2015

Single-stranded DNA-binding protein and its role in Okazaki fragment maturation

Yao Wang
University of Wollongong

Single-Stranded DNA-Binding protein and its Role in Okazaki Fragment Maturation

by

Yao Wang, *B.Sc.*

A thesis submitted in fulfillment of the requirements for the degree of Doctor of Philosophy

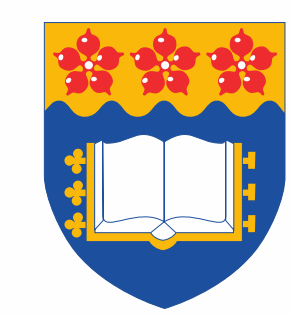

School of Chemistry, University of Wollongong

2015

DECLARATION

I, Yao Wang, declare that this thesis, submitted in fulfillment of the requirements for the degree of Doctor of Philosophy at University of Wollongong is the author's own work, unless otherwise stated, and was carried out within School of Chemistry, University of Wollongong. This document has not been submitted for qualifications at any other academic institution.

_____

Yao Wang

19th, March, 2015

ACKNOWLEDGEMENTS

The journey of my PhD had a start with great ups and downs, but an end with excitement and satisfaction, from the fulfillment of my curiosity during the pursuit of new knowlege in the world of science. None of this could be possibly achieved without the help of my mentor Prof. Nick Dixon. He brought me into the complex (and dark) world of macromolecular chemistry (I was a biologist). But his insight (like a light tower) powered by his vast knowledge often guided me when I was lost in the darkness. Many times I wished this was just the beginning of my Ph.D.; however, time has put a period on it. I hope (and I believe) it will be the beginning of something else.

The journey of my Ph.D. would not have been of such joy without our lovely group members (many of them became my friends). I would especially thank Dr. Allen Lo who taught techniques (such as SPR and MS) and with me many things shared (such as high quality proteins and columns) that turned out to be key parts of my Thesis. Even though my project overlapped with his in a very limited way, he spent his time with great patience in solving my endless problems. I felt extremely lucky to be able to work with him, and he certainly set a high mark for me. I would also thank A/Prof. Aaron Oakley who brought me into the structural world of protein science by trying to explain it to me on many occasions. I also thank him for his printed 3D *E. coli* SSB model, which really inspired me in an unexpected way. I would especially thank Drs Slobodan [whose many assays inspired me (and our collaborators) for my experiments in which his world-class quality proteins unveiled many exciting results], Nan, Zhi-Qiang, Robyn, and Claire who gave me great help in pursuing my Ph.D. From big projects and some brilliant ideas to bits and pieces, you guys are the “invisible” writers who “actually” constructed my thesis. Of course I thank “young” Nick (who lent me some of his quality proteins that are now weaving some nice stories in my Eppendorf tubes), and Fay, Michele, Jacob, David, Zorik, Amy, Joel, Jeff, *etc.* who accompanied me through various stages of my Ph.D.

I also thank our allies around Australia and the world, including Profs Gottfried, Guido, Joel, Samir, Jong-Bong and Antoine, who generated results from various platforms for my papers and thesis. I felt very lucky to be able to meet you and work in some of your

labs. I would thank Dr. Kiyoshi for demonstrating to me cell-free protein synthesis and old-fashioned plasmid purification, and Dr. Marylene for teaching me MST. I also thank our close ally Prof. Jenny Beck and her group members (especially Celine) at UOW. Without their constant help with mass spectrometry, many of our achievements would not be possible.

Scientists in the School of Chemistry with whom I exchanged talks and ideas shall also be thanked. Some thoughts from different fields very often inspired my study.

Last by not least, I would like to thank my family for their constant support. Their support clears out the path, and allows me to invest so much time in the things that I love.

I owe them too much.

LIST OF PUBLICATIONS

Marchetti, A., Jehle, S., Felletti, M., Knight, M.J., Wang, Y., Xu, Z.-Q., Park, A.Y., Otting, G., Lesage, A., Emsley, L., Dixon, N.E. and Pintacuda, G. (2012). Backbone assignment of fully protonated solid proteins by ^{1}H detection and ultrafast magic-angle-spinning NMR spectroscopy. *Angew. Chem. Int. Ed.*, *51*, 10756–10759.

Mason, C.E., Jergic, S., Lo, A.T.Y., Wang, Y., Dixon, N.E. and Beck, J.L. (2013). *Escherichia coli* single-stranded DNA-binding protein: A nanoESI-MS study of salt-modulated subunit exchange and DNA binding transactions. *J. Am. Soc. Mass Spectrom.*, *24*, 274–285.

Jergic, S., Horan, N.P., Elshenawy, M.M., Mason, C.E., Urathamakul, T., Ozawa, K., Robinson, A., Goudsmits, J.M.H., Wang, Y., Pan, X., Beck, J.L., van Oijen, A.M., Huber, T., Hamdan, S.M. and Dixon, N.E. (2013). A direct proofreader–clamp interaction stabilizes the Pol III replicase in the polymerization mode. *EMBO J.*, *32*, 1322–1333.

Shishmarev, D., Wang, Y., Mason, C.E., Su, X.-C., Yagi, H., Oakley, A.J., Graham, B., Huber, T., Dixon, N.E. and Otting, G. (2014). Intramolecular binding mode of the C-terminus of *E. coli* single-stranded DNA binding protein (SSB) determined by nuclear magnetic resonance spectroscopy. *Nucleic Acids Res.*, *42*, 2750–2757.

Yin, Z., Wang, Y., Whittell, L.R., Jergic, S., Liu, M., Harry, E., Dixon, N.E., Kelso, M.J., Beck, J.L. and Oakley, A.J. (2014). DNA replication is the target for the antibacterial effects ofnon-steroidal anti-inflammatory drugs. *Chem. Biol.*, *21*, 481–487.

Yin, Z., Whittell, L.R., Wang, Y., Jergic, S., Liu, M., Harry, E.J., Dixon, N.E., Beck, J.L., Kelso, M.J. and Oakley, A.J. (2014). Discovery of lead compounds targeting the bacterial sliding clamp using a fragment-based approach. *J. Med. Chem.*, *57*, 2799–2806.

Su, X.-C., Wang, Y., Yagi, H., Shishmarev, D., Mason, C.E., Smith, P.J., Vandevenne, M., Dixon, N.E. and Otting, G. (2014). Bound or free: interaction of the C-terminal domain of *Escherichia coli* single-stranded DNA-binding protein (SSB) with the tetrameric core of SSB. *Biochemistry*, *53*, 1925–1934.

Yin, Z., Whittell, L.R., Wang, Y., Jergic, S., Ma, C., Lewis, P.J., Dixon, N.E., Beck, J.L., Kelso, M.J. and Oakley, A.J. (2015). Bacterial sliding clamp inhibitors that mimic the sequential binding mechanism of endogenous linear motifs. *J. Med. Chem.*, *58*, 4693–4702.

In preparation:

Dunnant, H.R.W., Felletti, M., Jehle, S., Wang, Y., Emsley, L., Dixon, N.E., Lesage, A. and Pintacuda, G. (2015). Transient protein–protein interactions by solid state NMR: self-inhibition in *E. coli* single-stranded DNA-binding protein.

Li, N., Lo, A.T.Y., Robinson, A., Luzuriaga, J., Wang, Y., Ruiz, S., Dawes, F., Jergic, S., Oakley, A.J. and Dixon, N.E. (2015). Conservation of the DNA polymerase III χ–SSB and χ–ψ interactions in Gram-negative γ-proteobacteria.

Wang, Y., Li, N., Oakley, A.J. and Dixon, N.E. (2015). Intramolecular DNA wrapping mode and direction of *E. coli* and F-plasmid single-stranded DNA-binding protein.

ABBREVIATIONS

A_λ	absorbance at wavelength λ nm
AAA+	ATPase associated with various cellular activities
Ahx	aminohexanoic acid (spacer)
AMP	adenosine monophosphate
ATP	adenosine triphosphate
bp	base pair(s)
BRCT	the C-terminal domain of breast cancer susceptibility protein
BSA	bovine serum albumin
DEAE	diethylaminoethyl
DMSO	dimethyl sulphoxide
DnaGC	C-terminal domain of *E. coli* DnaG primase (residues 434–581)
dNTP	deoxyribonucleoside triphosphate
ds	double-stranded
DTT	dithiothreitol
ε_λ	extinction coefficient at wavelength λ nm
E.coli	*Escherichia coli*
Ec-SSB	*E. coli* single-stranded DNA-binding protein
EDTA	ethylenediaminetetraacetic acid
EM	electron microscopy
ESI-MS	electrospray ionization-mass spectrometry
EtBr	ethidium bromide
ExoI	exonuclease I
FPLC	fast protein liquid chromatography
F-SSB	*E. coli* F-plasmid derived SSB
F-SSBtrun	a serendipitously C-terminally truncated F-SSB
HEPES	4-(2-hydroxyethyl)-1-piperazineethanesulfonic acid
HhH	helix–hairpin–helix (domain)
HPLC	high-performance liquid chromatography
IPTG	isopropyl-β,D-1-thiogalactopyranoside
ITC	isothermal titration calorimetry
kb	kilo-base (pairs)
kDa	kilo-Daltons
K_D	equilibrium dissociation constant
LB(T)(A)	Luria-Bertani broth with supplement(s): (thymine) and/or (ampicillin)
MES	2-(*N*-morpholino)ethanesulfonic acid
mRNA	messenger RNA

MST	micro-scale thermophoresis
MW or mol. wt.	molecular weight
MWCO	molecular weight cut off
NAD^+	nicotinamide adenine dinucleotide
NH_4OAc	ammonium acetate
NMN	nicotinamide mononucleotide
NOE	Nuclear Overhauser Effect
Nt	nucleotide(s)
NTase	nucleotidyltransferase
OB fold	oligonucleotide/oligosaccharide-binding fold
OD_{600}	optical density at wavelength 600 nm
Q-Tof	quadrupole-time-of-flight
PCR	polymerase chain reaction
PEG	polyethylene glycol
PMSF	phenylmethylsulphonyl fluoride
Pol I	DNA polymerase I
Pol III HE	DNA polymerase III holoenzyme
RBS	ribosome-binding site
RMSD	root-mean-square deviation
RNase HI	ribonuclease HI
RNase HII	ribonuclease HII
RU	resonance units
R_{max}	resonance units at saturation for a given immobilized surface
SD	strand displacement (synthesis)
SDM	site-directed mutagenesis
SDS-PAGE	sodium dodecyl sulphate-polyacrylamide gel electrophoresis
SPR	surface plasmon resonance
SSB	single-stranded DNA-binding protein
SSB-Ct	highly conserved C-terminal peptide motif of *E. coli* SSB
ss	single-stranded
TAE buffer	Tris/acetate/EDTA buffer
TBE buffer	Tris/borate/EDTA buffer
TFII	tailed form II (DNA); i.e. fully ds circular DNA product derived using a flap-primed template
Tris	tris(hydroxymethyl)aminomethane
ZBD	zinc binding domain

ABSTRACT

All forms of life are defined by their DNAs. For organisms to survive, their chromosomes have to be replicated authentically and passed onto their next generations. This process is very complex – it involves a large number of proteins working in a very dynamic way. By elucidating this system, it helps us understand the basic mechanisms underlying life, to the eventual benefit of human beings.

Escherichia coli DNA replication is the best studied DNA replication system, and serves as a model in textbooks. In this model, Pol III HE (polymerase III holoenzyme), coordinated by DnaB helicase, replicates the leading strand continuously and the lagging strand discontinuously. The discontinuous DNA fragments, called Okazaki fragments, have to be processed and ligated. This process is called Okazaki fragment maturation. *Ec*-SSB (*E. coli* single-stranded DNA-binding protein), which binds to the single-stranded DNA ahead of the Pol III HE attracts more and more attention because of its versatility in DNA replication. This Thesis focuses on lagging-strand DNA synthesis, Okazaki fragment maturation and the role of *Ec*-SSB in these processes.

Ec-SSB is shown to stimulate DNA synthesis through many more residues than we thought. Previous studies have shown this process is stimulated through the interaction between *Ec*-SSB-Ct (C-terminal conserved residues of *Ec*-SSB) and the χ subunit of the Pol III clamp loader. The present study revealed a much higher level of involvement of the entire *Ec*-SSB sequence during DNA synthesis. The *Ec*-SSB N-terminal OB domain (oligonucleotide/oligosaccharide binding domain) and the C-terminal conserved residues (-DDDIPF) stimulate Pol III primer extension. This process is believed to be partially dependent on a newly structurally defined interaction between *Ec*-SSB-Ct and the single-stranded DNA binding site on the OB domain. This interaction may facilitate the removal of *Ec*-SSB on the ssDNA template ahead of the DNA polymerase. On the other hand, Pol III strand displacement (SD) synthesis is shown to be dependent on the entire *Ec*-SSB sequence. An additional role of the unconserved *Ec*-SSB C-terminal domain in SD was revealed by using elaborately designed chimeric SSBs. Interestingly, *Ec*-SSB does not always stimulate DNA synthesis. In a DNA replication assay with

DNA polymerase I (Pol I), *Ec*-SSB inhibits primer extension. However in both Pol III and Pol I systems, the OB domain of *Ec*-SSB is required for SD, as shown in assays at low salt concentration. Additionally, a single-molecule assay with fluorescently tagged *Ec*-SSB shows *Ec*-SSB is probably recycled at the DNA replication fork. These assays show for the first time a clear dependence on the OB domain and the unconserved C-terminal residues of *Ec*-SSB in SD, which sheds light on the understanding of this process. They also show a highly dynamic characteristic of *Ec*-SSB in DNA replication.

During Okazaki fragment maturation, Pol I is shown to remove the RNA primer and fill the gap with newly synthesized DNA. A nick is left behind, which is then sealed by ligase A. An alternative pathway involving RNase HI or RNase HII was proven to be infeasible in the *E. coli* replication system. RNase HI is able to remove RNA primers, but neither RNase HI nor HII (nor both of them together) is capable of properly processing the RNA at the RNA/DNA junction to leave a substrate (a nick) for ligase A to ligate. An additional role of the RNA primer is unveiled in the study, which shows longer RNA primers favour Okazaki fragment maturation by inhibiting the SD synthesis. This study supports the canonical pathway of Okazaki fragment maturation involving Pol I, and reveals the significance of RNA primers in the process. Additionally, interactions are identified between the Pol III χ subunit, the C-terminal domain of DnaG primase, RNase HI and the C-terminus of the *Ec*-SSB analogue F-SSB (*E. coli* F sex factor-encoded SSB). However, the functions of these interactions remain to be deciphered.

A crystal structure of the N-terminal OB domain of F-SSB in complex with ssDNA was solved. It shows a very similar tetrameric structure and the "baseball seam" type of ssDNA wrapping as a previous *Ec*-SSB:$(dC)_{35\times2}$ crystal structure (PDB code: 1EYG). However unlike the *Ec*-SSB, the bound $(dT)_{63}$ on the F-SSB is strikingly symmetric and adopts the opposite binding polarity. Further studies show that F-SSB and *Ec*-SSB can form hybrid tetramers with any combination of their monomers. DNA replication assays (with *E. coli* Pol III HE or a downsized *Ec*-SSB dependent system) with the hybrid tetramers as well as homogenous tetramers composed of elaborately made fusion monomers shows F-SSB can stimulate primer extension but not SD. Thus, DNA polymerase may be able to cope with both ssDNA binding polarities on SSBs. To further establish this, attempts to reproduce the *Ec*-SSB:$(dC)_{35}$ crystal structure were made, but the crystals obtained did not diffract X-rays to sufficiently high resolution to

define the ssDNA binding polarity. This has left the binding polarity of ssDNA on SSBs still an open question. Assuming ssDNA can wrap on SSBs in both polarities, a new ssDNA binding path on SSB is proposed. Finally, given extensive sequence similarities between F-SSB and *Ec*-SSB, the structure carries valuable information about SSB–DNA interactions.

This Thesis contributes to the understanding of *E. coli* DNA replication by revealing and defining numerous protein–protein and protein–DNA interactions biochemically and structurally. Importantly, it also provides insights into new protein–protein and protein–DNA interactions.

TABLE OF CONTENTS

TABLE OF FIGURES

TABLE OF TABLES

CHAPTER 1

INTRODUCTION

1.1 Background

1.1.1 DNA elongation during DNA replication in *Escherichia coli*

The bacterium *Escherichia coli* is widely used for carrying out molecular and protein studies, due to advantages such as short generation time, lack of pathogenicity and its completely sequenced chromosome. DNA replication mechanisms in *E. coli* are used as model systems for discovery of new anti-bacterial agents. This potential relies on thorough understanding of the replication process including protein–protein and protein–DNA interactions. However, there are many weak and transient interactions yet to be understood.

DNA replication is bidirectional (**Figure 1.1**) since copying of two DNA strands of the circular *E. coli* chromosome occurs at two replication forks progressing in opposite directions from the single origin of replication, *oriC* (Prescott and Kuempel, 1972). At the same time, it is semi-conservative since each daughter cell contains dsDNA (double-stranded DNA) composed of parental and complementary newly synthesized polynucleotide chains (Meselson and Stahl, 1958).

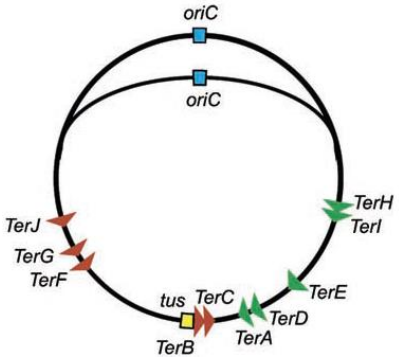

Figure 1.1 Schematic of the origin of *E. coli* DNA replication (from Mulcair *et al*., 2006). The origin (*oriC*) where DNA replication initiates is shown as blue squares on the DNA (represented as black threads). The *Ter* sites (red and green triangles) and the location of the *tus* gene (yellow square) are also shown.

At each replication fork, the replisome, the protein complex carrying out DNA replication, unidirectionally "unzips" double helical DNA strands while it copies both antiparallel strands (Watson and Crick, 1953a,b) of DNA simultaneously (Wu *et al*., 1992; Zechner *et al*., 1992). This creates a problem since all DNA polymerases

synthesize DNA in the 5'–3' direction by extending the 3'-OH group of a pre-existing "primer". The replication machinery solves this problem by synthesizing the two strands of DNA in continuous and discontinuous manners (**Figure 1.2**).

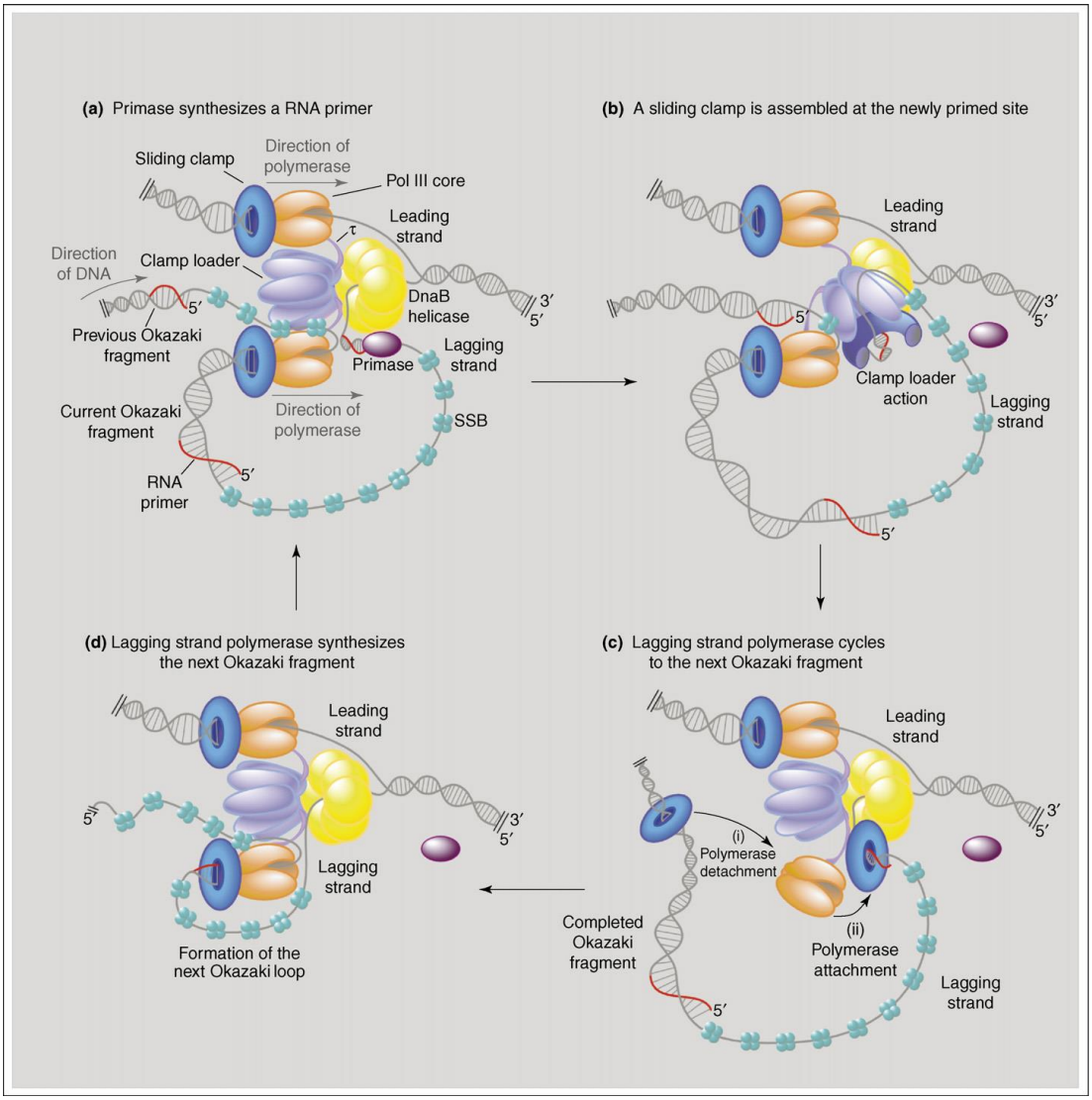

Figure 1.2 Proposed DNA replication mechanism showing polymerase cycling on the lagging strand (from Pomerantz and O'Donnell, 2007). The DNA helicase (yellow) unwinds the dsDNA (double-stranded DNA) into two ssDNA (single-stranded DNA) strands that are coated with the ssDNA-binding protein (SSB; cyan) tetramers. The DNA polymerase III (Pol III) HE (holoenzyme) moves along DNA unidirectionally while copying both stands of DNA simultaneously, during which the SSB is removed. The two newly replicated strands are called the leading and lagging strands, respectively, due to their distinct synthesis fashions. (**a**) A primase (dark magenta oval) interacts with the helicase and synthesizes a short RNA primer (red thread) on lagging strand DNA. (**b**) Primase dissociates from the completed primer. The clamp loader (purple) opens the β_2 clamp (blue toroid) and loads it on the primed site. (**c**) The polymerase on the lagging strand is cycled from the completed Okazaki fragment to the β_2 clamp on a newly primed site. The detached β_2 clamp is left behind. (**d**) The polymerase on the lagging strand starts synthesizing a new Okazaki fragment.

As depicted in **Figure 1.2**, the DnaB helicase first separates the two strands of dsDNA

and occasionally interacts with the DnaG primase, which synthesizes short RNA primers (Tougu and Marians, 1996a,b; Oakley *et al*., 2005), 11 ± 1 nucleotides in length, on single-stranded (ss) DNA. The ssDNA produced by helicase action is protected by being coated with ssDNA-binding protein (SSB). However additional functions of SSB other than protection of ssDNA from nuclease attack have been reported in recent years (discussed in **Chapter 4**, **Section 4.1.1**). The continuous strand, which is called the leading strand, needs to be primed only once at *oriC*, or again during replication restart after occasional fork stalling.

In contrast, the discontinuous lagging strand is synthesized in a more complicated way that needs numerous primed sites. On the lagging strand, DNA polymerase III holoenzyme (Pol III HE), with assistance of the β_2 clamp, extends a 3' end of an RNA primer and synthesizes 1000–2000 nucleotide (Nt) DNA segments called Okazaki fragments (Okazaki and Okazaki, 1969; Kornberg and Baker, 1992). Implication of a partially ssDNA loop has been made based on the geometry of the replication fork (Sinha *et al*., 1980). The Pol III HE dissociates when it encounters the 5' end of the previous RNA primer (Stukenberg *et al*., 1994; Li and Marians, 2000) and is recycled onto a new primed site. DNA polymerase I (Pol I) then replaces the RNA primer with DNA and leaves a nick which is later joined by DNA ligase (Kornberg and Baker, 1991).

1.1.2 Functions and structures of key components participating in DNA elongation during *E. coli* DNA replication

1.1.2.1 The Pol III αεθ core

The multi-subunit DNA polymerase III is the enzyme carrying out *E. coli* chromosomal DNA replication. The α polymerase subunit carries out DNA synthesis in the 5'–3' direction (Mitra and Kornberg, 1966). The ε subunit has proofreading 3'–5' exonuclease activity (Maki and Kornberg, 1987), which promotes the fidelity of DNA synthesis. The third subunit, θ, interacts with the ε subunit and stabilizes it (Taft-Benz and Schaaper, 2004). The three subunits are arranged in the form of 1:1:1 heterotrimers (Studwell-Vaughan and O'Donnell, 1993). Three αεθ polymerase cores are coordinated by the clamp loader complex through the α:τ interaction (there are probably three τs in the

clamp loader) at the replication fork, which enables simultaneous leading and lagging strand DNA replication (reviewed by and van Oijen, 2013).

The chemistry of DNA synthesis by α, involving two metal ions at the active site, is believed to be conserved in all DNA polymerases (Brody and Frey, 1981; Echols and Goodman, 1991; Rothwell and Waksman, 2005; Yang *et al.,* 2006). A detailed structural study recently captured snapshots of the DNA synthesis reaction by the error-prone human DNA polymerase η (Nakamura *et al.,* 2012). It showed a third metal ion is involved in the reaction (**Figure 1.3**). A nucleotidyl-transfer reaction is triggered at the active site between the α-phosphate of a complementary dNTP and the 3'-OH of the primer strand. A new phosphodiester bond is formed between the primer and the dNTP while a PP_i (pyrophosphate) group is released. The reaction is coordinated by two Mg^{2+} ions. A third Mg^{2+} probably coordinates the newly formed phosphodiester bond and the PP_i leaving group.

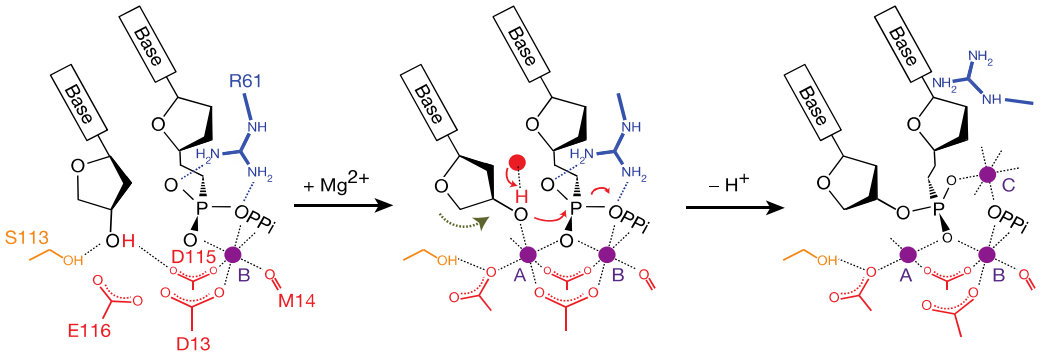

Figure 1.3 The proposed DNA polymerase reaction promoted by Pol η. The incoming dNTP is coordinated by an Mg^{2+} (purple dot) and the side chains of the polymerase. The dashed lines indicate the hydrogen bonds and the metal ion coordination. Deprotonation is triggered at the 3'-OH group by the involvement of the second Mg^{2+}. The arrows indicate the electron transfer process between the water molecules (red dot), 3'-OH and the dNTP. A third Mg^{2+} approaches and replaces the R61 side chain when the new phosphodiester bond is forming (from Nakamura *et al.,* 2012).

1.1.2.2 The β_2 clamp

Highly processive DNA replication requires attachment of DNA polymerase III to a ring-shaped sliding clamp, the β dimer (McHenry, 2003; Johnson and O'Donnell, 2005). When coupled to the sliding clamp, the DNA polymerase becomes exceedingly fast (~750 nt/s) and processive (>50 kb), provided that β had previously been bound to encircle the DNA template (Stukenberg *et al*., 1991). The β_2 clamp binds to many other

proteins to coordinate their access to dsDNA. It is reported that a clamp-binding motif (consensus: QL[S/D]LF) is widely conserved in most (or all) eubacterial proteins that interact with the clamp (Dalrymple *et al.,* 2001; Sutton, 2004). Eukaryotes also use similar ring-shaped sliding clamps during DNA replication, called proliferating cell nuclear antigen, or PCNA (Krishna *et al*., 1994; Gulbis *et al*., 1996).

The homodimeric bacterial sliding clamp is composed of two β subunits (the 41 kDa product of the *dnaN* gene). Each monomer has three similar globular domains and binds the other monomer in a head-to-tail manner, to form a six-domain ring (Kong *et al*., 1992; Argiriadi *et al*., 2006) capable of accommodating dsDNA in the central cavity (**Figure 1.4A**). The specific conformation of the β dimer results in two different faces on the ring (**Figure 1.4B**). The face from which the C-termini protrude contains an intermolecular binding site, which interacts with clamp-binding motifs in numerous proteins at different stages of DNA replication and repair processes (Naktinis *et al*., 1995, 1996; Johnson and O'Donnell, 2005). Pol III HE makes new DNA at very high speed when it is bound to the β_2 clamp. How does the clamp slide so easily on dsDNA? A high-resolution crystal structure suggests that water molecules (Oakley *et al*., 2003) and positive electrostatic potential (Blackburn and Gait, 1996; Barsky *et al*., 2011) at the inner face of the β_2 ring create a path for sliding on duplex DNA in the center of the toroid (**Figures 1.4C and D**).

The known β_2-binding partners also include MutL and MutS, DNA ligase, the Hda cell-cycle regulatory factor, the ε proofreading subunit of Pol III and all other known *E. coli* DNA polymerases (Pols I, II, IV and V) (MutS, DNA ligase and Pol I: López de Saro and O'Donnell, 2001; MutL: Johnson and O'Donnell, 2005; Hda: Kurz *et al.,* 2004; Pol II: Hughes *et al*., 1991; Bonner *et al*., 1992; the ε subunit of Pol III: Jergić *et al.,* 2013; Pol IV: Wagner *et al*., 2000; Tang *et al*., 2000; Kobayashi *et al*., 2002; Pol V: Tang *et al*., 2000; Dalrymple *et al*., 2001; López de Saro *et al*., 2003b). These enzymes are all involved in a variety of DNA metabolic pathways. Pol I is responsible for the maturation of Okazaki fragments and filling of single-stranded gaps in DNA. Pols II, IV and V are significantly upregulated as part of the cell's global SOS response to DNA damage. Both of MutL and MutS play critical roles in DNA mismatch repair, and ligase A acts at the last step of DNA replication where it is required for sealing nicks between Okazaki fragments on the newly formed lagging strand.

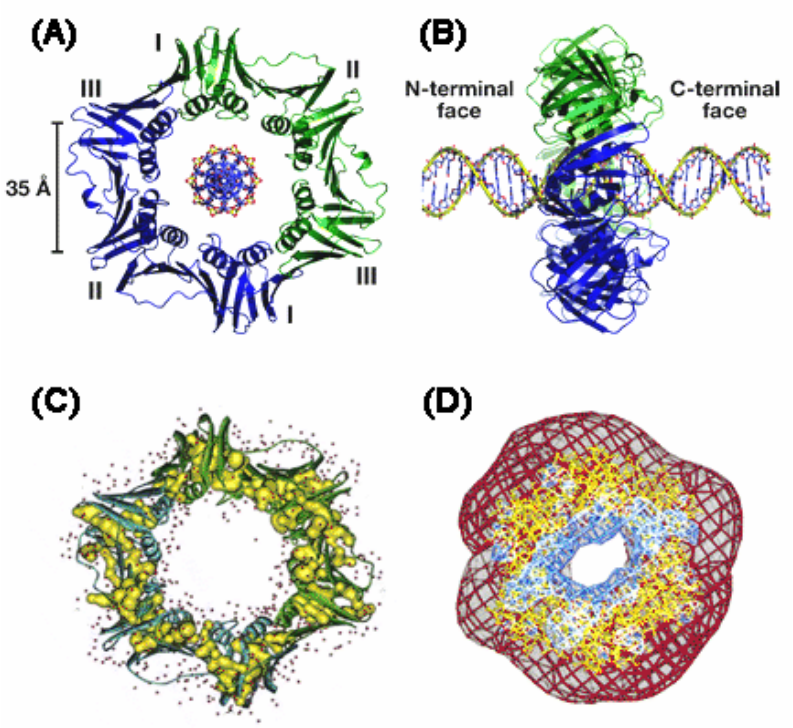

Figure 1.4 *E. coli* β_2 clamp crystal structures. (**A**) Ribbon structure of β_2 shows a ring structure with a modelled DNA residing in the central cavity. The β subunit is a crescent protein with three domains that dimerizes to form a six-domain ring. (**B**) Two distinct faces of the clamp are indicated. The C-terminal face contains a protein-binding site that binds other proteins (adapted from Johnson and O'Donnell, 2005). (**C**) Ordered water molecules (red spheres) are observed in a high-resolution structure of the clamp, predicted to form a layer of water molecules at the interface of DNA and the clamp (adapted from Oakley *et al*., 2003). (**D**) The electrostatic potential map shows positive potential at the central channel surrounded by negative potential at the outer region of the clamp (adapted from Blackburn and Gait, 1996)

MutS, a sensor of DNA mismatches, can interact with the β clamp (Clark *et al.*, 2000; López de Saro and O'Donnell, 2001). Two interaction sites are found (Dalrymple *et al.*, 2001; López de Saro *et al.*, 2006; Simmons *et al.*, 2008), a weaker N-terminal binding site and a strong one at the C-terminus. Studies show that interaction of *Bacillus subtilis* MutS with the β_2 clamp promotes the stabilization of MutS at mismatches *via* the C-terminal binding site, suggesting that mismatch recognition is coordinated and promoted by interaction with β_2 (Simmons *et al.*, 2008). MutL is regarded as a "matchmaker" among the mismatch repair factors (Ban and Yang, 1998; Ban *et al.*, 1999). MutL can bind to ssDNA, and this seems to be a prerequisite for its binding to the β clamp (Ban *et al.*, 1999; López de Saro *et al.*, 2006). It undergoes major conformational change as it undergoes its ATPase cycle, suggesting a possible on–off switch for the interaction (Ban *et al*, 1999). Speculation was made for a regulatory process modulated by DNA structure and ATP-induced conformational changes.

Being a dimer, the β_2 clamp can bind two different proteins simultaneously. For example, Pol I and ligase are also reported to bind to the β clamp, but it is not clear if their actions in Okazaki fragment maturation are coordinated by it. Evidence shows that human ligase can adopt open and closed conformations, and interaction with the PCNA clamp may rigidify the closed form and preclude other proteins from binding to the clamp (Pascal *et al.*, 2004). Perhaps the reason for this is that ligation is the last step in Okazaki fragment maturation. A longer introduction to the roles of Pol I and ligase in Okazaki fragment processing is given in **Chapter 4**.

These various proteins all bind to a hydrophobic site in each subunit of β_2 to which the δ subunit of the Pol III clamp loader also binds. The β subunit interacts with the isolated δ subunit of the clamp loader (K_D = 8 nM; Naktinis *et al*., 1995), as well as the fully assembled clamp loader complex ($\gamma_3\delta\delta'\psi\chi$), although with weaker strength (Leu and O'Donnell, 2001). These interactions induce a conformational change in the sliding clamp that leads to its opening and loading on dsDNA (Jeruzalmi *et al*., 2001a). It is found that clamp-binding proteins all bind the hydrophobic protein-binding pocket on the C-terminal face of the clamp, and some of them likely have other unique touch points as well (Gulbis *et al*., 1996; Shamoo and Steitz, 1999; Matsumiya *et al*., 2001; Sutton and Walker, 2001; Jeruzalmi *et al*., 2001a,b; Chapados *et al*., 2004).

It was later suggested that Pol III binds to the β subunit *via* two binding sites in the α subunit. One is located at the extreme C-terminus, and another is about 200 residues internal to it (López de Saro *et al*., 2003b; Dohrmann and McHenry, 2005). Moreover, an additional interaction between the ε subunit and the β clamp was identified recently (Jergić *et al.,* 2013). Pol IV also binds to β with two different sites (Bunting *et al*., 2003). A ternary complex formed by Pol III, Pol IV and β has led to speculation of a tool belt model where multiple proteins bind to and dissociate from β at various times during DNA synthesis (Indiani *et al*., 2005). The structure of the complex of Pol IV with β_2 revealed that Pol IV can adopt two conformations when it binds to β_2 through a flexible interaction, where it switches on and off the Pol III activity (Bunting *et al*., 2003; Indiani *et al*., 2005; Kath *et al.*, 2014).

A further study reveals that the β_2 clamp directly binds primed DNA as well as ssDNA in a tilted manner (Georgescu *et al*., 2007). In this structure, DNA resides in the centre of the ring with a sharp angle that is 22° from the *C*2 rotation axis of β_2 (**Figure 1.5A**).

Double-stranded DNA interacts with Arg-24 and Gln-149 on protruding loops of the C-terminal face of β. This face is the one that also binds the clamp loader (Naktinis *et al*., 1996). Interestingly, interaction was also uncovered between ssDNA and the protein-binding pocket, which might have an undefined role in clamp loading (**Figure 1.5B**). The ssDNA-binding surface contains two closely located tyrosines (Tyr-153 and Tyr-154) which stack with thymine (Thy-13) and adenine (Ade-15) bases of the DNA (**Figures 1.5B and 1.5C**). Other nucleotide bases (Thy-11 and Thy-12) are placed at two conserved residues (Val-247 and Met-362) in the protein-binding pocket of β. It is speculated that Thy-11 of the DNA may interact with Thr172 of β.

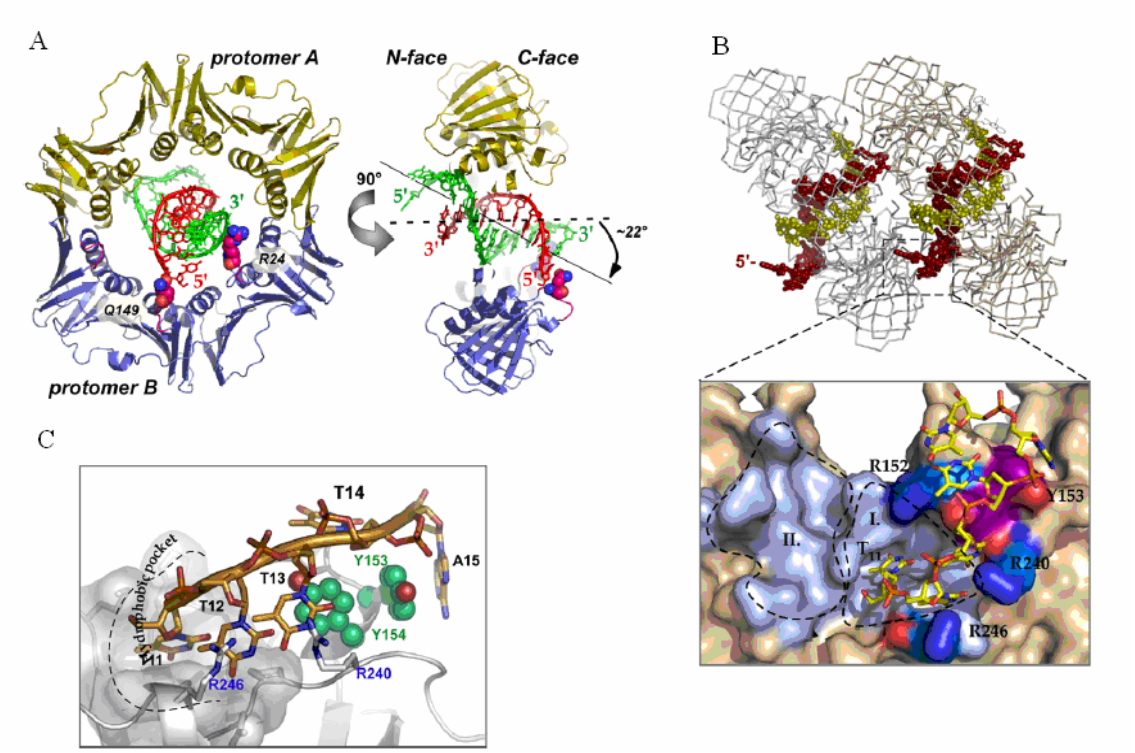

Figure 1.5 Structure of the β_2–DNA complex (from Georgescu *et al*., 2007). (**A**) Ribbon structure of the β_2–DNA complex shows that DNA resides in the channel of the clamp in a tilted manner at 22° from the *C*2 rotation axis of β_2 clamp. (**B**) Crystal lattice structure shows that two β_2 clamps are attached to each other by crystal contacts between ssDNA and the protein-binding site of the β_2 clamp. Below is a detailed picture of the interaction site. Basic residues are coloured blue. The protein-binding site is shaded purple and subsites I and II (defined in Burnouf *et al*., 2004) are indicated. (**C**) Close view of the interaction site shows the position of ssDNA (gold) inside the hydrophobic protein-binding pocket of β. The hydrophobic pocket, Thy-11 and Thy-12 and the exposed side chains (Arg-246 and Arg-240) interacting with the ssDNA backbone are shown. Stacking between Tyr-153 (green) and Ade-15, and Tyr-154 (green) and Thy-13 are shown.

1.1.2.3 The $\tau_2\gamma\delta\delta'\psi\chi$ clamp loader

Crystallographic and biochemical studies demonstrate that the *E. coli* clamp loader

assembles and dissembles the β_2 clamp on dsDNAs. The whole clamp loader is composed of seven subunits ($\tau_2\gamma\delta\delta'\psi\chi$; Pritchard *et al*., 2000). However it is shown that a smaller version called the γ complex ($\gamma_3\delta\delta'$) is sufficient for clamp loading (Jeruzalmi *et al*., 2001a). In this complex, two τ subunits are replaced by γ subunits. The γ subunit is encoded by the same gene (*dnaX*) as τ, but lacks a 24-kDa C-terminal sequence due to translational frameshifting (Flower and McHenry, 1990; Tsuchihashi and Kornberg, 1990). The additional C-terminal segment of τ coordinates leading and lagging strand synthesis by interacting with the DnaB helicase and the two Pol III cores (Onrust *et al*., 1995; Glover and McHenry, 2000; Pritchard *et al*., 2000; Gao and McHenry, 2001a,b). The ψ and χ subunits are not required in the clamp assembly but are involved in binding SSB and the RNA primer (Xiao *et al*., 1993a; Glover and McHenry, 1998; Kelman *et al*., 1998; Yuzhakov *et al*., 1999). Recently, it was shown that the interaction between χ and SSB is essential for strand displacement DNA synthesis by Pol III HE (Yuan & McHenry *et al*. 2009; further introduced in **Chapter 4**).

Crystal structures show that each of the five subunits of the γ complex ($\gamma_3\delta\delta'$) contains three similar domains and exhibits a C-shaped structure (**Figure 1.6A**). The subunits are held together by forming a circular collar at the C-terminal region. The three γ proteins flanked by δ and δ' are organized into a spiral-shaped asymmetric structure (**Figure 1.6B**). The γ subunit belongs to the AAA+ (ATPases associated with a variety of cellular activities) family, and so is called the "motor" of the clamp loader (Neuwald *et al*., 1999; Davey *et al*., 2002a). While the δ and δ' subunits have structures very similar to γ, they are not ATPases (Jeruzalmi *et al*., 2001a,b).

Clamp opening is accomplished through conformational changes of the clamp loader (γ complex in the case of *E. coli*). First, an ATP molecule is bound to each of the three ATP-binding sites, comprised of the conserved Ser-Arg-Cys (SRC) structure and the P-loop (phosphate binding loop) at three of the subunit interfaces of the γ-complex (**Figure 1.6C**). Then, the γ complex binds to the β_2 clamp *via* strong interactions with an α-helix on the δ subunit (not shown). ATP binding triggers rotations of four hydrophobic residues on the α-helix, where it loses interactions between residues Trp-61 and Phe-62 of the α-helix and δ', and exposes Leu-73 and Phe-74, which bind directly in the hydrophobic pocket of the β_2 clamp. Interestingly, in the absence of ATP, Trp-61 and Phe-62 of δ interact with δ', while Leu-73 and Phe-74 are sequestered in δ.

When hydrolysis of ATP and binding to primed DNA take place, the clamp is released and reclosed around the dsDNA or RNA–DNA primer-template (Jeruzalmi *et al.*, 2001a, b). The γ and τ subunits in isolation show weak interactions with the β_2 clamp (Leu and O'Donnell, 2001), suggesting their secondary involvement in clamp assembly.

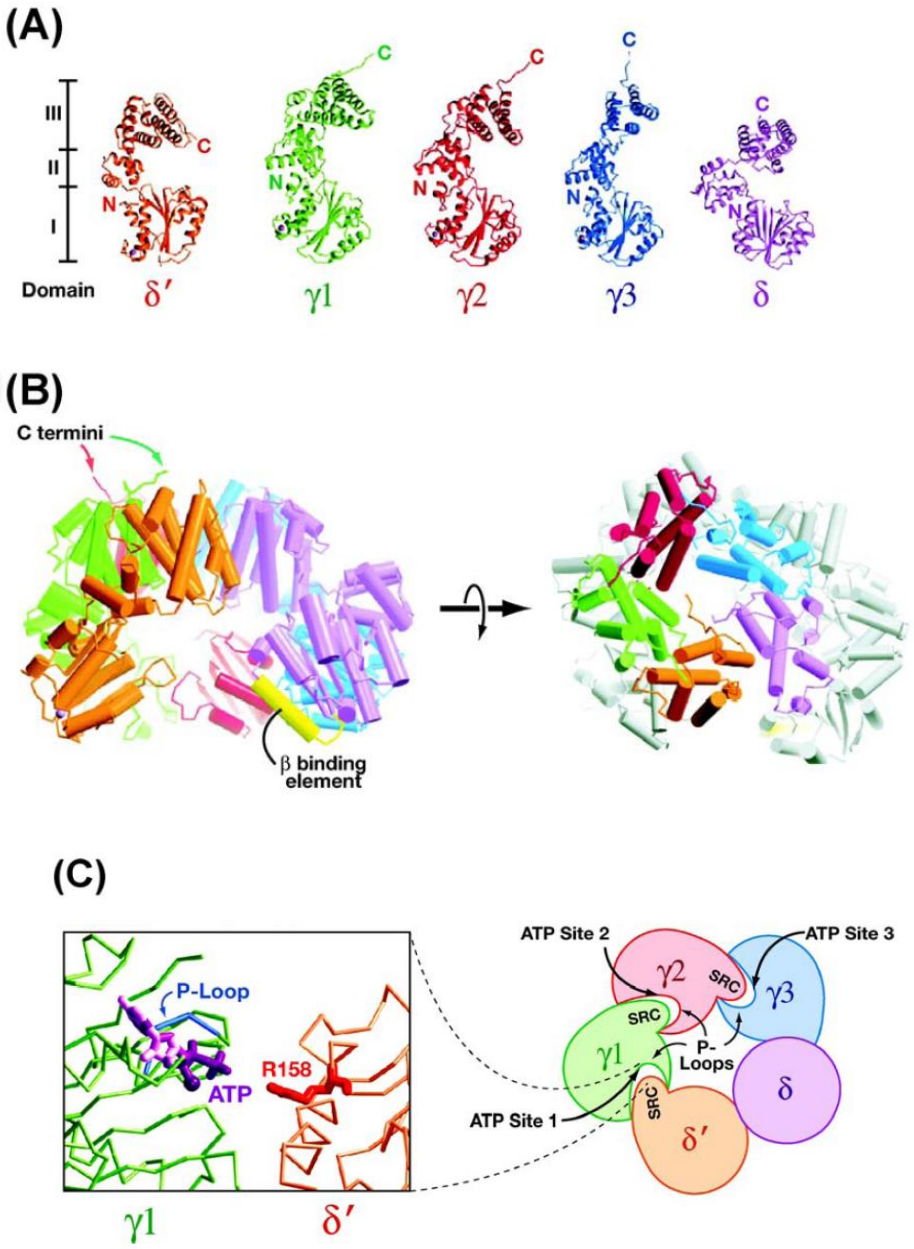

Figure 1.6 Crystal structures of the γ complex and its subassemblies solved by Jeruzalmi *et al.* (2001b). (**A**) Structures of δ, δ' and three γ(1–373) subunits show similar C-shapes with three domains (from Jeruzalmi *et al.* 2001b). (**B**) Structure of $\gamma_3\delta\delta'$ (left) shows that the clamp loader assembles in a way with adjacent domains from different subunit. Each subunit is coloured the same way as in panel **A**. The C-termini of δ', γ_1 and the β binding element in δ are indicated by arrows. The panel at right shows the C-terminal collar region where the clamp loader subunits hold together (from Jeruzalmi *et al.* 2001b). (**C**) Picture shows the spiral-shaped architecture of the clamp loader and a closer view of the ATP binding site at the interface of γ_1 and δ'. ATP (purple) is modelled against the P-loop (blue) with the arginine finger (red) from the conserved SRC (Ser-Arg-Cys) motif pointed towards it (from Johnson and O'Donnell, 2005).

The co-crystal structure (**Figure 1.7**) of the *E. coli* clamp loader and a primed DNA fragment reveals that interactions primarily occur at the phosphate backbone of the template strand as opposed to the primer strand (Simonetta *et al*., 2009). The clamp loader adopts a right-handed spiral conformation around the portion of dsDNA, while ssDNA is located out of the structure without tight contact with the protein.

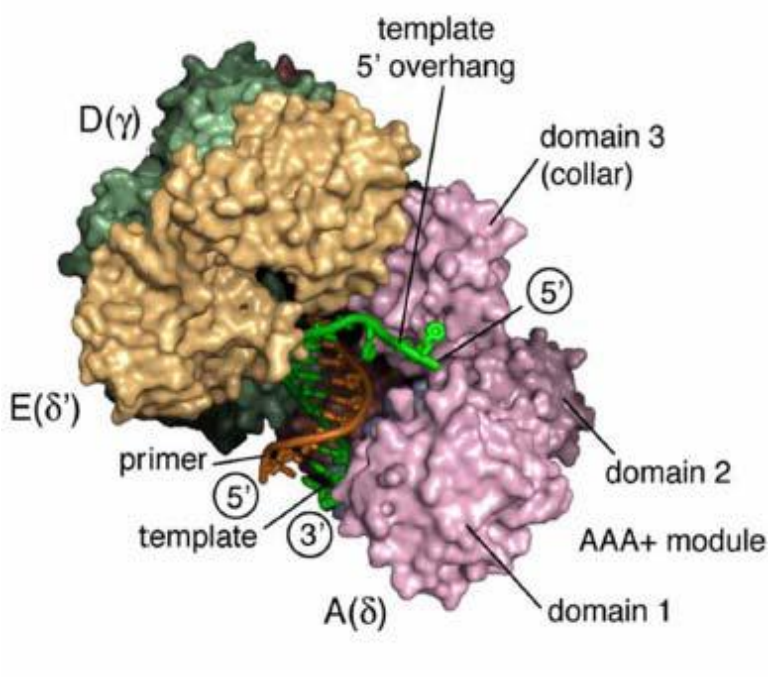

Figure 1.7 Co-crystal structure of the γ complex with primed DNA strands shows the critical interaction in primer recognition (from Simonetta *et al.,* 2009). The clamp loader holds the double-stranded portion of the template, and has the single-stranded portion escaping from it.

The χ and ψ subunits are not required in clamp loading but are thought to coordinate primase and SSB activities. The χ subunit encoded by the *holC* gene is a 17 kDa protein, while the ψ subunit encoded by *holD* is a 15 kDa protein (Carter *et al*., 1993a,b; Xiao *et al*., 1993b). The χ subunit does not bind to other parts of the clamp loader complex. However it does bind tightly to ψ (O'Donnell and Studwell, 1990), which interacts with Domain III (Gao and McHenry, 2001b) of γ *via* its N-terminal conserved but otherwise flexible residues (Gulbis *et al*., 2004; Ozawa *et al*., 2005). Thus, ψ acts as a bridge connecting the χ subunit to the clamp loader. **Figure 1.8** shows the crystal structure (Gulbis *et al.,* 2004) of the χψ complex (missing the flexible 26 N-terminal residues of ψ).

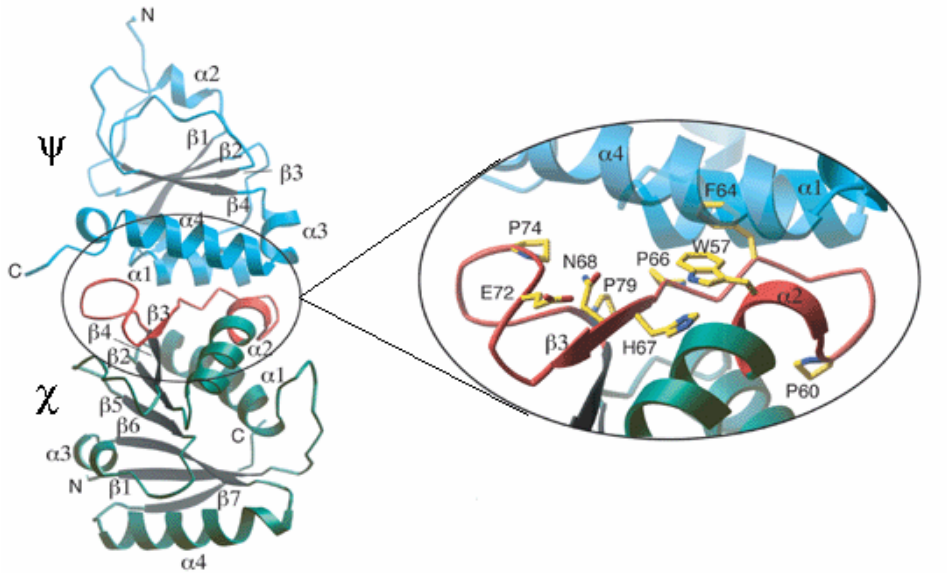

Figure 1.8 Crystal structure of the *E. coli* χψ complex with 26 N-terminal residues missing from ψ. The binding site (red) between the χ and the ψ subunits is shown in the enlarged picture on the right (from Gulbis *et al*., 2004).

Previously, it was proposed that the χψ complex binds the clamp loader through 28 conserved residues of the N-terminus of ψ (Gulbis *et al*., 2004; Ozawa *et al*., 2005). A recent study of binding affinities indicates that the isolated 2–28 peptide of ψ (ψ peptide) has similar effects on the clamp loader as intact ψ (Simonetta *et al.,* 2009). They both increase the binding affinity between the clamp loader and a primed DNA template. The ψ subunit binds the clamp loader on the collar region of all three γ subunits (**Figure 1.9**). An α-helix formed by residues 3–13 of the ψ peptide packs against the helices of C(γ) and D(γ) subunits that line the inner surface of the collar. Residues 14–19 of the ψ peptide form a β-strand that runs along the surface of the C(γ) subunit and into the interface between the C(γ) and B(γ) subunits, forming a short two-stranded antiparallel β hairpin with the C-terminal tail of the B(γ) subunit. The highly conserved Trp-17 in the ψ peptide is packed between Pro-361 and Arg-355 of the B(γ) subunit.

This arrangement, where the N-terminal peptide of ψ contacts all three γ subunits of the clamp loader in an asymmetric fashion explained a previously puzzling paradox. The ψ subunit was known to interact with both γ and τ (in isolation), yet there is only one ψ (and χ) subunit in the active, assembled clamp loader complexes.

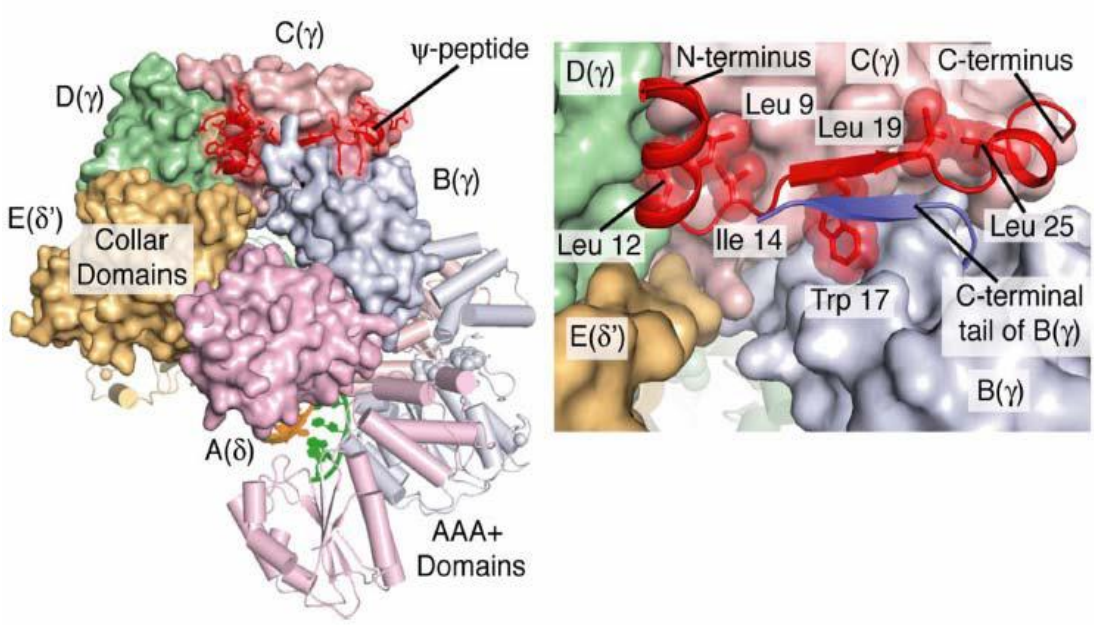

Figure 1.9 Co-crystal structure of the ψ-peptide (red) bound to the clamp loader collar (left panel) reported by Simonetta *et al.* (2009). The clamp loader is shown in the form of a surface representation. The right panel shows details of the interaction that occurs at the collar domains of the B(γ), C(γ), and D(γ) subunits. Hydrophobic side chains are shown as spheres. The C-terminal tail of B(γ), which forms a short anti-parallel β-sheet with the ψ-peptide, is shown as a blue ribbon (from Simonetta *et al.,* 2009).

Thus, ψ links χ to the clamp loader complex through its N-terminal peptide (**Figure 1.10**). By attaching to the clamp loader, the χ subunit coordinates DNA replication through interacting with SSB (Kelman *et al*., 1998; Witte *et al*., 2003). Structural and biochemical studies showed that χ binds the flexible C-terminal region of SSB (Kelman *et al*., 1998; Marceau *et al.,* 2011), and this interaction is further strengthened by SSB binding to ssDNA (Glover and McHenry, 1998). Study of the clamp loader structure (**Figure 1.10**) indicates that the N-terminus of ψ anchors the interface of two γ subunits at the collar region, while the χψ complex is located at the outer face (Simonetta *et al.,* 2009). The orientation of the χψ complex toward the emerging DNA stand makes it able to interact with the flexible tails of SSBs on ssDNA. It is suggested that the χ subunit destabilizes interaction between primase and SSB at the primed site, which is then available for clamp loading (Yuzhakov *et al*., 1999). This primase-to-polymerase switch contributes to transactions during lagging strand DNA synthesis.

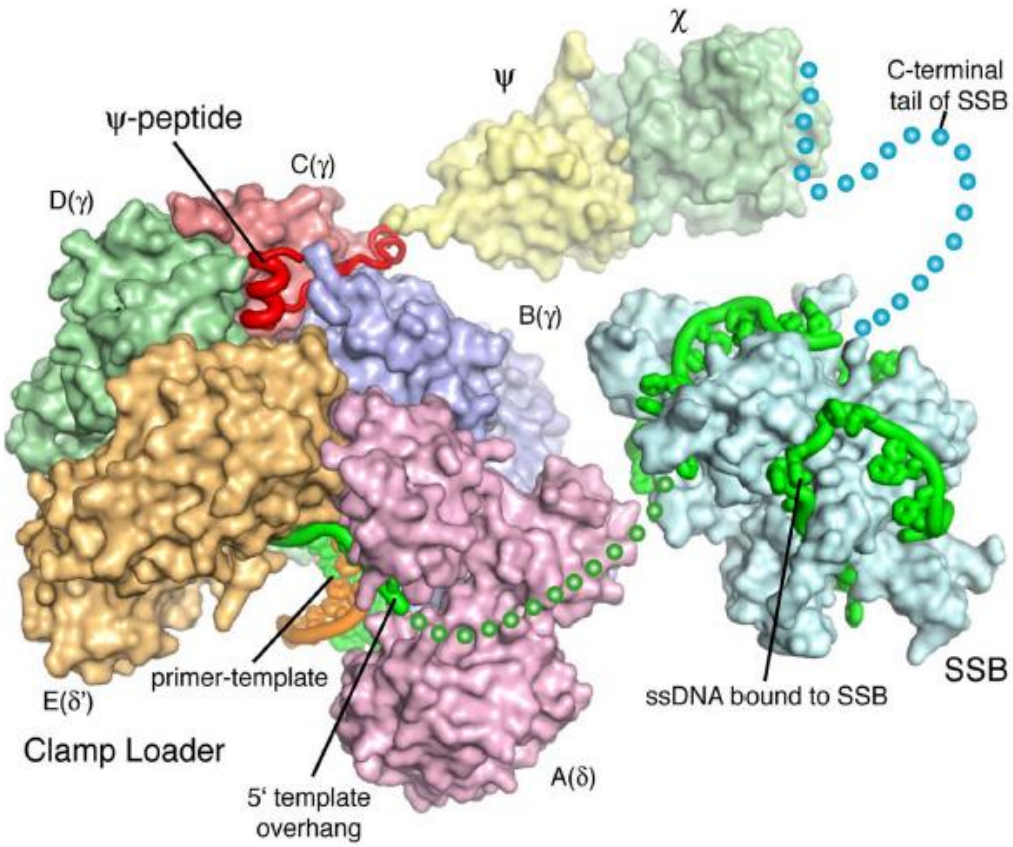

Figure 1.10 Model of the clamp loader:χψ:SSB complex. The ψ peptide binds the collar region of the clamp loader, orients the χψ complex in a direction capable of engaging the flexible C-terminal tail of SSB bound to the ssDNA ahead of a primer terminus (from Simonetta *et al.,* 2009). SSB engaging the 5' overhang of DNA (green spheres) is shown.

1.1.2.4 DNA ligase

NAD^+ (nicotinamide adenine dinucleotide) dependent DNA ligase, discovered 40 years ago (Gellert, 1967; Olivera and Lehman, 1967a,b; Weiss and Richardson, 1967a,b; Gefter *et al.,* 1967; Zimmerman *et al.,* 1967; Becker *et al.,* 1967) is an essential participant in DNA replication. It guarantees chromosome integrity by forming phosphodiester bonds between 3'-OH and 5'-phosphate groups at nicks in DNA. As a result, ligases have attracted a great deal of interest from scientists, and been widely used in research. It is found that multiple ligases exist and function differently in most organisms. In this case, study will focus on *E. coli* DNA ligase A, the enzyme that repairs lagging-strand nicks in the final stage of Okazaki fragment processing.

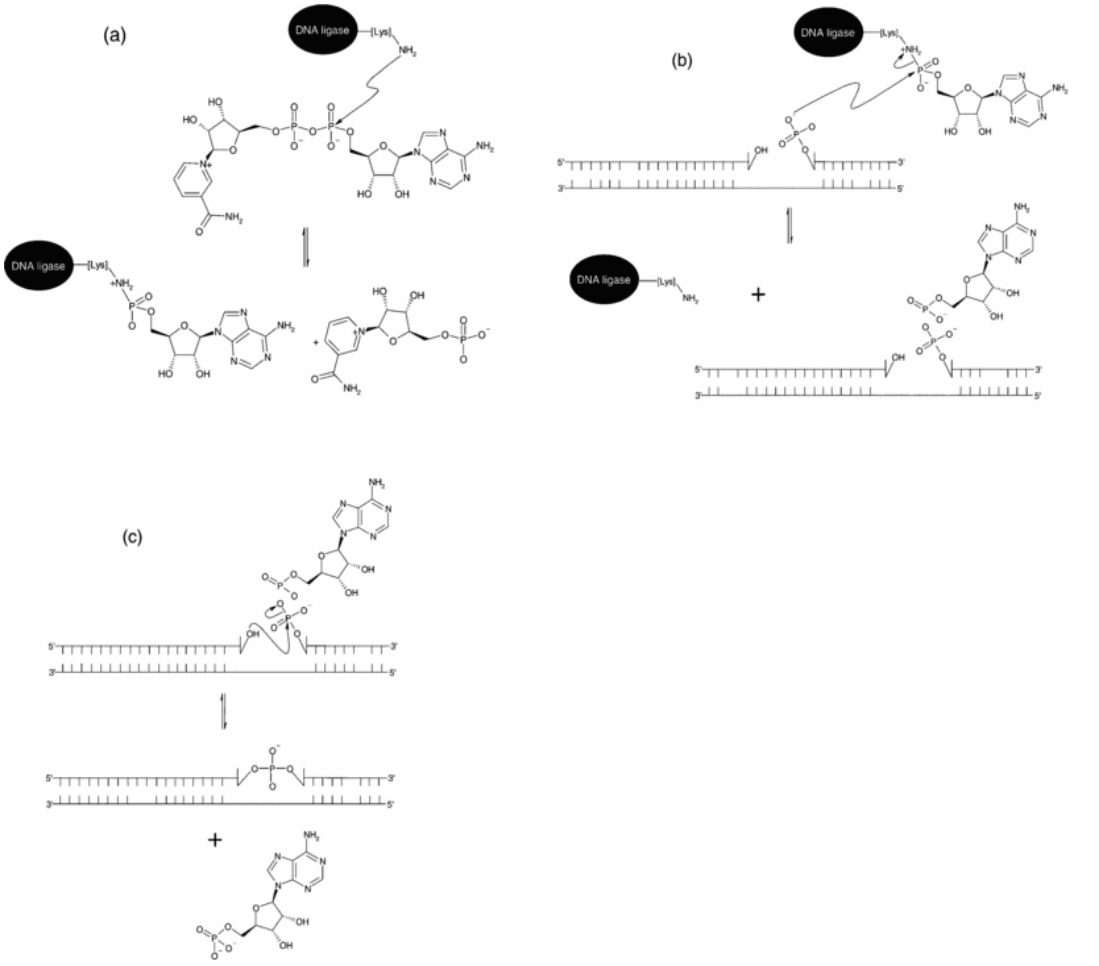

Figure 1.11 Schematic representation of the reaction mechanism of NAD^+-dependent ligases (from Shuman, 2009). (**a**) Formation of an enzyme–adenylate complex and NMN. (**b**) Activation of 5'-phosphate at the site of a nick in the DNA substrate. (**c**) Nick closure in which a covalent bond is formed between an adjacent 3'-hydroxyl group and activated 5'-phosphate in duplex DNA structures with the release of AMP.

Ligation by ligase A requires three nucleotidyl transfer reactions (**Figure 1.11**): (i) Ligase reacts with NAD^+ in the absence of nucleic acid to form a covalent ligase-(lysyl-N-)-AMP (adenosine monophosphate) intermediate and releases NMN (nicotinamide mononucleotide; Little *et al.,* 1967; Gumport and Lehman, 1971). (ii) Ligase-AMP binds to a nicked duplex DNA and transfers the adenylate from the active-site lysine to the 5'-phosphate terminus to form an adenylylated nicked intermediate, AppDNA (Olivera *et al.,* 1968). Ligase remains bound to the adenylylated nick and immediately catalyzes step (iii), the attack of the nick 3'-OH on the 5'-phosphoanhydride linkage, resulting in a repaired phosphodiester in the DNA and release of AMP.

The molecular structure **(Figure 1.12**) of the ligase A protein (671 amino acids in total)

exhibits a core nucleotidyltransferase (NTase) domain (amino acids 70–316) flanked by an N-terminal Ia domain (amino acids 1–69) and four C-terminal modules: an OB-fold domain (amino acids 317–404), a tetracysteine zinc finger domain (amino acids 405–432), a helix-hairpin-helix domain (HhH, amino acids 433–586), and a BRCT domain (named after the C-terminal domain of breast cancer susceptibility protein, amino acids 587–671; Singleton *et al*., 1999; Lee *et al.*, 2000; Gajiwala *et al.*, 2004; Srivastava *et al.*, 2005; Nandakumar *et al.*, 2007).

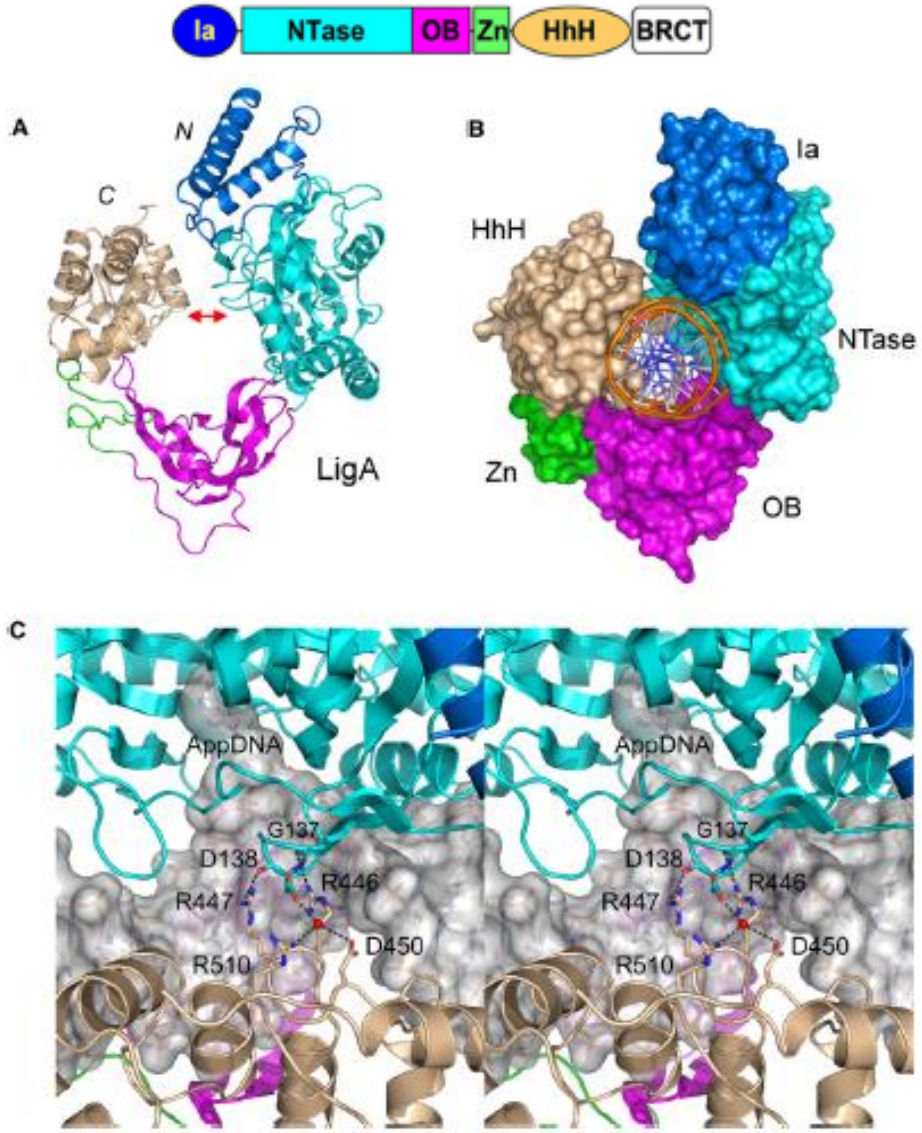

Figure 1.12 Co-crystal structure of *E. coli* ligase A with DNA is shown with the C-terminal BRCT domain missing in this case (from Nandakumar *et al.,* 2007). (**A**) Ribbon diagram of ligase A with DNA molecules omitted at the central cavity. The red arrow indicates the kissing contact between the HhH domain (beige) and the NTase domain (cyan). (**B**) A space-filling representation shows that ligase A engages the DNA template in the form of a clamp. (**C**) A closeup stereo-view the kissing contact shows that the interaction occurs at the DNA major groove opposite the nick. Arg-446 and Arg-447 of the HhH domain donate hydrogen bonds to the backbone carbonyls of NTase residues Gly-137 and Asp-138. Water molecules are shown in red spheres. The co-crystal structure captures the ligaseA–AppDNA intermediate.

Ligase A binds DNA, adopting a clamp form that involves interactions with DNA between the NTase and HhH domains (**Figures 1.12A and B**), while no interaction occurs between the HhH and la domains. Nicked DNA resides in the central cavity of the enzyme. A close view shows that the interaction occurs at opposite sides of the nick, where HhH residues Arg-446 and Arg-447 interact with backbone carbonyls of Gly-137 and Asp-138 in the NTase domain. Water mediated hydrogen bonds are also observed between the Asp-138, Arg-510 and Asp-450 side chains (**Figure 1.12C**). Details of contacts between the DNA template and the domains of ligase are shown in **Figure 1.13**.

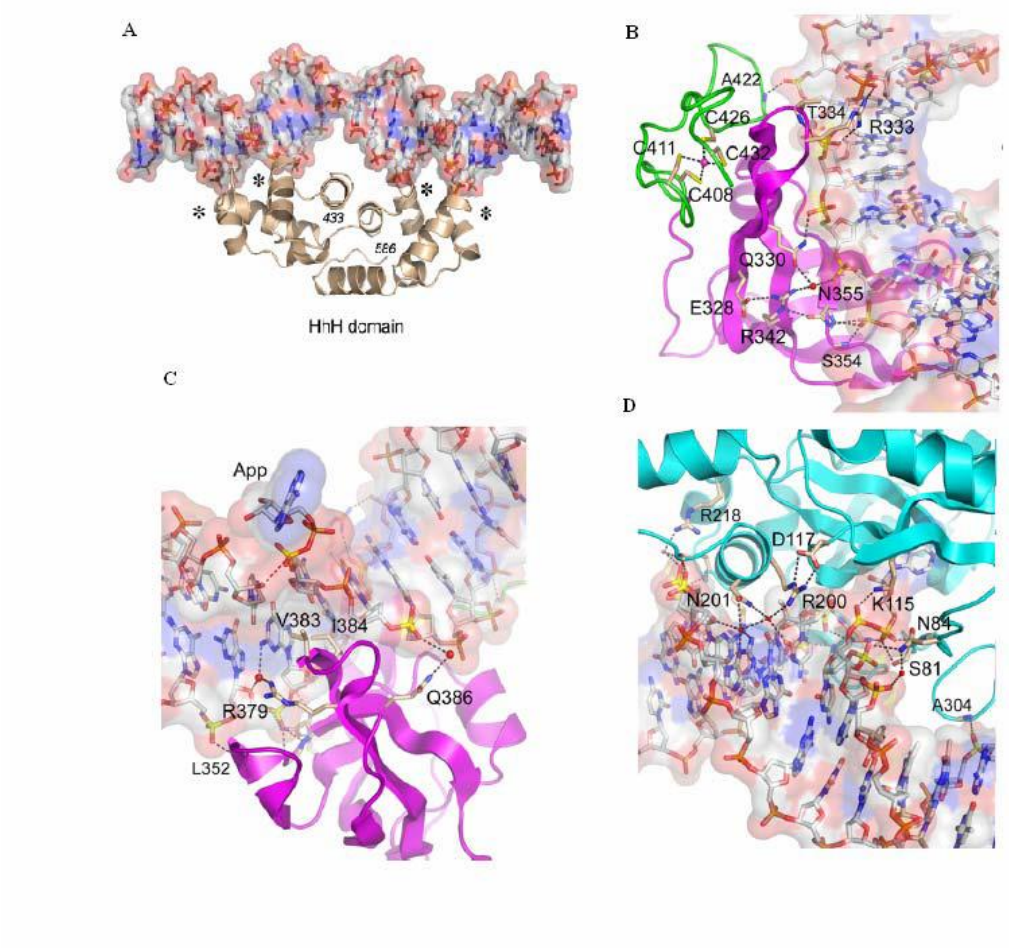

Figure 1.13 Detailed views of interactions between DNA and ligase A domains (from Nandakumar *et al.,* 2007). (**A**) Ribbon diagram of the *E. coli* ligase A HhH (gold) domain bound to nicked duplex DNA. Asterisks implicate the "loop-helix" motifs, which bind the backbone of the minor groove of the substrate. (**B**) Tetracysteine zinc coordination complex (green) distant from the DNA template. (**C**) β barrel of the OB domain (magenta) that contacts the backbone of DNA. (**D**) β strands of the nucleotidyltransferase domain surrounding the nick 5'-adenylate and the numerous interactions of the helix that inserts into the minor groove.

1.2 Aims and scope of this Thesis

The *E. coli* DNA replisome is a large, complex and dynamic multi-protein machine. At the replication fork, the DnaB helicase unwinds dsDNA, and interacts with DnaG primase to lay down short RNA primers. The ssDNA derived from helicase action is protected by SSB. DnaB helicase also interacts with the large complex of the clamp loader ($\tau_2\gamma\delta\delta'\psi\chi$), which coordinates two Pol III cores ($\alpha\varepsilon\theta$) on β_2 clamps for DNA synthesis. Once the Pol III cores finish DNA synthesis, the RNA primer is removed by DNA polymerase I, and the nick that remains is ligated by DNA ligase (Pomerantz and O'Donnell, 2007).

The understanding of this complex machinery has been experiencing changes in recent years. More and more weak interactions have been shown to be important to maintain the speed and fidelity of the replisome. This Thesis helps to further understand the significance of weak protein interactions for DNA synthesis on the lagging strand.

In **Chapter 2**, I present the general materials and methods used in this Thesis.

In **Chapter 3**, I first introduce the SSB protein and describe its structure and functions, highlighting the conserved C-terminal region that interacts with many partner proteins in DNA replication, repair and recombination (Shereda *et al.,* 2008). In that **Chapter**, an interaction between the highly conserved SSB C-terminus and RNase HI is characterized by SPR (surface plasmon resonance). A SSB analogue protein, F-SSB, encoded by the F plasmid of *E. coli*, is found also to be able to bind ssDNA and also interacts with RNase HI through its C-terminus. Furthermore, it is shown that the F-SSB C-terminus also binds to DnaGC (*E. coli* C-terminal helicase-binding domain of DnaG, residues 434–581) and the χ subunit of the Pol III HE, as does the *E. coli* SSB. The SSB OB domain is well conserved in F-SSB, but the C-terminal flexible region is highly diverged except for the very C-terminal 8 residues. Thus the similarity of DNA and protein binding properties of these two SSBs provides opportunities to explore the function of SSB in DNA replication (results are shown in **Chapters 4 and 5**). A long-standing question about the putative SSB C-terminus binding site on its OB-domain has been resolved by NMR (Shishmarev *et al.,* 2014). Further study using fluorescein labelled SSB in MST (micro-scale thermophoresis) shows the interaction is very weak

(K_D ~10 mM), and NMR results show the C-termini of SSB are most of time unbound to the binding sites (Su *et al.,* 2014). Therefore we conclude SSB is ready to bind to its binding partners through the highly conserved C-terminus with and without associating with ssDNA. These studies extend our understanding about the regulatory role of the SSB C-terminus. However, further study is needed for understanding the meaning of the interactions between SSB (and its analogue protein F-SSB) and RNase HI, DnaGC or the χ subunit in DNA replication, and how weak interactions between the SSB C-terminus and its OB domain regulate its ssDNA binding (Kozlov *et al.,* 2010; Mason *et al.,* 2013).

In **Chapter 4**, bulk phase DNA replication assays, DNA binding assays and single-molecule DNA replication assays are used to explore new functions of individual proteins and protein–protein interactions. A stimulatory role of the SSB OB-domain in Pol I and Pol III promoted SD DNA synthesis is revealed. Further study using SSB/F-SSB chimeric proteins shows the whole flexible C-terminal region is also important for DNA strand displacement. However it was thought that this process is stimulated by the interaction between the χ subunit and the SSB C-terminus (Yuan *et al*., 2009). Another stimulatory role of the SSB OB domain in Pol III α subunit promoted primer extension synthesis is revealed. This process is further stimulated by the C-terminus of SSB. Interestingly, SSB inhibits primer extension by Pol I, possibly though its tight interactions with the ssDNA template. This leads to speculation about a novel interaction between the α subunit and SSB. Single-molecule assays with fluorescent protein-labelled SSB shows SSB is probably recycled at the replication fork. However, further study is needed to understand which interactions keep SSB at the replication fork, and the significance of this observation. This Chapter also provides insight into an alternative pathway of Okazaki fragment maturation involving RNase HI and RNase HII. It is shown that RNase HI is able to digest RNA primers but fails to thoroughly process the RNA primer for ligase A to seal the nick. Pol I on the other hand shows ample ability to process the RNA primer to produce a sealed DNA strand in the presence of ligase A. This is in agreement with widely accepted belief. DNA replication assays with various RNA-primed DNA templates in the presence of Pol I and ligase A shows Okazaki fragment maturation also requires a certain length of RNA primer. Pol III can displace shorter RNA primers to carry out strand displacement synthesis, which interferes with Okazaki fragment maturation.

Chapter 5 describes the crystal structure of *apo*-F-SSB and F-SSB in complex with ssDNA. These are the first structures of F-SSB solved since its discovery 30 years ago (Chase *et al.,* 1983). They show a very similar tetrameric structure and the "baseball seam" type of ssDNA binding as the native *E. coli* SSB. However, the polarity of ssDNA wrapping on F-SSB is opposite to that reported for SSB (Raghunathan *et al.,* 2000). DNA replication assays with fusion and hybrid tetramers of SSB/F-SSB show Pol III HE may be able to carry out DNA replication with ssDNA wrapped on SSB in either polarity.

CHAPTER 2

GENERAL MATERIALS AND METHODS

2.1 Bacterial strains and plasmid vectors

2.1.1 Bacterial strains

Hosts used for plasmid storage include *E. coli* strain AN1459 (F⁻ *ilv leu thr supE recA srlA*::*Tn*10) (Vasudevan *et al*., 1991) and strain SURE 2 [e14⁻(McrA⁻) Δ*(mcrCB-hsdSMR-mrr)171 endA1 gyrA96 thi-1 supE44 relA1 lac recB recJ sbcC umuC*::Tn*5* (Kan^r) *uvrC*] from Stratagene. SURE 2 supercompetent cells derived from the Stratagene strain SURE (Stop Unwanted Rearrangement Events) are designed to overcome the difficulties in cloning certain repetitive DNAs using traditional *E. coli* strains. Strains used for protein expression include strains BL21(λDE3) *recA*, an *E. coli* B strain with a λ prophage carrying the T7 RNA polymerase gene under control of *lacOP* operator-promoter [F⁻ *ompT (lon) hsdS$_B$ (r_B^- m_B^-) recA srlA*::*Tn*10] (Williams *et al*., 2002) and BL21(λDE3)/pLysS (Studier *et al.*, 1990).

2.1.2 Plasmid vectors

Plasmids pND706 and pETMCSI (**Figure 2.1A** and **B**), or derivatives of them, were used as vectors for carrying target genes in this Thesis, unless otherwise specified.

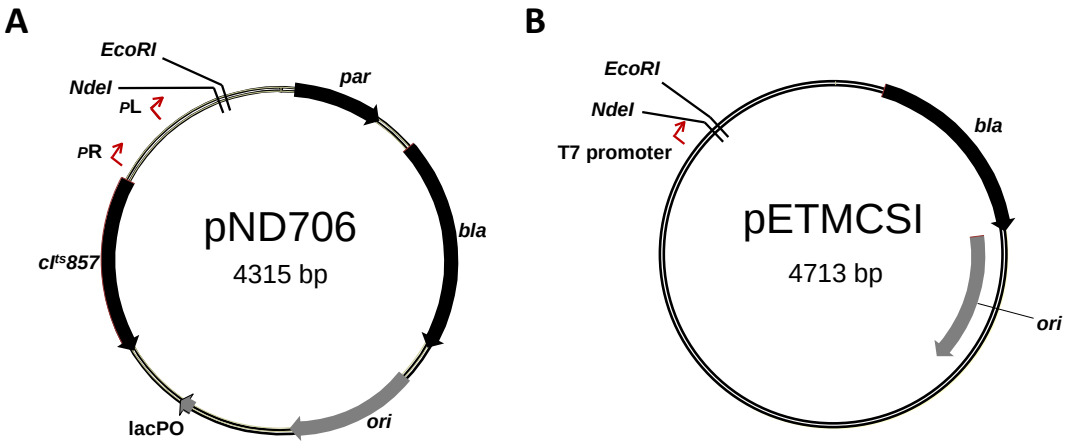

Figure 2.1 The physical maps of plasmid pND706 (**A**) and pETMCSI (**B**) used in this Thesis. Target genes were normally inserted between *Nde*I and *Eco*RI restriction sites.

Plasmid pND706 (Love *et al.*, 1996; **Figure 2.1A**) provides an *Nde*I restriction site (5'-CATATG) containing an ATG start codon downstream of a strong ribosome binding site (RBS). Target genes were inserted between *Nde*I and *Eco*RI restriction sites, unless

otherwise specified. Upstream of the *Nde*I site resides the tandem p_R and p_L promoters (from bacteriophage λ) which promote the transcription of the inserted gene. At lower temperatures (≤30˚C), the transcription of the gene is suppressed by the λ repressor encoded by the $cI^{ts}857$ gene. The expression of the target gene is typically enabled by a quick change of temperature to 42˚C, which inactivates the thermolabile λ repressor (Elvin *et al.*, 1990). Additionally, the *par* locus and the *bla* gene confer plasmid stability and ampicillin resistance, respectively (Love *et al.*, 1996). Plasmid pETMCSI (Neylon *et al*., 2000; **Figure 2.1B**) allows gene expression under the control of the phage T7 ϕ10 promoter. A target gene in pETMCSI was expressed in strains with the ability of induced expression of T7 RNA polymerase [*e.g*., BL21(λDE3)*recA*]. It also contains the *bla* gene that encodes ampicillin resistance. The origins of replication (*ori*) in both plasmids are also shown in **Figure 2.1**.

2.2 Growth media

2.2.1 LB medium

LB medium (Luria and Burrous, 1957) was generally used to grow *E. coli* strains. Strains containing plasmids with gene expression under the strict control of λ promoters (*e.g*., in pND706) were grown in 30˚C, and were switched to 42˚C for protein induction. The strains with T7 expression vectors (pETMCSI) were grown at 30 or 37˚C, and were treated with IPTG (isopropyl-*β*-D-thiogalactopyranoside) for induction of protein overproduction. The LB medium was supplemented with 25 mg/L thymine. Ampicillin (100–200 mg/L) and/or chloramphenicol (35 mg/L) were added into the LB medium according to the antibiotic resistance encoded by the plasmids. In this Thesis, LBTA refers to LB medium supplemented with thymine and ampicillin. Solid LBTA medium was made by adding 15 g/L of agar in LB liquid medium.

2.2.2 Minimal medium for isotope (^{13}C, ^{15}N or ^{2}H) labelled proteins

Minimal medium provides basic elements for bacteria to grow, thus eliminates un-required contaminants in rich medium (*e.g.,* LB). Carbon, nitrogen or hydrogen sources in this medium can be replaced with isotope labelled counterparts as the sole carbon,

nitrogen or hydrogen source to achieve uniform isotope-labelling of proteins. To make 1 L of minimal medium, 950 mL of milliQ water (or D_2O), 50 mL 20 × MM (made by dissolving 10.6 g of K_2HPO_4 and 6.1 g of NaH_2PO_4 in 50 mL of MilliQ water or D_2O) and 1 g of NH_4Cl (or ^{15}N-NH_4Cl) were mixed in a 1 L flask which was autoclaved. The medium was cooled to room temperature and supplemented with 1 mL of 1 M $MgSO_4$, 1 mL of 1000 × metal mix, 2 g of glucose (or ^{13}C-glucose) and 100 µL of 10 g/L vitamin B1, all of which had been filter sterilized. Bacteria were inoculated into a 5 mL minimal medium culture and incubated overnight at 30˚C before being transferred into a larger volume of medium for protein expression. Alternatively, bacteria were incubated in LB medium until OD_{600} ~0.7, and then centrifuged at ~3000 × g. The clear LB medium was discarded. The bacterial pellet was resuspended in minimal medium containing the required isotopes. Induction was immediately initiated by quickly shifting the temperature to 42˚C (for strains with λ-promoter plasmids) or adding IPTG (for strains with T7-promoter expression vectors), as required.

2.3 Molecular genetics procedures

2.3.1 Plasmid extraction

Bacteria were grown on an LBT agar plate (with required antibiotics) overnight at 30˚C, and then collected for small-scale plasmid extraction. For large-scale plasmid extraction, bacteria were grown in 1 L of LBT broth (with required antibiotics) overnight, and collected by centrifugation at 5,000 × g for 20 min. Small-scale and large-scale plasmid extractions were performed by using Miniprep and Maxiprep Kits (Qiagen GmbH, Hilden, Germany), respectively. Small-scale plasmid extraction was routinely performed during cloning. Large-scale plasmid extraction was performed for CsCl purified plasmids (**Section 2.3.10**).

2.3.2 Oligonucleotide synthesis

Oligonucleotide primers were designed manually using the original plasmid sequences, and were purchased from Gene Works (Adelaide). Briefly, two primers flanking the gene of interest were designed for polymerase chain reactions (PCRs) involved in

cloning procedures. The primers for these purposes were normally extended at the 5' end by adding additional dAMP residues to ensure efficient cleavage by restriction endonucleases. Two primers complementary to each other with one or multiple mutated nucleotides were designed for site-direct mutagenesis by PCR. The HPLC-purified $(dT)_{63}$, $(dT)_{62}$ and $(dC)_{31}$ used for crystallization were also purchased from and HPLC purified by Gene Works. The HPLC-purified 3' biotin labeled $(dT)_{35}$ used for immobilization on BIAcore chips was a kind gift from Dr. Allen Tak Yiu Lo.

2.3.3 Quantification of DNA

The concentration of double-stranded DNA was determined by Nanodrop (Thermo Scientific) assuming A_{260} of 1.0 corresponds to 50 μg/mL of DNA. Plasmid DNA was routinely stored in TE buffer (10 mM Tris-HCl, pH 7.6, 0.1 mM EDTA) at –20˚C. TE buffer was used as blank for DNA concentration measurement in the Nanodrop instrument.

2.3.4 Restriction endonuclease digestion of DNA

All restriction endonucleases were purchased from New England Biolabs. For the purpose of obtaining linear DNA fragments, digestions were carried out as recommended by the company.

2.3.5 Agarose gel electrophoresis

Mini-Sub Cell GT Systems (Bio-Rad) were used for both analytical and preparative agarose gel electrophoresis; 0.7% to 2% (w/v) agarose gels in TBE buffer (89 mM Tris-borate, 2 mM EDTA; Sambrook *et al*., 1989) containing 0.4 μg/mL ethidium bromide (EtBr), was used for analytical purposes. A potential difference of 20–60 V was applied to migrate the DNA samples. Preparative agarose gel electrophoresis was carried out in 1% (w/v) agarose gels in TAE buffer (40 mM Tris base, 20 mM acetic acid, and 2 mM EDTA; Sambrook *et al.,* 1989) in the presence of 0.4 μg/mL EtBr; 20–60 V were applied to migrate the digested DNA samples. As specified, 0.7% (w/v) agarose gels in TAE buffer, in the absence or presence of EtBr, were used for analytical purposes. The agarose gel without EtBr was stained afterwards in the same TAE buffer in the presence of 0.8 μg/mL ethidium bromide for 20 min followed by destaining with H_2O for 15 min.

Alternatively, gels were stained with 10,000-fold diluted SYBR® Gold nucleotide gel stain (Life Technologies) for 1 h with gentle shaking. The buffer was heated to ~30˚C for better staining. The DNA fragments were visualized using a UV transilluminator (ChemiDoc XRS system, Bio-Rad). DNA ligation assays and replication assays were quenched (unless otherwise specified) by adding 90 mM EDTA and 0.6% SDS in the reaction mixture, before being loaded into the gel. EDTA chelates the metal ions (normally ≤10 mM of Mg^{2+} in the reaction mixture) and SDS disrupts the DNA–protein interactions to enable visualization of naked DNA in the agarose gel after staining.

2.3.6 Isolation of DNA fragments

The DNA was recovered from agarose gels using the Agarose Gel Extraction kit (Qiagen). Briefly, DNA fragments were separated in agarose gels with EtBr, and visualized under a long-wavelength UV lamp to avoid DNA damage. The desired DNA fragment was cut out by using a scalpel, and transferred into an Eppendorf tube followed by extractions using the extraction kit. All the instruments in contact with the agarose gels were extensively washed beforehand using MilliQ water and 70% ethanol to avoid contamination by other DNAs.

2.3.7 DNA ligation

Target genes and vectors cut with restriction endonucleases were separated by agarose gel electrophoresis, followed by gel extraction (**Section 2.3.6**). Then, target genes and vectors with complementary ends were ligated with T4 DNA ligase (Fermentas). The procedures were as described by Sambrook *et al*. (1989). Reaction mixtures were incubated in 16˚C for 12 h to achieve optimum ligation.

2.3.8 Transformation of competent *E. coli* cells

For heat-shock DNA transformation, competent *E. coli* cells were prepared by using the procedures described by Morrison (1979). For electroporation, competent cells were prepared as described by Miller and Nickoloff (1995). The transformation procedures were also as described by Miller and Nickoloff (1995) for electro-transformation or Morrison (1979) for heat-shock transformation except that 42˚C for 1 min was used in the latter.

2.3.9 Colony polymerase chain reactions

The cloned genes were analyzed by conducting colony PCR with the plasmid (contained in a single bacterial colony) potentially containing the desired gene as the template. Primers complementary to the sequences flanking the gene insertion site were used in the PCR. Specifically, the reaction mixtures were made by mixing 0.3 μM primers, 0.25 mM of each dNTP, 1.25 units of Taq DNA polymerase (Roche), and a bacterial colony in 25 μL of Taq buffer (10 mM Tris-HCl, pH 8.3, 1.5 mM $MgCl_2$ and 50 mM KCl). The colony was taken from a LB agar plate by using a sterilized pipette tip or a tooth pick, and then dipped into the reaction mixture. The reaction took place in a thermo cycler using the following PCR protocol:

Cycles	Temperature	Time
1	94˚C	3 min
30	94 / 55 / 72˚C	30 / 15 / 60 s
1	72˚C	5 min

2.3.10 Determination of nucleotide sequences

DNA samples for sequencing were prepared using the BigDyeTerminator sequencing reaction kit (Applied Biosystems). Primers p9 (5'-GGCAGCATTCAAAGCAGAAG) and p10 (5'-GTTGGGTAACGCCAGGG) were used for sequencing genes inserted in vector pND706 (Love *et al.*, 1996). Primers p3 (5'-CGACTCACTATAGGGAGAC CACAAC) and p4 (5'-CTTTCGGGCTTTGTTAGCAG) were used for sequencing genes inserted in vector pETMCSI (Neylon *et al.*, 2000). These primers are complementary to the sequences of the vector flanking the *Nde*I and *Eco*RI cloning sites. The reagents were mixed according to the instruction manual from the company. The reaction mixture was incubated in thermo cycler using the following PCR protocol:

Cycles	Temperature	Time
1	96˚C	1 min
14	96 / 50 / 60˚C	10 / 5 / 75 s
4	96 / 50 / 60˚C	10 / 5 / 90 s
4	96 / 50 / 60˚C	10 / 5 / 2 s

The reaction mixtures were then purified by the QIAGEN Dye EX 2.0 Spin kit. The

samples were analyzed by capillary electrophoresis at the School of Biological Science at the University of Wollongong.

2.3.11 Plasmid purification by CsCl gradient centrifugation

Purification of DNA plasmids was performed at the Research School of Chemistry, Australian National University. Purification was done as described by Sambrook *et al.* (2000), except that DNA sample was mixed with 1.025 g/mL CsCl, EtBr added, and centrifuged at 83500 × *g* for 48 h in a Sorvall T-1270 rotor. Bands were collected using a syringe, and after extraction of the EtBr, were dialyzed extensively against TE buffer.

2.3.12 Site-directed mutagenesis (SDM) PCR

The SDM PCR was carried out following procedures described in the manual accompanying the QuikChange Site-Directed Mutagenesis kit (Stratagene), except for small modifications in the PCR protocol listed below.

Cycles	Temperature	Time
1	95˚C	1 min
18	95 / 56 / 68˚C	30 s / 50 s / 8 min
1	68˚C	8 min

2.4 Manipulation of proteins

2.4.1 Collection of bacterial cells

After protein induction for specified times, bacterial cultures were quickly chilled by immersing the container into ice-water. Cell pellets were collected by centrifugation at 11,000 × *g* for 10 min in a Sorvall SLA-3000 rotor (Thermo Scientific). Cleared media were decanted from the centrifuge tubes, which were then re-centrifuged briefly, before the remaining liquid was removed with a Pasteur pipette. The tubes were weighed before and after, and finally frozen with the cell pellet by immersion in liquid nitrogen. All frozen pellets were then stored at –80˚C until use.

2.4.2 FPLC purification of proteins

Purification of proteins was carried out by using fast performance liquid chromatography (FPLC) systems (GE Healthcare). The AKTApurifier system was controlled by a UNICORN software system. Chromatography was carried out at 4˚C.

2.4.3 Denaturing SDS-polyacrylamide gel electrophoresis

Denaturing SDS-polyacrylamide gel electrophoresis was carried out by using Novex NuPAGE 4–12% Bis-Tris Midi Gels (Invitrogen) in an XCell 4 Surelock Midi-cell electrophoresis system (Invitrogen), or Mini-PROTEAN® TGX™ Precast Gels (Bio-Rad) in a Mini-PROTEAN Tetra cell. Buffers for the electrophoresis were made following the instructions of the company.

2.4.4 Staining of protein with Coomassie brilliant blue

Polyacrylamide gels were stained in 40% (v/v) methanol, 10% (v/v) acetic acid and 0.3% (w/v) Coomassie brilliant blue for 20 min followed by destaining in buffer containing 40% (v/v) methanol and 10% (v/v) acetic acid. The destaining buffer was normally heated to 100˚C to speed up the process.

2.4.5 Determination of protein concentrations

Protein concentrations were determined by measuring the A_{280} (absorbance at 280 nm wavelength) of the sample by using a Nanodrop 2000C spectrophotometer (Thermo Scientific). The molar extinction coefficients of highly-purified proteins at 280 nm (ε_{280}) were derived from the online program ProtParam (ExPASy bioinformatics resource portal).

2.4.6 Concentration of proteins

Protein samples were concentrated either by precipitation by addition of ammonium sulphate (0.4–0.5 g/mL) followed by resuspension and dialysis in an appropriate buffer, or by ultrafiltration using Amicon Ultra centrifugal filter devices (Millipore). Centrifugation for ammonium sulphate precipitation was carried out at 16,000 × g in a Sorvall SS-34 rotor. Centrifugation for ultrafiltration was carried out at 5000 × *g* by using a swinging bucket rotor in a Sorvall Super T21 centrifuge.

2.4.7 Mass spectrometry

All nanoESI-MS (nanoelectrospray ionization mass spectrometry) data were collected on an SYNAPT HDMS system (Waters, Manchester, UK) equipped with a nanolockspray source. The system, controlled by MassLynx v4.1 software (Waters), was calibrated using cesium iodide (10 mg/mL in 70% v/v isopropanol) before all experiments.

Proteins were dialyzed into appropriate buffers before they were analyzed. To obtain the spectrum of proteins under denaturing condition, ~3 μM proteins were dialyzed into 0.1% formic acid. To obtain spectra of proteins under native conditions, proteins were dialyzed into 0.01 to 1 M NH_4OAc (pH 6.8–8.5) at 4–55°C, as specified. Generally the buffer conditions were explored before the measurement to obtain the optimal spectrum. All spectra were obtained in positive ion mode.

All samples were loaded in a gold coated borosilicate glass capillary (1.0 mm outer diameter, 0.78 mm inner diameter; Harvard Apparatus) which had a sharp needle-shaped tip. It was created by pulling the capillary with a Flaming/Brown P-97 micropipette puller (Sutter Instruments), and then coated with gold by using an Emitech K500x sputter coater (EM technologies).

Spectra were obtained and processed using MassLynx v4.1. The typical parameters for all experiments are listed below:

Parameter	**Denaturing condition**	**Native condition**
Capillary voltage (kV)	1.5	1.5
Sampling cone (V)	20–50	150–200
Scan time (s)	2	2
Tof (kV)	9.1	9.1
MCP detector voltage (V)	1800	1800
Source temperature (˚C)	50	50
Desolvation temperature (˚C)	100	100
Backing pressure (mbar)	1.5–2	4.0–4.5

CHAPTER 3

REGULATION OF THE C-TERMINI OF *E. coli* SSB AND ITS HOMOLOGUE F-SSB

3.1 Introduction

3.1.1 *Ec*-SSB structure and regulation through its C-terminus

The *Escherichia coli* single-stranded DNA-binding protein (*Ec*-SSB) is a homotetramer with a subunit mol. wt. of 18843.8 (177 residues; the initiating methionine is processed by methionine aminopeptidase *in vivo*) and a predicted isoelectric point of 6.0 (Weiner *et al.,* 1975; Williams *et al.,* 1983). Each subunit has a structured and highly-conserved N-terminal DNA-binding domain (OB-fold; residues 1–115) followed by an unstructured and generally poorly conserved C-terminal segment. *Ec*-SSB binds to single-stranded DNA (ssDNA) that is generated during DNA replication, repair and recombination. Due to the vulnerability of ssDNA to nucleolytic attack, one role of SSB is to protect it during DNA metabolic processes. Recent discoveries revealed a rather versatile feature of *Ec*-SSB other than just to act as an ssDNA "guardian". It has been shown that more than a dozen different proteins bind to it through its short, highly-conserved acidic C-terminal region, SSB-Ct (**Figure 3.1**; reviewed by Shereda *et al.*, 2008). It was also reported that the C-terminal region of *Ec*-SSB has a higher susceptibility to proteolysis when it is bound to ssDNA (Williams *et al.,* 1983). It is speculated that the *Ec*-SSB-Ct is sequestered within the OB-fold in the free protein and released on its interaction with ssDNA to coordinate the access of various SSB-binding proteins to ssDNA.

In one study, *E. coli* SSB-interacting partners were isolated from cell extracts using genome-wide dual affinity-tagging and identified by mass spectrometry (Butland *et al.*, 2005). For example, the α subunit of DNA polymerase III (Pol III) and RNase H, as baits, were found to interact with *Ec*-SSB. Recently, studies have shown that *Ec*-SSB interacts with the α subunit through its N-terminus (Pant *et al.,* 2013), and RNase HI (Petzold *et al*., 2012; Dr. James Keck, personal communication) through its Ct. The interactions between *Ec*-SSB and two other binding partners, DnaGC (C-terminal helicase-binding domain of *E. coli* DnaG primase; residues 434–581) and the χ subunit of the Pol III clamp loader, were described biochemically and structurally by Marceau *et al.* (2011), as well as Lo (2012) in our research group. The binding affinity (K_D) between χ and *Ec*-SSB C-terminus is about 4 μM, as measured by surface plasmon

resonance (SPR). The crystal structure showed residues 171–177 (FDDDIPF) of *Ec*-SSB form a complex with the χ subunit through amphipathic interactions. The binding affinity between DnaGC and *Ec*-SSB Ct is ~13 μM. The crystal structure showed residues 173–177 (DDIPF) of *Ec*-SSB form a complex with the DnaGC through similar amphipathic interactions. Although it isnot totally clear how the C-terminal tail of *Ec*-SSB selects specific binding partners, some studies show it favours the binding of some proteins over others. By comparing the enthalpy of PriA and Pol III χ subunit binding to the *Ec*-SSB C-terminal peptide by ITC (isothermal titration calorimetry), a more favoured interaction of PriA was revealed (Kozlov *et al.*, 2010). In this Chapter, the interaction between RNase HI and *Ec*-SSB-Ct is confirmed.

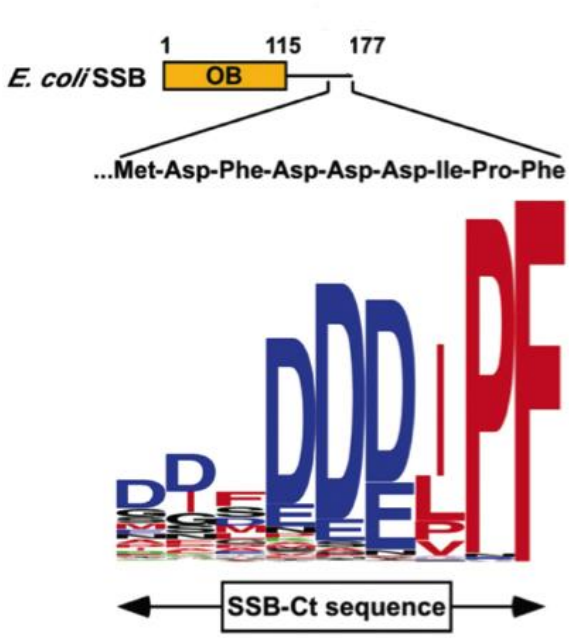

Figure 3.1 The *Ec*-SSB C-terminal tail is highly conserved throughout 280 eubacterial species (from Shereda *et al.*, 2008). *Ec*-SSB is symbolized by a yellow bar (representing its OB domain from residues 1 to 115) and a black line (representing its C-terminal region from residues 116 to 177). The sequence of the last 9 residues is shown in both three-letter and single-letter form. The height and colour of the single letter in the WebLogo representation (Crooks *et al.*, 2004) represent the frequency and the property of the residue (the red, blue or black color indicate hydrophobic, electronegative, or polar residues, respectively).

Ec-SSB forms a homotetramer through its N-terminal OB (oligonucleotide- and oligosaccharide-binding)-domain, and associates with ssDNA with various binding modes (Raghunathan *et al.*, 2000). It adopts a highly cooperative ssDNA binding mode, called the $(SSB)_{35}$ mode, in conditions of low ionic strength and high SSB-to-ssDNA ratios. In this mode, each tetramer binds approximately 35 nucleotides of ssDNA and two of the four ssDNA-binding sites are occupied. On the other hand, another ssDNA binding mode, called the $(SSB)_{65}$ mode, is preferred at high ionic strength or when

ssDNA is in excess (Chrysogelos and Griffith, 1982; Griffith *et al*., 1984; Lohman and Overman, 1985; Bujalowski and Lohman, 1986; Lohman *et al*., 1986; Wei *et al*., 1992). Structures of the *Ec*-SSB:ssDNA complexes based on X-ray crystallography (**Figure 3.2**) propose that two or all four monomers of the *Ec*-SSB homotetramer are occupied by ssDNA in the $(SSB)_{35}$ or $(SSB)_{65}$ modes, respectively (Raghunathan *et al.,* 2000). The structure also reveals that many interactions occur with positively charged or aromatic residues in the OB-fold, accounting for the lack of sequence specificity of SSB–DNA interactions.

More recent studies show *Ec*-SSB slides, rather than rolls, on ssDNA even when its C-terminal flexible tail is occupied by its binding partner RecO (Zhou *et al.,* 2011). It was also shown that a pulling force as low as 1 to 6 pN on the two ends of ssDNA progressively dissociated pre-attached *Ec*-SSB. When the force reached about 10 pN, *Ec*-SSB was completely detached from ssDNA.

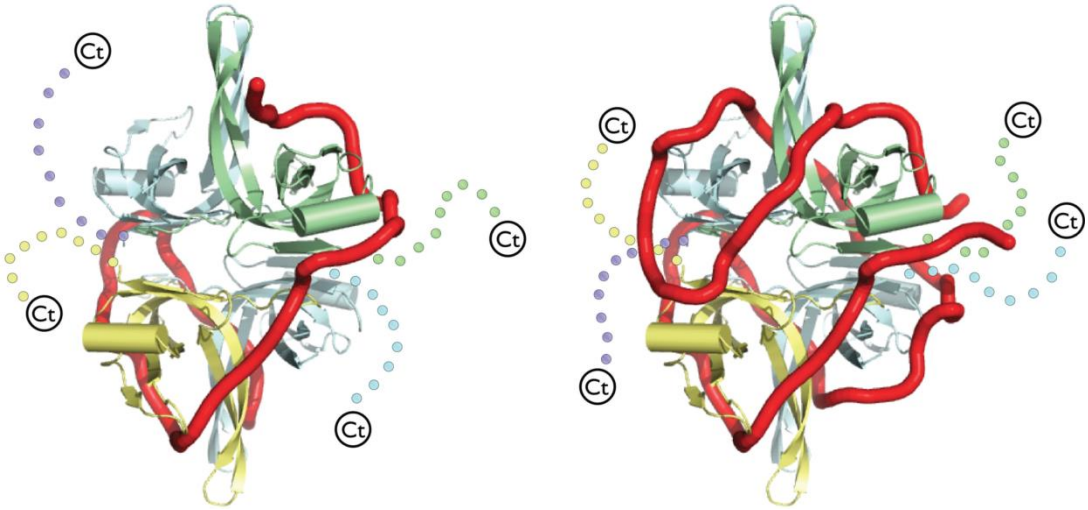

Figure 3.2 Models of *Ec*-SSB:ssDNA complexes show how it adopts two ssDNA (represented by red lines) binding modes. The highly cooperative $(SSB)_{35}$ mode is shown on the left, and the less cooperative $(SSB)_{65}$ binding mode is shown on the right. Monomers (structures of the OB-fold are shown) are coloured differently, with the flexible C-terminal regions represented by dots (from Raghunathan *et al.*, 2000).

Other than recruiting arrays of proteins, the *Ec*-SSB-Ct also shows signs of regulating ssDNA binding. An early study (Curth *et al.,* 1996) showed that the *Ec*-SSB C-terminus helps discriminate DNA from RNA. Although the interaction with RNA is weak, deletion of the C-terminus of *Ec*-SSB slightly enhanced the binding to poly(rU). Some other studies showed that removal of the C-termini of phages T4 gene 32 (Lonberg *et al.*,

1981) and T7 gene 2.5 SSB proteins (Marintcheva *et al.,* 2006; 2008) render them able to bind with higher affinity to ssDNA (though their structures are distantly related to that of *Ec*-SSB). A recent study of subunit exchange using nanoESI-MS (Mason *et al.,* 2013) showed that the last 8 residues (DFDDDIPF) of *Ec*-SSB contributes to the stabilization of the *Ec*-SSB tetramer, proposed to be by its interaction with the OB-domain of its adjacent subunits. This confirmed work reported in several other papers. For example, Kozlov *et al.* (2010) showed that deletion of the last eight residues strengthened the interaction of *Ec*-SSB with ssDNA. The interaction site of SSB-Ct on the OB-domain was determined recently by us using NMR (Shishmarev *et al.,* 2014) and the binding affinity was measured using micro-scale thermophoresis (Su *et al.,* 2014). Details are described in this Chapter.

Another single-stranded DNA binding protein, F-SSB (F-plasmid derived SSB), encoded by the *ssf* gene on the F sex factor plasmid was identified in F^+ *E. coli* (Chase *et al.,* 1983). Despite the lack of thorough investigation since it was discovered, alignment of its full-length sequence (58.9% conserved residues) with that of *Ec*-SSB showed high conservation of the OB-domain (87% conserved residues reported by Raghunathan *et al.* 2000) and less similarity in the C-terminal region, with the exception of the SSB-Ct **(Figure 3.3)**. Many of the aromatic *Ec*-SSB residues that were previously identified to be involved in ssDNA binding, including Trp-40, Trp-54, Trp-88, His-55, Phe-60 and Tyr-70 are conserved in F-SSB (Ruvolo *et al.,* 1991).

The secondary structure alignment of the *Ec*-SSB tetramer (residues 1–112; Raghunathan *et al*., 2000) and F-SSBT* (residues 1–114; **Chapter 5**), and amino acid sequence alignment of full-length *Ec*- and F-SSB are shown in **Figure 3.3**. Although another crystal structure (Matsumoto *et al.*, 2000) showed the structure beyond Gly-114 of *Ec*-SSB, reexamination of their data showed an error in register of residues beyond residue 90 and that the electron density map beyond Gly-114 is weak and discontinuous (Shishmarev *et al.,* 2014). The N-terminal region, which forms the *Ec*-SSB tetramer, is very well conserved in F-SSB, but the flexible C-terminal region (residues 115–172) of *Ec*-SSB, which has never been resolved in previous crystal structures, is poorly conserved in F-SSB except for the last five residues (-DDIPF) that interact with SSB-binding partners. These five residues are especially highly conserved in SSBs from all of the eubacteria (**Figure 3.1**).

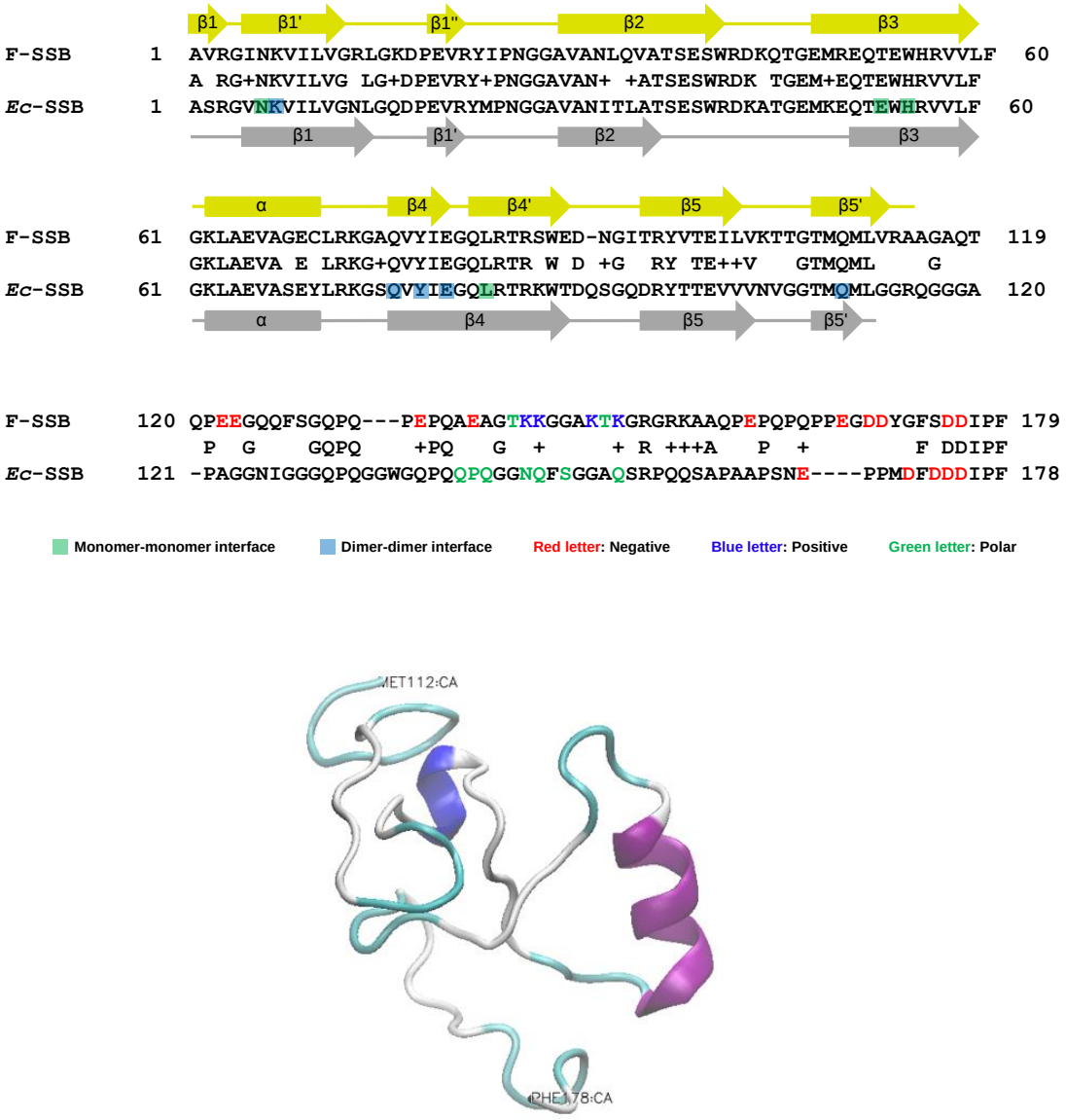

Figure 3.3 Secondary structure alignment for OB-folds of *Ec*-SSB (residues 1–112; Raghunathan *et al*., 2000) and F-SSBT* (residues 1–114; **Chapter 5**), amino acid sequence alignment of full-length *Ec*-SSB and F-SSB, and a simulated structure of SSB C-terminal residues. The first methionines of *Ec*-SSB and F-SSB are removed *in vivo* by methionine aminopeptidase. As shown in the upper picture, the residues involved in tetramer binding (Raghunathan *et al.*, 2000) are labelled with green and blue squares. The acidic residues in the C-terminal region of both *Ec*-SSB (residues 113–177) and F-SSB (residues 115–178) are shown in red. The residues between 140 and 152 in *Ec*-SSB and aligned F-SSB residues are also labelled based on the properties of their side chains. This region that forms transient alpha helix (purple) is depicted in a simulated structure of SSB C-terminus (residues 112–178; conducted by A/Prof. Aaron Oakley, personal communication) in the lower picture.

Interestingly, there are twice as many acidic residues distributed in the C-terminal region of F-SSB than *Ec*-SSB. The residues that were confirmed to participate in monomer–monomer and dimer–dimer interactions in *Ec*-SSB (Raghunathan *et al.*, 2000;

Ruvolo *et al.,* 1991) are also present in F-SSB (**Figure 3.3**). A molecular dynamics simulation conducted by A/Prof. Aaron Oakley shows transient formation of a helix at residues 140–152 of *Ec*-SSB (lower picture in **Figure 3.3**). Interestingly, sequence alignment shows this region is poorly conserved in F-SSB.

Despite the similarity between *Ec*-SSB and F-SSB, it was shown that F-SSB does not stimulate strand elongation by DNA polymerase III holoenzyme (Pol III HE; Ruvolo *et al.,* 1991). In contrast, F-SSB can support the viability of *E. coli* cells that completely lack the *ssb* gene (Porter and Black, *et al.,* 1991). Recently in our laboratory, a well-established bulk-phase DNA replication assay showed the significance of the *Ec*-SSB-Ct for helicase independent Pol III DNA extension and strand displacement synthesis. Using F-SSB as an *Ec*-SSB analogue offered a valuable opportunity to further investigate the role of *Ec*-SSB in DNA replication, as described in **Chapters 4** and **5**.

Since this Thesis involves two different *E. coli* SSB species, *Ec*-SSB will be used throughout to denote the native SSB while F-SSB is used to denote the F-plasmid derived SSB.

3.1.2 Microscale thermophoresis (MST)

Microscale thermophoresis (MST) was used to estimate the binding affinity of the *Ec*-SSB-Ct for the OB-domain of *Ec*-SSB in this work. MST is a newly emerged technique for measuring bimolecular interactions. Due to its characteristics of easy handling, small sample volume requirement, and operation in close-to-native conditions, it is beginning to find wide applications in biochemistry.

The foundation of thermophoresis in the liquid phase was laid by Charles Soret and Carl Ludwig in the 19th century (Ludwig, 1856). They found molecules with different surface properties diffuse differently in a temperature gradient. Following studies found that molecules' hydration shells, sizes and shapes all contribute to their diffusion in aqueous solution (**Figure 3.4A**).

Modern MST, empowered by laser technology, enables accurate measurement of biomolecular (such as protein) interactions (**Figure 3.4B**). An infrared (λ = 1480 nm) laser creates a small heating point (1–6˚C) in the water in a glass capillary containing

fluorescent labelled proteins. A temperature gradient surrounded the heating point is then formed. A fluorescence excitation light source (using LED) excites the fluorescent label on the protein. The fluorescence distribution of labelled protein in the vicinity of the heating point is immediately measured by a light detector. Since the infrared light is incorporated in the fluorescence excitation light, and guided into the same objective, it enhances the accuracy and sensitivity of the measurement.

The fluorescence is measured as a relative value in MST:

$$F_{\text{norm}} = \frac{F_1}{F_0}$$

where F_{norm} is the normalized fluorescence, F_1 is fluorescence after thermodiffusion, and F_0 is initial fluorescence or fluorescence after T-jump.

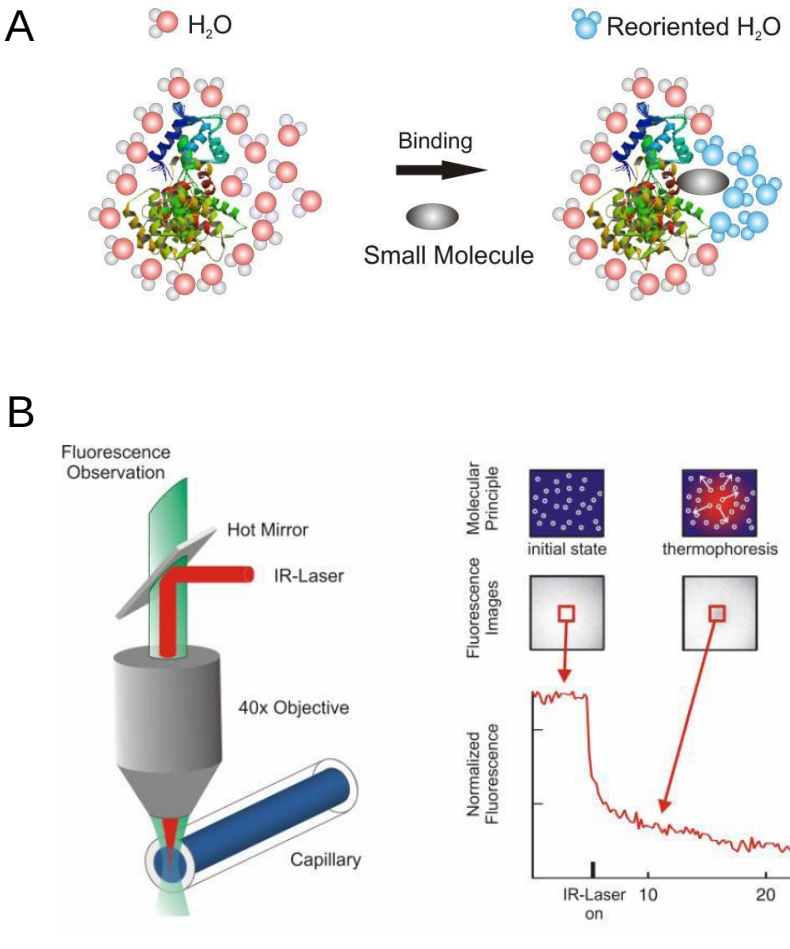

Figure 3.4 The mechanism of microscale thermophoresis (MST). The migration of large molecules, such as proteins, in aqueous solutions is largely dependent on their hydration shells (**A**). Binding of a small molecule, such as a peptide, can alter the hydration shell and lead to a

change of thermophoresis. The mechanism of MST is shown in the schematic diagram (**B**). The incorporated IR laser and excitation LED pass through an objective and focus on a glass capillary that contains the fluorescently labelled protein and the binding partners. The thermophoresis is recorded continuously from several seconds before turning on the laser and 15 s after turning off the laser, while the LED is constantly on throughout the process (from Nano Temper Handbook).

The fluorescence measured around the heating point carries information about the concentration of the labelled molecules; it corresponds to the Soret coefficient (S_T):

$$\frac{c_{hot}}{c_{cold}} = \exp(-S_T \Delta T) \approx 1 - S_T \Delta T$$

where c_{hot} is the fluorophore concentration in the hot area, c_{cold} is the fluorophore concentration in the cold area, and ΔT is a given spatial temperature difference.

One can choose to use F_0 with or without the inclusion of the *T*-jump. Normally the MST results are shown without the *T*-jump as the fluorescence signal measured at the *T*-jump may sometimes oppose the signals after the *T*-jump and thus cancel the resulting data points. F_1 is the fluorescence measured after the *T*-jump, which carries the information about binding.

The binding is very often described by a simple 1:1 binding model as is shown below, although other models are used occasionally for more complex binding events. The binding affinity is represented by K_D (equilibrium dissociation constant):

$$K_D = \frac{[A]_{free}[B]_{free}}{[AB]} = \frac{([A] - [AB])([B] - [AB])}{[AB]}$$

where K_D is the equilibrium dissociation constant; $[A]_{free}$ is the concentration of free partner A; $[B]_{free}$ is the concentration of free partner B; $[AB]$ is the concentration of bound complex; $[A]$ is the total concentration of titrated partner A, which has variable values; and $[B]$ is the total concentration of the fluorescent labelled binding partner B, which has a constant value. Based on this equation, the fraction of bound molecule (*FB*) can be solved:

$$FB = \frac{[AB]}{[B]} = \frac{[A] + [B] + K_D - \sqrt{([A] + [B] + K_D)^2 - 4[AB]}}{2[B]}$$

which can be used for calculating the K_D by fitting it into the following equation:

$$F_{\text{norm}} = (1 - FB)F_{\text{norm, unbound}} + (FB)F_{\text{norm, bound}}$$

where FB is fraction bound, $F_{\text{norm, unbound}}$ is normalized fluorescence of the unbound state, and $F_{\text{norm, bound}}$ is normalized fluorescence of the bound state. Because $F_{\text{norm, unbound}}$ and $F_{\text{norm, bound}}$ can be derived by fitting the curve where a lower plateau shows the fluorescence of the unbound sate and a higher plateau shows that of the saturated bound state, K_D is the only unknown value in the equation and can be calculated.

3.2 Materials and methods

3.2.1 Purification of *Ec*-SSB, F-SSB and their mutants

To study the proteins involved in *E. coli* DNA replication, proteins of interest were overexpressed to high levels in *E. coli* cells and purified. To define the roles of specific regions of the proteins, mutations or labels were introduced site-specifically. In this Section (and **Sections 4.2** and **5.2**), procedures (gene cloning, protein overexpression, purification and *in vitro* labelling) used to achieve these goals are described.

3.2.1.1 Plasmids directing expression of *Ec*-SSB, F-SSB and their mutants

Plasmids pND72 (encoding the wild-type *Ec*-SSB; Mason *et al.,* 2013), pAL1379 (encoding *Ec*-SSBΔC8 with the last eight C-terminal residues removed; Mason *et al.,* 2013), pND541 (encoding *Ec*-SSBT* with the last 62 *Ec*-SSB C-terminal residues removed; Su *et al.,* 2014), pCL547 encoding *Ec*-SSB(K43C) (C.A. Love, unpublished), and pPH302 (encoding the wild-type F-SSB; P. Hendry, unpublished), with the corresponding genes under the control of tandem temperature inducible phage λ promoters (Elvin *et al.*, 1990) were previously constructed in our laboratory. Note that the capital letters within brackets indicate the original residue and the residue into which it was mutated. For example, K43C means the original Lys-43 residue was mutated to cysteine. Plasmids encoding mutant proteins were made by site-directed mutagenesis as described in **Section 2.3.12**, using the following oligonucleotide primer pairs. All mutations were confirmed by nucleotide sequence determination using vector primers flanking the *ssb* gene.

Ec-SSB mutant	Primer number	Oligonucleotide sequence (5' to 3')
Ec-SSB(Y22C)	671	GACCCGGAAGTACGCTGCATGCCAAATGGTGG
	672	CCACCATTTGGCATGCAGCGTACTTCCGGGTC
Ec-SSB(E65C/E69D)	694	TTCGGCAAACTGGCATGTGTGGCGAGCGATTATCTGCGTAAAGGT
	695	ACCTTTACGCAGATAATCGCTCGCCACACATGCCAGTTTGCCGAA
Ec-SSB(T89C)	673	CGTACCCGTAAATGGTGCGATCAATCCGGTCAG
	674	CTGACCGGATTGATCGCACCATTTACGGGTACG
Ec-SSB(G114C)	675	CATGCAGATGCTGGGTTGCCGTCAGGGTGGTGGC
	676	GCCACCACCCTGACGGCAACCCAGCATCTGCATG
Ec-SSB(CysApp)	690	GATGATGACATTCCGTTCTGCTAATTTGTCATTAAAACAATAGG
	691	CCTATTGTTTTAATGACAAATTAGCAGAACGGAATGTCATCATC
Ec-SSB(S164C)	677	GCTCCGGCAGCGCCGTGTAACGAGCCGCCGATG
	678	CATCGGCGGCTCGTTACACGGCGCTGCCGGAGC

Construction of plasmids pYW1673 encoding *Ec*-SSB(Y22C), pYW1666 encoding *Ec*-SSB(E65C/E69D), pYW1670 encoding *Ec*-SSB(T89C), pYW1664 encoding *Ec*-SSB(G114C), and pYW1671 encoding *Ec*-SSB(CysApp) used pND72 as the template. The "CysApp" means an extra cysteine was added after the last C-terminal residue of the protein. Plasmids pYW1661 encoding *Ec*-SSB(G114C/CysApp) and pYW2110 encoding *Ec*-SSB (G114C/S164C) were made by a two-step procedure with pYW1671 and pYW1664, respectively, as templates for the second mutagenic PCR.

To make the plasmid pYW1663 encoding *Ec*-SSBΔC8(K43C), a similar procedure was used to that described by Mason *et al.* (2013) to make pAL1379 (encoding *Ec*-SSBΔC8). Specifically, the mutagenic PCR was conducted with pCL547 as template with primers 178 and 179 of Mason *et al.* (2013), which resulted in incorporation of a TAA stop codon eight codons before the end of the *Ec-ssb* gene.

3.2.1.2 Overproduction and purification of *Ec*-SSB, F-SSB and their mutants

Plasmids that directed overexpression of *Ec*-SSB, F-SSB and their mutants including *Ec*-SSBΔC8, *Ec*-SSBT*, *Ec*-SSB(Y22C), *Ec*-SSB(E65C/E69D), *Ec*-SSB(T89C), *Ec*-SSB(G114C), *Ec*-SSB(CysApp), *Ec*-SSB(G114C/CysApp), *Ec*-SSB(G114C/S164C) and *Ec*-SSBΔC8(K43C) were all transformed into the *E. coli* strain BL21(λDE3)*recA* (Williams *et al.,* 2002) for overproduction.

The bacteria were first streaked onto a LBTA agar plate (**Section 2.2.1**) and grown overnight at 30˚C. A single colony was picked and streaked on another LBTA agar plate. After growth at 30˚C, the bacteria were used to inoculate a 2 mL LBTA broth culture for

overnight incubation. This culture was then used to inoculate a 1 L LBTA culture. It was incubated at 30˚C with vigorous shacking until OD_{600} reached ~0.7. The temperature was quickly changed into 42˚C and the culture incubated at that temperature with continuous shaking for 3 h. Cultures were chilled on ice, and then the bacteria were collected by centrifugation and snap-frozen in liquid nitrogen (**Section 2.4.1**). All bacterial pellets were stored in –80˚C until use.

3.2.1.3 Buffers and storage of proteins

Buffers were: lysis buffer I (50 mM Tris-HCl, pH 8.0, 20 mM spermidine, 1 mM EDTA, 2 mM DTT, 10% w/v sucrose, 2 M NaCl); lysis buffer II (50 mM Tris-HCl, pH 8.0, 20 mM spermidine, 1 mM EDTA, 1 mM DTT, 500 mM NaCl); lysis buffer III (50 mM Tris-HCl, pH 8.0, 1 mM EDTA, 2 mM DTT, 0.5 mM PMSF); lysis buffer IV (50 mM Tris-HCl, pH 8.0, 1 mM EDTA, 2 mM DTT, 500 mM NaCl, 0.18 g/mL $(NH_4)_2SO_4$, 0.5 mM PMSF; buffer A (50 mM Tris-HCl, pH 8.0, 1 mM EDTA); buffer B (70 mM Tris-HCl, pH 8.0, 1 mM EDTA); buffer C (20 mM sodium phosphate, pH 6.9, 1 mM EDTA, 10% v/v glycerol); buffer D (50 mM Tris-HCl, pH 8.0, 1 mM EDTA, 1 mM DTT); buffer E (50 mM Tris-HCl, pH 8.0, 1 mM EDTA, 2 mM DTT, 20 mM NaCl); storage buffer (50 mM Tris-HCl, pH 8.0, 1 mM EDTA, 1 mM DTT, 30% v/v glycerol, 500 mM NaCl).

Purified proteins were generally concentrated by ammonium sulphate precipitation (**Section 2.4.6**), resuspended in and dialyzed against storage buffer, snap frozen in aliquots using liquid nitrogen, and stored at –80˚C. Their concentrations were determined spectrophotometrically (A_{280}) using calculated values of ε_{280} based on their tryptophan and tyrosine content (**Section 2.4.5**).

3.2.1.4 Purification of *Ec*-SSB

For purifying *Ec*-SSB, a protocol established by Prof. Nick Dixon in our laboratory (Mason *et al.*, 2013) was used. Specifically, the *E. coli* cell pellets from a 1 L culture were resuspended to 0.07 g/mL in lysis buffer I and the cells were lysed by being passed through a French press at 12000 psi.

Following centrifugation for 40 min at 35000 × *g*, the supernatant containing the soluble

Ec-SSB was stirred with 1.5% streptomycin sulphate for 30 min at 4˚C to precipitate DNA, which was removed by centrifugation in 35000 × *g* for 80 min.

The supernatant was transferred to a clean beaker, and a solution of 0.5 g/mL $(NH_4)_2SO_4$ in 50 mM Tris-HCl, pH 8.0 and 1 mM EDTA was added to a final concentration of 0.28 g/mL $(NH_4)_2SO_4$. The mixture was stirred in 4˚C for 30 min and then centrifuged in 35000 × *g* for 30 min to collect the precipitated *Ec*-SSB.

The pellet was resuspended in a minimum volume of buffer A + 300 mM NaCl, and then dialyzed against two changes (3 h each) of 2 L of buffer B. *Ec*-SSB is very insoluble and precipitated in the bottom of the dialysis bag. The sample including precipitated *Ec*-SSB was centrifuged in 35000 × *g* for 30 min.

The supernatant was removed, and the pellet was resuspended in about 3 mL of buffer A, which was centrifuged in 35000 × *g* for 30 min. The supernatant was added drop wise with stirring to a slurry of Toyopearl DEAE resin that had been equilibrated in buffer A + 30 mM NaCl. The resin was stirred gently at 4˚C for 20 min, and then repacked into a column (2.5 × 16 cm).

The column was washed with 100 mL of buffer A + 30 mM NaCl followed by application of a linear gradient (450 mL) of 30–600 mM NaCl in buffer A. *Ec*-SSB eluted between 200 and 300 mM NaCl. Fractions containing *Ec*-SSB were pooled and stored as described in **Section 3.2.1.3**. The typical yield was 80 mg of highly-purified *Ec*-SSB from 1 L of culture.

3.2.1.5 Purification of *Ec*-SSBΔC8

To purify *Ec*-SSBΔC8, the *E. coli* cell pellets were resuspended to 0.07 g/mL in lysis buffer II and the cells were lysed by passage through a French press at 12000 psi.

Following centrifugation for 40 min at 35000 × *g*, the supernatant containing the soluble *Ec*-SSBΔC8 was stirred with 0.15 g/mL of $(NH_4)_2SO_4$ for 30 min at 4˚C to precipitate the protein, which was collected by centrifugation in 35000 × *g* for 30 min.

The precipitated *Ec*-SSBΔC8 was resuspended in buffer C, and then dialyzed against two changes (3 h each) of 2 L of buffer C. *Ec*-SSBΔC8 is very insoluble and precipitated in the dialysis bag. The sample including the precipitate was centrifuged at

35000 × *g* for 30 min.

The supernatant was removed and the pellet was resuspended in a minimum volume of buffer C with 300 mM NaCl and 30% (v/v) glycerol. The sample was added drop wise to the surface of a column (2.5 × 16 cm) of phosphocellulose P11 (Whatman) resin that had been equilibrated in buffer C.

The column was washed with 10 mL of buffer C followed by application of a linear gradient (400 mL) of 0–1.4 M NaCl in buffer C. Fractions containing *Ec*-SSBΔC8 were pooled and stored at –80˚C (**Section 3.2.1.3**).

3.2.1.6 Purification of *Ec*-SSBT*

Ec-SSBT* was purified in the same way as *Ec*-SSBΔC8 through the phosphocellulose chromatography step (**Section 3.2.1.5**), except that 0.075 g/mL $(NH_4)_2SO_4$ was used to precipitate *Ec*-SSBT* from the cleared cell lysate.

Phosphocellulose fractions containing *Ec*-SSBT* were pooled and concentrated to 1 mL by $(NH_4)_2SO_4$ precipitation (**Section 2.4.6**). The sample was then dialyzed into buffer D. The *Ec*-SSBT* again precipitated, and was collected by centrifugation at 35000 × *g* for 30 min. The pellet was resuspended in 1 mL of buffer D containing 500 mM NaCl and 30% (v/v) glycerol, and gel filtered through a Hiload 26/60 Superdex 75 column (GE Healthcare) equilibrated in buffer D supplemented with 10% (v/v) glycerol and 500 mM NaCl. Fractions containing pure *Ec*-SSBT* were pooled, and stored at –80˚C (**Section 3.2.1.3**).

3.2.1.7 Purification of F-SSB

For purifying F-SSB, the *E. coli* cell pellets were resuspended to 0.07 g/mL in lysis buffer III (no spermidine was added since sheared DNA helps solubilize F-SSB) and the cells were lysed using a French press at 12000 psi.

Following centrifugation for 40 min in 35000 × *g*, the supernatant containing F-SSB was stirred with 0.18 g/mL $(NH_4)_2SO_4$ for 30 min in 4˚C to precipitate F-SSB, which was collected by centrifugation at 35000 × *g* for 30 min. The pellet was resuspended in buffer D + 20 mM NaCl, dialyzed against two changes (3 h each) of 2 L of the same

buffer, and then centrifuged for 30 min in 35000 × *g*.

The supernatant was loaded into a phosphocellulose P11 column (2.5 × 16 cm) that had been equilibrated in buffer D + 20 mM NaCl. The column was washed with 150 mL of buffer D and F-SSB was eluted in a linear gradient (360 mL) of 0–1.4 M NaCl in buffer D. Fractions containing F-SSB were pooled and stored at –80˚C (**Section 3.2.1.3**).

3.2.1.8 Purification of F-SSBtrun

A truncated form of F-SSB (denoted as F-SSBtrun), likely produced by intracellular proteolysis, was observed during F-SSB purification. As the F-SSB C-terminal region is speculated to be structurally disordered, as in *Ec*-SSB (see **Chapters 4** and **5**), it is likely that proteolysis occurs in this region. As F-SSB's very C-terminal residues (DDIPF) are conserved in *Ec*-SSB, this truncated form of F-SSB was potentially useful in various assays for studying the functionality of the C-termini of *Ec*- and F-SSB.

To purify F-SSBtrun, the *E. coli* cells containing the overexpressed F-SSB were resuspended to 0.07 g/mL in lysis buffer IV and the cell lysate was obtained following passage through a French press at 12000 psi.

The lysate was centrifuged for 40 min at 35000 × *g* to obtain the pellet containing insoluble F-SSBtrun. The pellet was mixed with 20 mL of buffer containing 50 mM Tris-HCl, pH 8.0, 1 mM EDTA, 2 mM DTT, 500 mM NaCl and 10% glycerol. It was pipetted until it became an homogeneous opaque suspension, which was clarified by centrifugation at 35000 × *g* for 30 min.

The supernatant containing F-SSBtrun was dialyzed against two changes (3 h each) of buffer E, and then clarified at 35000 × *g* for 30 min. The supernatant was loaded into a phosphocellulose P11 column (2.5 × 16 cm) that had been equilibrated in buffer D. The column was washed with 150 mL of buffer B followed by application of a linear gradient (360 mL) of 0–1.4 M NaCl in buffer D. The fractions containing F-SSBtrun were pooled and stored at –80˚C (**Section 3.2.1.3**).

It was estimated by nanoESI-MS in 0.1% formic acid that F-SSBtrun is a mixture of two truncated F-SSBs: F-SSBΔC29 (16358.17 ± 0.83 Da; calcd. 16350.5 Da) and F-SSBΔC31 (16128.90 ± 1.00 Da; calcd. 16121.2 Da; data not shown).

3.2.1.9 Purification of *Ec*-SSB mutants

The purification procedures for *Ec*-SSB(Y22C), *Ec*-SSB(E65C/E69D), *Ec*-SSB(T89C), *Ec*-SSB(G114C), *Ec*-SSB(CysApp), *Ec*-SSB(G114C/CysAPP) and *Ec*-SSB(G114C/S164C) were the same as that for *Ec*-SSB except that all buffers contained 2 mM DTT.

3.2.1.10 Purification of isotope labelled *Ec*-SSB, *Ec*-SSBΔC8 and *Ec*-SSBT*

The procedures for expression (**Section 2.2.2**) and purification of isotope (^{13}C, ^{15}N and/or ^{2}H) labelled *Ec*-SSB, *Ec*-SSBΔC8 and *Ec*-SSBT* were the same as those for unlabelled proteins, except for ^{13}C,^{15}N-labelled *Ec*-SSBΔC8.

The same procedure as used for *Ec*-SSB (**Section 3.2.1.4**) was followed to partially purify double-labelled ^{13}C,^{15}N-*Ec*-SSBΔC8. The fractions eluted from the DEAE column containing labelled *Ec*-SSBΔC8 were combined and 0.4 g/mL $(NH_4)_2SO_4$ added to precipitate the protein. The samples were centrifuged for 20 min at 35000 × *g*, and the pellet was resuspended in and dialyzed against storage buffer.

The sample was gel filtered using a Hiload 26/60 Superdex 75 column that was equilibrated and washed with buffer A + 500 mM NaCl. Fractions containing labelled *Ec*-SSBΔC8 were pooled and mixed with 0.4 g/mL $(NH_4)_2SO_4$ to precipitate the protein, which was collected by centrifugation for 20 min at 35000 × *g*.

The pellet was resuspended in buffer D + 500 mM NaCl, and then dialyzed into buffer A. Labelled *Ec*-SSBΔC8 was very insoluble and precipitated in the dialysis bag; the suspension was transferred into a centrifuge tube. After centrifugation (20 min at 35000 × *g*), the pellet containing pure labelled *Ec*-SSBΔC8 was resuspended in storage buffer, and then stored in –80˚C.

This improved purification procedure will most likely work for the unlabelled *Ec*-SSBΔC8 as well (*cf.* **Section 3.2.1.5**).

3.2.1.11 Isolation of fluorescein-5-maleimide labelled *Ec*-SSBΔC8(K43C), *Ec*-SSB(K43C), *Ec*-SSBT*(K43C), and hybrid tetramers

Approximately 1.7 mL of purified *Ec*-SSBΔC8(K43C) (7.3 mg/mL; 102 μM; mol. wt. 4 × 17853.7) was dialyzed at room temperature into buffer F, yielding ~3 mL at 4 mg/mL.

A 500 μL sample was concentrated to 100 μL in an Amicon Ultra centrifugal concentrator (MWCO 10K; Millipore). The sample was diluted 5 times in the same device by adding buffer F without DTT, and concentrated again. This was repeated three more times to reduce the concentration of DTT to ~1.5 μM (the final volume of sample was ~300 μL).

To this sample was added 15 μL of a solution of 160 mM fluorescein-5-maleimide (ThermoFisher Scientific) in *N*,*N*-dimethylformamide (DMF), and the mixture was left to stand at room temperature for 3 h. The mixture was then dialyzed against 3 changes (2 L each) of buffer F (without DTT) at room temperature over 48 h. A bright yellow colour could be seen in the buffer after the first dialysis, but the final buffer was colourless. About 300 μL of sample (containing 5 mg/mL, 68 μM protein) was obtained; it was stored at –80˚C.

For subunit exchange, 10 μL of the fluorescein-tagged protein was mixed with 250 μL of "wild-type" *Ec*-SSBΔC8 (5 mg/mL in storage buffer; 25-fold excess), and incubated at 30˚C for 6 h. Under these conditions, subunit exchange among *Ec*-SSBΔC8 tetramers is expected to be complete (Mason *et al.*, 2013), so the majority of fluorescein (FAM) labelled hybrid tetramers in the sample will have been [*Ec*-SSBΔC8]$_3$[*Ec*-SSBΔC8(K43C-FAM)]$_1$.

Fluorescein-5-maleimide labelled *Ec*-SSB(K43C) and *Ec*-SSBT*(K43C) and the hybrid tetramers of [*Ec*-SSB]$_3$[*Ec*-SSB(K43C-FAM)]$_1$ and [*Ec*-SSBT*]$_3$[*Ec*-SSBT*(K43C-FAM)]$_1$ were prepared by using the same procedures.

3.2.1.12 The χ subunit, DnaGC and RNases HI and HII

The χ subunit of the Pol III clamp loader assembly and DnaGC, the C-terminal helicase binding domain of DnaG primase, were gifts of Dr. Allen Tak Yiu Lo. Procedures for producing RNases HI and HII are described in **Section 4.2**.

3.2.2 Surface plasmon resonance (SPR)

A Biacore T200 instrument (GE Healthcare) was used to carry out all SPR measurements at 25˚C using Series S Sensor Chips SA (GE Healthcare), which have

streptavidin on the surface. Ligands with a biotinylated tag were immobilized on the surface *via* strong interaction between streptavidin and biotin. The response in *RU* (resonance units) was obtained by subtracting the signals of a blank surface from the surface with ligands or analytes. Various concentrations of ligands were injected over the surface to produce corresponding values of *RU*, and the resulting binding isotherm was fit to a steady state 1:1 interaction model to derive values of the equilibrium dissociation constant, K_D and maximum response, R_{max}:

$$K_D = \frac{C \times (R_{max} - RU)}{RU}$$

Parameters in this equation (Biacore T100 Software Handbook, 2008) are:

Parameters	**Stands for:**	**Obtained:**
C	analyte concentration	selected
RU	response (resonance units)	during measurement
K_D	equilibrium dissociation constant (M)	by fitting
R_{max}	analyte binding capacity of the surface (RU)	by fitting

Stoichiometries (n) of the interactions were estimated by:

$$n = \frac{R_{max}}{RU_{IM}} \times \frac{MW_L}{MW_A}$$

Parameters in this equation (Biacore Sensor Surface Handbook, 2007) are:

Parameters	**Stands for:**	**Obtained:**
MW_A	molecular weight of analyte	by calculation
MW_L	molecular weight of ligand	by calculation
RU_{IM}	immobilization level of ligand	during measurement
R_{max}	analyte binding capacity of the surface (RU)	by fitting

Unless specified otherwise, the SPR buffer used for all measurements contained 10 mM HEPES, pH 7.4, 3 mM EDTA, 1 mM DTT, 150 mM NaCl and 0.005% surfactant P20 (GE Healthcare), and a constant flow rate of 5 µL/min was used throughout.

Two different chip surfaces were used. The $(dT)_{35}$ surface was prepared by injection of 100 nM 3'-biotinylated $(dT)_{35}$ (GeneWorks) in SPR buffer for 60 s (to obtain 100 *RU*) or 120 s (to obtain 220 *RU*). The *Ec*-SSB-Ct surface was prepared by injection of 10 nM N-terminally biotinylated *Ec*-SSB-Ct [sequence: Biotin-(Ahx)-GSAPSNEPPMDFD DDIPF; Ahx, amino-hexanoate spacer; Biomolecular Resource Facility, John Curtin

School of Medical Research, ANU)] in SPR buffer for 60 s (to obtain ~47 *RU*).

To measure interactions between the χ subunit or DnaGC and F-SSB or *Ec*-SSB, proteins were first dialyzed into SPR buffer without P20. A $(dT)_{35}$ chip surface (100 *RU*) was used as follows: 100 nM of F-SSB or *Ec*-SSB was injected for 60 s with a dissociation time of 300 s. The SSB proteins bound stably and stoichiometrically to the $(dT)_{35}$ surface under these conditions. A selected concentration of the χ subunit was then injected for 60 s with a 60 s dissociation time. The surface was regenerated with 1 M or 4 M $MgCl_2$ after the dissociation. The whole procedure was repeated, starting from injection of F-SSB or *Ec*-SSB, for injection of another concentration of the χ subunit. A second $(dT)_{35}$ chip surface (200 *RU*) was used similarly for measuring interactions between DnaGC and F-SSB or *Ec*-SSB.

To measure interactions between RNase HI and F-SSB or *Ec*-SSB, proteins were dialyzed into SPR buffer (without P20) or a high salt SPR buffer (with 300 mM instead of 150 mM NaCl, without P20). The buffers were then supplemented with 0.05% P20 (in the high salt SPR buffer) or 0.005% P20 (in the regular SPR buffer), and used as the running buffers during measurement. The chip surfaces used for measurements in SPR buffers with 150 and 300 mM NaCl had 100 and 220 *RU*, respectively, of immobilized $(dT)_{35}$. F-SSB or *Ec*-SSB (100 nM) were injected on the $(dT)_{35}$ chip surfaces for 60 s with a dissociation time of 300 s. A selected concentration of RNase HI was then injected for 60 s (unless otherwise specified) with a 60 s dissociation time. The surface was regenerated with 4 M $MgCl_2$ after the dissociation. The whole procedures were repeated, starting from injection of F-SSB or *Ec*-SSB, for injection of another concentration of RNase HI.

To measure interactions between RNase HI and the *Ec*-SSB-Ct peptide, the protein was dialyzed in SPR buffer (without P20), and measurements were made in SPR buffer. A selected concentration of RNase HI was injected for 60 s with a 60 s dissociation time. The surface was regenerated with 1 M $MgCl_2$ after the dissociation. This procedure was repeated for injecting another concentration of RNase HI.

Interactions between RNase HI and immobilized $(dT)_{35}$ (100 *RU*) in SPR buffer were studied similarly, except that the chip surface was regenerated with 4 M $MgCl_2$ between injections of different concentrations of RNase HI.

3.2.3 Microscale thermophoresis (MST)

All MST measurements were carried out on a Monolith NT 115 microscale thermophoresis (Nanotemper Technologies) instrument controlled by NT 2.0.2.29 software, and data were collected and processed by NT Analysis software. The instrument was kindly supplied by Prof. Joel Mackay at the University of Sydney, and the experiments were conducted under the supervision of Dr. Marylène Vandevenne.

Ec-SSB C-terminal peptide (sequence: PSNEPPMDFDDDIPF) was purchased from *Mimotopes*. It was dissolved in 10 mM Tris base, and then neutralized to pH 7.5 by adding 5 M KOH. Fluorescein labelled mixed SSB tetramers, [*Ec*-SSBΔC8]$_3$[*Ec*-SSBΔC8(K43C-FAM)]$_1$, [*Ec*-SSB]$_3$[*Ec*-SSB(K43C-FAM)]$_1$ and [*Ec*-SSBT*]$_3$[*Ec*-SSBT*(K43C-FAM)]$_1$ were prepared as described in **Section 3.2.1.11**.

Before the measurements, mixtures containing 1.6 μM fluorescein labelled mixed SSB tetramers and 0.05, 0.10, 0.20, 0.40, 0.80, 1.61, 3.22, 6.44, 12.88, 25.75, 51.50 or 103.00 mM of *Ec*-SSB C-terminal peptide were prepared in a buffer containing 10 mM Tris-HCl, pH 7.6 and 0.01% Tween 20 surfactant. The mixtures were then loaded into Monolith NT capillaries (hydrophilic) and inserted into the instrument. Blue LED light (power 50%) was used to excite the fluorescein. Before measurements, each capillary was exposed just under the LED (without MST power) to ensure each mixture contained the same amount of fluorescent labelled proteins. All the samples in capillaries gave similar fluorescence. For the MST measurement, 90% MST power was used to create the heat gradient.

3.3 Results and discussion

3.3.1 Sequence alignment, ssDNA binding property and subunit exchange of *Ec*-SSB and F-SSB

The secondary structure alignment of the *Ec*-SSB tetramer (residues 1–112; Raghunathan *et al*., 2000) and F-SSBT* (residues 1–114; **Chapter 5**), and amino acid sequence alignment of full-length *Ec*-SSB and F-SSB are shown in **Figure 3.3** (**Section 3.1.1**). The N-terminal OB domains of both proteins share extensive sequence and

structural similarity, but the C-termini, which lack any structural information, are very different in term of their sequences.

Further studies (see **Chapter 4**) using agarose gel electrophoresis show that F-SSB also has ssDNA binding ability as does *Ec*-SSB, and native-state nanoESI-MS shows that F-SSB is a tetramer in its native state. When *Ec*-SSB and F-SSB tetramers were mixed, they were able to form hybrid tetramers with any combinations of *Ec*-SSB and F-SSB monomers (see **Chapter 4**). This suggests that the N-terminus of F-SSB adopts the same OB fold as that of *Ec*-SSB, and the conserved residues at the monomer–monomer and dimer–dimer interfaces are probably located at the same positions. This was confirmed by a new F-SSB crystal structure, which shows the residues at both interfaces are well conserved in both SSBs (see **Chapter 5**). The similarity of their N-termini and diversity of their C-terminal region allows us to use F-SSB in DNA replication assays, as a comparison, to help us understand the functions of the C-terminus of *Ec*-SSB (see **Chapter 4**).

3.3.2 Purification of SSB proteins

New procedures for purification of F-SSB and many derivatives of *Ec*-SSB were developed as part of this work (see **Section 3.2.1**). SDS-PAGE was used to verify their purity (see **Chapter 4**, **Figure 4.5**).

3.3.3 DnaGC and the χ subunit interact with F-SSB and *Ec*-SSB with similar affinities

Interactions of the C-terminus of *Ec*-SSB with DnaGC, the C-terminal helicase binding domain of DnaG primase, and the χ subunit of the Pol III clamp loader complex were well characterized both chemically and structurally by Dr. Allen Tak Yiu Lo (Lo, 2012). The interactions were proposed to be involved in both helicase independent strand displacement DNA synthesis by the Pol III holoenzyme (**Chapter 4**) and priming events during lagging strand DNA replication. To extend our understanding of these mechanisms, especially strand displacement DNA synthesis, F-SSB was used as an *Ec*-SSB analogue to provide a valuable alternative “link” in the “chain” of protein interactions. Here the interactions of F-SSB with DnaGC and χ were probed by SPR using similar conditions to those previously described for *Ec*-SSB (Lo, 2012).

SPR measurements show F-SSB interacts similarly to *Ec*-SSB with both DnaGC and χ under physiological salt (150 mM NaCl) conditions (**Figures 3.5** and **3.6)**. Aligned intact sensorgrams for individual injections of *Ec*-SSB or F-SSB on a $(dT)_{35}$ surface and following injections of DnaGC are shown in **Figures 3.5A(i) and B(i)**. They show firstly that F-SSB and *Ec*-SSB have similar binding kinetics on $(dT)_{35}$, and that both SSBs form stable 1:1 complexes. The characterization of ssDNA binding by F-SSB is explored using other techniques in **Chapter 4**.

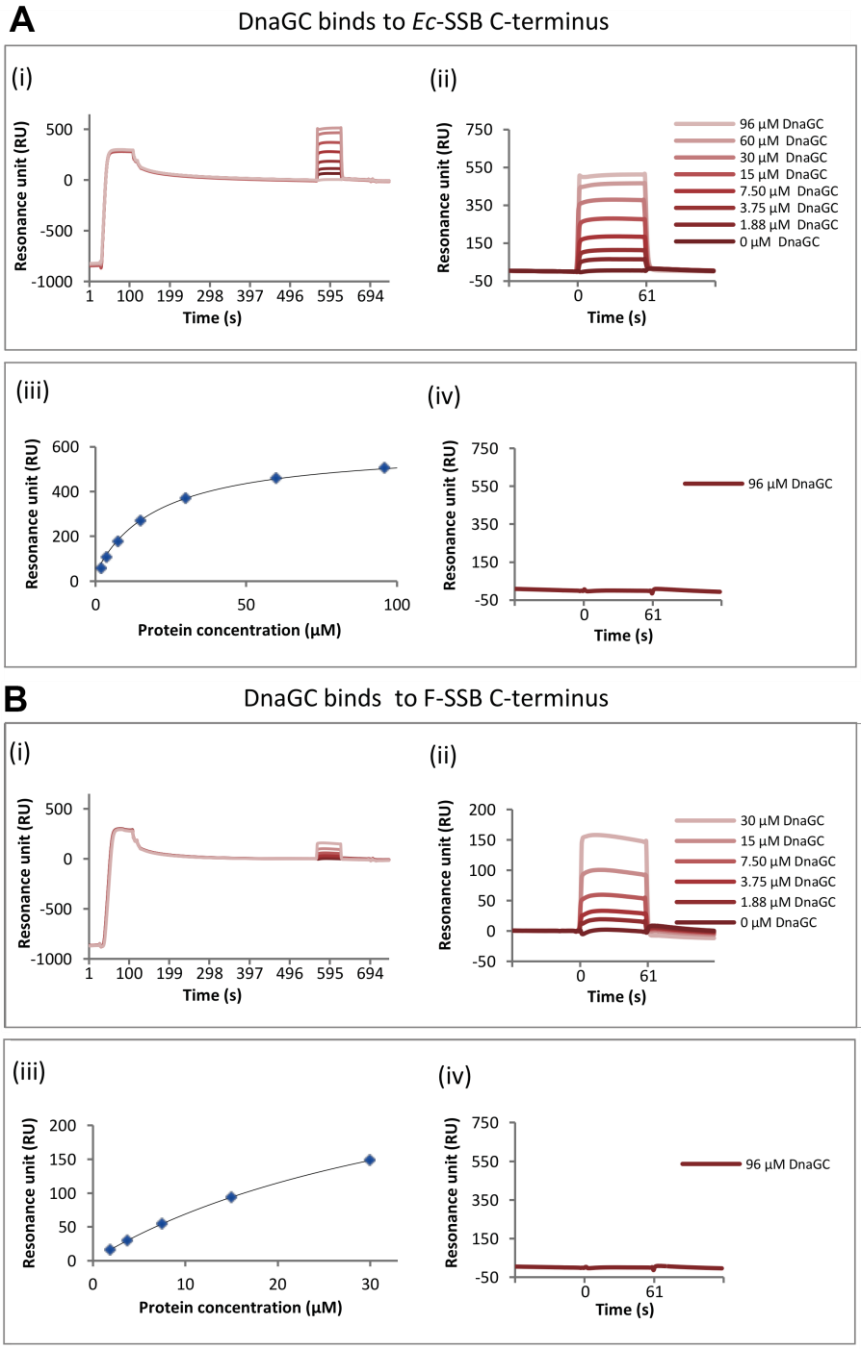

Figure 3.5 SPR sensorgrams (representative data) and equilibrium binding isotherms showing interactions of DnaGC with *Ec*-SSB (**A**) and F-SSB (**B**) in physiological salt (150 mM NaCl)

conditions. Aligned sensorgrams derived from injection of 100 nM *Ec*-SSB [**A(i)**] or F-SSB [**B(i)**] on $(dT)_{35}$ surfaces and the following injections of various concentrations of DnaGC are shown. **A(ii)** and **B(ii)** show the enlarged sensorgrams of the injections of DnaGC on *Ec*-SSB or F-SSB surfaces. Concentrations of DnaGC are listed in the insets. **A(iii)** and **B(iii)** show binding isotherms. The fit curves (steady state 1:1) correspond to values of K_D and R_{max} given in **Table 3.1**. At the right are sensorgrams derived from injection of 96 μM DnaGC on SSBΔC8 [**A(iv)**] or F-SSBtrun [**B(iv)**] surfaces.

Figures 3.5A(ii) and **B(ii)** show aligned sensorgrams from 60 s before to 60 s after injection of DnaGC over the SSB–$(dT)_{35}$ surfaces. DnaGC clearly interacts with both F-SSB and *Ec*-SSB with rapid binding and dissociation kinetics. The resulting binding isotherms [**Figures 3.5A(iii)** and **B(iii)**] were fit well using a "steady state 1:1" interaction model. Negative controls using C-terminally truncated *Ec*-SSB and F-SSB [**Figures 3.5A(iv)** and **B(iv)**] confirmed that interactions with both SSBs occurred, as expected, through the conserved C-terminal peptide. In the rest of this Thesis, SPR data will be shown as in **Figure 3.5,** except that the intact sensorgrams are not shown unless needed; the sensorgrams derived using *Ec*-SSB or F-SSB bound to $(dT)_{35}$ are very similar and highly reproducible.

Calculated equilibrium dissociation constants (K_D) and the stoichiometry (n) for interactions of DnaGC with F-SSB and *Ec*-SSB are shown in **Table 3.1**. According to the K_D values, DnaGC binds *Ec*-SSB about 2-fold more strongly than F-SSB, and based on the calculated stoichiometry, only half of the F-SSB C-termini (n = 2.1) were occupied by DnaGC under conditions where the C-termini of *Ec*-SSB were almost saturated by DnaGC (n = 3.4). The reason for this difference in stoichiometry is unclear at the moment. The highest concentration used in the SPR measurement for DnaGC and F-SSB interaction is 30 μM (**Figure 3.5B**) which is lower than the K_D value (42.4 μM **;Table 3.1**). Higher concentrations of F-SSB were used in the measurement. However, due to the distortion of the SPR sensorgram they were not shown in **Figure 3.5,** although attempted fitting showed very similar K_D and n values in **Table 3.1**.

Table 3.1 Calculated equilibrium dissociation constants (K_D) and stoichiometries (n) for interactions between DnaGC and *Ec*-SSB or F-SSB in physiological salt (150 mM NaCl) conditions. Errors are standard errors from non-linear regression.

	K_D (μM)	n	R_{max}
DnaGC:*Ec*-SSB	18.9 ± 0.4	3.40 ± 0.02	597 ± 3
DnaGC:F-SSB	42.4 ± 1.0	2.10 ± 0.03	355 ± 6

F-SSB also interacts with the χ subunit of the Pol III clamp loader through its C-terminus in physiological salt (150 mM NaCl) conditions (**Figure 3.6** and **Table 3.2**). Loss of the C-terminus of F-SSB in F-SSBtrun disables the interaction. The stoichiometry of interaction between F-SSB and χ shows that about three F-SSB C-termini can be occupied by the χ subunit at saturation (**Table 3.2**). This is very close to the data for the interaction between χ and *Ec*-SSB, although the interaction between χ and F-SSB is 4–5 times weaker than that with *Ec*-SSB.

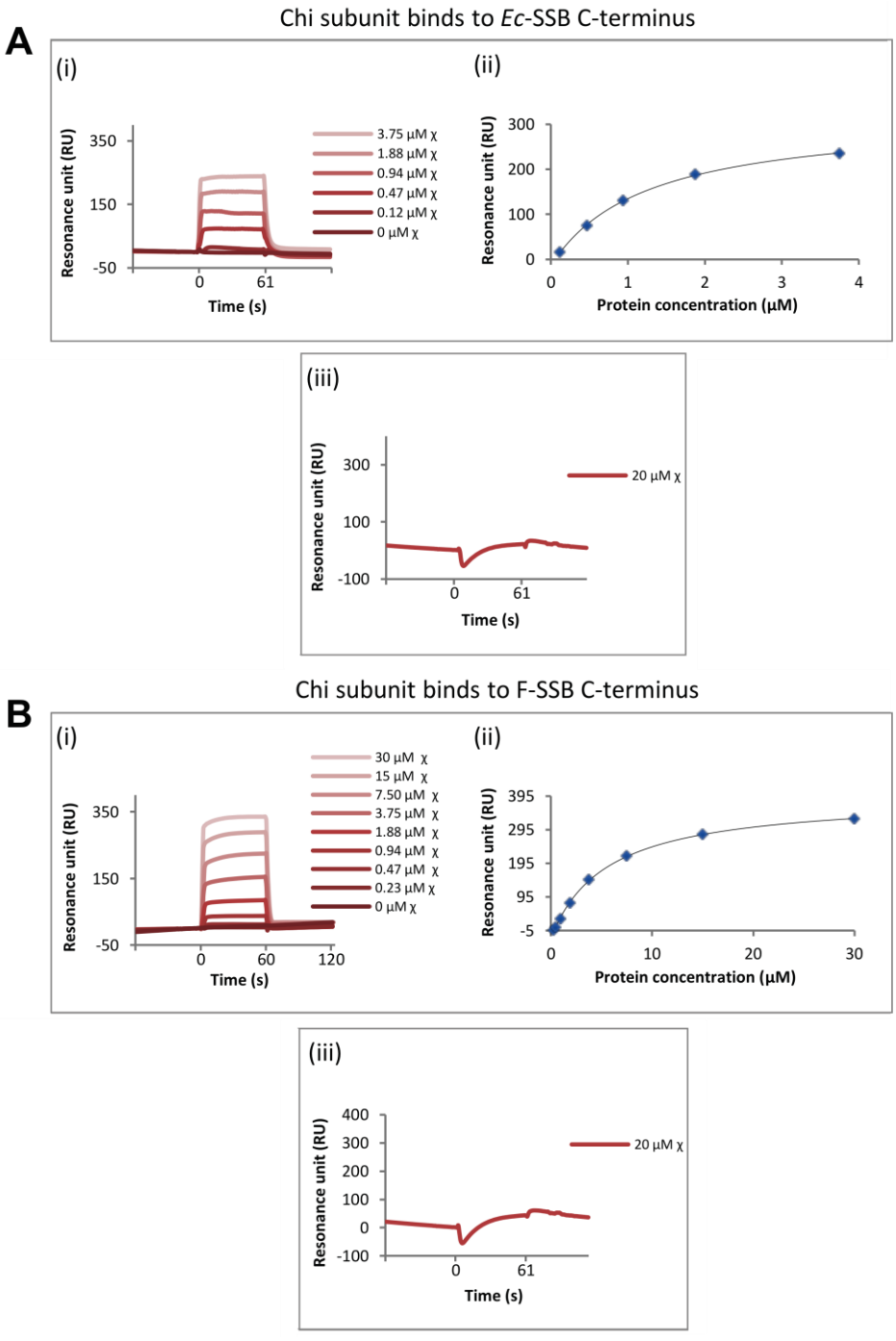

Figure 3.6 SPR sensorgrams (representative data) and equilibrium binding isotherms showing interactions between the Pol III χ subunit and *Ec*-SSB (**A**) or F-SSB (**B**) in physiological salt (150 mM NaCl) conditions. **A(i)** and **B(i)** show aligned sensorgrams for the injections of χ over *Ec*-SSB and F-SSB surfaces created by prior injection of *Ec*-SSB or F-SSB over $(dT)_{35}$ surfaces. The various concentrations of χ injected are listed in the insets. **A(ii)** and **B(ii)** show the binding isotherms. The fit curves (steady state 1:1) correspond to values of K_D and R_{max} given in **Table 3.2**. The panels at the right show sensorgrams from injecting 20 μM χ on surfaces with bound *Ec*-SSBΔC8 [**A(iii)**] and F-SSBtrun [**B(iii)**].

Interestingly, Dr. Lo has shown that only the last residues (-FDDDIPF) of *Ec*-SSB are involved in its interaction with χ and DnaGC (Lo, 2012). These residues are well conserved in F-SSB. This raises the question: what causes the difference in interactions of these two SSBs with DnaGC and the χ subunit? The differences in affinities is probably due to the extended F-SSB C-terminal sequence being somewhat less acidic that that of *Ec*-SSB (sequence: -YGFSDDIPF *cf.* -MDFDDDIPF; **Figure 3.3**). An SPR experiment with the F-SSB C-terminal peptide immobilized on the surface could elucidate this, as could a mutagenesis study where the C-terminal regions of the two SSBs are interchanged. Unfortunately, such experiments have not been done yet.

Table 3.2 Calculated equilibrium dissociation constants (K_D) and the stoichiometries (n) for interactions between the χ subunit and *Ec*-SSB or F-SSB in physiological salt (150 mM NaCl) conditions. Errors are standard errors from non-linear regression.

	K_D (μM)	n	R_{max}
χ subunit:*Ec*-SSB	1.2 ± 0.1	3.00 ± 0.06	333 ± 7
χ subunit:F-SSB	5.5 ± 0.3	3.30 ± 0.05	421 ± 6

3.3.4 RNase HI interacts with *Ec*-SSB and F-SSB through their conserved C-terminal residues

Interactions between *Ec*-SSB and most of its binding partners occur through its highly conserved C-terminal residues (-DDDIPF). The population of the characterized binding partners has rapidly grown over recent years. RNase H is the protein found in *E. coli* for digesting RNAs in RNA–DNA hybrid duplexes and possibly helping to identify the replication origin (see **Chapter** 4, **Section 4.1.2**). There are two RNase Hs in *E. coli*: RNase HI and RNase HII. It is possible that RNase HI (and maybe RNase HII) accesses its substrates through recognition of *Ec*-SSB on nearby ssDNA. The interaction between *Ec*-SSB and RNase HI has been determined biochemically and structurally (Petzold *et al.*, 2012; Dr. James Keck, unpublished communication), however no such studies have been reported for F-SSB. Our well-established SPR system and high-quality purified

proteins provided a good opportunity to probe these interactions. In this Section, interactions of RNase HI with *Ec*-SSB or F-SSB are described. No interaction between RNase HII and *Ec*-SSB or F-SSB was found (data not shown).

SPR measurements showed interactions between RNase HI and *Ec*-SSB through its conserved C-terminal residues in physiological (150 mM NaCl) as well as high salt (300 mM NaCl) conditions. In 150 mM NaCl, RNase HI interacts with *Ec*-SSB and also $(dT)_{35}$ with fast association and slow dissociation kinetics [**Figures 3.7A(i)** and **3.8(i)**], and removal of the last eight residues from *Ec*-SSB abolishes the *Ec*-SSB interaction [**Figure 3.7A(iii)**]. The binding affinities are shown in **Table 3.3**. The data indicate that RNase HI binds *Ec*-SSB through its C-terminus.

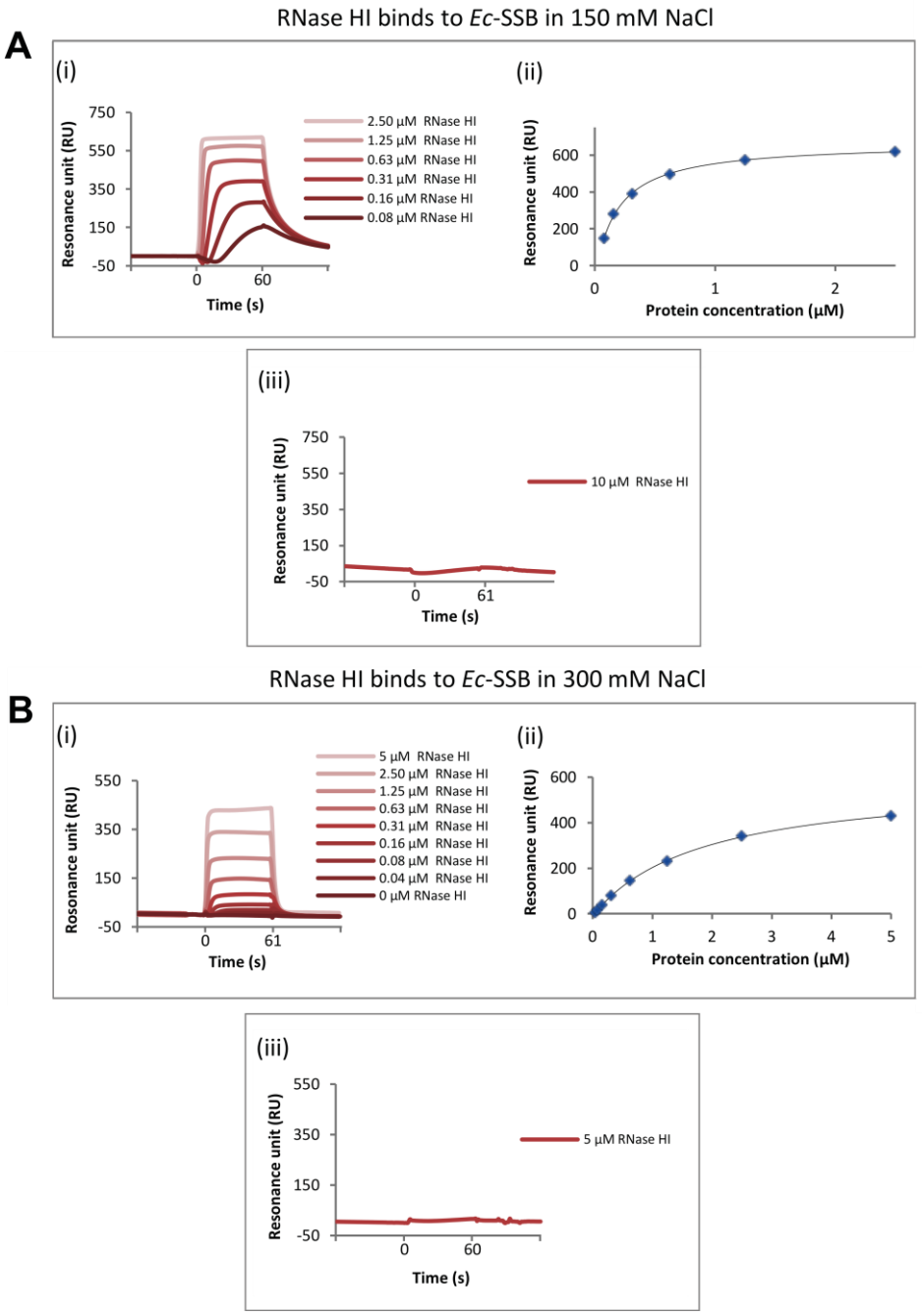

Figure 3.7 SPR sensorgrams (representative data) and equilibrium binding isotherms showing interactions between RNase HI and *Ec*-SSB in physiological (150 mM NaCl) and higher (300 mM NaCl) salt conditions. Aligned sensorgrams of the injections of RNase HI on the *Ec*-SSB surface are shown in **A**(**i**) for 150 mM NaCl, and **B**(**i**) for 300 mM NaCl. The fit curves (steady state 1:1) based on the data points from the aligned sensorgrams are shown in (**ii**) in **A** and **B**. **A**(**iii**) and **B**(**iii**) show the sensorgrams from injection of RNase HI over the *Ec*-SSBΔC8 surface.

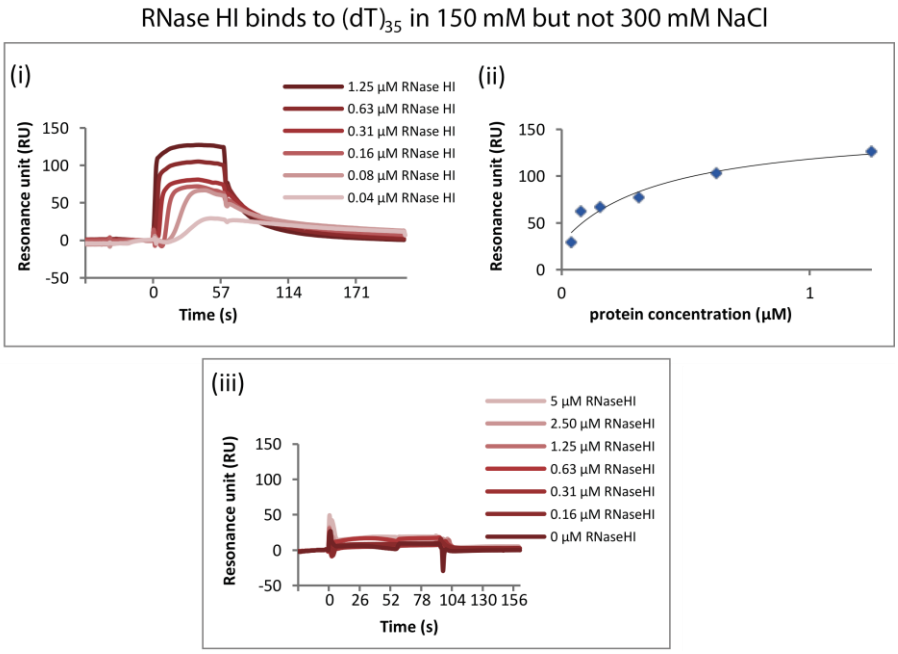

Figure 3.8 SPR sensorgrams (representative data) and equilibrium binding isotherms showing interactions between RNase HI and $(dT)_{35}$ in physiological (150 mM NaCl) and higher (300 mM NaCl) salt conditions. Aligned sensorgrams of the injections of RNase HI on the $(dT)_{35}$ surface are shown in (**i**) for 150 mM NaCl, (**iii**) for 300 mM NaCl. The fit curves (steady state 1:1) based on the data points from the aligned sensorgrams are shown in (**ii**).

The experiments were repeated in the same buffer supplemented with higher salt concentration (300 mM NaCl). At higher salt, interaction of RNase HI and $(dT)_{35}$ was abolished [**Figure 3.8(iii)**] and the RNaseHI:*Ec*SSB interaction showed rapid dissociation kinetics [**Figure 3.7B(i)**]. This may suggest that the response from injecting RNase HI on the $(dT)_{35}$ surface at lower salt is due to a nonspecific (electrostatic) interaction. Using a buffer with higher ionic strength and surfactant concentrations counteracts this effect. Therefore, the response in **Figure 3.7A(i)** may represent a combination of two binding events [RNase HI:$(dT)_{35}$ interaction and RNase HI:*Ec*-SSB interactions], although the abolition of the RNase HI interaction by use of the SSBΔC8 surface [**Figure 3.7A(iii)**] suggests that the $(dT)_{35}$ on the surface is saturated with SSB in all conditions in **Figure 3.7**.

To finally confirm that RNase HI binds to *Ec*-SSB through its C-terminus, a chip surface with immobilized (N-terminally biotinylated) *Ec*-SSB-Ct peptide was used (**Figure 3.9**). Interactions were measured in 150 mM NaCl. Interestingly, typical fast-on and fast-off kinetics were observed. This supports the possibility of two binding events in **Figure 3.7A(i)** and the complication of electrostatic interaction of RNase HI with $(dT)_{35}$. The value of K_D (1.47 µM) for the RNase HI:*Ec*-SSB-Ct (150 mM NaCl)

interaction was very close to that (1.83 μM) for RNase HI:*Ec*-SSB (300 mM NaCl), but the RNase HI:*Ec*-SSB interaction in 150 mM NaCl was apparently 10-fold stronger (**Table 3.3**). This may indicate that *Ec*-SSB has a site additional to the C-terminal peptide for weak interaction with RNAse HI. The stoichiometry (*n*) suggests that four RNase HI molecules can simultaneously bind to one *Ec*-SSB tetramer.

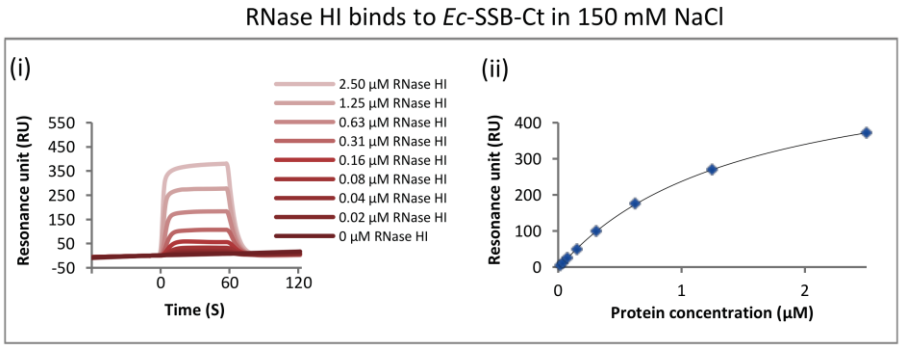

Figure 3.9 SPR sensorgrams (representative data) and equilibrium binding isotherms showing interactions between RNase HI and *Ec*-SSB-Ct in physiological (150 mM NaCl) salt conditions. Aligned sensorgrams of the injections of RNase HI on the *Ec*-SSB-Ct surface are shown in (**i**), The fit binding isotherm (steady state 1:1) based on the data points from the aligned sensorgrams is shown in (**ii**).

Table 3.3 Calculated equilibrium dissociation constants (K_D) and stoichiometries (*n*) for interactions between RNase HI and *Ec*-SSB, $(dT)_{35}$ or *Ec*-SSB-Ct in physiological (150 mM NaCl) and high (300 mM) salt conditions. Errors are standard errors from non-linear regression.

	NaCl (mM)	K_D (μM)	*n*	R_{max}
RNase HI:*Ec*-SSB	150	0.18 ± 0.02	3.9 ± 0.1	733 ± 23
	300	1.83 ± 0.05	3.80 ± 0.04	599 ± 6
RNase HI:$(dT)_{35}$	150	0.4 ± 0.3	0.7 ± 0.1	126 ± 25
	300	n/a	n/a	n/a
RNase HI:*Ec*-SSB-Ct	150	1.47 ± 0.05	0.80 ± 0.01	599 ± 9

SPR measurements show RNase HI binds to F-SSB in a similar way as it binds to *Ec*-SSB. **Figure 3.10A(i)** and **B(i)** show that RNase HI interacts with F-SSB with fast-on and fast-off kinetics in both 150 and 300 mM NaCl. Comparing this with the fast-on and slow-off type of *Ec*-SSB:RNase HI interaction in 150 mM NaCl [**Figure 3.7A(i)**] suggests that F-SSB may have stronger affinity for $(dT)_{35}$, resulting in a smaller population of unoccupied $(dT)_{35}$ on the chip surface. This is also reflected in the binding curve of F-SSB on the $(dT)_{35}$ surface where F-SSB dissociates more slowly than does *Ec*-SSB [**Figure 3.5A(i)** and **B(i)**].

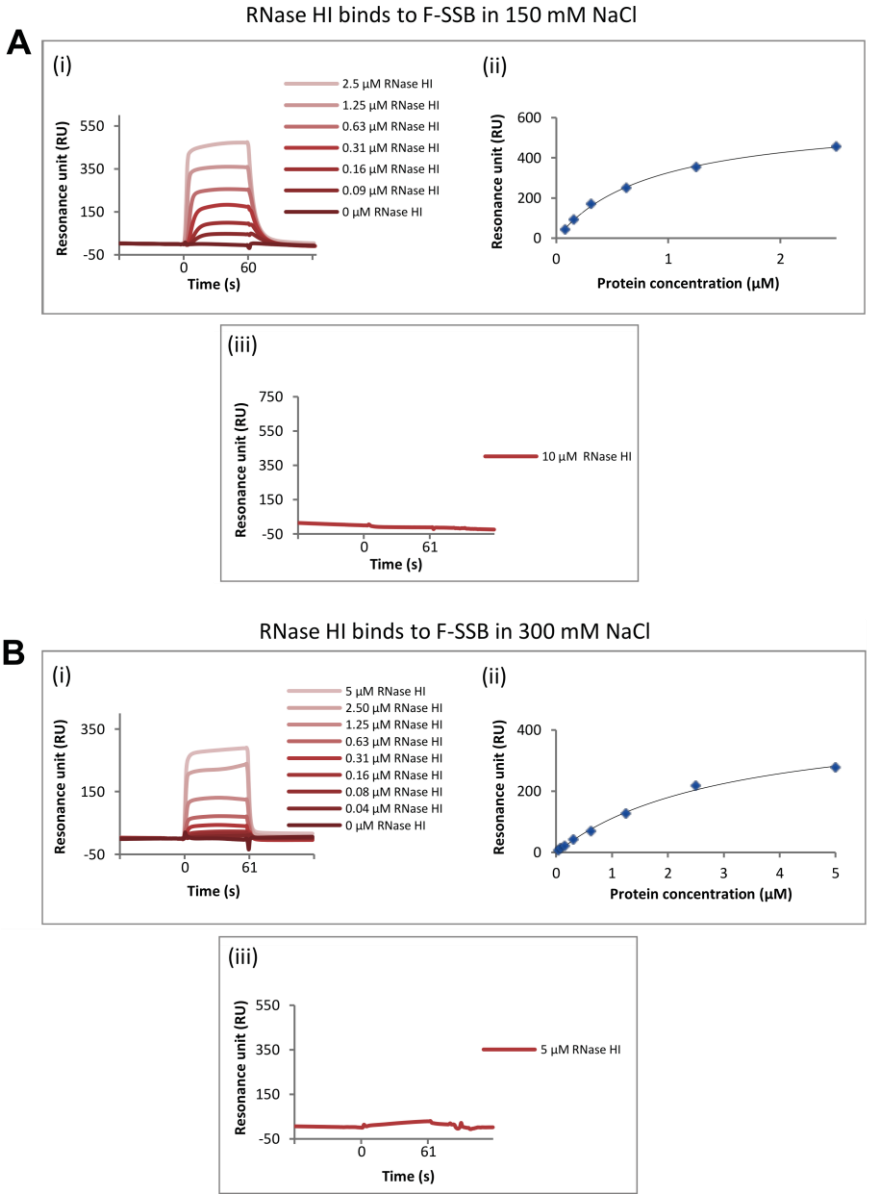

Figure 3.10 SPR sensorgrams (representative data) and equilibrium binding isotherms showing interactions between RNase HI and F-SSB in physiological (150 mM NaCl) and higher (300 mM NaCl) salt conditions. **A(i)** and **B(i)** show the aligned sensorgrams of the injections of RNase HI on F-SSB surfaces created by injecting F-SSB on $(dT)_{35}$ surfaces in 150 mM and 300 mM NaCl, respectively. The fit curve (steady state 1:1) based on the data points from the aligned sensorgrams are shown in (**ii**) in both **A** and **B** (**Table 3.4**). Panels **A(iii)** and **B(iii)** show the sensorgrams from injection of RNase HI on F-SSBtrun surfaces.

Table 3.4 Calculated equilibrium dissociation constants (K_D) and the stoichiometries (n) for interactions between RNase HI and F-SSB in physiological (150 mM NaCl) and higher salt (300 mM NaCl) conditions. Errors are standard errors from non-linear regression.

	NaCl (mM)	K_D (µM)	n	R_{max}
RNase HI:F-SSB	150	0.9 ± 0.1	3.1 ± 0.1	614 ± 20
	300	3.0 ± 0.5	2.9 ± 0.2	456 ± 34

All in all, the results show RNase HI binds to *Ec*-SSB through its conserved C-terminal residues (DFDDDIPF) with a similar K_D to the *Ec*-SSB:χ interaction. The *Ec*-SSB analogue protein F-SSB interacts with RNase HI with similar strength and stoichiometry through its C-terminal region, though the interaction is somewhat weaker than with *Ec*-SSB (**Table 3.4** *cf.* **Table 3.3**). Studies have shown that *Ec*-SSB stimulates hydrolysis of RNA in RNA/DNA hybrids by RNase HI (Petzold *et al*., 2012). However, the function of the F-SSB:RNase HI interaction is not clear. My results hint that the activity of RNase HI is likely to be coordinated by both ssDNA-bound *Ec*-SSB and F-SSB, and that F-SSB probably interacts with RNase HI, DnaGC and the χ subunit through the same *Ec*-SSB binding pockets.

3.3.5 The C-terminal peptide of *Ec*-SSB interacts with its OB domain

Collaboration between Profs Gottfried Otting (ANU) and Nick Dixon has led to identification of the binding site for the *Ec*-SSB C-terminus on the *Ec*-SSB OB-domain by NMR. Previously the laboratory of Prof. Otting found that *Ec*-SSB adopts a fully-folded monomeric structure (instead of a tetramer) in acidic (pH 3.4) conditions. This was advantageous for use of NMR spectroscopy for studying *Ec*-SSB, and allowed near-complete assignments of resonances in the HSQC spectrum of monomeric SSB (see **Figure 3.12**). Dr. Dmitry Shishmarev in the Otting group has recorded excellent NMR spectra in this condition (using proteins purified by Mr Yao Wang in Nick Dixon's lab), and identified the binding site for the *Ec*-SSB C-terminus on the OB domain (Shishmarev *et al.,* 2014). These data provided direct evidence for this interaction, which had been just an assumption for a long time.

Uniformly ^{15}N-labelled and ^{15}N,^{13}C-double-labelled *Ec*-SSB, as well as ^{15}N-labelled *Ec*-SSB(E65C/E69D) were used in the NMR experiments. Protein production was induced in cultures grown in minimal medium (**Section 2.2.2**) with $^{15}NH_4Cl$ and/or ^{13}C-glucose as the sole nitrogen and carbon sources, respectively. Purification procedures used for the proteins were the same as for unlabelled *Ec*-SSB (**Section 3.2.1.4**). The proteins eluted from the DEAE column were analyzed by SDS-PAGE (**Figure 3.11**); appropriate fractions were pooled and used in the NMR experiments.

The integrity of the OB-fold structure was retained at pH 3.4. The ^{15}N-HSQC spectrum of ^{15}N-labelled *Ec*-SSB at pH 3.4 showed excellent dispersion of chemical shifts

(**Figure 3.12**), indicating that its 3D structure was conserved, and this was further examined by comparison with the coordinates of a crystal structure of *Ec*-SSB (PDB code: 4MZ9). The structure was then confirmed by measuring pseudocontact chemical shifts (PCS) generated using paramagnetic lanthanide tags attached to residue 65 using the ^{15}N-labelled *Ec*-SSB(E65C/E69D) (Shishmarev *et al.*, 2014).

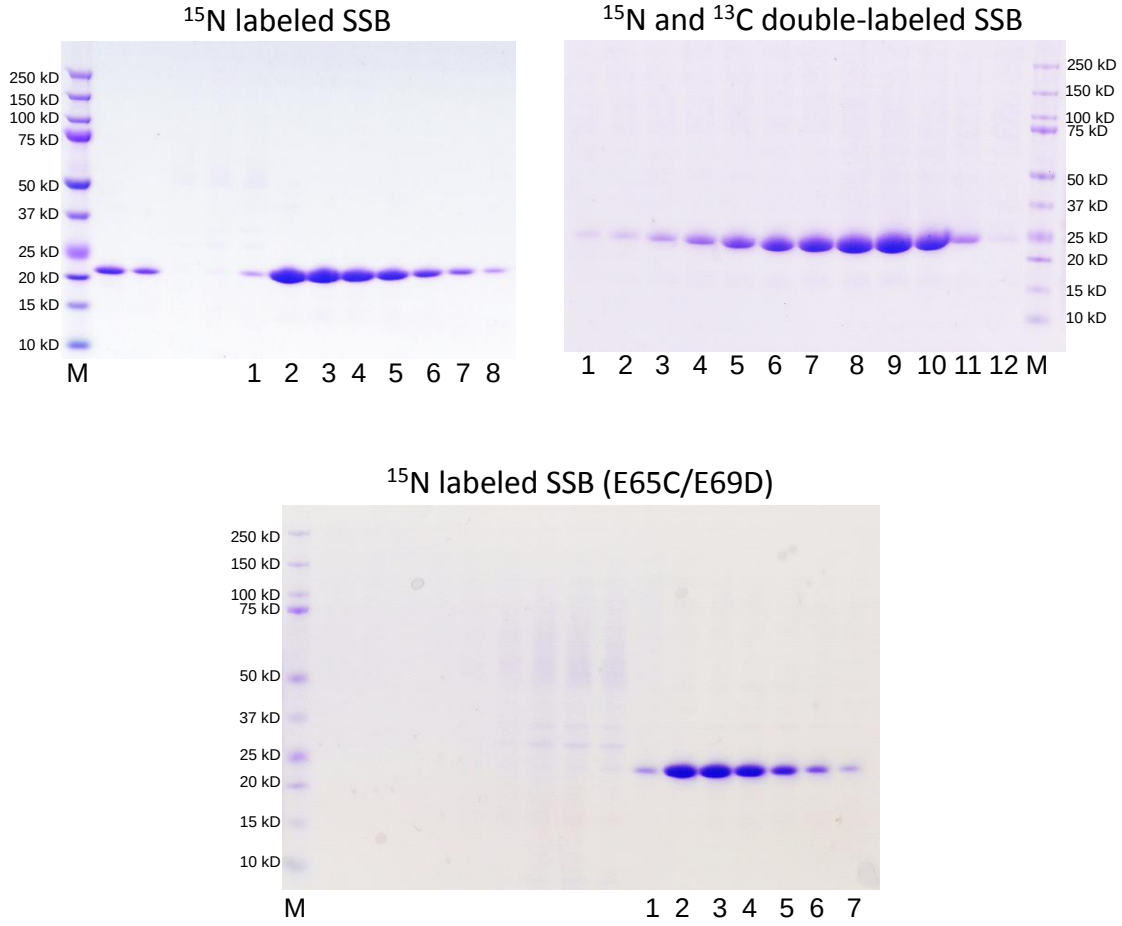

Figure 3.11 SDS-PAGE showing the eluted ^{15}N-labelled, ^{15}N and ^{13}C double-labelled *Ec*-SSB and ^{15}N labelled *Ec*-SSB(E65C/E69D) used for the NMR measurements. Fractions 1–8 for ^{15}N-labelled *Ec*-SSB, fractions 1–11 for ^{15}N,^{13}C double-labelled *Ec*-SSB, and fractions 1–7 for ^{15}N-labelled *Ec*-SSB(E65C/E69D) were combined.

NOEs could be assigned between side chain protons of Asp-174 and Val-30, and Phe-172 and Val-59 at the *Ec*-SSB C-terminus and in the OB domain, respectively (**Figure 3.13A**). Although there were no other clear NOEs assigned between the C-terminus and the OB domain, the three other acidic C-terminal residues (Asp-171, Asp-173 and Asp-175) close to the binding site (*i.e.*, within 8 Å of the valine residues) are assumed to facilitate the interaction by binding through electrostatic interactions to the positively charged surface (Arg-20, Arg-55, Arg-83 and Arg-85) that is close to Val-30 and Val-59

of the OB domain. Furthermore, we speculated that the interaction at neutral pH will be stronger, because the low pH conditions could potentially disrupt the interaction by protonation of side chains of the acidic residues at the C-terminus of *Ec*-SSB.

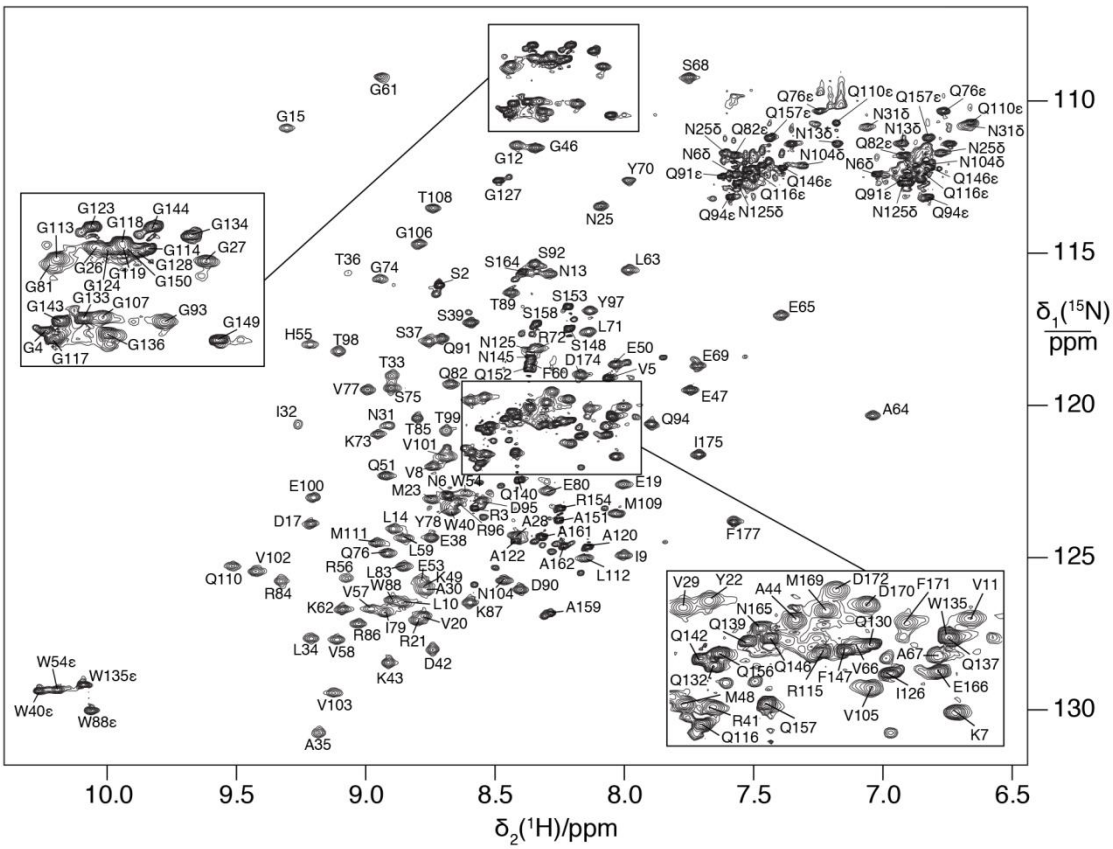

Figure 3.12 ^{15}N-HSQC spectrum of monomeric *Ec*-SSB. The spectrum was generated by using ^{15}N-labelled *Ec*-SSB at pH 3.4 and 25°C in a Bruker 800 MHz NMR spectrometer (from Shishmarev *et al.,* 2014). The backbone amides are labelled with the name of amino acid and a number indicating its position. The side chain NH groups are labelled with an additional Greek letter. Certain areas are enlarged to show assignments.

3.3.6 The interaction of the C-terminal peptide with the OB domain of *Ec*-SSB is very weak

We sought a method to directly measure the binding affinity between the *Ec*-SSB C-terminal peptide and its OB domain at neutral pH where the protein is a stable tetramer (Su *et al.*, 2014). The NOEs between the C-terminus and OB domain had been identified at low pH in solutions without salt. To measure the affinity of a C-terminal peptide for the OB-fold by NMR (or other methods such as SPR), one would need to titrate *Ec*-SSBΔC8 in a low salt buffer into a constant concentration of the C-terminal peptide. Since this interaction is expected to be weak in the absence of covalent tethering of the peptide to the globular domain, this would require a relatively high

initial concentration of protein. A solubility test was carried out by dialysis of *Ec*-SSBΔC8 (at 40 μM) into three different low salt buffers (buffer X containing 5 mM HEPES, pH 7.2, 1 mM DTT and 1 mM EDTA; buffer Y containing 5 mM sodium phosphate, pH 7.2, 1 mM DTT and 1 mM EDTA; "buffer" Z containing MQ water and 1 mM DTT). The dialyzed protein samples were then centrifuged, and the concentration of soluble protein was determined by measuring the A_{280} of the supernatant. The result showed there in 0.7 μM soluble protein in buffers X and Y, and 1.4 μM in buffer Z. The poor solubility of *Ec*-SSBΔC8 thus seriously limits methods available for affinity measurement.

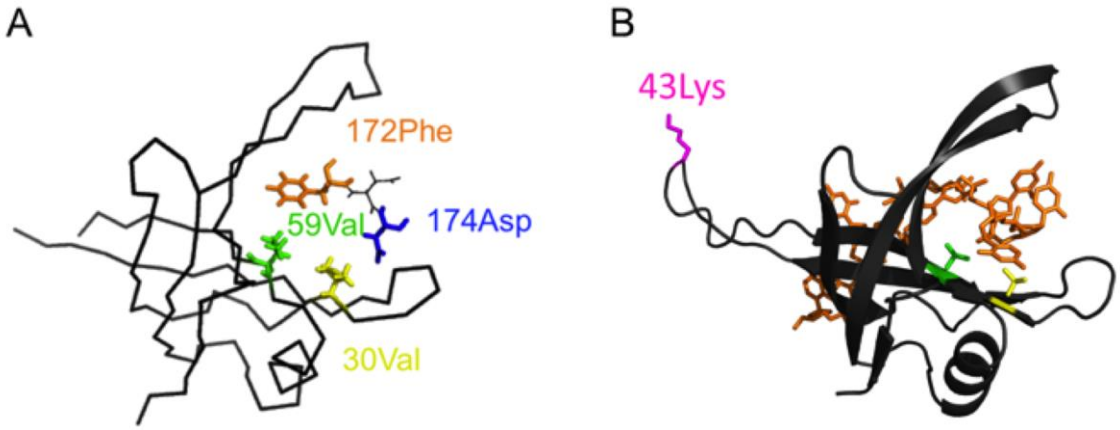

Figure 3.13 A model of the *Ec*-SSB C-terminal residues (Asp-174 and Phe-172) binding close to residues (Val-30 and Val-59) in the OB domain of *Ec*-SSB (**A**; from Shishmarev *et al.,* 2014), and a model showing the Lys-43 (mutated into Cys for the MST experiment) is far away from the ssDNA-binding site (**B;** PDB code: 1EYG). The 3D NMR structure in model **A** was generated (by Dr. Shishmarev) based on the NOEs assigned from spectra of 0.37 mM ^{13}C,^{15}N-labelled *Ec*-SSB at pH 3.4 and 25˚C at a ^{1}H NMR frequency of 800 MHz. PCS-Rosetta (Schmitz *et al.,* 2012) was used to identify the conformations that fulfill the NOEs as well as the PCSs and van-der-Waals' restraints provided by the structure of the OB-domain of a crystal structure (PDB code: 4MZ9). The backbone of the *Ec*-SSB monomer is shown as black lines. The residues involved in the interaction are shown as sticks. The model in **B** (adapted from PDB: 1EYG) shows the Val-30 (green), Val-59 (yellow) and the bound ssDNA (orange) are far away from the Lys-43 chosen as the fluorescein labelling site. Therefore the fluorescein should not interfere with SSB C-domain binding site in the MST measurements.

MST (micro-scale thermophoresis) is a recently developed method (**Section 3.1.2**) that allowed us to make the required affinity measurements. Use of MST requires that one of the binding partners be labelled with a fluorophore. For this, I used fluorescein-5-maleimide conjugation to the single cysteine in the *Ec*-SSB(K43C) mutant. Since Lys-43 is far away from the ssDNA binding site (**Figure 3.13B)**, the fluorescein should not interfere with the MST measurement.

Preparations of fluorescein-5-maleimide labelled *Ec*-SSB(K43C-FAM), *Ec*-SSBΔC8 (K43C-FAM) and *Ec*-SSBT*(K43C-FAM) tetramers (**Section 3.2.1.11)** were analyzed by SDS-PAGE (**Figure 3.14**). All the bands could be visualized in bright yellow colour without staining, and were in the same positions of the bands after Coomassie blue staining, indicating the proteins contain conjugated fluorescein labels.

To minimize the possible interference of the fluorescein tag with the binding of SSB-Ct, tagged SSBΔC8(K43C) was allowed to equilibrate by subunit exchange (Mason *et al.*, 2013) with a 25-fold excess of "wild-type" SSBΔC8 to produce a population of tetramers (**Section 3.2.1.11**) in which a maximum of one subunit should be fluorescent.

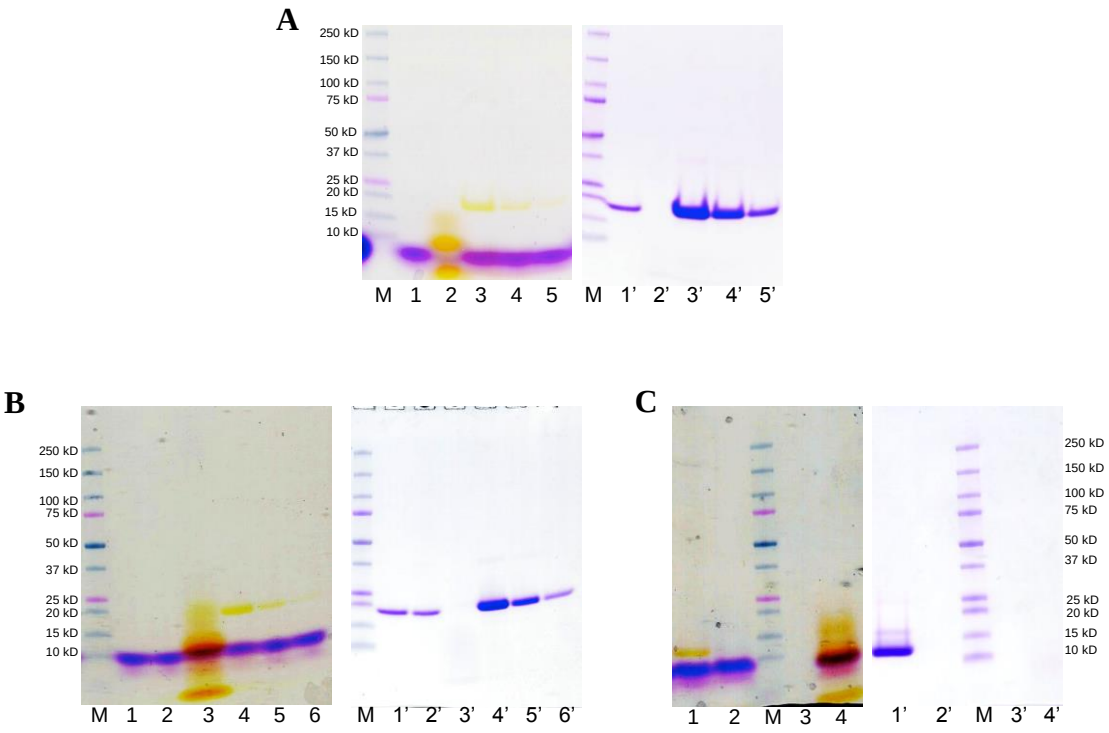

Figure 3.14 SDS-PAGE for unlabelled and fluorescein-5-maleimide labelled *Ec*-SSBΔC8(K43C), *Ec*-SSB(K43C) and *Ec*-SSBT*(K43C), used for MST measurements. **A.** *Ec*-SSBΔC8(K43C). Lanes contain 2 µg of unlabelled *Ec*-SSBΔC8(K43C) (lanes 1 and 1'), 10 µg of fluorescein-5-maleimide (presumably as the DTT conjugate; lanes 2 and 2'), and 15 (lanes 3 and 3'), 5 (lanes 4 and 4') and 2 µg of labelled *Ec*-SSBΔC8(K43C) (lanes 5 and 5'). **B.** *Ec*-SSB(K43C). Lanes contain 2 µg of unlabelled *Ec*-SSB (lanes 1 and 1'), 2 µg of unlabelled *Ec*-SSB(K43C) (lanes 2 and 2'), 10 µg of fluorescein-5-maleimide (lanes 3 and 3'), and 14 (lanes 4 and 4'), 5 (lanes 5 and 5') and 2 µg of labelled *Ec*-SSB(K43C) (lanes 6 and 6'). **C.** *Ec*-SSBT*(K43C). Lanes contain 5 µg of labelled *Ec*-SSBT*(K43C) (lanes 1 and 1') and 10 µg of fluorescein-5-maleimide (lanes 4 and 4'). Lanes 2 and 2' contain dialyzed fluorescein-5-maleimide (initially at the same concentration used for labelling SSB species). The left panels of **A**, **B** and **C** were photographed before being stained with Coomassie brilliant blue, and the panels on the right were photographed after staining. The purple bands below the yellow bands (the protein) in the left panels are the bromophenol blue dye in the protein loading buffer.

For the MST measurements, we titrated a high concentration of C-terminal peptide into solutions containing a relatively low concentration (1.6 μM) of fluorescein labelled mixed tetramers of *Ec*-SSBΔC8, *Ec*-SSBT* and *Ec*-SSB. We considered using two peptides (a short peptide: WMDFDDDIPF, and a long peptide: PSNEPPMDFDDDIPF), both of which had been previously used in various experiments. A solubility test was carried out for both peptides by dissolving them (in powder form) in 10 mM Tris, and neutralizing them to pH ~7.5 by adding 5 M KOH. The samples were then centrifuged. Concentrations of soluble peptides were measured spectrophotometrically, which showed the concentrations to be 5 mM for the short peptide and 206 mM for the long peptide. Therefore, the long peptide was used in the following MST measurement (**Figure 3.15**).

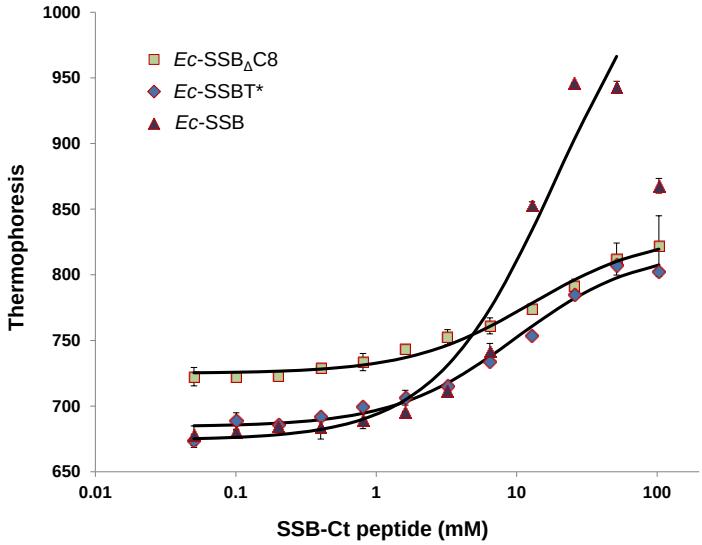

Figure 3.15 C-terminal *Ec*-SSB peptide binds to the OB-domain. MST measurements were carried out by adding 0.05, 0.10, 0.20, 0.40, 0.80, 1.61, 3.22, 6.44, 12.88, 25.75, 51.5 and 103.0 mM of a non-labelled *Ec*-SSB C-terminal peptide (PSNEPPMDFDDDIPF) into a constant concentration (1.6 μM) of each of the fluorescein-5-maleimide labelled proteins [*Ec*-SSBΔC8]$_3$[*Ec*-SSBΔC8(K43C-FAM)]$_1$, [*Ec*-SSB]$_3$[*Ec*-SSB(K43C-FAM)]$_1$ and [*Ec*-SSBT*]$_3$[*Ec*-SSBT*(K43C-FAM)]$_1$ in buffer containing 10 mM Tris-HCl, pH 7.6 and 0.01% Tween 20. 50% LED power (blue) and 90% MST power were used. Each measurement was repeated twice. Raw fluorescence curves are plotted as corresponding fluorescence ratios. The averaged MST data points were used for fitting to a 1:1 binding model, based on which the K_D is derived. The last data point (at 103 mM) with the [*Ec*-SSB]$_3$[*Ec*-SSB(K43C-FAM)]$_1$ was not taken into the fitting since its unusual value is likely due to the artifact of high concentration of peptide. All the measurements were conducted in a Monolith NT 115 microscale thermophoresis instrument. The K_D (in mM) for [*Ec*-SSBΔC8]$_3$[*Ec*-SSBΔC8(K43C-FAM)]$_1$, [*Ec*-SSB]$_3$[*Ec*-SSB(K43C-FAM)]$_1$ and [*Ec*-SSBT*]$_3$[*Ec*-SSBT*(K43C-FAM)]$_1$ interactions were 13 ± 3, 19 ± 5 and 11 ± 2 mM, respectively.

The result shows a K_D of 13 ± 3 mM for the peptide–[*Ec*-SSBΔC8]$_3$[*Ec*-SSBΔC8 (K43C-FAM)]$_1$ interaction by fitting the data to a 1:1 binding model. To probe whether

there are additional binding sites elsewhere in the C-terminal tail or OB domain, the same measurement was repeated using [*Ec*-SSBT*]$_3$[*Ec*-SSBT*(K43C-FAM)]$_1$. A very similar value of K_D (11 ± 2 mM) was obtained. As a negative control, the measurement was also made using [*Ec*-SSB]$_3$[*Ec*-SSB(K43C-FAM)]$_1$. Surprisingly, a similar K_D value (19 ± 5 mM) was also derived. However, to fit the curve, we needed to exclude the point at the highest concentration (103 mM). Due to the constraints of concentration of the peptide, the K_D is likely to be higher than 19 mM.

The similarity of the dissociation constants suggests that residues in the C-domain preceding the C-terminal peptide make no significant contribution to the binding of SSB-Ct to the OB domain. The result with full-length *Ec*-SSB, and the poor fitting, may hint that the native C-terminus is not bound to the OB fold most of the time. This is also reflected by the high mobility of the *Ec*-SSB C-terminus in ^{15}N-relaxation measurements by NMR, indicating a substantial fraction of the C-termini remain unbound at low pH (Shishmarev *et al.,* 2014). Studies at neutral pH showing at most one-third of C-termini of *Ec*-SSB bound to its OB-domain, were also consistent with this hypothesis (Su *et al.,* 2014). This seems to contradict results from previous studies (**Sections 3.1.1** and **4.1.1**), which show signs that the C-terminus of *Ec*-SSB regulates itself on binding to ssDNA. It now seems more likely that there are alternate explanations for those observations (as discussed in Su *et al*., 2014).

In work reported in this Chapter, interactions between the *Ec*-SSB C-terminus and RNase HI, the χ subunit of Pol III and DnaGC were studied by SPR. Repeating the experiments with F-SSB yield similar values of K_D and stoichiometry. The functional importance of the SSB:χ interaction is further explored in **Chapter 4** in studies that revealed an additional function of the C-terminal flexible region of SSB. The functional implications of the interactions between SSB and RNase HI or DnaGC were not explored further in this Thesis.

A novel SSB C-terminal binding site on its OB domain, where Asp-174 and Phe-172 are close to the residues Val-30 and Val-59 was also described in this Chapter. Additional MST and NMR measurements showed that although the C-terminus of SSB can bind to its OB domain, it stays unbound most of the time. This seems to contradict previous suggestions that release of the C-terminal tail of SSB on DNA binding provides a way for SSB-Ct interacting proteins to sense the presence of ssDNA. There are likely other

potential explainations how *Ec*-SSB regulates it's C-terminus, one of which is explored in Chapter 4. Little is known to date about how the DNA polymerase removes SSB during DNA synthesis. These studies extend our understanding about the regulation of the SSB C-terminus. However more studies are needed to fully interpret the results and to reconcile all of the theories.

CHAPTER 4

DNA ELONGATION AND OKAZAKI FRAGMENT MATURATION DURING *E. coli* DNA REPLICATION

4.1 Introduction

Single-stranded DNA-binding proteins (SSBs) form very stable complexes with ssDNA, and how DNA polymerases quickly remove SSBs ahead of them when they replicate DNA is a question that is yet to be answered by researchers in the field. A recent study (Zhou *et al.,* 2011) showed that a certain applied physical force can dissociate *E. coli* (*Ec*-) SSB from ssDNA. Other studies show *Ec*-SSB in the $(SSB)_{35}$-binding mode can transfer rapidly from one ssDNA template to another without dissociating into solution (Kozlov & Lohman, 2002; Mason *et al.,* 2013) or simply dissociate from ssDNA over a long period of time (Shlyakhtenko *et al.*, 2012). However, there is a lack of evidence showing the direct "communication" between the DNA polymerase III holoenzyme (Pol III HE) and *Ec*-SSB except for the now well-established χ:SSB-Ct interaction (see **Chapter 3**).

The model for Okazaki fragment maturation in *E. coli* involving DNA polymerase I (Pol I) and DNA ligase (**Sections 1.1** and **4.1.2**) has been long accepted; Pol I removes RNA primers using its flap endonuclease ("5'–3' exonuclease") activity while filling in DNA behind it, to produce a DNA–DNA nick that is sealed by ligase. However there are still many aspects of this mechanism that remain uncertain, including the potential roles of *Ec*-SSB and the β_2 subunit of Pol III HE. Previously in our research group, Dr. Slobodan Jergić has undertaken an extensive study of the mechanism of helicase-independent, SSB-dependent strand displacement (SD) synthesis by Pol III HE (Jergić *et al.*, 2013) on encountering the RNA- or DNA-primed 5' end of an Okazaki fragment (S. Jergić, unpublished data). He demonstrated that in the presence of *Ec*-SSB, Pol III HE could displace short, but not long, RNA primers. SD synthesis by Pol III has the potential to hinder normal Okazaki fragment maturation. Would the presence of Pol I or longer RNA primers facilitate Okazaki fragment maturation? Additionally, an endonuclease mechanism involving RNA primer removal by RNase HI or RNase HII, instead of Pol I, has been proposed; the RNase Hs are enzymes that remove RNA when it is hybridized to DNA. Does RNase H provide a "backup" mechanism for Pol I in *E. coli*? This Chapter will focus on resolving some of these issues.

4.1.1 ssDNA-binding properties of *Ec*-SSB

The way in which *Ec*-SSB binds to ssDNA is affected by various factors including buffer condition, temperature, the integrity of its C-terminus, *etc.*

The ionic strength of the buffer influences the binding of *Ec*-SSB to ssDNA. An early study showed addition of 320 mM NaCl decreased the strength of association of an *Ec*-SSB:poly(dT) complex by about a factor of 40 (Molineux *et al.,* 1975). Another study reported a large drop of binding affinity of *Ec*-SSB for ssDNA by increasing the NaCl concentration from 100 to 300 mM (William and James, 1975). C-terminally truncated *Ec*-SSBs, including *Ec*-SSBC* (N-terminal fragment after chymotryptic cleavage after Trp-135) and *Ec*-SSBT* (tryptic cleavage after Arg-115), bind so strongly to ssDNA-cellulose that it required 6 M guanidine hydrochloride to separate the complex, whereas it only need 1–2 M NaCl for full-length *Ec*-SSB to dissociate (Williams *et al.,* 1983). This behaviour is similar to the effect of truncation of phage T4 SSB (Williams & Konigsberg, 1978).

The binding affinity of *Ec*-SSB for ssDNA is affected by buffer conditions as well as the integrity of its C-terminus, especially the last 8 residues. Williams *et al.* (1983) reported the K_D (derived by using fluorescence quenching methodology) for the *Ec*-SSB:poly(dT), *Ec*-SSBC*:poly(dT) and *Ec*-SSBT*:poly(dT) complexes in buffer containing 50 mM Na_2HPO_4, pH 7.7, 1 mM EDTA and 1 mM β-mercaptoethanol at 25˚C to be 510 nM, 33 nM and 10 nM, respectively. Very similar values were obtained with circular phage fd ssDNA. A K_D of 30 nM was obtained when the *Ec*-SSB:poly(dT) interaction was measured in a different buffer (20 mM Tris-HCl, pH 7.4) at lower temperature (5˚C). This was in good agreement with an earlier study that reported a K_D of 1 nM for the *Ec*-SSB:poly(dT) interaction using the same fluorescence quenching method in the same buffer condition (Molineux *et al.,* 1975). When Williams *et al*. used another methodology, poly[d(AT)] melting temperature depression, to measure K_D in another buffer (10 mM Tris-HCl, pH 8.1, 0.1 mM EDTA and 150 mM NaCl), they observed a large decrease (more than 100-fold) of K_D for the *Ec*-SSBC* complex. The association constants were 1.8, 0.03 and 85 nM for the single-stranded poly[d(A-T)] complex formed with *Ec*-SSB, *Ec*-SSBC* and *Ec*-SSBT*, respectively. Interestingly, the affinity of *Ec*-SSBT* for ssDNA almost stayed the same, as did that for *Ec*-SSB.

This may be due to a contribution of the residues between 116 and 135 of *Ec*-SSB to the stability of the *Ec*-SSB tetramer (Williams *et al.* 1983). It is noteworthy that various studies have shown that *Ec*-SSBC* binds ssDNA with higher affinity than does wild type *Ec*-SSB.

It was found more recently that the last eight residues of *Ec*-SSB have an inhibitory effect on ssDNA binding, and this effect is weakened when the salt concentration increases (Kozlov *et al.*, 2010). Varied values of K_D for complexes of wild-type *Ec*-SSB and ssDNA have been reported from other studies. Krauss *et al.* (1981) reported a value of 30 nM with $(dT)_{35}$ in buffer containing 20 mM potassium phosphate, pH 7.4, 200 mM KCl, and 1 mM EDTA at 8˚C by using fluorescence titration, while Ruyechan *et al.* (1975) reported K_D = 0.38–0.76 nM using electron microscopy for *Ec*-SSB:λ ssDNA in 10 mM Tris-HCl buffer, pH 7.8, with 1 mM EDTA and 150 mM NaCl at 4˚C.

Ec-SSB has DNA helix-destabilizing activity, which is enhanced by removal of its C-terminus (Chase *et al.*, 1984). This passive temperature-dependent activity results from SSB progressively trapping thermally-unwound termini of dsDNA. It has also been shown that the apparent DNA unwinding activity of the phage T4 gp32 SSB protein was enhanced by removing its C-terminus (Moise & Hosoda, 1976; Hosoda & Moise, 1978; Greve *et al.*, 1978). In the case of *Ec*-SSB, *Ec*-SSBT* and *Ec*-SSBC*, the poly[d(AT)] melting temperature was lowered by 8.5, 15 or 19.5˚C, respectively, in buffer containing 10 mM Tris-HCl, pH 8.1, 0.1 mM EDTA and 150 mM NaCl (Williams *et al.* 1983). The melting temperature of poly[d(AT)] itself was reported to be 66˚C.

The dissociation of ssDNA from the *Ec*-SSB:ssDNA complex was measured in early times by looking at the transfer of *Ec*-SSB from labelled to non-labelled heat-denatured intact (or sonicated) phage T7 ssDNA in 50 mM Tris-HCl, pH 7.5 with 1 mM EDTA at 25˚C (Williams *et al.,* 1983). No dissociation was observed for the *Ec*-SSB:T7 ssDNA or *Ec*-SSBC*:T7 ssDNA complexes in 2 h. This is different from another study that showed 50% dissociation of *Ec*-SSB from *Ec*-SSB:fd ssDNA in 300 min, measured by glycerol gradient sedimentation at 5˚C in buffer containing 10 mM Tris-HCl, pH 7.6, 0.1 mM EDTA (Molineux *et al.,* 1975). In contrast, 35% of *Ec*-SSBT* was dissociated from T7 ssDNA in 20 min. However when the ssDNA had been sonicated, it only need 90 s for 50% dissociation of *Ec*-SSBT*:T7 ssDNA(sonicated) complex, 5 min for the

Ec-SSBC*:T7 ssDNA(sonicated) complex or 450–600 min for *Ec*-SSB:T7-ssDNA (sonicated) (Williams *et al.,* 1983).

More recent studies have shown that the availability of free ssDNA binding sites on *Ec*-SSB determines the transfer rate of *Ec*-SSB from one ssDNA template to another, so that exchange occurs rapidly when DNA is in excess over *Ec*-SSB when SSB is bound to DNA in the $(SSB)_{35}$ mode (Kozlov & Lohman, 2002). In 10 mM Tris-HCl, pH 8.1 and 0.1 mM EDTA at 25˚C, *Ec*-SSB associated with $(dT)_{35}$ [$(SSB)_{35}$ mode] transfers to other ssDNAs much faster than *Ec*-SSB associated on $(dT)_{70}$, where all four ssDNA binding sites are occupied. These transactions of *Ec*-SSB on ssDNA were confirmed more directly by using native-state ESI mass spectrometry in ammonium acetate buffers at neutral pH (Mason *et al.,* 2013.). *Ec*-SSB also shows preference for binding poly(dT) and poly(dA) over poly(dC) (Molineux *et al.,* 1975). Interestingly, *Ec*-SSB also binds to ribohomopolymers [poly(rU)] and to tRNA, although much more weakly than to ssDNA (Molineux *et al.,* 1975).

The Pol III HE is able to move on an *Ec*-SSB-coated ssDNA template to synthesize DNA at a rate of ~750 Nt/s (Stukenberg *et al*., 1991). It is of interest to know how DNA polymerase dissociates SSB bound tightly on the ssDNA ahead of it.

4.1.2 Pol I activity during Okazaki fragment maturation

E. coli Pol I was the first DNA polymerase to be discovered (Kornberg *et al.,* 1956). It can be separated by proteolysis into a small fragment containing the 5'–3' exonuclease domain and a large fragment (Klenow) with 3'–5' proofreading exonuclease and 5'–3' polymerase activities (Ollis *et al.*, 1985; Beese and Steitz, 1991; Ricchetti and Buc, 1993). Although the other activities were already well understood, the 5'–3' exonuclease mechanism was not well characterized until the 1980s. It was shown that, instead of nick translation occurring by sequential removal of dNMPs ahead of the polymerase, the concurrent DNA polymerase activity stimulates the 5'–3' exonuclease to remove not only one but sometimes many nucleotides (Lundquist and Olivera, 1982). Subsequently, the 5'–3' exonuclease domain of Pol I was shown to specifically hydrolyze the phosphodiester bond at the junction of a single-stranded overhang, leaving a nick behind, a process now known as flap endonuclease (FEN) activity. The

nick is closed afterwards by DNA ligase A (**Chapter 1**). This process of coordinated removal of RNA primers and DNA ligation is known as Okazaki fragment maturation. The small fragment of Pol I was identified as a homologue of human FEN1 and yeast RAD27 flap endonucleases in the 1990s (Robins *et al.,* 1994), and consensus was reached for Pol I being the essential protein required for processing RNA primers during Okazaki fragment maturation. Surprisingly, *in vivo* studies later showed that the *polA* gene (encoding Pol I) is dispensable in *E. coli*, although deletion of *polA* leads to high mutation frequencies and a temperature-sensitive phenotype (Nagata *et al.,* 2002; Fukushima *et al.,* 2007). Further examination showed that the 5'–3' exonuclease domain is much more important for the viability of *E. coli* than the rest of Pol I (Joyce & Grindley, 1984; Fukushima *et al.,* 2007), and is conserved in all eubacteria, in a pool of 250 genomes.

The other potential primer processing proteins in *E. coli*, RNase HI and RNase HII, have been shown to be dispensable in the presence of Pol I in living *E. coli* (Fukushima *et al.* 2007). Moreover, the fact that unlike eukaryotic RNase H, *E. coli* RNase H1 can only digest RNA from the 3' to 5' direction and always leaves at least one RNA nucleotide behind (Hogrefe *et al.,* 1990; Crooke *et al.,* 1995) further strengthens the status of Pol I in the Okazaki fragment maturation process. Although the dispensability of *polA* in *E. coli* could in principle be explained in terms of compensation by other analogous genes (Kunst *et al.,* 1997), the identity of these genes are still unknown. In this Chapter, various DNA replication assays were conducted to verify the important role of Pol I and the dispensibility of RNase HI and RNase HII during Okazaki fragment maturation.

4.1.3 Helicase-independent Pol III strand-displacement DNA synthesis

Helicase-independent strand-displacement (SD) DNA synthesis, which is a phenomenon whereby a DNA polymerase displaces one strand of dsDNA with concurrent DNA synthesis on the complementary strand, has drawn a lot of attention in the field, most recently with the demonstration that Pol III HE can carry out such a DNA synthesis reaction under certain conditions (Yuan & McHenry, 2009; Jergić *et al.,* 2013). Although it is not entirely clear what is the function of SD synthesis in bacteria *in vivo,* or whether it might be an aberrant process that needs to be controlled, it has

nevertheless been used successfully *in vitro* as a probe to obtain new information about the protein–protein interactions and protein complex stability of the replisome (*e.g.*, see Jergić *et al.*, 2013). This is because this synthetic reaction shows a requirement for all known component subunits of Pol III HE (except θ), as well as *Ec*-SSB.

A Pol III-τ-ψ-χ-SSB interaction model for *E. coli* Pol III SD synthesis was proposed according to the essential interactions among the components (Yuan & McHenry, 2009). In this model (**Figure 4.1**), *Ec*-SSB bound to the displaced DNA strand interacts through its conserved C-terminal tail with the ψ:χ complex, which is connected to Pol III core by domains III–V of the τ subunit within the clamp loader complex. Current interrogation of this model in our laboratory has led to further understanding of the mechanism. Besides the known α:β interaction, another interaction occurring between the ε proofreading exonuclease subunit of the Pol III core and the β clamp has proven to be essential for stabilizing the Pol III core to stimulate SD (Jergić *et al.*, 2013).

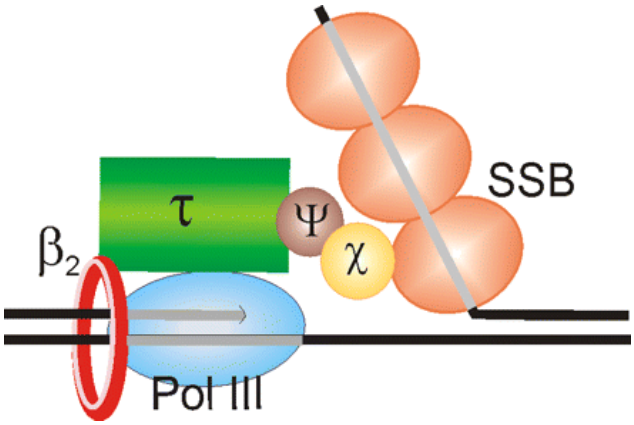

Figure 4.1 *E. coli* Pol III-τ-ψ-χ-SSB model proposed by Yuan & McHenry (2009). This model depicts the Pol III HE SD reaction as being stimulated through the interaction between the C-terminus of *Ec*-SSB and χ. The intersecting areas among various proteins indicate the essential interactions for stimulating SD (from Yuan & McHenry, 2009).

The χ:ψ unit is identified as a 1:1 complex (Xiao *et al.*, 1993b). The χ subunit does not interact with the clamp loader without the ψ subunit, and ψ interacts with all three of the γ/τ subunits of the clamp loader through its 24 amino acid N-terminal unstructured portion (Simonetta *et al.*, 2009); this explains the unusual 1:3 (ψ:τ/γ) stoichiometry of these subunits (Xiao *et al.*, 1993b). The ψ:χ complex has been shown to stimulate Pol III activity in higher salt conditions, which is a likely result of its contribution to stabilizing the clamp loader (O'Donnell & Studwell 1990; Xiao *et al.*, 1993b; Kelman *et*

al., 1998). Since the χ:SSB interaction is so far the only identified interaction between *Ec*-SSB and the rest of the Pol III HE (reviewed by Pomerantz and O'Donnell, 2007), it is likely that *Ec*-SSB stimulates Pol III activity through this interaction. There are many data that indicate this is indeed true (Weiner *et al.,* 1975; Scott *et al.,* 1977; LaDuca *et al.,* 1983; Kelman *et al.,* 1998). However we are still unable to explain how the tight ssDNA:SSB complex ahead of the polymerase stimulates instead of blocks the DNA polymerization reaction. SSB is known to disrupt secondary structures in ssDNA, which might otherwise impede the action of the polymerase, but there must also be an uncharacterized mechanism for disruption of the ssDNA:SSB interaction. In this Chapter, *in vitro* DNA replication assays were carried out to probe the interactions among the components of interest, and various new roles of those proteins were revealed.

There are more and more studies showing SD activities of polymerases from various organisms, although the mechanism is not entirely clear. Studies have implied that the inefficiency of SD by DNA polymerase is probably caused by the fork regression pressure (Manosas *et al.,* 2012). This study, using magnetic tweezers, showed that applying opposite pulling forces >16 pN on the two strands of long hairpin DNA can separate them. Application of a 10 pN applied force on the hairpin DNA stimulated SD by both the phage T4 and T7 holoenzymes. However, primer extension was slightly stimulated at forces <6 pN and hindered at >6 pN. This implies that 16 pN is probably the force proteins exert on the replication fork during SD synthesis, and primer extension probably needs a more stringent conformation of the polymerase–DNA complex. Other studies show that DNA SD can in fact take place in the absence of proteins like helicases, polymerases or recombinases under conditions where one complementary DNA strand can replace another (Zhang & Seelig, 2011). This probably occurs by transient thermal melting of the DNA, allowing strand invasion (Frank-Kamenetskii, 1987; Gueron *et al.,* 1987; Gueron & Leroy, 1995; Russu *et al.,* 2004). Like *Ec*-SSB's helix-destabilizing activity, strand-displacement synthesis by polymerases could similarly rely on the protein trapping transiently strand-separated species.

4.2 Materials and methods

4.2.1 Plasmids directing expression of mutant *Ec*-SSB, mutant F-SSB, their fusion proteins, and *Ec*-SSB~KikGR-His_6

Plasmids pPH180 (encoding *Ec*-SSBΔC27, also called SSB151) and pSM823 (encoding F-SSBT*, also called F-SSBΔC64), which express proteins under the control of temperature inducible phage λ promoters were gifts of Drs Phillip Hendry and Shadi Moghaddas, respectively.

Plasmid pYW1656 (directing expression of a gene encoding F-SSB–*Ec*-SSBc, with the eight C-terminal residues of F-SSB, -GFSDDIPF, mutated into the corresponding residues of *Ec*-SSB, DFDDDIPF; **Figure 3.3**) and pYW1660 (directing expression of the reciprocal mutant, *Ec*-SSB–F-SSBc) were constructed by SDM PCR (**Section 2.3.12**) using template plasmids pPH302 and pND72 (**Section 3.2.1.1**), respectively. The primer pair used for constructing the gene encoding F-SSB–*Ec*-SSBc was 589 (5'-GAGGGTGACGATTACGACTTTGATGACGATATCCCGTTCTGA) and 590 (5'-TCAGAACGGGATATCGTCATCAAAGTCGTAATCGTCACCCTC), while the pair used to make the gene encoding *Ec*-SSB–F-SSBc was 587 (5'-AACGAGCCGCCGA-TGGGTTTTTCTGATGACATTCCGTTCTGA) and 588 (5'-TCAGAACGGAATGTC-ATCAGAAAAACCCATCGGCGGCTCGTT). Plasmid pPH396 (encoding *Ec*-SSB–F-SSB with 79 *Ec*-SSB N-terminal residues spliced to 99 F-SSB C-terminal residues) and pPH397 (encoding F-SSB–*Ec*-SSB with 79 F-SSB N-terminal residues spliced to 98 *Ec*-SSB C-terminal residues) were gifts from Dr. Phillip Hendry. All of these plasmids direct expression of genes under control of temperature inducible phage λ promoters. Schematic maps of all *Ec*-SSB and F-SSB fusion proteins are shown in **Figure 4.2**.

Plasmid pCM1444, a derivative of pND706 (Love *et al.*, 1996) containing a gene construct encoding the N-terminal KigGR fusion protein KikGR~*Ec*-SSB under control of temperature inducible phage λ promoters was a gift from Dr. Claire Mason. It was used to make the plasmid pYW1653 encoding the C-terminal fusion *Ec*-SSB~KikGR-His_6. In pCM1444, the *mKikGR* gene (encoding a monomeric photo-switchable fluorescent protein; Habuchi *et al.,* 2008) is contained between unique *Nde*I and *Mlu*I

restriction sites, and the *ssb* gene (encoding *Ec*-SSB) is between unique *Bam*HI and *Eco*RI sites. A DNA fragment encoding a linker "~" (TRESGSIGS) was introduced between the *Mlu*I and *Bam*HI sites. The gene encoding KikGR-His_6 with a His_6 tag followed by a stop codon (TAA) was obtained by PCR with pCM1444 as template and primers 584 (5'-AAAAAA**GGATCC**AGTGTGATTACATCAGAAATGAAGATC-GAGCTG, bold letters indicate an incorporated *Bam*HI site) and 585 (5'-AAAAAA-**GAATTC***TTA*GTGATGGTGATGGTGATGGGCTTCAAATTCATACTTGGCGCCCC T, bold letters indicate an incorporated *Eco*RI site and italics the complement of the stop codon; the His_6 encoding sequence is underlined). The PCR product was digested by restriction enzymes *Bam*HI and *Eco*RI, and then ligated with vector pCM1444 (digested with the same restriction enzymes to remove the *ssb* gene) to obtain pYW1659, encoding KikGR~KikGR-His_6 (selected in SURE 2 supercompetent cells; **Section 2.1.1**). This plasmid was then extracted and digested with restriction enzymes *Nde*I and *Mlu*I, and then ligated with the *ssb* gene, which had in turn been amplified by PCR using primers 581: 5'-AAAAAAAAAA**CATATG**GCCAGCAGAGGCGTAAA-CAAGGTTATT (bold letters indicate an incorporated *Nde*I site containing an ATG start codon) and 582: 5'-AAAAAA**ACGCGT**GAACGGAATGTCATCATCAAAGT-CCATCGG (bold letters indicate an incorporated *Mlu*I restriction site) with pND72 as template, and digested with the same restriction enzymes. The resulting plasmid pYW1653 containing the *Ec*-SSB~KikGR-His_6 encoding construct.

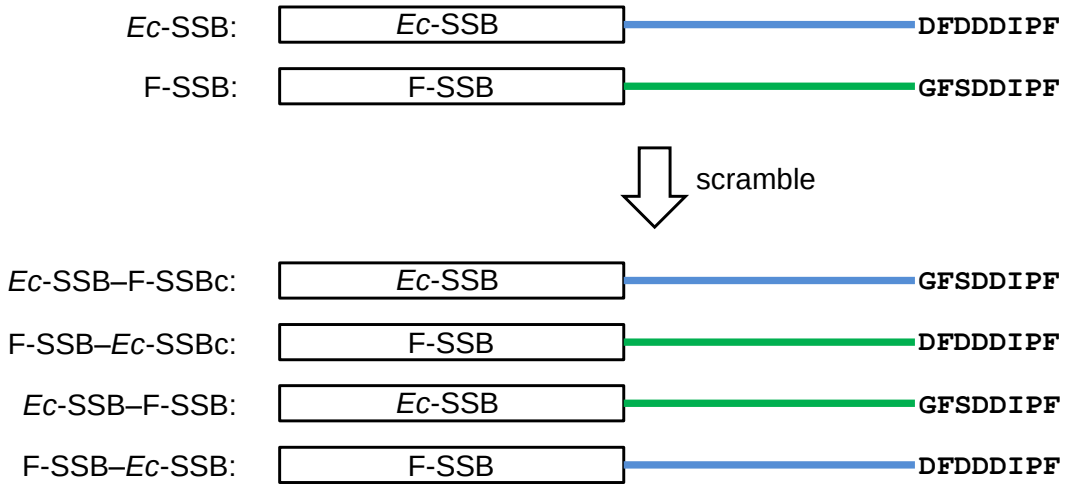

Figure 4.2 Schematic maps of *Ec*-SSB, F-SSB and their chimeric derivatives used in this work. The boxes represent the conserved N-terminus (79 residues) of *Ec*-SSB or F-SSB. The blue and green lines represent the C-termini of *Ec*-SSB (98 residues) and F-SSB (99 residues), respectively. The sequences of the last 8 residues of *Ec*-SSB and F-SSB are shown at the right side of the lines. The name used for each fusion protein is shown at the left side of each schematic map.

4.2.2 Overproduction and purification of *Ec*-SSB and F-SSB chimeric proteins

The λ-promoter plasmids encoding *Ec*-SSBΔC27, F-SSBT*, *Ec*-SSB–F-SSBc, F-SSB–*Ec*-SSBc, *Ec*-SSB–F-SSB, F-SSB–*Ec*-SSB, and *Ec*-SSB~KikGR-His_6 were all transformed into the *E. coli* strain BL21(λDE3)*recA* for overexpression. The procedure for overexpression is described in **Section 3.2.1.2**.

4.2.2.1 Purification of *Ec*-SSBΔC27

For purifying *Ec*-SSBΔC27, the *E. coli* cell pellets (7.5 g) were resuspended to 0.07 g/mL of lysis buffer (50 mM Tris-HCl, pH 8.0, 1 mM EDTA, 1 mM DTT and 10% glycerol) additionally with 150 mM NaCl, and the cells were lysed by being passed through a French press at 12000 psi.

Following centrifugation for 40 min at 35000 × *g*, the supernatant containing the soluble *Ec*-SSBΔC27 was stirred with 1.5% streptomycin sulphate for 30 min at 4˚C to precipitate DNA, which was removed by centrifugation in 35000 × *g* for 30 min. To the supernatant was added 0.243 g/mL of $(NH_4)_2SO_4$ with stirring for 30 min at 4˚C, to precipitate the *Ec*-SSBΔC27.

After centrifugation at 35000 × *g* for 30 min, precipitated proteins containing the *Ec*-SSBΔC27 were resuspended in lysis buffer with 300 mM NaCl, and then dialyzed against two changes (3 h each) of 2 L of lysis buffer without NaCl. *Ec*-SSBΔC27 is very insoluble and precipitated in the bottom of the dialysis bag. The sample including the precipitate was centrifuged at 35000 × *g* for 30 min.

The pellet containing *Ec*-SSBΔC27 was resuspended in a minimum volume (~1 mL) of lysis buffer containing 500 mM NaCl, and then added drop wise to Toyopearl DEAE resin that had been equilibrated in lysis buffer. The resin was stirred gently for 20 min at 4˚C, and then packed into a column (2.5 × 16 cm). The column was washed with 100 mL of lysis buffer followed by a linear gradient (400 mL) of 30–1400 mM NaCl in lysis buffer. Fractions containing *Ec*-SSBΔC27 were pooled and concentrated by $(NH_4)_2SO_4$ precipitation. The sample was then dialyzed into lysis buffer containing 500 mM NaCl.

The sample was gel filtered through a Hiload^{TM} 26/60 Superdex^{TM} 75 column (GE Healthcare) equilibrated in the same buffer. Fractions containing pure *Ec*-SSBΔC27 were pooled and dialyzed into storage buffer (50 mM Tris-HCl, pH 8.0, 1 mM EDTA, 1 mM DTT, 30% glycerol and 500 mM NaCl), and then stored at –80˚C.

4.2.2.2 Purification of F-SSBT*, *Ec*-SSB–F-SSBc, F-SSB–*Ec*-SSBc, *Ec*-SSB–F-SSB and F-SSB–*Ec*-SSB

The purification procedure for F-SSBT* was as the same as that for *Ec*-SSBT* (**Section 3.2.1.6**) except that 2 mM DTT was present in all the buffers used. The purification procedures for *Ec*-SSB–F-SSBc and F-SSB–*Ec*-SSB were the same as that for *Ec*-SSB (**Section 3.2.1.4**) except that all buffers used for F-SSB–*Ec*-SSB contained 2 mM DTT. The purification procedures for F-SSB–*Ec*-SSBc and *Ec*-SSB–F-SSB were the same as that for F-SSB (**Section 3.2.1.7**).

4.2.2.3 Purification and validation of [*Ec*-SSB]$_{2.6}$[*Ec*-SSB~KikGR-His$_6$]$_{1.4}$

To purify [*Ec*-SSB]$_{2.6}$[*Ec*-SSB~KikGR-His$_6$]$_{1.4}$, the *E. coli* cells containing over-expressed *Ec*-SSB~KikGR-His$_6$ (7.5 g) were resuspended to 0.07 g/mL in lysis buffer (50 mM Tris-HCl, pH 8.0, 1 mM EDTA, 2 mM DTT, 10% sucrose, 2 M NaCl, and 0.5 mM PMSF), and the cells were lysed by being passed through a French press at 12000 psi. After centrifugation for 40 min at 35000 × *g*, the pellet containing insoluble *Ec*-SSB~KikGR-His$_6$ was washed by pipetting in 20 mL of buffer A (50 mM Tris-HCl, pH 7.6, 1 mM EDTA, 2 mM DTT and 500 mM NaCl). The sample was then centrifuged in the same buffer. This washing procedure was repeated three times in buffer A and another three times in buffer A without NaCl. This procedure would presumably remove large amount of lipid, DNA and contaminant proteins.

The pellet was then resuspended in 2 mL of buffer A without NaCl followed by slowly adding 6 M guanidine hydrochloride (~5 mL) until the sample became transparent. Subsequently, a ~25-fold molar excess of purified *Ec*-SSB (as assessed by SDS-PAGE) was added and the sample was dialyzed into refolding buffer (50 mM Tris-HCl, pH 7.6, 1 mM DTT, 30% glycerol and 500 mM NaCl) to refold the SSB proteins.

After centrifugation for 40 min at 35000 × *g*, the supernatant was injected into a 1 mL Histrap HP column (GE Healthcare). The column was washed with 5 mL of refolding

buffer followed by 10 mL of buffer B (refolding buffer + 500 mM imidazole). [*Ec*-SSB]$_{2.6}$[*Ec*-SSB~KikGR-His$_6$]$_{1.4}$ eluted 1 mL after injection of buffer B. The protein samples were dialyzed in storage buffer (50 mM Tris-HCl, pH 7.6, 3 mM DTT, 1 mM EDTA, 40% glycerol and 500 mM NaCl) and analyzed by SDS-PAGE. The ratio of 2.6:1.4 was determined by comparison of the protein sample with a known protein KikGR~*Ec*-SSB purified previously by Dr. Claire Mason (see **Section 4.3.9.2**).

4.2.3 Plasmids for overexpression of *E. coli* Pol I, ligase A, RNase HI and RNase HII

Four proteins (Pol I, ligase A, RNase HI and RNase HII) possibly involved in *E. coli* Okazaki fragment maturation were purified. They were used in DNA replication assays as described in this Chapter. Additionally, RNase HI and RNase HII were used in the SPR study described in **Chapter 3**.

Chromosomal DNA used as the DNA template for PCR amplification of the genes *ligA*, *rnhA* and *rnhB*, respectively encoding *E. coli* ligase A, RNase HI and RNase HII was extracted from the *E. coli* K12 strain AN1459 (**Section 2.1.1**) by use of a Miniprep kit (Qiagen).

Forward PCR primers for amplification of *ligA*, *rnhA* and *rnhB* were designed to incorporate an ATG start codon as part of an *Nde*I restriction site (5'-CATATG). Reverse PCR primers were designed to incorporate an *Eco*RI restriction site (5'-GAATTC) just after a TAA stop codon. Sequences of oligonucleotide primers are shown below with *Nde*I and *Eco*RI restriction site highlighted in bold letters:

Proteins	Oligonucleotide No.	Oligonucleotide sequence (5' to 3')
RNase HI	497	AAAAAAAA**CATATG**CTTAAACAGGTAAAATTTTC
	498	AA**GAATTC**TTAAACTTCAACTTGGTAGCC
RNase HII	499	AAAAAAAA**CATATG**ATCGAATTTGTTTATCCG
	500	AA**GAATTC**TTAGGACGCAAGTCCCAGTGC
ligase A	501	AAAAAAAA**CATATG**GAATCAATCGAACAACAAC
	502	AA**GAATTC**TTAGCTACCCAGCAAACGCAG

The PCR products were separated by electrophoresis following digestion with the restriction enzymes *Nde*I and *Eco*RI, and were extracted from the agarose gel. The PCR

fragments of *ligA, rnhA* and *rnhB* were inserted between the *Nde*I and *Eco*RI sites in the T7 promoter vector pETMCSI (**Section 2.1.2**) to generate plasmids pYW1496, pYW1495 and pYW1494, respectively. The integrity of the inserts was in each case confirmed by nucleotide sequence determination.

Plasmid pJC666, containing the *polA* gene under control of phage λ p_R and p_L promoters, was a gift of Dr. Jeffrey Crowther (Australian National University).

4.2.4 Overproduction and purification of ligase A, RNase HI, RNase HII and DNA polymerase I

Plasmids pYW1496, pYW1495 and pYW1494 containing *ligA, rnhA* and *rnhB* genes were transformed into *E. coli* strain BL21(λDE3)/pLysS, which has the T7 RNA polymerase gene integrated in the chromosome under control of the *lacP* promoter. The *polA*$^+$ plasmid pJC666 was transformed into *E. coli* strain AN1459. Induction of expression was tested and perfected first on a small scale in 20 mL of LB medium supplemented with the required antibiotics (ampicillin and/or chloramphenicol). Large scale cultures were prepared as follows. A single colony containing each of constructs of *ligA, rnhA* and *rnhB* was inoculated into 3 L of LB medium with 100 mg/L ampicillin and 35 mg/L chloramphenicol, and then shaken vigorously at 37˚C until the value of OD_{600} reached 0.7. Then 0.5 mM IPTG was added to each culture, which then underwent 3 h incubation at 37˚C. A single colony of AN1459 containing pJC666 (*polA*$^+$) was inoculated into 3 L of LB medium with 100 mg/L ampicillin, and shaken vigorously in 30˚C until OD_{600} reached 0.7. Then the culture was heated quickly to 42˚C, and incubated for 3 h. *E. coli* cells were collected by centrifugation at 17000 × *g* for 8 min, and then the pellets were stored at –80˚C.

4.2.4.1 Purification of ligase A

The 4.5 g of *E. coli* cells collected by centrifugation were resuspended in 60 mL of lysis buffer (50 mM Tris-HCl, pH 7.6, 10 mM spermidine, 1 mM EDTA, 1 mM DTT, 10% glycerol, 0.5 mM PMSF and 20 mM NaCl). A cell-free lysate (Fraction I) was obtained from the bacteria by passing the suspension through a French press at 12000 psi. The lysate was then centrifuged for 25 min at 35000 × *g* to obtain the supernatant with

soluble ligase A. $(NH_4)_2SO_4$ (0.30 g/mL of supernatant) was added, and the precipitate collected by centrifugation at 35000 × *g* for 25 min.

The pellet was resuspended in 10 mL of buffer A (50 mM Tris-HCl, pH 7.6, 1 mM EDTA, 1 mM DTT and 10% glycerol) supplemented with 20 mM NaCl, and then dialyzed against two changes (3 h each) of 2 L of buffer A + 150 mM NaCl to obtain Fraction II.

Fraction II was applied at 1 mL/min to a column (2.5 × 16 cm) of Toyopearl DEAE-650M resin that had been equilibrated in buffer A + 150 mM NaCl. Proteins that did not bind to the column were pooled and dialyzed against two changes (3 h for each change) of 2 L of buffer A + 20 mM NaCl to obtain Fraction III, which was subsequently applied to the same column with the same resin equilibrated in buffer A + 20 mM NaCl. The column was washed with 80 mL of the same buffer followed by application of a linear gradient (420 mL) of 20–350 mM NaCl in buffer A. Ligase A eluted between 100 and 200 mM NaCl. Fractions containing ligase A were pooled and dialyzed against two changes (3 h each) of 2 L of buffer A, to obtain Fraction IV.

Fraction IV was applied at 1 mL/min to a Mono Q 10/100 GL column (8 mL), which had been equilibrated in buffer A + 20 mM NaCl. The column was washed with 24 mL of the same buffer, followed by a linear gradient (120 mL) of 20–800 mM NaCl in buffer A. Ligase A eluted at about 260 mM NaCl. Fractions containing ligase A were pooled and dialyzed against two changes (3 h each) of 2 L of buffer C (50 mM Na.MES, pH 6.5, 1 mM EDTA, 1 mM DTT, and 10% glycerol), to obtain Fraction V.

Fraction V was applied at 1 mL/min to a column (2.5 × 13 cm) of phosphocellulose P11 (Whatman), which had been equilibrated in buffer B (30 mM sodium phosphate, pH 6.5, 1 mM EDTA, 1 mM DTT and 10% glycerol) supplemented with 20 mM NaCl. The column was washed with 90 mL of the same buffer followed by a linear gradient (480 mL) of 20–400 mM NaCl in buffer B. Ligase A eluted at about 160 mM NaCl. Fractions containing highly-purified ligase A were pooled and concentrated by ammonium sulphate precipitation (**Section 2.4.6**) and stored at –80˚C.

4.2.4.2 Purification of Pol I

The 4.0 g of *E. coli* cells collected by centrifugation were resuspended in 60 mL of lysis

buffer (50 mM Tris-HCl, pH 7.6, 10 mM spermidine, 1 mM EDTA, 1 mM DTT, 10% glycerol, and 0.5 mM PMSF), and lysed by being passed through a French press at 12000 psi. After centrifugation, the supernatant containing soluble Pol I was dialyzed into buffer A (50 mM Tris-HCl, pH 7.6, 1 mM EDTA, 1 mM DTT and 10% glycerol) with 160 mM NaCl to yield Fraction I.

Fraction I was applied at 1 mL/min to a column (2.5 × 16 cm) of Toyopearl DEAE-650M resin which had been equilibrated in buffer A + 160 mM NaCl. Proteins that did not bind to the column were pooled and dialyzed against two changes (3 h each) of 2 L of buffer A to obtain Fraction II, which was subsequently applied to the same column with the same resin equilibrated in buffer A. The column was washed with 90 mL of the same buffer followed by a linear gradient (480 mL) of 0–300 mM NaCl in buffer A. Pol I eluted at about 140 mM NaCl. Fractions containing Pol I were pooled and dialyzed against two changes (3 h each) of 2 L of buffer B (20 mM sodium phosphate, pH 6.5, 1 mM DTT, and 10% glycerol), to obtain Fraction III.

Fraction III was applied at 1 mL/min to a column (2.5× 13 cm) of phosphocelullose P11, which had been equilibrated in buffer B. The column was washed with 70 mL of the same buffer followed by a linear gradient (420 mL) of 20–200 mM sodium phosphate, pH 6.5. Pol I eluted between 140 and 160 mM sodium phosphate. To the pooled fractions containing Pol I (Fraction IV) was added 0.40 g/mL $(NH_4)_2SO_4$ and the precipitate of Pol I was collected by centrifugation at 35000 × *g* for 25 min. Precipitated Pol I was resuspended in storage buffer (30 mM Tris-HCl, pH 7.6, 1 mM DTT, 1 mM EDTA, 20% glycerol and 150 mM NaCl), and then dialyzed in 2 L of the same buffer. The purified protein was stored at –80˚C.

4.2.4.3 Purification of RNase HI

The 5.5 g of *E. coli* cells collected by centrifugation were resuspended in 60 mL of lysis buffer (50 mM Tris-HCl, pH 7.6, 10 mM spermidine, 1 mM EDTA, 1 mM DTT, 10% glycerol, 0.5 mM PMSF and 20 mM NaCl), and lysed by being passed through a French press (12000 psi). Centrifugation for 25 min at 35000 × *g* yielded a lysate with soluble RNase HI. The supernatant was dialyzed against two changes (3 h each) of 2 L of buffer A (50 mM Tris-HCl, pH 7.6, 1 mM EDTA, 1 mM DTT and 10% glycerol) supplemented with 20 mM NaCl to obtain Fraction I.

Fraction I was applied at 1 mL/min to a column (2.5 × 16 cm) of Toyopearl DEAE-650M resin that had been equilibrated in buffer A + 20 mM NaCl. The column was washed with 80 mL of the same buffer followed by a linear gradient (300 mL) of 20–350 mM NaCl in buffer A. RNase HI eluted between 20 and 100 mM NaCl. Fractions containing RNase HI were pooled and dialyzed against two changes (3 h each) of 2 L of buffer A, to obtain Fraction II.

Fraction II was applied at 1 mL/min to a column (2.5 × 13 cm) of phosphocellulose, which had been equilibrated in buffer A + 20 mM NaCl. The column was washed with 90 mL of the same buffer, followed by a linear gradient (480 ml) of 20–400 mM NaCl in buffer A. RNase HI eluted between 340 and 400 mM NaCl. Fractions containing RNase HI were pooled and dialyzed in the storage buffer (30 mM Tris-HCl, pH 7.6, 1 mM DTT, 1 mM EDTA, 20% glycerol and 150 mM NaCl), and stored at –80˚C.

4.2.4.4 Purification of RNase HII

The 5.5 g of *E. coli* cells collected by centrifugation were resuspended in 60 mL of lysis buffer (50 mM Tris-HCl, pH 7.6, 10 mM spermidine, 1 mM EDTA, 1 mM DTT, 10% glycerol, 0.5 mM PMSF and 20 mM NaCl) and lysed using a French Press (12000 psi). Centrifugation for 25 min at 35000 × *g* yielded a lysate with soluble RNase HII. The supernatant was dialyzed against two changes (3 h each) of 2 L of buffer A (50 mM Tris-HCl, pH 7.6, 1 mM EDTA, 1 mM DTT and 10% glycerol) to obtain Fraction I.

Fraction I was applied at 1 mL/min to a column (2.5 × 16 cm) of Toyopearl DEAE-650M resin that had been equilibrated in buffer A. The column was washed with 90 mL of the same buffer followed by a linear gradient (480 mL) of 0–320 mM NaCl in buffer A. RNase HII eluted between 0 and 160 mM NaCl. Fractions containing RNase HII were pooled and dialyzed against two changes (3 h each) of 2 L of buffer A, to obtain Fraction II (140 mL).

Ammonium sulphate (56 g) was added into Fraction II, which was then centrifuged at 35000 × *g* for 25 min. The precipitated proteins were resuspended in 30 mL of buffer B (50 mM Tris-HCl, pH 8.3, 1 mM EDTA, 1 mM DTT and 10% glycerol), and dialyzed against two changes (3 h each) of 2 L of buffer B, to obtain Fraction III.

Fraction III was applied at 1 mL/min to a Mono Q 10/100 GL column (8 mL), which

had been equilibrated in buffer B. The column was washed with 24 mL of the same buffer followed by a linear gradient (120 mL) of 0–350 mM NaCl in buffer B. RNase HII eluted between 0 and 20 mM NaCl. Fractions containing RNase HII were dialyzed against two changes (3 h each) of 2 L of buffer C (50 mM MES, pH 6.5, 1 mM EDTA, 1 mM DTT and 10% glycerol), to obtain Fraction IV.

Fraction IV was applied at 1 mL/min to a Mono S 5/50 GL column (1 mL), which had been equilibrated in buffer C. The column was washed with 5 mL of the same buffer followed by a linear gradient (20 mL) of 0–400 mM NaCl in buffer C. RNase HII eluted between 180 and 220 mM NaCl. Fractions containing RNase HII were pooled and dialyzed against 2 L of storage buffer (30 mM Tris-HCl, pH 7.6, 1 mM DTT, 1 mM EDTA, 20% glycerol and 150 mM NaCl). The purified protein was stored at –80˚C.

4.2.5 Subunits of DNA polymerase III holoenzyme

The Pol III clamp loader subunits (including τ, γ, δ, δ') and $\gamma_3\delta\delta'$ clamp loader complex were purified using previously described protocols: γ (Ozawa *et al*, 2005); τ, δ and δ' (Tanner *et al*, 2008); $\gamma_3\delta\delta'$ (Jergić *et al.*, 2013). The Pol III α subunit was purified using a new procedure with a final affinity chromatography step devised by Mr. Nicholas Horan (to be published). The Pol III ε, θ and β subunits and αεθ complex were kind gifts of Mr. Horan, and the χψ complex and the $\tau_3\delta\delta'\chi\psi$ clamp loader complex were kind gifts of Dr. Allen Tak Yiu Lo.

4.2.6 SDS-PAGE analysis of purified proteins

SDS-PAGE was used to verify the purity of the proteins prepared for the studies reported here (**Figure 4.3**). With the exception of a few that are shown elsewhere, proteins described in **Chapter 3** were also analyzed in the SDS-PAGE gels shown in **Figure 4.3.**

4.2.7 Preparation of DNA templates

4.2.7.1 Synthetically primed circular phage M13 templates

Wild-type phage M13, a gift of Professor Nick Dixon, was purified from infected culture supernatants by PEG precipitation and banding (twice) in CsCl gradients. Phage were lysed, phenol extracted, and the ssDNA precipitated with ethanol, resuspended in and dialysed extensively against 10 mM Tris.HCl pH 8.0, 1 mM EDTA and stored frozen at –80˚C.

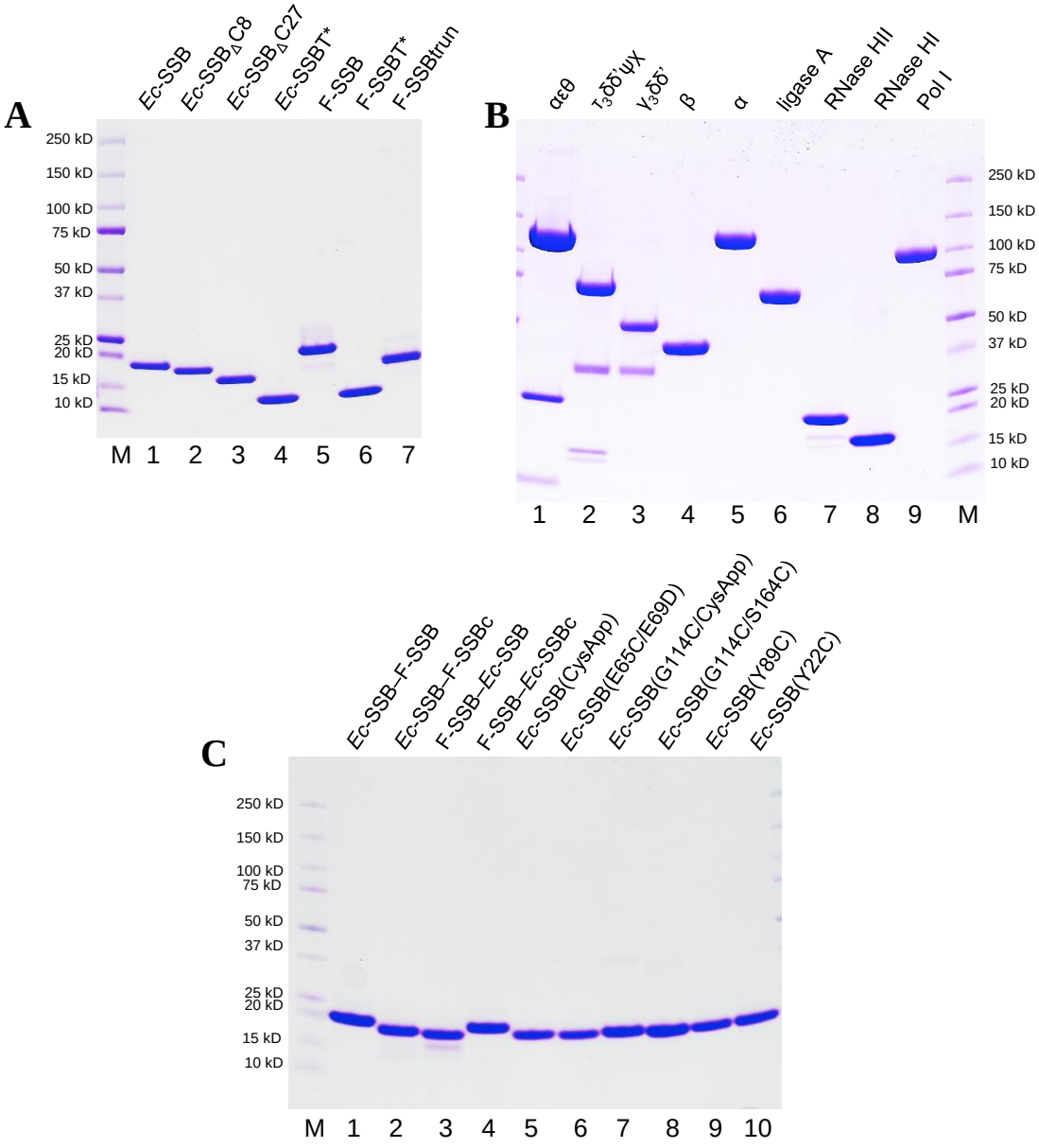

Figure 4.3 SDS-PAGE analysis of all purified proteins [except *Ec*-SSB~KikGR-His$_6$, *Ec*-SSB(K43C), *Ec*-SSBΔC8(K43C) and *Ec*-SSBT*(K43C), which are shown elsewhere]. **A.** Wild type and truncated *Ec*-SSBs and F-SSBs used in DNA binding assays, DNA replication assays and SPR measurements; 5 µg of each protein, as indicated, were loaded in each lane. **B.** Pol III HE subunits and complexes, and proteins involved in Okazaki fragment maturation. Lanes (as indicated) contained 15 µg of αεθ, 7 µg of $\tau_3\delta\delta'\psi\chi$, 5 µg of $\gamma_3\delta\delta'$, 5 µg of β_2, 5 µg of α, 5 µg of ligase A, 5 µg of RNase HII, 5 µg of RNase HI and 5 µg of Pol I. Note that the δ and δ' subunits of the clamp loader complexes (at ~35 kDa) are not resolved. **C.** The *Ec*-SSB and F-SSB fusion proteins and the single-site mutant *Ec*-SSBs involved in the DNA replication assay, SPR measurements and NMR studies; 5 µg of each protein, as indicated, were loaded in each lane.

Synthetic oligonucleotide primers were purchased from GeneWorks (Adelaide, Australia). The standard oligodeoxynucleotide (DNA) primer for flap-priming of M13 ssDNA (6408 Nt) had the sequence: 5'-T_{36}TATGTACCCCGGTTGATAATCAGAA-AAGCCCCA-3', consisting of a 33-mer complementary to wild-type M13 DNA preceded at the 5' end by a non-complementary $(dT)_{36}$ flap. Other oligodeoxy-nucleotide primers used, as specified in the text, were the same 33-mer sequence, without the flap, and a synthetically 5'-phosphorylated version of the same. The 33-Nt oligoribonucleotide (RNA) primer had the sequence: 5'-UAUGUACCCCGGUUGAU-AAUCAGAAAAGCCCCA-3'. The mixed oligoribo-deoxyribonucleotide primers, as described in the text, had the same sequence with *n* ribonucleotides followed by (33 – *n*) deoxyribonucleotides, where *n* = 1, 5, 10, or 15.

To prepare synthetically primed templates, M13 ssDNA (35 nM, as circles) was mixed with 1 μM of the appropriate primer in 30 mM Tris.HCl pH 7.6, 15 mM $MgCl_2$, 130 mM NaCl and 0.1 mM EDTA. The mixture was treated at 55˚C for 10 min and then cooled slowly to room temperature over a period of 8 h. This mixture was diluted ~10-fold in replication assays (final DNA concentrations are specified in the text).

4.2.7.2 Topological forms of plasmid DNAs

Supercoiled, nicked (open-circular, relaxed) and covalently-closed relaxed plasmid DNAs were prepared as follows. Plasmid p1644 (7.3 kb), with a single *Bbv*CI restriction site, was a gift of Dr. Jeff Barrett. A modified restriction enzyme Nb.*Bbv*CI (New England Biolabs) containing only one of two active domains of the wild-type enzyme was used to produce the nicked plasmid.

The supercoiled plasmid was first extracted from 3 L of overnight bacterial culture of an *E. coli recA* strain containing p1644 using a Maxiprep kit (Qiagen) to yield a 6.0 mL sample of DNA at 125 μg/mL, and then further purified by CsCl gradient ultracentrifugation in the presence of ethidium bromide, EtBr (**Section 2.3.11**); 4.8 mL of 60 μg/mL supercoiled plasmid (lower band of two in the gradient) was recovered, and a 400 μL sample was stored at –80˚C. The rest of the sample was nicked in a reaction mixture containing 4.4 mL of the purified supercoiled plasmid, 500 μL of buffer 2 (New England Biolabs) and 55 μL (550 units) of Nb.*Bbv*CI restriction enzyme. The reaction was conducted in 37˚C for 1 h and then quenched by heating (80˚C) for 20

min. Subsequently, the mixture was again separated into two bands by CsCl/EtBr gradient ultracentrifugation; the upper band was collected, yielding 3.4 mL of nicked plasmid at 80 μg/mL. A 1.7 mL sample was stored in –80˚C. The rest (1.7 mL) was religated in a reaction mixture with 94 μL of H_2O, 200 μL of ligase A reaction buffer (500 mM Tris-HCl, pH 7.8, 100 mM $MgCl_2$, 100 mM DTT, 2.6 mM NAD^+, 250 μg/mL BSA), and 6.47 μL of 8 mg/mL ligase A. The reaction was carried out at 30˚C for 30 min and then quenched by adding EDTA to 500 mM and 220 μL of 10% (w/v) SDS. The reaction mixture was then separated by CsCl/EtBr gradient centrifugation, and the lower of the two bands in the centrifuge tube was retained; 2.7 mL of religated plasmid at 10 μg/mL was recovered. The sample was stored in –80˚C.

4.2.8 DNA replication assays

In general, for DNA replication assays, mixtures were first prepared on ice containing all of the components whose concentrations were not varied (except DNA), and these were then distributed to tubes. Additional components were then added, with the DNA added last to a total volume of 10–15 μL, and the tubes were immediately incubated at temperatures as specified in the text and/or figure legends. The final compositions of all assay mixtures are specified in the figure legends. Reactions were generally quenched at indicated times by addition of 11 μl of 200 mM EDTA, pH 8.0, 0.08% (w/v) bromophenol blue, 0.08% (w/v) xylene cyanol, 10% (v/v) glycerol, 2% (w/v) SDS. Reaction mixtures were treated for 2 min at 42˚C, loaded onto a 0.8% agarose gel in 2×TBE buffer and electrophoresis carried out at 45 V for 180 min. Gels were stained in 200 ml of SYBR® gold nucleic acid stain (Tuma *et al*, 1999) at the concentration suggested by the supplier (Invitrogen, Carlsbad, CA), or with 0.5 μg/mL ethidium bromide in TBE buffer, as specified. DNA bands were visualized under 302-nm UV light using a Gel Doc™ XR+ system (Bio-Rad, Hercules, CA). A corresponding DNA template sample was loaded in one lane of each gel as a reference, as well as a sample of GeneRuler™ 1 kb Plus DNA Ladder (Thermo Fisher Scientific).

4.3 Results and discussion

4.3.1 Preparation of topological forms of plasmid DNA templates

Supercoiled, nicked and religated forms of a 7.3 kb plasmid DNA were used in DNA binding assays, ligation assays and DNA replication assays. These various forms can be resolved by agarose gel electrophoresis in the presence or absence of ethidium bromide (EtBr) to analyse the products of various enzymatic reactions (e.g., DNA ligation and topoisomerase activity). Supercoiled (Form I) DNA migrates more rapidly than the relaxed (Form II; nicked or relaxed covalently-closed forms) in the presence or absence of EtBr, while the two different Form II DNAs can be resolved by electrophoresis in the presence of EtBr.

Plasmid p1644 (7.3 kb) with a single *Bbv*CI restriction site was used to make supercoiled, nicked and covalent-closed relaxed (religated) plasmids, which were purified separately by three sequential CsCl density gradient centrifugations steps, beginning with a sample prepared from a bacterial culture using a commercial kit Qiagen Maxiprep). The crude DNA product was analyzed (lane 4 in **Figure 4.4A**) by agarose gel electrophoresis in the absence of EtBr. The DNA sample showed a three-band pattern: contaminating (relaxed) chromosomal DNA migrating most slowly, nicked (relaxed) DNA migrating at an intermediate position, and supercoiled plasmid migrating farthest. The first CsCl/EtBr gradient step was used to purify the negatively supercoiled plasmid (lane 1 in **Figure 4.4A**), which has the highest density (lower band in the gradient) because it intercalates larger amounts of EtBr.

In a second step, the supercoiled DNA was used as substrate for site- and strand-specific nicking by the modified restriction enzyme Nb.*Bbv*CI, containing only one of two active domains of the wild-type enzyme. The relaxed DNA product (lane 2 in **Figure 4.4A**) was again isolated, now as the upper band in a CsCl/EtBr gradient.

Nb.*Bbv*CI produces a single nick in the backbone of one of the DNA double stands, leaving termini with a 5'-phosphate group (5'-P) and a 3'-hydroxyl group (3'-OH) at the restriction site. This provided a substrate for nick sealing by purified *E. coli* ligase A in the third step. The relaxed, covalently closed product is now cabable of becoming

positively supercoiled on intercalation of EtBr, so it bands again at higher density in the CsCl/EtBr gradient.

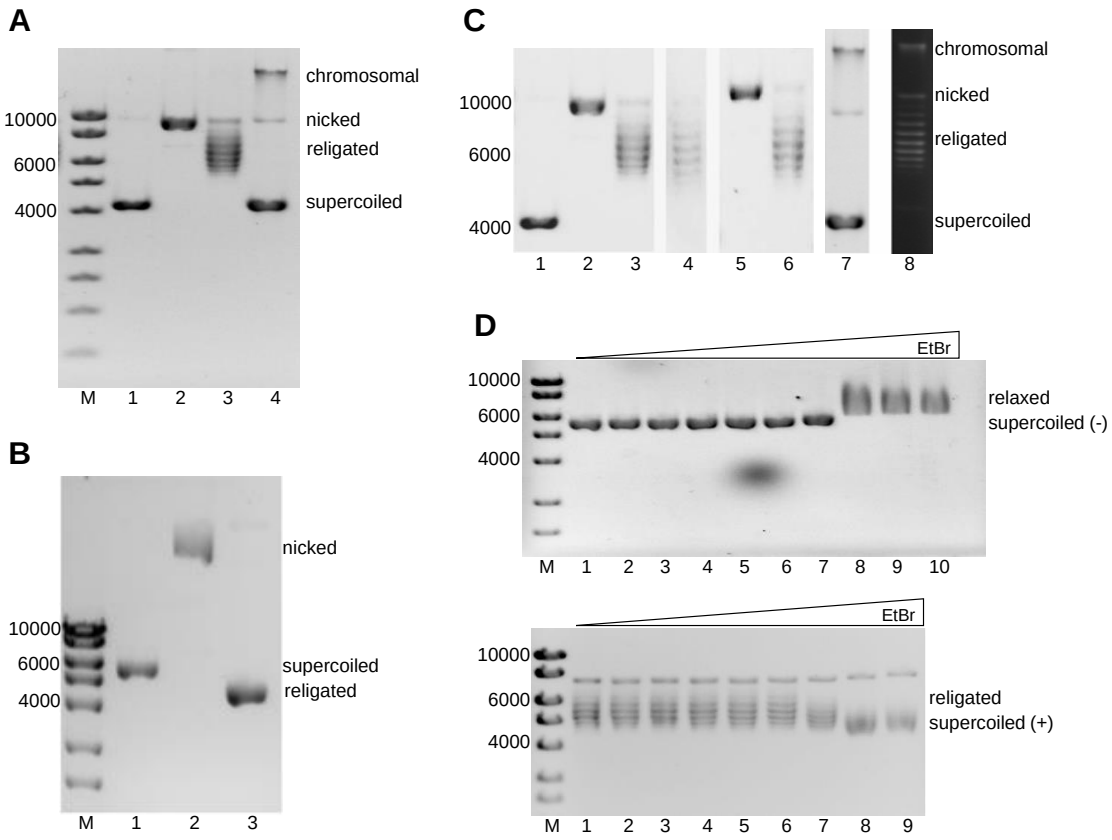

Figure 4.4 Analysis of purified plasmids by agarose gel electrophoresis. **A.** Migration of 20 ng of purified plasmid (untreated plasmid, lane 1), nicked plasmid (lane 2), religated plasmid (lane 3) and unpurified plasmid (lane 4) in a 0.7% agarose gel electrophoresed at 20 V for 7 h. The gel was stained with EtBr after electrophoresis. **B.** Migration of 20 ng of purified DNA samples (lanes 1–3 as in **A**), analyzed in a 1% agarose gel run in the presence of EtBr. The religated plasmid in lane 3 is a single band instead of multibands in lane 3 of **A**. **C.** Migration of 20 ng of purified plasmid (untreated plasmid, lane 1), purified nicked plasmid (lane 2), purified religated plasmid (lane 3), purified religated plasmid after ethanol precipitation (lane 4), purified nicked plasmid after ethanol precipitation (lane 5), religated plasmid of the same sample in lane 5 (lane 6), unpurified plasmid (lane 7) and religated pre-nicked unpurified plasmid (lane 8) in 0.7% agarose gels electrophoresed at 20 V for 8 h. The gels were stained with EtBr after electrophoresis. **D.** EtBr titration with purified plasmid (upper panel) and purified religated plasmid (lower panel) in 0.7% agarose gels electrophoresed in 20 V for 7 h. Upper panel: 80 ng of purified supercoiled plasmid was mixed with (lanes 1–10, respectively): 7×10^{-8}, 7×10^{-7}, 7×10^{-6}, 7×10^{-5}, 7×10^{-4}, 0.007, 0.07, 0.7, 1.0 and 10 μg of EtBr. Lower panel: 40 ng of nicked and religated plasmid was mixed with (lanes 1–9, respectively): 7×10^{-9}, 7×10^{-8}, 7×10^{-7}, 7×10^{-6}, 7×10^{-5}, 7×10^{-4}, 0.007, 0.07, 0.7 μg of EtBr before electrophoresis at 20 V for 7 h. The gels were stained with EtBr after electrophoresis. The numbers on the left of all gel photographs are the size of the markers (linear fragments) in base pairs (bp). Different species (multimer, supercoiled, nicked and religated) of plasmids are labelled on the right side of all panels.

A multi-band pattern of topoisomers was observed for the religated plasmid (lane 3 in **Figure 4.4A**). These bands indicate that the religated plasmid retains a small number of supercoils (either positive or negative), from one to eight, with the distribution centred

on four or five. This was confirmed when the plasmids were analyzed in a 0.7% agarose gel in the presence of EtBr, where the religated plasmid showed a single band (lane 3 in **Figure 4.4B**) due to its becoming fully overwound by intercalation of ethidium. The reason that it migrates slightly faster than the negatively supercoiled plasmid (lane 1 in **Figure 4.4B**) could be because it binds less ethidium than the negatively supercoiled plasmid, due to the retained supercoils (*i.e.*, positive supercoiling). Several assays were carried out in attempts to explain why the religated plasmid was not fully relaxed. One possibility was that residual ethidium remained in the nicked DNA preparation during the religation reaction (generating negative supercoils on its removal), or that the religated plasmid contained residual EtBr (positively supercoiled). To eliminate the latter possibility of EtBr contamination, the ligated sample was purified by ethanol precipitation, which efficiently removes EtBr. The product showed a very similar multi-band pattern of topoisomers (lane 4 in **Figure 4.4C**). The CsCl- purified nicked plasmid was also further purified by ethanol precipitation (lane 5 in **Figure 4.4C**). It was subsequently ligated, and again showed the multi-band pattern (lane 6 in **Figure 4.4C**). To further investigate this, the unpurified supercoiled plasmid (lane 7 in **Figure 4.4C**) was then nicked and religated. The religated unpurified plasmid (lane 8 in **Figure 4.4C**) again showed a similar multi-band pattern of topoisomers as the purified religated plasmid. As EtBr is known to positively supercoil relaxed covalently closed circular dsDNA (Dougherty, 1983), an EtBr titration assay was carried out to determine whether the religated plasmid is positively or negatively supercoiled (**Figure 4.6D**). The upper panel shows that elevating the EtBr concentration to introduce positive supercoils counteracts the supercoiling of the untreated, supercoiled plasmid, which must therefore have intrinsic negative supercoils, as expected. The lower panel in **Figure 4.6D** shows increasing EtBr concentration uniformly caused the purified religated plasmid to migrate faster in the agarose gel. This implies that the religated plasmid must possess a small number of positive supercoils, and intercalation of ethidium further supercoils it. These supercoils appear to arise during the ligation reaction by DNA ligase A, which must overwind the DNA during the ligation reaction. This recalls a recent study showing a transient transformation from B- to A-form DNA during DNA synthesis by eukaryotic polymerase η (Nakamura *et al.,* 2012) and a more relevant study that showed formation of a range of topoisomers during phage T4 ligase activity (Jo *et al.,* 1998). Another study using *T. aquaticus* DNA ligase showed it rather produces negative supercoiling in DNA (Hsieh & Capp, 2005). Further studies are needed to work out the

significance of these interesting observations. For example, positively supercoiled DNA may be produced by ligase A during DNA replication or repair, and how these DNA are reprocessed, presumably by topoisomerase, into uniform negative supercoils (**Figure 4.4A**) need to be addressed. A topoisomerase assay with the religated DNA can shed light on how various supercoiled DNA influence the activities of topoisomerases.

This Section showed agarose gel electrophoresis to be a good tool for separating various topological forms of plasmids, and ligase A as an active enzyme to ligate nicked DNA, attributes that were exploited in more experiments in the following part of the Thesis. Since all of the DNA markers (Hyperladder 1, Bioline) used throughout the Thesis are the same, in the following sections the sizes of markers are not labelled (unless otherwise necessary).

4.3.2 Further characterization of *Ec*-SSB and its homologue F-SSB in DNA binding and subunit exchange

DNA binding abilities of *Ec*-SSB have been extensively studied during the past several decades. But its homologue, F-SSB, lacks thorough investigation. It was shown in **Chapter 3** that F-SSB binds to $(dT)_{35}$ and interacts with DnaGC, RNase HI and the Pol III χ subunit through its conserved C-terminal residues. Amino acid sequence alignment of *Ec*- and F-SSB showed a very well conserved N-terminal OB domain through which the *Ec*-SSB tetrmer is formed. However, whether F-SSB adopts a similar tetrameric structure and DNA binding ability was still a question due to the lack of structural data thus far. This part of this Thesis describes properties of *Ec*- and F-SSB examined biochemically by using various techniques including agarose gel electrophoresis, nanoESI-MS, and SPR.

Before conducting all DNA replication and DNA binding assays, samples of *Ec*-SSB, F-SSB, their truncated versions and fusion proteins were prepared by dialysis into the SSB storage buffer (50 mM Tris-HCl, pH 7.6, 1 mM DTT, 1 mM EDTA, 500 mM NaCl, 30% v/v glycerol), and were then diluted to the same concentration (40 μM, as tetramers). When conducting SSB-dependent DNA replication assays, the reaction mixtures without SSB were always compensated with the same volume of the SSB storage buffer, so as to eliminate unwanted salt effects in the assays. Similarly, when

examining the roles of other components in DNA replication assays, the reaction mixtures without certain protein components were always (unless otherwise specified) compensated with buffer containing 20 mM Tris-HCl, pH 7.6, 10 mM $MgCl_2$ and 120 mM NaCl to minimize salt effects, since this buffer is similar to all the storage buffers that contained the protein samples (except SSB species).

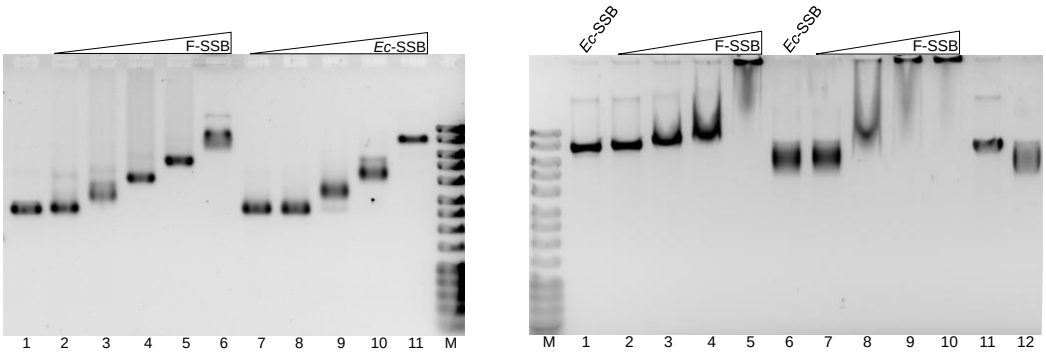

Figure 4.5 Agarose gel electrophoresis for ssDNA (left) and dsDNA (right) interactions of *Ec*-SSB and F-SSB. In the left panel, lanes 2–6 shows the migration pattern of M13 (6408 Nt; 4 nM) mixed with elevating concentrations (89, 179, 357, 536 and 714 nM) of F-SSB, and lanes 7–11 shows that of *Ec*-SSB at the same concentrations (as tetramers). Lane 1 is naked M13 template. The panel on the right shows migration of 1.6 nM nicked (lanes 2–5) and 0.33 nM religated (lane 7–10) plasmid (7.3 kb) mixed with various concentrations (179, 357, 536 and 714 nM) of F-SSB. As controls, lanes 1 and 6 show *Ec*-SSB (714 nM) mixed with nicked and religated plasmid, respectively. Lanes 11 and 12 are nicked and religated plasmid templates without SSB. All reactions were carried out in 11.2 μL reaction mixtures containing 10 mM Tris-HCl, pH 7.6, 10 mM $MgCl_2$, 1 mM DTT and 46 mM NaCl. The reaction mixtures were incubated for 5 min at 30˚C before being analyzed by 0.7% agarose gel electrophoresis without EtBr. The gel was stained with SYBR® Gold nucleic acid gel stain.

A titration assay of F-SSB showed its ssDNA and dsDNA binding properties in agarose gel electrophoresis (**Figure 4.5**). *Ec*-SSB was known to bind ssDNA but not dsDNA (**Sections 3.1** and **4.1**). The result shows that both *Ec*-SSB and F-SSB bind to ssDNA in a progressive manner with increasing concentration of protein (left panel of **Figure 4.5**). The concentration of SSB required to coat 4 nM M13 DNA in the 35-mode of binding is 740 nM, and the result is consistent with binding in this mode at saturation. *Ec*-SSB is known to bind ssDNA but not dsDNA, and this is confirmed by the *Ec*-SSB controls in the right panel of **Figure 4.5**. Unexpectedly, F-SSB showed extensive dsDNA binding ability, moving the plasmid bands to the wells at high concentrations. Since relaxed plasmids were used, that do not contain any significant amount of ssDNA, F-SSB must bind to the dsDNA, and since it binds equally well to the relaxed, but covalently-closed ligated plasmid, it cannot be unwinding dsDNA by its helix destabilizing activity. This is the first time that an assay clearly shows dsDNA binding by a bacterial SSB.

However the function for the dsDNA binding is not clear. Futher studies are needed.

The four monomers in the *Ec*-SSB tetramer were previously shown to be able to exchange with subunits of other *Ec*-SSB species that retain the OB fold (Mason *et al.,* 2013); subunit exchange was stimulated by omitting the C-terminal residues of *Ec*-SSB, but was inhibited by association with ssDNA. To find out if full length F-SSB can exchange subunits with *Ec*-SSB, a native-state nanoESI-MS measurement (**Section 2.4.7**) was carried out. This experiment will show us whether the F-SSB adopts a tetrameric structure and is able to exchange its subunits in solution as does *Ec*-SSB. It will also show us whether the two SSB species can form hybrid tetramers, which is likely to occur in F^+ *E. coli* cells when F-SSB is expressed. To obtain hybrid tetramers, equimolar concentrations of *Ec*-SSB and F-SSB were mixed and incubated at 30˚C. At various time points (ranging from 1–15 h), samples were analyzed by nanoESI-MS. No hybrid tetramers were observed (data not shown). However, repeating the experiment at 55˚C led to essentially complete subunit exchange between *Ec*-SSB and F-SSB within 2 h (**Figure 4.6**). As a control experiment, equimolar concentrations of *Ec*-SSB and *Ec*-SSBΔC8 showed a similar extent of subunit exchange under the same conditions. The lack of subunit exchange at the lower temperature, at which *Ec*-SSB subunit exchange is readily observable within 15 h (Mason *et al.*, 2013), may be an effect of the C-terminus of F-SSB (between residues 115–178), which has twice as many acidic residues as the *Ec*-SSB C-terminus (**Figure 3.3**), or it may simply be that the OB domains of F-SSB form more stable tetramers than *Ec*-SSB. In order for subunit exchange between *Ec*-SSB and F-SSB to occur, the tetramers have to transiently dissociate into dimers and/or monomers. Mason *et al.* (2013) showed that removal of the last eight C-terminal residues (containing 5 acidic residues) of *Ec*-SSB enhanced subunit exchange, and NMR and MST measurements both showed interaction between the C-terminal region and the OB domain (**Chapter 3**). The acidic residues of the F-SSB C-termini might bind even more tightly to the basic OB domain in neighbouring protomers in the tetramer (**Chapter 5**), which would slow down its dissociation into dimers and/or monomers. The result provides important information about the two different dimer–dimer interfaces in the F-SSB tetramer. The fact that F-SSB can form hybrid tetramers with any numbers of *Ec*-SSB subunits from one to three reveals the likelihood of F-SSB possessing very similar structures to *Ec*-SSB at the interfaces. Further structural studies are described in **Chapter 5**.

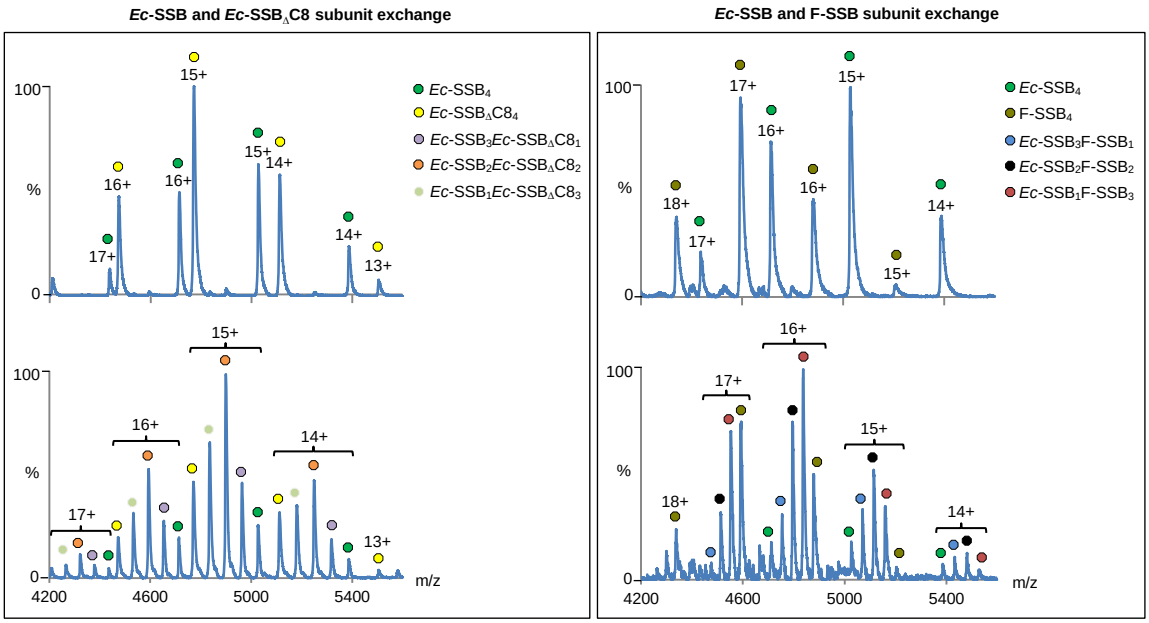

Mass (Da)	*Ec*-SSB$_4$	*Ec*-SSBΔC8	*Ec*-SSB$_3$*Ec*-SSBΔC8$_1$	*Ec*-SSB$_2$*Ec*-SSBΔC8$_2$	*Ec*-SSB$_1$*Ec*-SSBΔC8$_3$
Theoretical	75375	71515	74410	73445	72480
In nanoESI-MS	75410 ± 2.4	71579 ± 2.5	74457 ± 14.6	73494 ± 6.4	72527 ± 10.3

Mass (Da)	F-SSB$_4$	*Ec*-SSB$_3$F-SSB$_1$	*Ec*-SSB$_2$F-SSB$_2$	*Ec*-SSB$_1$F-SSB$_3$
Theoretical	78020	76036	76698	77359
In nanoESI-MS	78060 ± 6.8	76063 ± 7.8	76730 ± 7.3	77405 ± 5.9

Figure 4.6: Subunit exchange between *Ec*-SSB and F-SSB (right panel) as well as *Ec*-SSB and *Ec*-SSBΔC8 (left panel). Spectra were obtained by using nanoESI-MS. *Ec*-SSB, SSBΔC8 and F-SSB were dialyzed individually into 10 mM NH_4OAc (pH 7.2), 1 M NH_4OAc (pH 7.2) and 1 M NH_4OAc (pH 7.2) with 0.5 mM 2-mercaptoethanol, respectively. Equimolar (10 µM) proteins were mixed and spectra were recorded immediately after mixing (upper spectra) and after 2 h at 55˚C (lower spectra). All the tetrameric species are labelled with subscripts showing the numbers of monomers of each kind they contain in the tetramer. The charge state of each species is labelled on the spectrum also. The calculated mass (theoretical) and the mass derived from nanoESI-MS are shown below.

4.3.3 Establishment of bulk phase DNA replication assays

A wide variety of DNA replication assays involving synthesis by *E. coli* Pol III HE or its sub-assemblies have been established in our laboratory. Generally, proteins are mixed on ice in a reaction buffer containing a fixed concentration of salt ($MgCl_2$ and NaCl), energy source (ATP), DNA precursors (dNTPs) and oligonucleotide-primed DNA template. The reaction mixture is enclosed in an Eppendorf tube, which is incubated in a heating block. Unlike the single-molecule experiments, the bulk phase

assay creates a relatively static and stable condition, similarly as in the bacterial cell, with only heat promoting to the reaction.

Here, a bulk phase primer extension plus helicase-independent Pol III SD replication assay (Jergić *et al.*, 2013) was first re-evaluated. In this assay, a 5'-flapped oligodeoxynucleotide primer annealed to M13 circular ssDNA is extended to produce a circular dsDNA product. Under appropriate conditions, the Pol III HE can then displace the flapped product strand while further extending the primer to produce long ssDNA tails. Following quenching with EDTA and SDS to denature the proteins, the DNA products (**Figure 4.7**) are visualized following 0.7% agarose gel electrophoresis by staining with SYBR gold, which detects both ss and ds DNA (**Section 2.3.5**)

Since the assay is conducted manually, human error is the major cause of inconsistent results. The assay (**Figure 4.7A**) was first carried out at various temperatures (0, 20, 30 and 37˚C). Reaction at 30˚C showed the highest efficiency of primer extension and SD. Thus, 30˚C was used in all further work. The quenching buffer was also tested for its robustness since the assays often need a tight control of stopping points. The quenching buffer was added into an assay mixture at zero time, and incubated at 30˚C for 30 min. It showed a completely quenched reaction (lane 3 in **Figure 4.7B**) while the control showed robust DNA replication (lane 2 in **Figure 4.7B**).

Assays were also used to show the importance of a static (no turbulence) environment for Pol III HE dependent DNA replication. Vortex mixing is known to give rise to covalent bond breakage in long dsDNA molecules, and our DNA replication assays always involve pipetting samples containing DNA templates. Deliberate pipetting (about 120 rounds/min using a 20 μL pipette) or stirring (about 180 rpm) with a small magnetic stirring bar was imposed on reaction mixtures while they were heated at 30˚C for 5 min (lane 3 in **Figure 4.7C**) or at 20˚C for 30 min (lane 4 in **Figure 4.7B**), respectively. Control reactions without pipetting (lane 2 in **Figure 4.7C**) or stirring (lane 1 in **Figure 4.7B**) were conducted. Surprisingly, no SD synthesis was observed in the reactions with either pipetting or stirring, although primer extension seemed not to be influenced by these actions. This probably reflects the greater efficiency of processive strand extension; it takes less than 10 s to fully replicate M13 DNA once Pol III HE is fully assembled under these conditions, while Pol III SD synthesis is believed to be a slow and much less processive process. This explains why in the bulk phase assay, a

clear fully replicated M13 circle is always observed before SD. The accumulated full circle M13 in the gel, instead of a smear, means the polymerase stalls at the "finish line" of primer extension, and then readjusts itself for the next stage (SD).

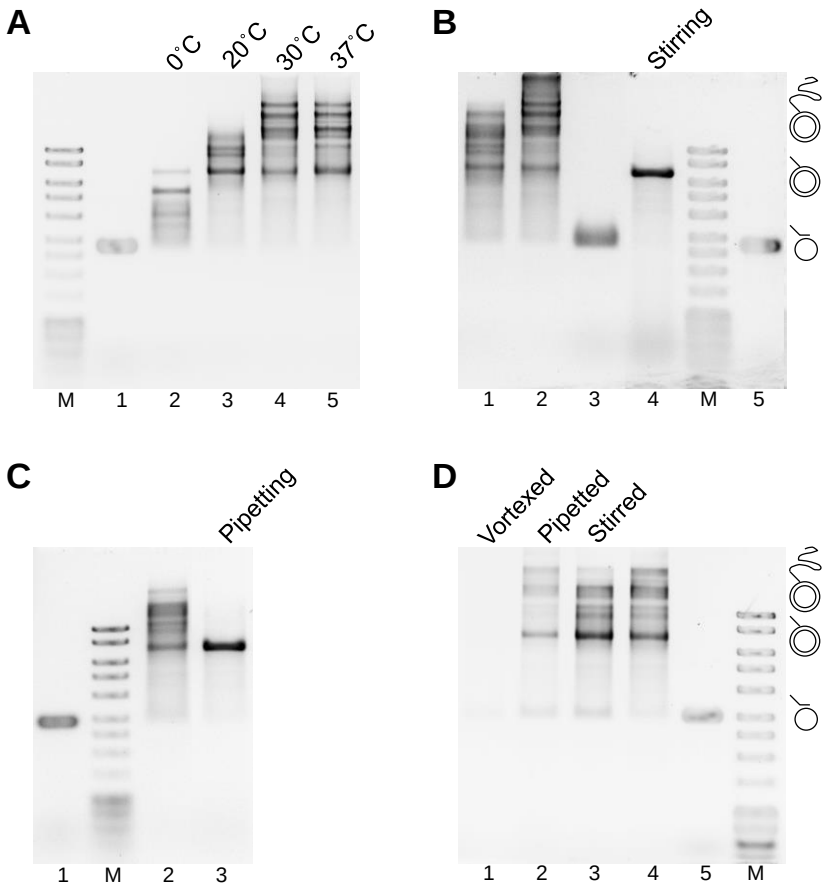

Figure 4.7 Establishment of DNA replication assay. All the reactions were analyzed by agarose gel electrophoresis in the absence of EtBr. Lane 1 in **A**, lane 5 in **B**, lane 1 in **C** and lane 5 in **D** are naked flap-primed M13, while lanes 1 and 2 in **B**, lane 2 in **C** and lane 4 in **D** are positive control reactions without mechanical treatment. Assays (for 20 min unless specified in the text) contained 20 mM Tris-HCl, pH 7.6, 10 mM $MgCl_2$, 110 mM NaCl, 1 mM ATP, 6.8 mM DTT, 423 μM of each dNTP, 68 nM αεθ, 32 nM $\tau_3\delta\delta'\chi\psi$, 420 nM β_2, 700 nM *Ec*-SSB and 4 nM flap-primed M13 ssDNA (Jergić *et al.,* 2013). After 20 min, the reaction mixtures were quenched in the quenching buffer (finally ~90 mM EDTA and ~0.6% SDS) and analyzed by 0.7% agarose gel electrophoresis. In all following assays, the same concentrations of EDTA and SDS were applied for quenching.

Finally, to prove the lack of SD synthesis in reactions with disturbances (pipetting or stirring, as above) was not the result of the breakage of the primed M13 ssDNA template or the protein components, the same disturbances were exerted on the flap-primed M13 ssDNA in the buffer (20 mM Tris-HCl, pH 7.6, with salts and nucleotides). Then, the protein components were added before further incubation at 30˚C for 20 min. A control reaction containing the same components without any disturbance was

conducted (lane 4 in **Figure 4.7D**). Instead of hindered SD synthesis, relatively robust DNA synthesis was observed (lanes 2 and 3 in **Figure 4.7D**). However in a parallel reaction imposed with 5 min of vigorous vortex mixing, the complete absence of DNA replication products was shown (lane 1 in **Figure 4.7D**). This means the ssDNA templates could be sheared by the physical force of prolonged vortex mixing.

Therefore, in all following assays, disturbance was reduced to the minimum amount. Since Pol III HE seems to be active during mixing, even at 0˚C (lane 2 in **Figure 4.7A**), the time for mixing reaction components on ice was also reduced to the minimum, and DNA templates or polymerases were always added last into the reaction mixtures.

The purity of the proteins, especially with respect to trace nuclease contamination, is another important factor for successful DNA replication assays. All newly purified proteins or protein complexes were tested in parallel with the previously purified ones in the bulk phase DNA replication assay before use (data not shown). Proteins or protein complexes that failed to give the expected results were discarded.

4.3.4 The roles of *Ec*-SSB, clamp loader and the β clamp in Pol I primer extension and SD synthesis

Pol I plays a key role at Okazaki fragment maturation. As an isolated protein, it has been very well characterized by extensive studies in the past, beginning with the Nobel Prize winning work of Arthur Kornberg in the mid-1950s. Perhaps because of this and the time elapsed until other replisomal components were discovered, the enzymatic activities of Pol I in the presence of other key components of the replisome have not been extensively studied. Work described here shows that *Ec*-SSB inhibits Pol I primer extension but stimulates Pol I SD DNA synthesis (**Figure 4.8A**). Pol I was titrated in an *in vitro* DNA replication assay similar to the Pol III assays described above, with flap-primed M13 as template. Reactions took place at 30˚C for 2 h. Comparison of lanes 4 and 12 shows that *Ec*-SSB modestly inhibits the slow and distributive Pol I primer extension reaction.

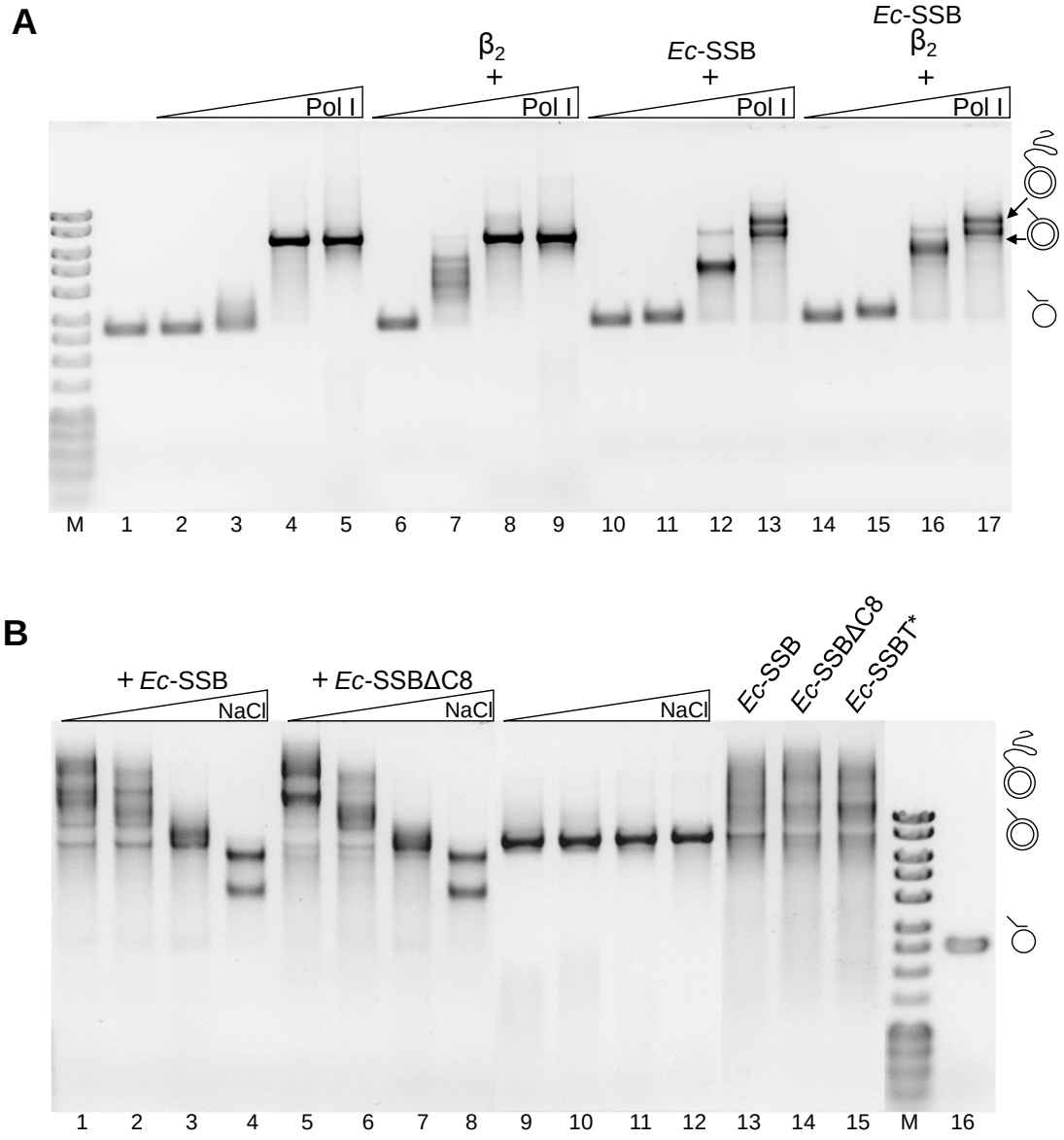

Figure 4.8: *Ec*-SSB inhibits Pol I primer extension and stimulates Pol I SD DNA synthesis. **A.** A Pol I titration assay (5, 20, 100, and 400 nM, from left to right in each set of four lanes from 2–17) was carried out without *Ec*-SSB and β_2 (lanes 2–5), with 200 nM β_2 (lanes 6–9), with 800 nM *Ec*-SSB (lanes 10–13) or with 800 nM *Ec*-SSB and 200 nM β_2 (lanes 14–17). All assays contained 20 mM Tris-HCl, pH 7.6, 10 mM $MgCl_2$, 1 mM ATP, 7 mM DTT, 470 µM of each dNTP and 44 nM $\gamma_3\delta\delta$', with 130 mM NaCl. **B.** NaCl titration assays (0, 50, 100, 145 mM from left to right in each set of four lanes from 1–12) were carried out with 878 nM *Ec*-SSB (lanes 1–4) or *Ec*-SSBΔC8 (lanes 5–8), or without SSB (same volume of SSB storage buffer; lanes 9–12). All reactions contained 20 mM Tris-HCl, pH 7.6, 10 mM $MgCl_2$, 1.2 mM ATP, 7.2 mM DTT, 500 µM of each dNTP, 428 nM Pol I and 4 nM flap-primed M13 template. To make comparisons, M13 primed with a fully complementary 5'-phosphorylated primer (4 nM) was used with 878 nM *Ec*-SSB (lane 13), *Ec*-SSBΔC8 (lane 14) or *Ec*-SSBT* (lane 15) in the presence of Pol I (428 nM) in 50 mM NaCl. All reaction mixtures in **A** and **B** were incubated in 30˚C for 2 h, and then analyzed by 0.7% agarose gel electrophoresis. Lane 1 in **A** and lane 16 in **B** contain naked flap-primed M13.

The *dnaN* gene encodes the β clamp. It was known already that β stimulates Klenow and Pol I primer extension (Maul *et al.,* 2007), and that elevated Pol I concentration can

suppress the temperature sensitivity of a *dnaN*^{ts} mutant strain (Maul *et al.,* 2007). Bacterial Pol Is are also known to have a (poorly-characterized) clamp binding motif (Dalrymple *et al.*, 2001) that is presumed to interact with loaded β_2 to increase their processivity and/or facilitate their loading at a primer terminus. To see whether *Ec*-SSB inhibits Pol I primer extension in the presence of β_2 that had been loaded on the primer–template by the $\gamma_3\delta\delta$' clamp loader complex, Pol I was titrated (5–400 nM) in the presence of 200 nM β_2 with 800 nM *Ec*-SSB (**Figure 4.8A**, lanes 14–17) or the same volume of *Ec*-SSB storage buffer (lanes 6–9). By comparison of lane 7 and 15, it was noticed that *Ec*-SSB moderately inhibits Pol I primer extension in the presence of β_2. By comparison of lanes 3 and 7 as well as lanes 12 and 16, it was also noticed that β_2 indeed stimulates Pol I primer extension, though the effect was modest. Furthermore, results in **Figure 4.8A** reveal that elevating concentrations of Pol I can compensate for the activity of β_2; this is also consistent with the *in vivo* study by Maul *et al.* (2007).

In lanes 13 and 17 of **Figure 4.8A**, small quantities of SD products greater in size than unit-length M13 dsDNA were observed in the presence of *Ec*-SSB. The occurrence of these products is discussed below. In another *in vitro* DNA replication assay that examined the salt dependence, *Ec*-SSB and its C-terminally truncated versions showed stimulation of Pol I SD synthesis (**Figure 4.8B**). Extensive SD was observed in the presence of *Ec*-SSB (lanes 1–4) or *Ec*-SSBΔC8 (lanes 5–8) at 0 (lane 1 or 5) and 50 mM NaCl (lanes 2 or 6). Higher NaCl concentration (lanes 3, 4, 7 and 8) inhibited Pol I SD as well as primer extension. Interestingly at high NaCl concentration, the reaction without *Ec*-SSB still gave fully replicated M13, demonstrating again that *Ec*-SSB (or *Ec*-SSBΔC8) inhibits Pol I primer extension. It was noticed that at even 0 mM NaCl (lane 9) no SD was observed in the absence of *Ec*-SSB.

To see whether a non-flapped primed M13 template or the rest of C-terminal region of *Ec*-SSB affects Pol I SD, *Ec*-SSB (lane 13), *Ec*-SSBΔC8 (lane 14) and *Ec*-SSBT* (lane 15) were mixed with the same reaction buffer with 50 mM NaCl, using 4 nM of M13 primed with a 33-Nt fully complementary 5'-phosphorylated primer (**Section 4.2.7.1**). The results showed very similar SD patterns, indicating two important features of Pol I SD: (1) Pol I does not discriminate between flapped or fully complementary primers in the presence of *Ec*-SSB; (2) The entire C-terminal flexible region of *Ec*-SSB has no significant role in Pol I SD in lower salt conditions.

Ec-SSB is known to protect ssDNA from digestion by nucleases. Pol I has 5'–3' flap endonuclease activity as well as 3'–5' proofreading exonuclease activity. In lanes 9 and 10 of **Figure 4.8B**, smears of fragments shorter than M13 ssDNA were observed. They are likely to be from ssDNA digested by Pol I, most probably from small amounts of linerized M13 ssDNA in the template preparation. However other lanes do not show such bands when *Ec*-SSB is present in the reactions. As reviewed in the introduction to this Chapter, the regression force at replication forks is likely to be the reason for the inefficiency of SD by various polymerases (Manosas *et al.,* 2012). Since binding of thermally separated single-stranded ends to the OB-domain of *Ec*-SSB is known to reduce the melting temperature of dsDNA, and so far there has been no report of interactions between *Ec*-SSB and Pol I, this *Ec*-SSB dependent Pol I SD assay might indicate the OB-domain of *Ec*-SSB imparts a counter force to fork regression by binding to the displaced strand (Raghunathan *et al.*, 2000). This leads to the speculation that during Pol I SD synthesis, the OB-domain of *Ec*-SSB protects the displaced ssDNA from digestion by the flap endonuclease activity of Pol I, at the same time keeping the replication fork open. This is the first reported experiment that clearly shows that *Ec*-SSB stimulates Pol I SD synthesis. This simple DNA replication model might shed light to the much more complex Pol III SD synthesis reaction. It is shown later in this Chapter that Pol III also does not discriminate between flapped and fully complementary DNA primers. It is also shown later for the first time that *Ec*-SSB missing the C-terminal region still stimulates Pol III SD (**Sections 4.3.6** and **4.3.7**) in low salt conditions. These results suggest that a similar SD mechanism probably underlies these two systems (Pol I and Pol III). Both Pol I and Pol III normally replicate SSB-coated ssDNA in the cell, so the important question to be resolved is how unwanted strand-displacement DNA synthesis is controlled in the cell to prevent formation of long recombinogenic tracts of ssDNA at replication forks as they approach the 5'-end of Okazaki fragments. These are questions I will address later.

Surprisingly, the $\gamma_3\delta\delta'$ and $\tau_3\delta\delta'$ clamp loaders were observed to modestly stimulate Pol I primer extension, even in the absence of SSB and the β sliding clamp. Clamp loaders have been used in almost all Pol III DNA replication assays, where one of their roles is to load the clamp, and the clamp also stimulates Pol I activity (**Figure 4.8A**). However direct evidence showing that the clamp loader itself ($\gamma_3\delta\delta'$ or $\tau_3\delta\delta'$) affects Pol I activity is lacking. It was shown here that the clamp loader seems to stimulate primer extension

by Pol I (**Figure 4.9**). NaCl (138–162 mM) was titrated in the reaction buffer that contained 40 nM Pol I and flap-primed M13 ssDNA template, in the presence of $\gamma_3\delta\delta'$ (lanes 8–10), $\tau_3\delta\delta'$ (lanes 2–4), or absence of clamp loaders (lanes 5–7). The result shows that both clamp loaders $\gamma_3\delta\delta'$ and $\tau_3\delta\delta'$ stimulate Pol I primer extension across the whole salt concentration range. Interestingly, $\tau_3\delta\delta'$ (lane 4) seems to have a more positive effect on Pol I primer extension in comparison with $\gamma_3\delta\delta'$ (lane 10), especially at higher ionic strength condition. However the effect is small. Since there are no known interactions between Pol I and the clamp loader, the results lead to the speculation of new interactions between these components, or of the clamp loaders with the DNA template.

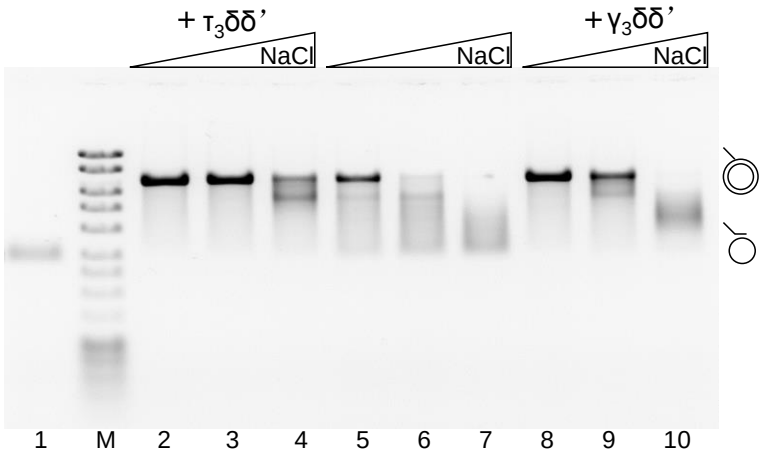

Figure 4.9: Pol I primer extension is stimulated by both $\gamma_3\delta\delta'$ and $\tau_3\delta\delta'$ clamp loaders, even in the absence of the clamp. This NaCl titration (138 mM NaCl in lanes 2, 5 and 8; 150 mM NaCl in lanes 3, 6 and 9; 162 mM NaCl in lanes 4, 7 and 10) assay was carried out with 4 nM flap-primed M13 ssDNA template in 20 mM Tris-HCl, pH 7.6, 10 mM $MgCl_2$, 1 mM ATP, 7 mM DTT, 500 μM of each dNTP, with 40 nM Pol I in the presence of 64 nM $\gamma_3\delta\delta'$ (lanes 8–10), 61 nM $\tau_3\delta\delta'$ (lanes 2–4), or absence of any clamp loaders (lanes 5–7). All reaction mixtures were incubated at 30˚C for 2 h, and then analyzed by 0.7% agarose gel electrophoresis. Lane 1 contained naked flap-primed M13.

4.3.5 The roles of *Ec*-SSB in primer extension by Pol III core

Ec-SSB stimulates primer extension by the Pol III α subunit (alone) in an *in vitro* DNA replication assay involving a downsized Pol III HE. Previously in our laboratory, bulk phase and single-molecule assays were carried out for studying Pol III HE activity during DNA replication. However, a relatively inefficient reaction with a more limited number of components can help reveal hidden interactions among smaller numbers of proteins (*e.g.*, see Jergić *et al.*, 2013 for an example). Reported here is an *Ec*-SSB

dependent α subunit primer extension assay with a minimized Pol III system, which might reveal the previously unknown interplay between the Pol III α subunit and *Ec*-SSB. The result shows that in buffer with physiological salt conditions (about 150 mM NaCl), the α subunit with a preloaded β clamp on the DNA primer–template carries out DNA replication only in the presence of *Ec*-SSB (lanes 2 and 3 in **Figure 4.10C**). Further investigation indicates that *Ec*-SSB dependent α subunit primer extension is stimulated by the presence of the last 8 residues in *Ec*-SSB. The C-terminus of *Ec*-SSB draws increasing amount of attention nowadays because of its versatile functions in many protein–protein interactions. Since all the binding partners of *Ec*-SSB interact through the C-terminal 8 residues, a salt titration assay (98–207 mM NaCl; **Figure 4.10A**) was first conducted to interrogate its possible functions in this DNA replication assay. By comparing primer extension by α at 116 and 134 mM NaCl in the presence of *Ec*-SSB (lanes 2 and 3) and *Ec*-SSBΔC8 (lanes 7 and 8), a stimulatory effect of the *Ec*-SSB C-terminal 8 residues is revealed. However with lower ionic strength (98 mM NaCl in lanes 1, 6 and 16), *Ec*-SSB, *Ec*-SSBΔC8 and *Ec*-SSBT* equally stimulate the reactions. Interestingly, the α subunit is unable to carry out DNA replication alone in the whole range of salt conditions (lanes 11–15), indicating a stimulatory role of the OB domain of *Ec*-SSB. On the other hand, *Ec*-SSB acts as an inhibitor in Pol I primer extension (**Figure 4.8A**). The contradictory effects of *Ec*-SSB in these two replication systems leads to the speculation of some specific interaction between *Ec*-SSB and the α subunit, perhaps during the process of removal of SSB ahead of the polymerase. Note that Pol I, in its normal role of RNA primer removal by nick translation, does not need to remove SSB, but Pol III needs to do so during Okazaki fragment synthesis.

To see if the rest of the C-terminus of *Ec*-SSB has more subtle functions in primer extension by the α subunit, a time course assay was carried out in the presence of the other truncated *Ec*-SSB proteins: *Ec*-SSBΔC27 and *Ec*-SSBT* (**Figure 4.10B**). At the 5-min time point, the α subunit with truncated *Ec*-SSBs show very similar, inefficient primer extension compared to full-length *Ec*-SSB. At the 20-min time point, proficient primer extension was observed only in the reaction with full-length *Ec*-SSB (lane 4). However, *Ec*-SSBΔC27 and *Ec*-SSBT* did not show any difference from *Ec*-SSBΔC8, which focussed our scope to the last 8 residues of *Ec*-SSB.

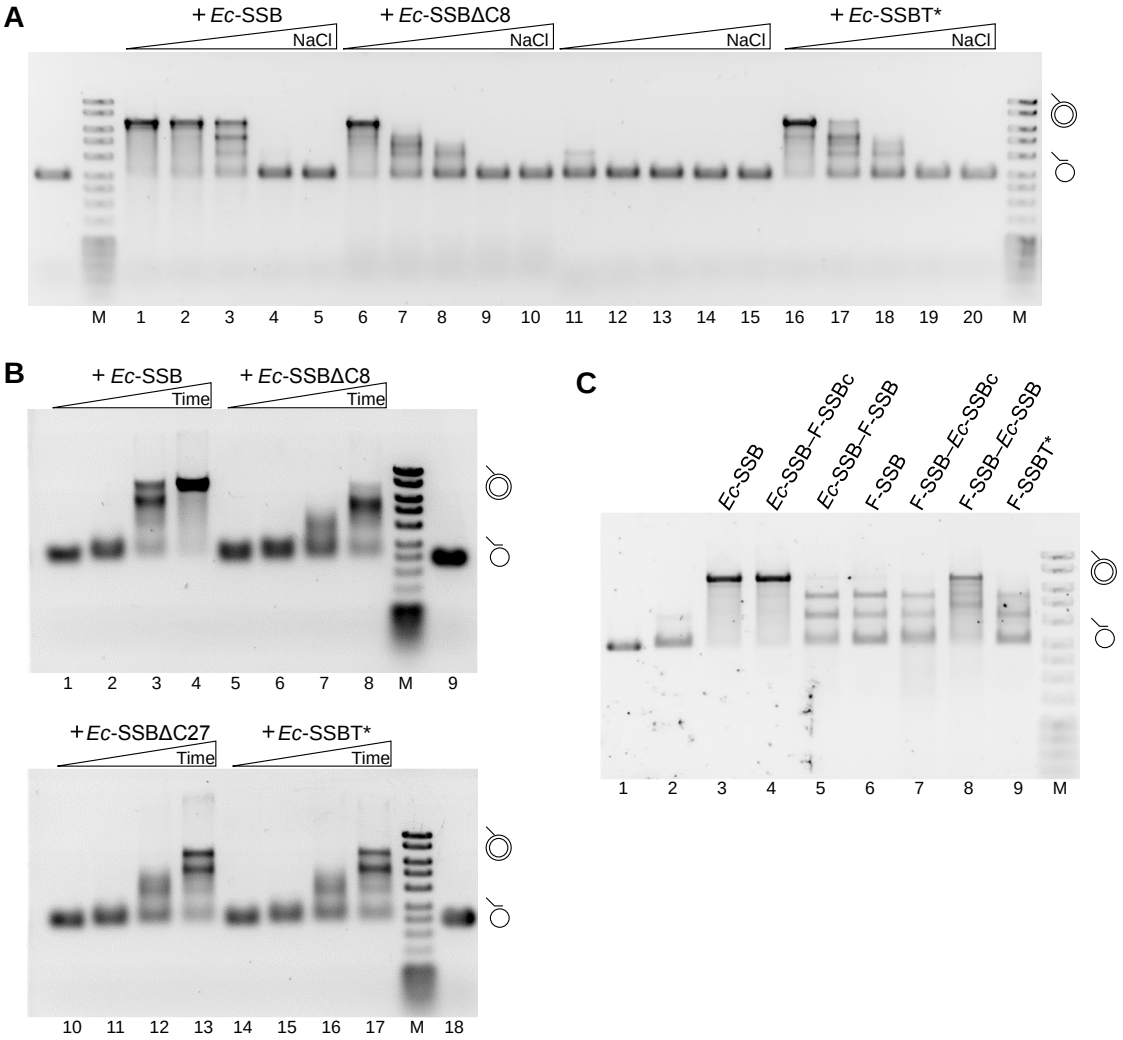

Figure 4.10: *Ec*-SSB dependent β_2-dependent primer extension by the Pol III α subunit. **A.** A salt titration assay shows higher DNA replication efficiency at higher NaCl concentration with the C-terminus of *Ec*-SSB intact. NaCl was at 98, 116, 134, 153, and 207 mM NaCl, respectively, left to right in each set of five lanes as indicated. Assays contained 727 nM *Ec*-SSB (lanes 1–5), *Ec*-SSBΔC8 (lanes 6–10), *Ec*-SSBT* (lanes 16–20), or absence of SSB (storage buffer, lanes 11–15), as well as 224 nM β_2, 42 nM $\gamma_3\delta\delta$', 197 nM α subunit and 3 nM flap-primed M13 ssDNA template in 20 mM Tris-HCl, pH 7.6, 10 mM $MgCl_2$, 0.9 mM ATP, 9 mM DTT, and 505 μM of each dNTP, and were incubated at 30˚C for 20 min. **B.** The *Ec*-SSB C-terminus dependency was further examined in a time-course assay with 545 nM *Ec*-SSB, *Ec*-SSBΔC8, *Ec*-SSBΔC27 or *Ec*-SSBT* at a fixed salt concentration (120 mM NaCl) in reactions containing 23 mM Tris-HCl, pH 7.6, 11 mM $MgCl_2$, 0.9 mM ATP, 9.2 mM DTT, 505 μM of each dNTP, 229 nM β_2, 43 nM $\gamma_3\delta\delta$', and 201 nM α. Reactions containing individual *Ec*-SSB species were quenched at 0, 5, 10 and 20 min time points, from left to right. **C.** Reactions (at 30˚C for 20 min) with full-length *Ec*-SSB and various *Ec*-SSB and F-SSB fusion proteins in the presence of 130 mM NaCl. In the reactions, 197 nM α subunit was mixed with 707 nM of *Ec*-SSB (lane 3), *Ec*-SSB–F-SSBc (lane 4), *Ec*-SSB–F-SSB (lane 5), F-SSB (lane 6), F-SSB–*Ec*-SSBc (lane 7), F-SSB–*Ec*-SSB (lane 8), F-SSBT* (lane 9) or the same volume of the SSB storage buffer (lane 2) in reaction buffer (20 mM Tris-HCl, pH 7.6, 10 mM $MgCl_2$, 0.9 mM ATP, 9 mM DTT, 505 μM of each dNTP, 224 nM β_2 and 42 nM $\gamma_3\delta\delta$') with 4 nM flap-primed M13 ssDNA template. The unlabelled lane in **A,** lanes 9 and 18 in **B**, and lane 1 in **C** contained naked flap-primed M13 ssDNA.

This then raises questions about the function of the OB domain and the rest of C-

terminus of *Ec*-SSB in this system. A series of α subunit-dependent primer extension assays with various *Ec*-SSB and F-SSB fusion proteins was used to address this question (**Figure 4.10C**). Interestingly *Ec*-SSB–F-SSBc stimulates α DNA replication equally to the wild type *Ec*-SSB, indicating switching the last eight-residue segment of *Ec*-SSB to F-SSB does not interfere with its functionality in this system. On the other hand, *Ec*-SSB–F-SSB, F-SSB, F-SSB–*Ec*-SSBc, F-SSB–*Ec*-SSB and F-SSBT* were incompetent in fully stimulating DNA replication. This indicates that *all* portions of the structure of *Ec*-SSB (the OB domain, C-terminal domain and C-terminus) are required to fully stimulate α-dependent DNA replication. However this is contradictory to previous studies where SSB shows sign of inhibition to the Pol III DNA synthesis in the absence of NaCl (Fay *et al.,* 1981; Glover and McHenry, 1998). DNA replications assays described in this Thesis were conducted in buffers with relatively higher inonic strength, mostly between 100–150 mM NaCl which is more biological relevant. Futher studies are described in **Chapter 5**.

Ec-SSB also stimulates α subunit-dependent primer extension in a further downsized Pol III replication system without the β clamp. Previously, Dr. Slobodan Jergić demonstrated *Ec*-SSB- and $\gamma_3\delta\delta$'-dependent αεθ primer extension in a low salt condition. Since there are no known interactions among *Ec*-SSB, $\gamma_3\delta\delta$' and αεθ, the assay provides an opportunity to extend knowledge about the roles of *Ec*-SSB and $\gamma_3\delta\delta$' during DNA replication. A large reservoir of purified individual subunits gives an opportunity to further downsize this system, which may help to find the key interactions. It was found that ε, θ and the flexible C-terminus of *Ec*-SSB can be omitted, although it seems to lead to lower efficiency of DNA replication. The results are shown in **Figure 4.11**. A time-course assay (**Figure 4.11A**) showed both *Ec*-SSB (lanes 5–8) and *Ec*-SSBT* (lanes 9–12) could promote some degree of primer extension to produce full circles within 10–20 min, but full-length *Ec*-SSB was more proficient than *Ec*-SSBT*. This indicates a role for the C terminal region of SSB in this reaction. As controls, reactions (20 min) were conducted with αεθ and just *Ec*-SSB (lane 3) or just $\gamma_3\delta\delta$' (lane 4). In accord with Dr. Jergić's results, αεθ-dependent primer extension at low salt required both SSB and the $\gamma_3\delta\delta$' clamp loader.

It was then found in another assay using variously truncated versions of *Ec*-SSB that the stimulatory region on the C-terminus is located primarily in the highly conserved last

eight residues (**Figure 4.11B**). The result shows the various C-terminally truncated *Ec*-SSBs have almost equal inefficiency in terms of stimulating αεθ primer extension.

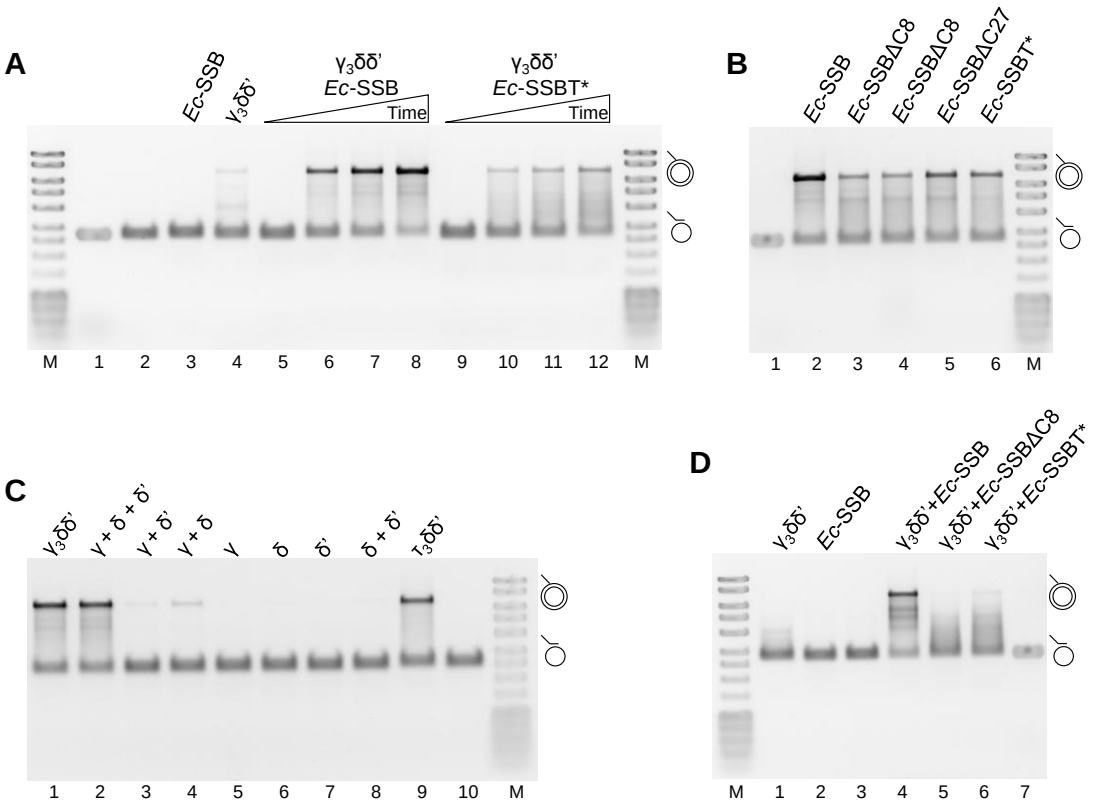

Figure 4.11 Clamp loader and *Ec*-SSB dependent, clamp independent primer extension by αεθ and α at low ionic strength. **A.** Time course (0, 5, 10, 20 min in lanes 5–8 and 9–12, respectively) of αεθ-dependent DNA replication in the presence of 70 nM $\gamma_3\delta\delta$' with 750 nM *Ec*-SSB (lanes 5–8) or *Ec*-SSBT* (lanes 9–12). Control reactions (in 20 min) contained αεθ alone (lane 2), or αεθ with only *Ec*-SSB (lane 3) or only $\gamma_3\delta\delta$' (lane 4). Reactions (at 30˚C) contained 20 mM Tris-HCl, pH 7.6, 10 mM $MgCl_2$, 1 mM ATP, 6.4 mM DTT, 400 μM of each dNTP, 100 nM αεθ and 4 nM flap-primed M13 template. **B.** Adding various C-terminally truncated *Ec*-SSBs (all at 750 nM) in the reaction containing $\gamma_3\delta\delta$' and αεθ resulted in different extents of stimulation. The reactions (20 min at 30˚C) were conducted as in **A** with *Ec*-SSB (lane 2), *Ec*-SSBΔC8 (batch 1, lane 3), *Ec*-SSBΔC8 (batch 2, lane 4), *Ec*-SSBΔC27 (lane 5) or *Ec*-SSBT* (lane 6). **C.** Omitting one or two subunits of the $\gamma_3\delta\delta$' complex abolishes the αεθ primer extension, suggesting a full clamp loader complex has to form to promote αεθ primer extension. $\tau_3\delta\delta$' (lane 9) was added as a comparison. Reactions (20 min at 30˚C) were conducted in 20 mM Tris-HCl, pH 7.6, 10 mM $MgCl_2$, 1 mM ATP, 6.4 mM DTT, 350 μM of each dNTP, 100 nM αεθ and 750 nM *Ec*-SSB, with 4 nM flap-primed M13 template, in the presence of 63 nM $\gamma_3\delta\delta$' (lane 1), 535 nM γ, 173 nM δ and 180 nM δ' (lane 2), 535 nM γ and 180 nM δ' (lane 3), 535 nM γ and 173 nM δ (lane 4), 535 nM γ (lane 5), 173 nM δ (lane 6), 180 nM δ' (lane 7), 173 nM δ and 180 nM δ' (lane 8) or 63 nM $\tau_3\delta\delta$' (lane 9). **D.** The ε and θ subunits of the Pol III core are not required for SSB and clamp-loader dependent primer extension. DNA synthesis (in 45 min at 30˚C) by the α subunit (200 nM) with only $\gamma_3\delta\delta$' (63 nM; lane 1), only *Ec*-SSB (750 nM; lane 2), both $\gamma_3\delta\delta$' and *Ec*-SSB (lane 4), *Ec*-SSBΔC8 (750 nM; lane 5) or SSB-T* (750 nM, lane 6) shows similar stimulatory roles of $\gamma_3\delta\delta$' and *Ec*-SSB as in the reactions involving αεθ, suggesting the ε and θ subunits are dispensable in this system. The reaction buffer otherwise had the same composition as in **A**. All the reactions were analyzed by 0.7% agarose gel electrophoresis. The DNA template (flap-primed M13 at 4 nM) used in the assays was run in parallel in lane 1 of gels **A** and **B**, lane 10 of gel **C**, and lane 7 of gel **D**.

To find which part of $\gamma_3\delta\delta$' stimulates the reaction, individual clamp loader subunits and mixtures of them were used (**Figure 4.11C**). The result shows that all three components of the $\gamma_3\delta\delta$' complex have to present in the reaction to stimulate $\alpha\varepsilon\theta$ primer extension. It is also worth noticing that the $\tau_3\delta\delta$' clamp loader gives the same extent of stimulation as $\gamma_3\delta\delta$', suggesting the underlying mechanism for stimulating the reaction is probably not through the well-defined α:τ interaction. Since $\gamma_3\delta\delta$', $\alpha\varepsilon\theta$ and *Ec*-SSB all interact with DNA, it is likely certain weak interactions among them are cooperatively mediated by DNA.

Finally, ε and θ were omitted from the system, and proved to be dispensable (**Figure 4.11D**). The reactions with α alone retain the dependence on both $\gamma_3\delta\delta$' and *Ec*-SSB, and furthermore, the clamp loader dependence is similar to that seen in the Pol I primer extension reaction (**Figure 4.9**). Both assays show a stimulatory role of the clamp loader on polymerase activity through previously unknown interactions. These results suggest the clamp loader ($\tau_3\delta\delta'\chi\psi$) is not only a clamp-loading complex and Pol III coordinator, but also directly facilitates DNA synthesis. Although these results might eventually lead to discoveries of new protein interactions among $\gamma_3\delta\delta$', *Ec*-SSB and α, it could also be that the observed effects are mediated through DNA binding; note that the presence of the last eight amino acids in *Ec*-SSB does have an effect on DNA binding by its OB domain, and some of the effects seen here could reflect that (see **Section 4.1.1**).

4.3.6 The roles of *Ec*-SSB in primer extension and SD DNA synthesis by Pol III holoenzyme

The last eight residues of *Ec*-SSB are known also to stimulate primer extension by Pol III HE, in part through the known interaction with the χ subunit of the full $\tau_3\delta\delta'\psi\chi$ clamp loader complex (see **Chapter 3** and **Section 4.1.3**). In the reactions described above, minimal downsized assays were used to reveal additional stimulatory roles of the *Ec*-SSB OB-domain and C-terminus, as well as the $\gamma_3\delta\delta$' clamp loader. In the following assays, the function of *Ec*-SSB was studied in a much more complex system with the $\tau_3\delta\delta'\chi\psi$ complex, which acts as a bridge connecting the Pol III core and *Ec*-SSB

(**Section 4.1.3**). The results will be much harder to interpret since they arise from an ensemble of effects resulting from many interactions among individual subunits.

A stimulatory role of the last eight residues at the C-terminus of *Ec*-SSB was revealed in a time-course DNA replication assay (**Figure 4.12A**) involving Pol III HE and various *Ec*-SSBs. Unlike truncated *Ec*-SSBs, full-length *Ec*-SSB stimulates the reaction dramatically, and the rest of the C-terminus apart from the last 8 residues does not show an evident effect on Pol III HE primer extension. This is similar to *Ec*-SSB stimulation of primer extension by α (**Figure 4.10)**, although the mechanism is probably different. Since *Ec*-SSB interacts with the χ subunit, it was speculated that *Ec*-SSB stimulates the Pol III HE reaction, at least partially, through interaction with χ. To confirm this, a similar assay was carried out with clamp loader lacking the χ and ψ subunits (**Figure 4.12B**); $\tau_3\delta\delta'$ was used instead of $\tau_3\delta\delta'\chi\psi$ and an additional longer time point (lanes 5, 10, 15 and 20) was added to capture slow processes. The overall efficiency of DNA replication with χ and ψ was much higher than without them. The distinct difference between these two assays shows the great importance of the χ:SSB interaction in terms of maintaining the speed of DNA replication; the absence of χ has very nearly the same effect as removal of the last eight residues of *Ec*-SSB, so the concomitant absence of ψ is likely to have a relatively small effect.

However, it is not entirely known how this single interaction functions in the entire Pol III HE. *Ec*-SSB is well known to have high affinity for ssDNA, which might impede the progress of a DNA polymerase on a ssDNA template (*e.g.*, for Pol I, **Figure 4.8A**). One can speculate that the *Ec*-SSB C-terminus helps maintain Pol III HE on the template through interaction with χ, which at the same time helps an unidentified HE component to eject *Ec*-SSB from ssDNA to make way for the polymerase. Furthermore, *Ec*-SSB aids polymerase translocation by elimination of secondary structures in the template. This view is partially supported by an *in vivo* study, which shows accumulation of the clamp loader complex at the replication fork in a wild-type strain (Reyes-Lamothe *et al.,* 2010). In contrast, no such accumulation occurred in the absence of the χ subunit (*i.e.*, in a *holC* strain). All in all, the results in **Figure 4.12** show a pronounced stimulatory effect of the last eight residues of *Ec*-SSB in Pol III primer extension, which might not just be the result of the χ:SSB interaction; it could also depend on an SSB

OB:α subunit interaction and/or even the SSB C-terminus:OB-domain interaction. Futher studies are needed to clarify the mechanism.

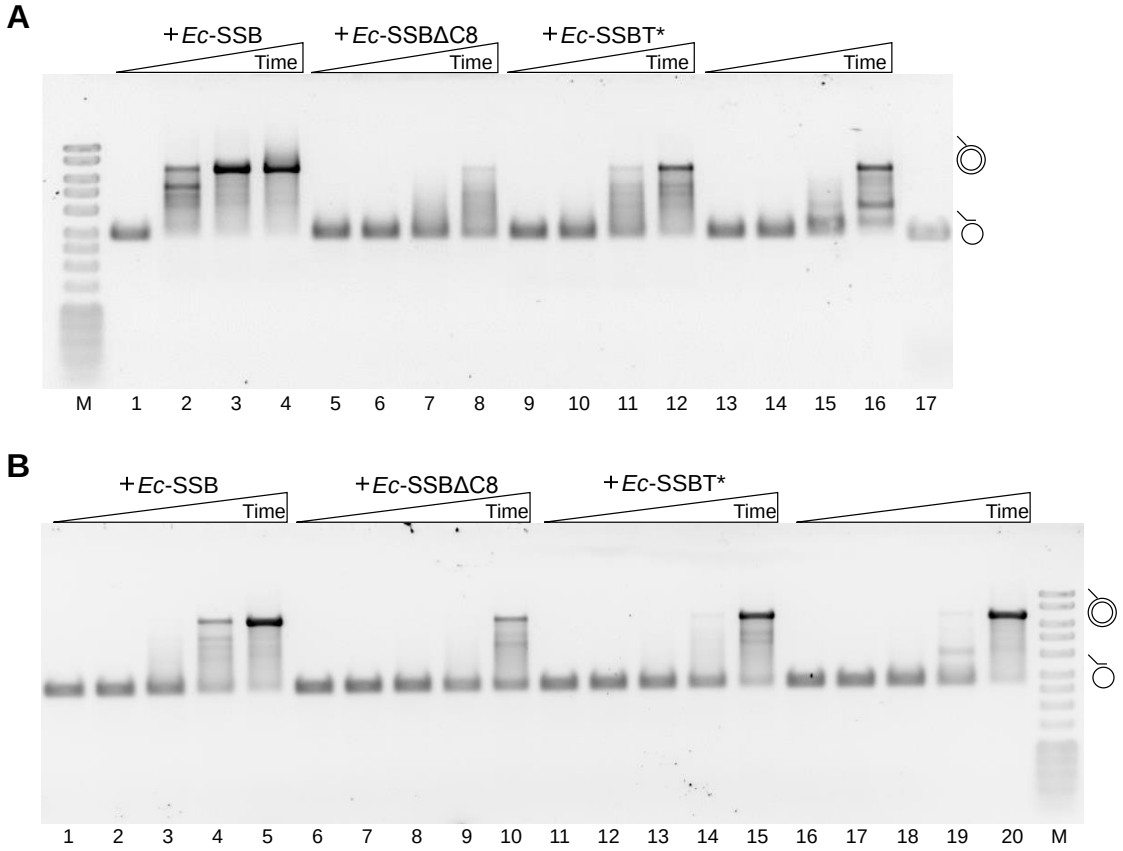

Figure 4.12 *Ec*-SSB stimulates Pol III HE primer extension by interaction between its last eight residues (DFDDDIPF) and the χ subunit. **A.** The time-course assay was conducted in the presence of Pol III HE (32 nM $\tau_3\delta\delta'\psi\chi$, 68 nM αεθ and 420 nM β_2) with 740 nM *Ec*-SSB (lanes 1–4), *Ec*-SSBΔC8 (lanes 5–8), or *Ec*-SSBT* (lanes 9–12), or the same volume of SSB storage buffer (lanes 13–16). Reaction mixtures containing individual *Ec*-SSB species were quenched at 0 (lanes 1, 5, 9 and 13), 10 (lanes 2, 6, 10 and 14), 30 (lanes 3, 7, 11 and 15) and 60 s (lanes 4, 8, 12 and 16). **B.** A similar time-course assay was conducted with Pol III HE in the absence of the χ and ψ subunits (*i.e.*, with 32 nM $\tau_3\delta\delta'$ in place of $\tau_3\delta\delta'\psi\chi$). Reaction mixtures containing individual *Ec*-SSB species were quenched at 0 (lanes 1, 6, 11 and 16), 10 (lanes 2, 7, 12 and 17), 30 (lanes 3, 8, 13 and 18), 60 (lanes 4, 9, 14 and 19) and 300 s (5, 10, 15 and 20). All reaction mixtures were incubated at 30˚C, and contained 20 mM Tris-HCl, pH 7.6, 10 mM $MgCl_2$, 110 mM NaCl, 1 mM ATP, 6.8 mM DTT, and 423 μM of each dNTP. Products were analyzed by 0.7% agarose gel electrophoresis.

Ec-SSB's entire flexible C-terminus is important for strand displacement (SD) synthesis by Pol III HE in physiological salt conditions. A bulk phase strand displacement assay involving Pol III HE has been established in our group (Jergic *et al.*, 2013). It shows a clear dependence on the conserved *Ec*-SSB C-terminus. It was speculated that the interaction between *Ec*-SSB and χ stimulates the reaction by stabilizing the whole complex. However, information about the functions of the N-terminal domain of *Ec*-

SSB in the process was missing. Therefore, a set of *Ec*-SSB and F-SSB fusion proteins (*Ec*-SSB–F-SSBc, F-SSB–*Ec*-SSBc, *Ec*-SSB–F-SSB and F-SSB–*Ec*-SSB; **Figure 4.2**) was introduced into the system. A salt titration assay first showed the absolute requirement of *Ec*-SSB for Pol III HE strand displacement synthesis, even at very low ionic strength (**Figure 4.13A**).

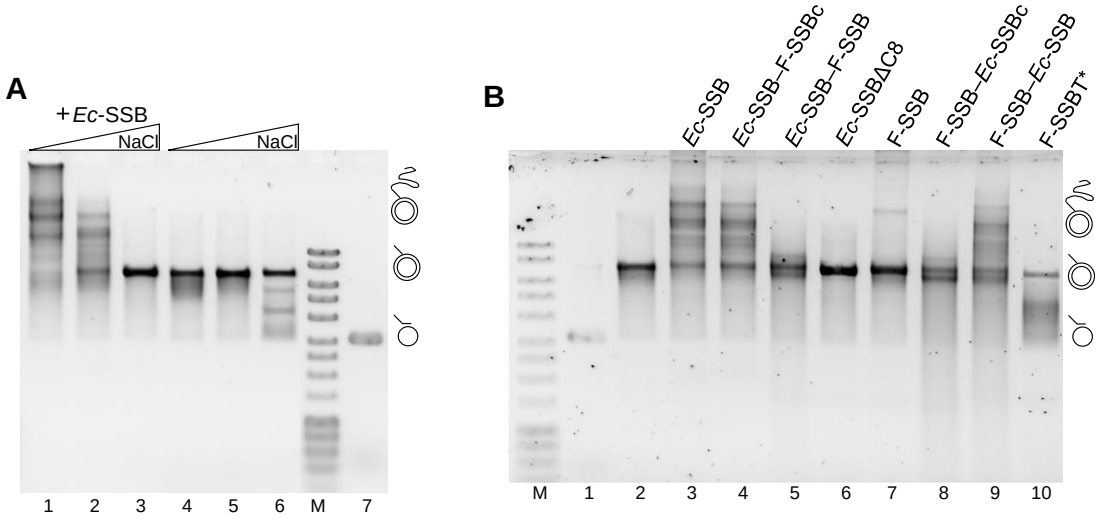

Figure 4.13: Pol III HE strand displacement is stimulated by *Ec*-SSB, and two *Ec*-SSB/F-SSB fusion proteins (*Ec*-SSB–F-SSBc and F-SSB–*Ec*-SSB). **A.** Salt titration (0, 55 and 110 mM NaCl, left to right) assay of Pol III HE strand displacement in the presence (750 mM; lanes 1–3) or absence of *Ec*-SSB (storage buffer added; lanes 4–6). Assays contained 20 mM Tris-HCl, pH 7.6, 20 mM $MgCl_2$, 1 mM ATP, 6.8 mM DTT, 423 µM of each dNTP, 68 nM αεθ, 32 nM $\tau_3\delta\delta'\chi\psi$ and 400 nM β_2, with 4 nM flap-primed M13 template. Reaction mixtures were incubated at 30˚C for 30 min. **B.** A similar reaction (at 30˚C for 40 min), except with 110 mM NaCl and 20 mM $MgCl_2$, using 750 nM *Ec*-SSB, *Ec*-SSBΔC8, F-SSB, F-SSBT* or various *Ec*-SSB/F-SSB fusion proteins, as indicated. The products in lane 2 were from a reaction that contained the same volume of storage buffer instead of the SSBs. DNA products were analyzed by 0.7% agarose gel electrophoresis. Lane 7 in **A** and lane 1 in **B** contain naked flap-primed M13.

To further examine the significance of the N-terminus of *Ec*-SSB, a similar assay (**Figure 4.13B**) was conducted with a range of SSBs, SSB truncations and *Ec*-SSB/F-SSB chimeras. Interestingly, F-SSB–*Ec*-SSB and *Ec*-SSB–F-SSBc stimulated Pol III HE strand displacement synthesis to a similar extent as *Ec*-SSB; however, reactions with F-SSB, *Ec*-SSB–F-SSB and F-SSB–*Ec*-SSBc did not give clear strand displacement products. As it was known the interaction of *Ec*-SSB C-terminal residues (DFDDDIPF) and the χ subunit is needed for strand displacement, and F-SSB also interacts with χ through its C-terminus (**Chapter 3**), it was necessary to know if the *Ec*- and F-SSB fusion proteins interact with the χ subunit in a similar way.

Therefore, interactions between χ and F-SSB–*Ec*-SSB, F-SSB–*Ec*-SSBc, *Ec*-SSB–F-

SSB or *Ec*-SSB–F-SSBc proteins were measured by SPR, essentially as described in **Chapter 3** (**Figure 4.14**). Calculated equilibrium dissociation constants (K_D) and the stoichiometries (n) are given in **Table 4.1**.

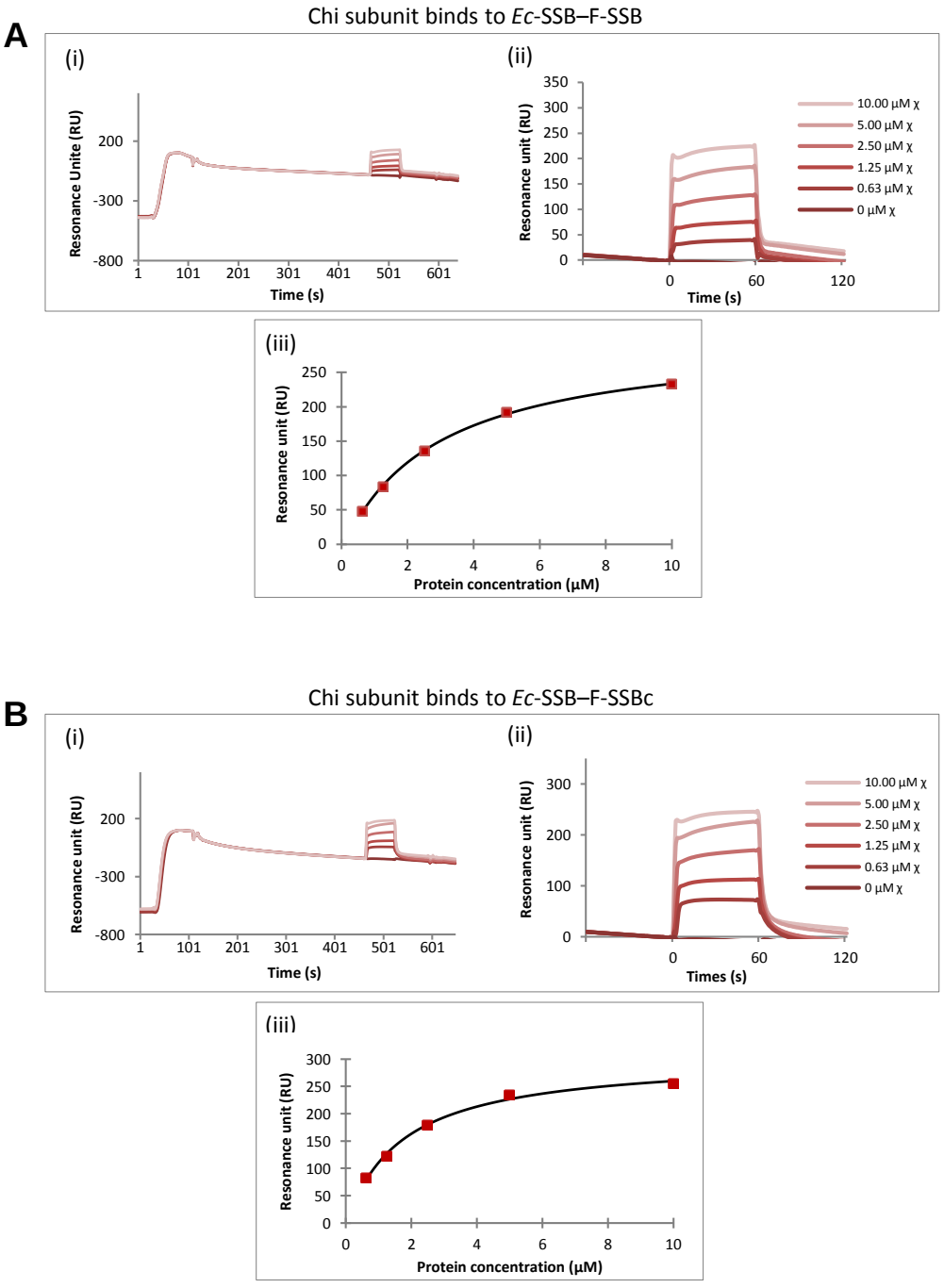

Figure 4.14 SPR sensorgrams (representative data) and equilibrium binding isotherms showing interactions between χ and tetramers composed of *Ec*-SSB and F-SSB fusion proteins. Results of interactions of χ with *Ec*-SSB–F-SSB **(A)** and *Ec*-SSB–F-SSBc **(B)** are shown. Proteins were dialyzed in buffer containing 10 mM HEPES, pH 7.4, 3 mM EDTA, 1 mM DTT and 150 mM NaCl before measurement. A fraction of this buffer was then supplemented with 0.005% surfactant P20, and used as the running buffer for SPR measurements. A 3'-biotinylated-$(dT)_{35}$ chip surface (100 RU) was used, and 100 nM of the SSBs were first injected for 60 s at 5 μL/min with a dissociation time of 450 s. A concentration series of the χ subunit was then injected for 60 s followed by a 60-s dissociation time. The surface was regenerated with 1 M $MgCl_2$ after the

dissociation. The whole procedure was repeated, starting from injection of the appropriate SSB, for injection of another concentration of the χ subunit. Aligned sensorgrams derived from injection of SSBs and the following injections of χ are shown at the left in the upper panel. At the right in the upper panel show enlarged sensorgrams of the injections of χ over the SSB surface. The fit binding isotherms (steady state 1:1) of χ binding are shown in the lower panel. (Figure continued on the next page).

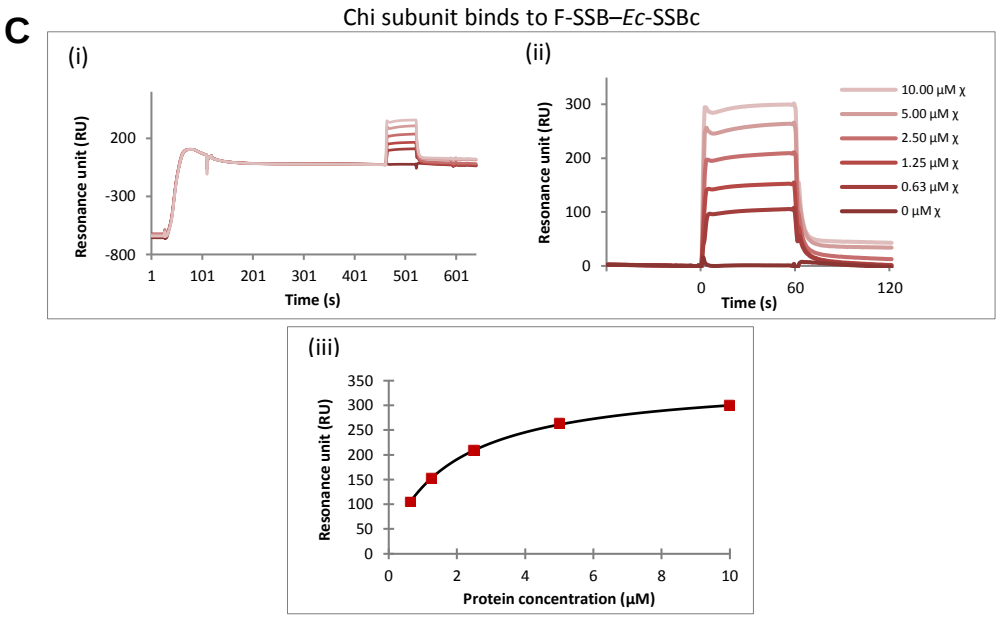

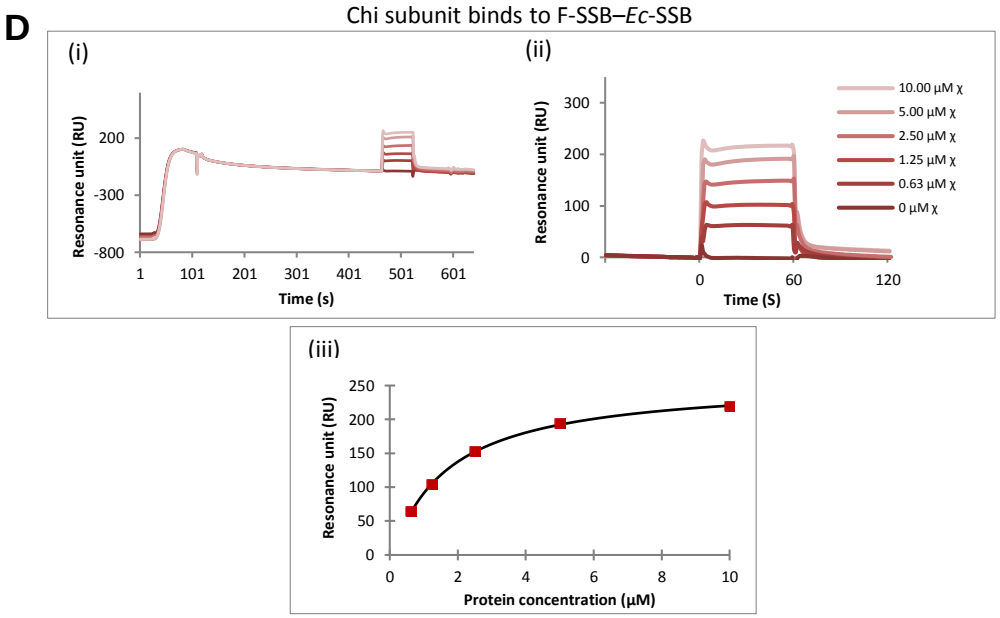

Figure 4.14 (continued from previous page). SPR sensorgrams (representative data) and equilibrium binding isotherms showing interactions between χ and tetramers composed of *Ec*-SSB and F-SSB fusion proteins. Results of interactions of χ with F-SSB–*Ec*-SSBc **(C)** and F-SSB–*Ec*-SSB **(D)** are shown. Experimental procedures were the same as those used in **A** and **B** (previous page).

According to the K_D, χ binds to *Ec*-SSB–F-SSBc (K_D = 1.7 μM), F-SSB–*Ec*-SSB (1.6 μM) and F-SSB–*Ec*-SSBc (2.0 μM) slightly more strongly than to *Ec*-SSB–F-SSB (2.9 μM), but the differences are small, and the K_D values are very close to the K_D (1.3 μM) for the intraction between χ and *Ec*-SSB (**Section 3.3.3**), suggesting that the residues before the last five (DDIPF) that vary between *Ec*- and F-SSB do not influence the binding affinity very much. Interestingly, the calculated stoichiometry of χ binding to *Ec*-SSB–F-SSB is double that of χ binding to F-SSB–*Ec*-SSB, but all the calculated stoichiometries are between 2 and 4, which are in the range of those for *Ec*- and F-SSB (**Section 3.3.3**).

Table 4.1 Calculated equilibrium dissociation constants (K_D) and the stoichiometries (n) for interactions between χ and *Ec*-SSB–F-SSB, *Ec*-SSB–F-SSBc, F-SSB–*Ec*-SSBc or F-SSB–*Ec*-SSB in physiological (150 mM NaCl) salt conditions. Errors are standard errors from non-linear regression.

	K_D (μM)	n	R_{max}
χ:*Ec*-SSB–F-SSB	2.9 ± 0.1	3.9 ± 0.03	313 ± 15
χ:*Ec*-SSB–F-SSBc	1.7 ± 0.2	3.2 ± 0.05	309 ± 5
χ:F-SSB–*Ec*-SSBc	2.0 ± 0.1	2.4 ± 0.02	330 ± 7
χ:F-SSB–*Ec*-SSB	1.6 ± 0.1	2.0 ± 0.01	271 ± 10

The fact that *Ec*-SSB, F-SSB–*Ec*-SSB and *Ec*-SSB–F-SSBc stimulate Pol III HE promoted strand displacement synthesis, but F-SSB, *Ec*-SSB–F-SSB and F-SSB–*Ec*-SSBc do not suggests that the stimulation effect is probably not related to the stoichiometry of the χ:SSB interaction. This is supported by data presented later that [*Ec*-SSB]$_{2.6}$[*Ec*-SSB~KikGR-His$_6$]$_{1.4}$, which has only 2–3 *Ec*-SSB C-termini accessible to χ also stimulates Pol III HE strand displacement synthesis (**Figure 4.25**). Interestingly, although the binding affinities between χ and *Ec*-SSB, F-SSB or *Ec*-SSB/F-SSB fusion proteins are very similar, those that stimulate strand displacement (*Ec*-SSB, F-SSB–*Ec*-SSB and *Ec*-SSB–F-SSBc) all have lower K_D values than those that do not (F-SSB, F-SSB–*Ec*-SSBc and *Ec*-SSB–F-SSB). It is thus possible that a stronger χ:*Ec*-SSB complex is a prerequisite condition for Pol III strand displacement synthesis, rather than the availability of free *Ec*-SSB C-termini close to the replisome. It is also noticeable that the SSBs that do not stimulate strand displacement (F-SSB, F-SSB–*Ec*-SSBc and *Ec*-SSB–F-SSB) all contain F-SSB residues 116–170, which are poorly conserved in *Ec*-SSB. Since the *Ec*-SSB OB-domain (residues 1–115) is well conserved in F-SSB, we speculate that some unrevealed properties of the unstructured *Ec*-SSB C-terminus (not incluing the last eight residues) also determine the propensity

for Pol III HE strand displacement synthesis (discussed further in **Chapter 5**).

The preliminary data from single-molecule DNA replication experiments (see later in **Section 4.3.9**) suggest that *Ec*-SSB is recycled at the replication fork. The unstructured C-terminal domain might be involved in the recycling pathway of *Ec*-SSB, and this pathway may be hindered by the C-terminus of F-SSB. This may be reflected in the lack of subunit exchange between F-SSB and *Ec*-SSB at 30˚C, a condition sufficient for *Ec*-SSB subunit exchange (**Section 4.3.2**). The different chemistry of the F-SSB C-terminus might be responsible for the lack of a recycling pathway as well. A subunit exchange experiment and a single-molecule assay with the *Ec*-SSB and F-SSB fusion proteins may shed further light on this speculation.

4.3.7 Additional roles of *Ec*-SSB's OB-domain and the χ subunit in Pol III HE primer extension and strand displacement synthesis

We found that in *low ionic strength conditions*, *Ec*-SSBΔC8 and *Ec*-SSBT* can also sustain Pol III HE strand displacement synthesis (data not shown). With the *Ec*-SSB:χ interaction abolished in this assay, the result shows that *Ec*-SSB's OB-domain is likely also to play a significant role in strand displacement synthesis. Therefore, with the help of Dr. Jergić, another assay with more combinations of proteins and a wider range of salt concentrations was carried out to explore the roles of the OB-domain of *Ec*-SSB (**Figure 4.15**). An unexpected new contribution of χ in DNA replication was revealed in this assay.

Ec-SSB's OB-domain by itself is able to stimulate Pol III HE strand displacement in low salt conditions. A salt titration assay was carried out with αεθ, β_2 and combinations of $\tau_3\delta\delta'\psi$ (assembled *in situ* from $\tau_3\delta\delta'$ and ψ) or $\tau_3\delta\delta'\psi\chi$, with *Ec*-SSB or *Ec*-SSBT* (**Figure 4.15**). The results showed that even in the absence of χ (lanes 5 and 6), the *Ec*-SSB OB-domain could still stimulate strand displacement synthesis in low salt conditions. However in the presence of 100 mM NaCl (lanes 8–13), strand displacement could only occur with intact SSB:χ interactions (lane 8). When the NaCl concentration was increased to 200 mM, strand displacement was suppressed in all reactions (lanes 14–19). The mechanism is unknown, but the results imply one function of the SSB OB-domain is likely to be to prevent the displaced ssDNA from reannealing with its

complementary strand. This provides a constant open fork, which facilitates the "invasion" of the Pol III core into the downstream dsDNA. The mechanism, therefore, is probably similar to that of strand displacement synthesis by Pol I (**Section 4.3.4**).

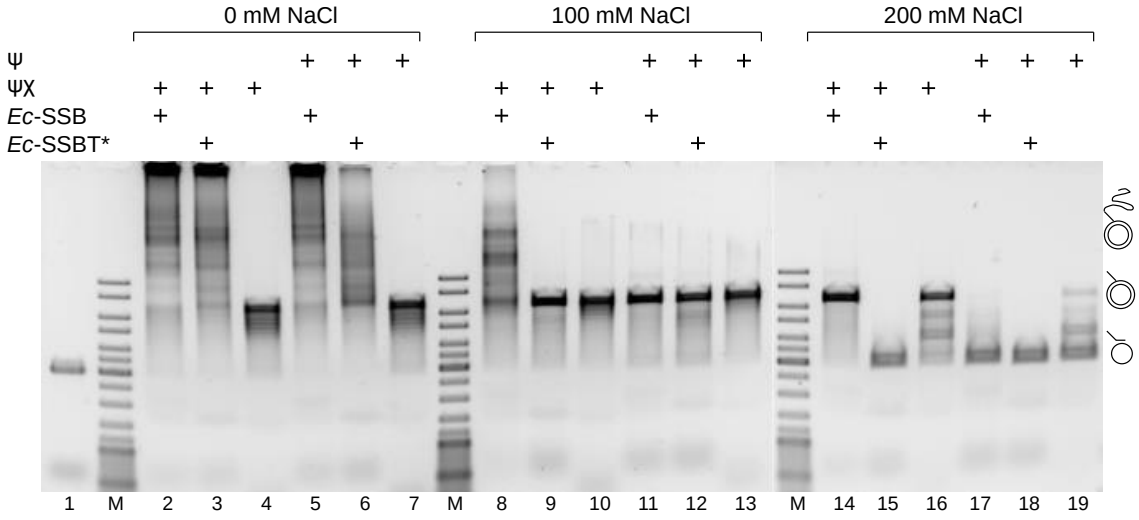

Figure 4.15: *Ec*-SSB OB-domain stimulates Pol III strand displacement at low salt, and a stimulatory role of the χ subunit is revealed in Pol III primer extension at high salt. All reactions contain 100 nM αεθ and 300 nM β_2, with various combinations of 30 nM $\tau_3\delta\delta'$ + 183 nM ψ (labelled ψ) or 31 nM $\tau_3\delta\delta'\psi\chi$ (labelled ψχ), with 750 nM *Ec*-SSB or *Ec*-SSBT* (as indicated by "+"). NaCl at 0, 100 or 200 mM was supplemented (as labelled above the gel) in the reaction buffer (20 mM Tris-HCl, pH 7.6, 10 mM $MgCl_2$, 1 mM ATP, 11 mM DTT, 600 μM of each dNTP). Flap-primed M13 template (3 nM) was added into each reaction mixture; after 20 min incubation at 30˚C, the products were analyzed by 0.7% agarose gel electrophoresis. Lane 1 contained the naked flap-primed M13 ssDNA.

A stimulatory role of χ in Pol III primer extension was also revealed in this experiment. In low salt conditions with abolished SSB:χ interaction, the reaction containing χ (lane 3) seemed to have a higher efficiency of strand displacement than that without χ (lane 6). And at high salt, with strand displacement suppressed, reactions with χ (lanes 14–16) had significantly higher primer extension efficiency than those without χ (lanes 17–19) except in the cases with *Ec*-SSBT* present, where both reactions were totally inhibited (lanes 15 and 18). The presence of ψχ has been shown previously to render strand extension synthesis by Pol III HE more salt resistant (Olson *et al.*, 1995; Glover and McHenry, 1998); the results shown here suggest that this involves the interaction of χ with the C-terminal domain of *Ec*-SSB in addition to stabilization of the clamp loader by interaction with the N-terminal region of ψ.

4.3.8 Pol I is indispensable during Okazaki fragment maturation

It was widely accepted that Pol I is the protein processing the RNA primers at the Okazaki fragments junctions (**Section 4.1.2**). However RNA exonuclease activity of RNase H in *E. coli* has stimulated the speculation of an alternative pathway for Okazaki fragment maturation. This speculation has not yet been tested in any functional assays. Thanks to the well-established bulk phase DNA replication assays in our laboratory, this alternative pathway could be investigated. To examine Okazaki fragment maturation, ligase A was added into a reaction system with an RNA primed M13 template as an indicator for a processed nick; ligase should covalently close the nick remaining after primer removal and the resulting dsDNA will migrate faster in the agarose gel in the presence of EtBr. Pol I, as the known nick-translation protein in *E. coli*, was used as a positive control. The enzymatic activities for ligase A, RNase HI, RNase HII and Pol I were tested before all the assays.

The activity and concentration of ligase A required for the nick-sealing ligation was explored with a singly-nicked plasmid. For the assay (**Figure 4.16A**), CsCl density gradient purified plasmid (**Section 4.3.1**) with a single nick in one of the DNA strands was used. The result showed about 3.5 nM of ligase A (lane 10) is able to ligate about half of the nicked plasmid (1.3 nM), and convert them to the covalently closed circular form. It was noticed that even with 56 nM (lane 14) of ligase A in the reaction, some remaining nicked template was still observed in the gel.

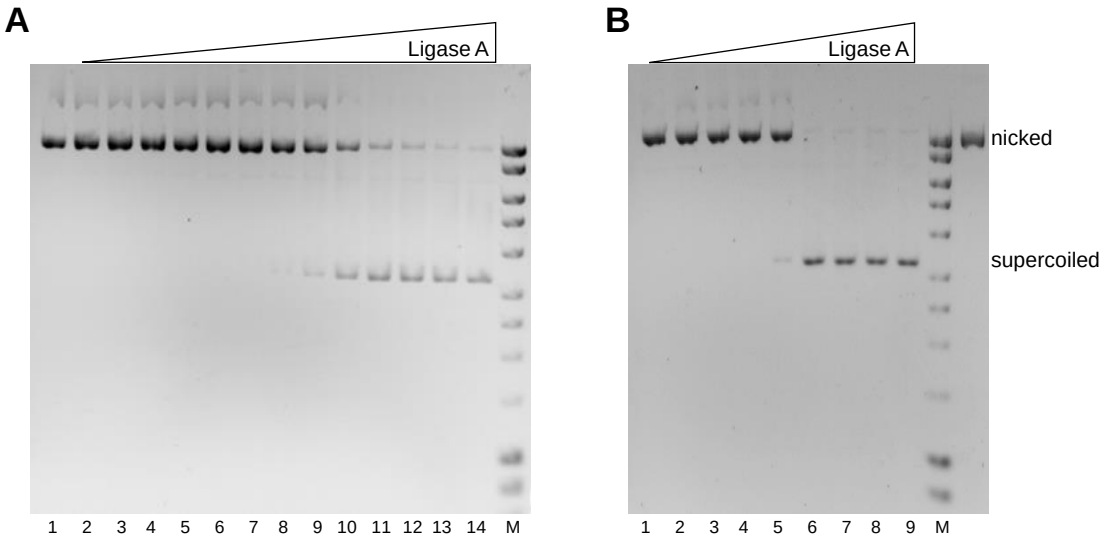

Figure 4.16 Characterization of ligase A activity by DNA ligation assays. **A.** Ligase A at 0.02 (lane 2), 0.03 (lane 3), 0.05 (lane 4), 0.11 (lane 5), 0.22 (lane 6), 0.44 (lane 7), 0.88 (lane 8), 1.75 (lane 9), 3.5 (lane 10), 7 (lane 11), 14 (lane 12), 28 (lane 13) and 56 nM (lane 14) was titrated in reaction buffer containing 50 mM Tris-HCl, pH 7.8, 10 mM $MgCl_2$, 10 mM DTT, 26 μM NAD^+,

25 μg/mL BSA and 1.3 nM nicked plasmid. After incubation at 30˚C for 30 min, reactions were quenched, and products analyzed by 0.7% agarose gel electrophoresis in the presence of EtBr. **B.** In the same reaction buffer, 1000 (lane 9), 100 (lane 8), 10 (lane 7), 1 (lane 6), 0.1 (lane 5), 0.01 (lane 4), 0.001 (lane 3), 0.0001 (lane 2) and 0.00001 nM (lane 1) of ligase A was titrated. The resulting products were analyzed in the same way as in **A**. Lane 1 in **A** and the unmarked lane in **B** contain nicked plasmid substrates.

Another titration assay was conducted with a higher concentration of ligase A (**Figure 4.16B**). A small amount of nicked template was still visible with the highest concentration (1 μM) of ligase A present, indicating that the template is possibly damaged at the nicked site (e.g., loss of 5'-phosphate or 3'-OH group), so cannot serve as the substrate for ligase. However the substantial closing of the nicked template proved that the ligase A is active, and 1–10 nM of ligase A is able to convert 1.3 nM nicked DNA template at 30˚C in 30 min in the presence of 26 μM NAD^+ (*E. coli* ligase uses NAD^+ rather than ATP for adenylation of the 5'-phosphate).

The activity and concentration of ligase A required for the ligation was also explored in a DNA replication assay (**Figure 4.17**). It shows that an RNA-primed M13 was replicated by the Pol III holoenzyme and became double-stranded (lane 11). In the presence of Pol I and a certain concentration of ligase A (lanes 1–4), the fully replicated M13 template was able to be converted cleanly to the covalently closed circular form that in the presence of EtBr migrates faster in the agarose gel than the fully replicated, but relaxed, circular product.

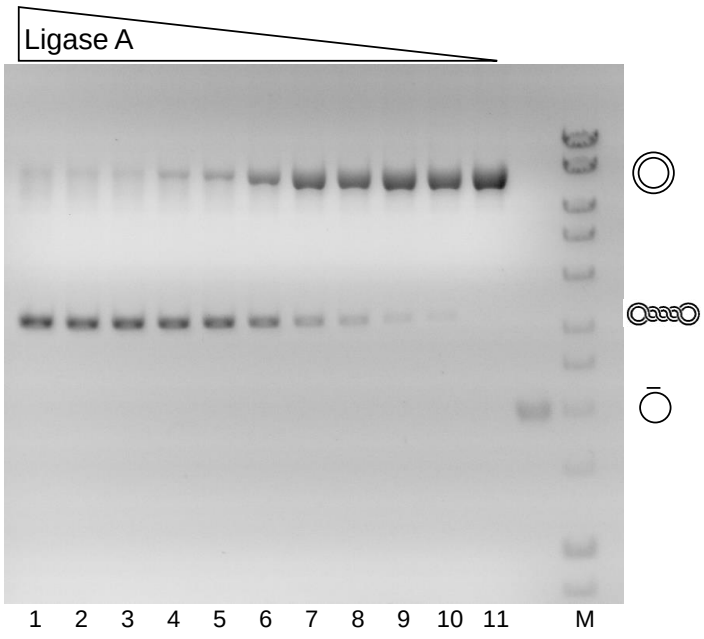

Figure 4.17 Ligase A titration in a Pol III DNA replication assay in the presence of Pol I. Ligase A (188, 94, 47, 23, 11.5, 5.8, 2.9, 1.4, 0.72, 0.36, 0.18 nM in lanes 1–11, respectively) was titrated into a DNA replication assay with $\tau_3\delta\delta'$, $\alpha\varepsilon\theta$, β_2, *Ec*-SSB, Pol I and RNA primed M13 template.

Specifically, the reaction buffer contained 20 mM Tris-HCl, pH 7.6, 10 mM $MgCl_2$, 120 mM NaCl, 0.96 mM ATP, 8.8 mM DTT, 288 μM of each dNTP, 210 nM β_2, 24 nM $\tau_3\delta\delta'$, 75 nM $\alpha\varepsilon\theta$, 510 nM *Ec*-SSB, 28 μM NAD^+, 137 nM Pol I and 3 nM RNA-primed M13 template. The reaction was carried out in 30˚C for 20 min. The products were separated on a 0.7% agarose gel in the presence of EtBr. The unmarked lane contains the naked RNA-primed M13.

This indicates that the RNA primer on the M13 had been converted into DNA by the 5'–3' (flap-) endonuclease activity of Pol I in concert with gap filling (with DNA) by its 5'–3' polymerase activity (i.e., nick translation). The Pol I is clearly active in the assay. Importantly, it shows that 23 nM of ligase A (lane 4) is able to fully ligate the fully replicated M13 template (3 nM); 20 nM (or a higher concentration) of ligase A was used for the following assays whenever it was required.

The ligase A titration assay relied on the Pol I activity for nick translation, without which the ligation could not occur. This highlights the importance of Pol I for Okazaki fragment maturation. To deliberately look at the dependence on Pol I for nick translation, a Pol I titration was carried out in a similar assay system with a fixed concentration of ligase A (20 nM; **Figure 4.18**).

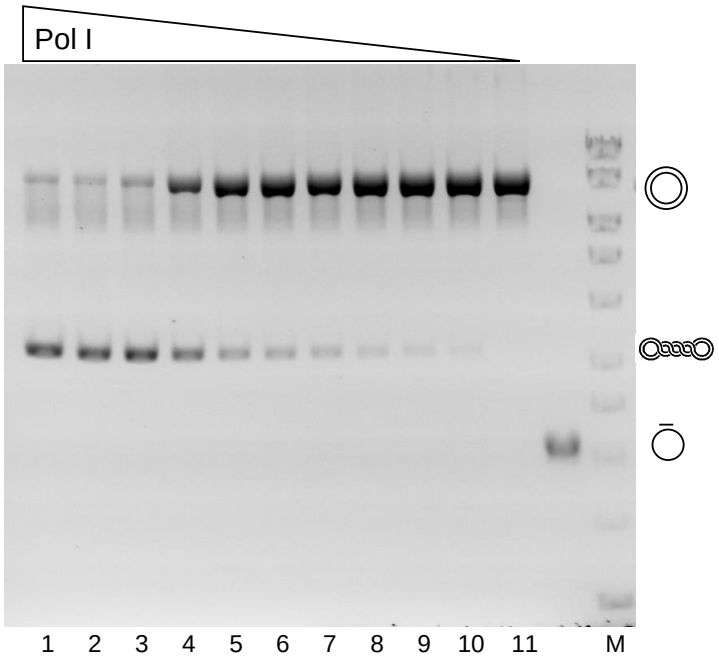

Figure 4.18 Pol I titration in a Pol III DNA replication assay in the presence of ligase A. Pol I was titrated in to a DNA replication assay in the presence of $\tau_3\delta\delta'$, $\alpha\varepsilon\theta$, β_2, *Ec*-SSB, ligase A (20 nM) and RNA-primed M13 template. Specifically, 134 (lane 1), 67 (lane 2), 33.5 (lane 3), 16.8 (lane 4), 8.4 (lane 5), 4.2 (lane 6), 2.1 (lane 7), 1.05 (lane 8), 0.52 (lane 9), 0.26 (lane 10) and 0.13 nM (lane 11) of Pol I were titrated in the reaction buffer containing 20 mM Tris-HCl, pH 7.6, 10 mM $MgCl_2$, 120 mM NaCl, 0.96 mM ATP, 8.8 mM DTT, 288 μM of each dNTP, 210 nM β_2, 24 nM $\tau_3\delta\delta'$, 75 nM $\alpha\varepsilon\theta$, 510 nM *Ec*-SSB, 28 μM NAD^+, 20 nM ligase A and 3 nM RNA-primed M13 template. The reaction was carried out at 30˚C for 20 min. The products were analyzed in a 0.7% agarose gel in the presence of EtBr. The unmarked lane contains the RNA-primed M13 template.

The result shows fully replicated M13 was achieved in all the reactions. However with a low concentration of Pol I, no ligation was observed (lane 11), which means the RNA primer was still intact (or partially intact) and could not serve as the substrate for ligase A. With a certain concentration of Pol I in the reaction, full ligation occurred (lanes 1–3). At 33.5 nM Pol I (lane 3), almost all of the fully replicated templates were converted into ligated covalently closed circular products, and could be distinguished from the unligated products in the agarose gel with EtBr present. **Figures 4.17** and **4.18** clearly show the dependence on the 5'–3' endonuclease and 5'–3' DNA polymerase activities of Pol I for nick translation and ligation in Okazaki fragment processing. However, to show the third activity of Pol I, which is the 3'–5' exonuclease (proofreading) activity, a different DNA replication system with a different template had to be used.

The nicked plasmid was used to probe the 3'–5' exonuclease activity of Pol I. In previous assays (see **Section 4.3.4**), Pol I showed 5'–3' DNA polymerase activity and (surprisingly) SD activity in the presence of the OB-domain of *Ec*-SSB. By using a similar combination of proteins but with the singly-nicked plasmid instead of primed M13 template, the third activity (3'–5' exonuclease) of Pol I could be probed. This assay (**Figure 4.19**), shows that in the presence of ligase A, the nicked plasmids were ligated and transformed into supercoiled plasmid, which migrate faster in the gel in the presence of EtBr (lanes 1–3). However, in the reactions without ligase A, Pol I was able to give strand displaced DNA species in the presence of *Ec*-SSB, as well as shortened products (lane 4). However, the reaction without *Ec*-SSB did not show Pol I SD activity, although the resulting DNA product (lane 6) seemed a little larger than the plasmid template (lane after 6).

This may result from weaker *Ec*-SSB-independent SD activity of Pol I, which is dramatically reduced without the *Ec*-SSB. The fact that Pol I was able to displace the strand in the 5'–3' direction with the nicked plasmid (*cf.* the primed M13 template) hints that Pol I has to digest a few nucleotides in the 3'–5' direction to allow the polymerase active site to recognize the 3' end of the DNA for 5'–3' DNA synthesis. This theory is supported by the fact that the 5'–3' endonuclease activity of Pol I is highly stimulated by the concurrent 5'–3' polymerase activity (Lundquist and Olivera, 1982). However ligase A seems to prevent this from happening (**Figure 4.19**).

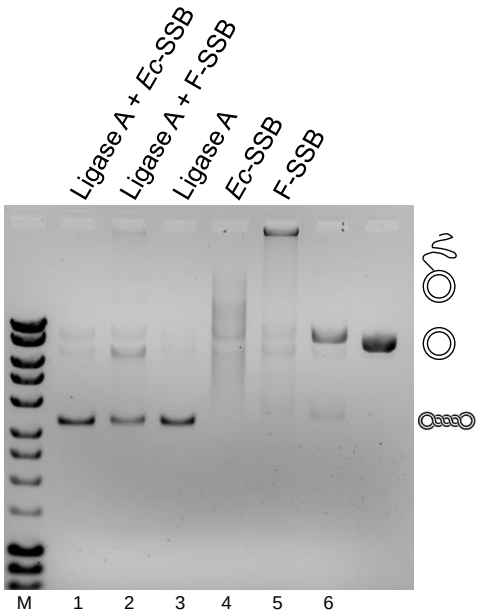

Figure 4.19 3'–5' exonuclease activity of Pol I probed in a *Ec*-SSB dependent SD assay with and without ligase A. Various combinations (labelled above the gel) of *Ec*-SSB, F-SSB and ligase A were mixed with the reaction buffer containing Pol I and the nicked plasmid (lanes 1–6). Specifically, 800 nM of *Ec*-SSB (lane 1), F-SSB (lane 2) or an equal volume of the SSB storage buffer (lane 3) were mixed with the reaction buffer containing 20 mM Tris-HCl, pH 7.6, 10 mM $MgCl_2$, 40 mM NaCl, 1 mM ATP, 8.8 mM DTT, 500 μM of each dNTP, 440 nM Pol I, 3 nM nicked plasmid and 390 nM ligase A. In parallel, 800 nM of *Ec*-SSB (lane 4), F-SSB (lane 5) or an equal volume of the SSB storage buffer (lane 6) were mixed with the same reaction buffer without the presence of ligase A. The reaction mixtures were incubated at 30˚C for 2 h. The products were analyzed by 0.7% agarose gel electrophoresis in the presence of EtBr. The unmarked lane contains the naked nicked plasmid.

It is worth noting that a mistake was made in the experiment in **Figure 4.19.** NAD^+ as the energy source of ligase A (**Section 1.1.2.4**) was not added in the experiment. Nevertheless, efficient ligation occurred in the presence of ligase A at a high concentration (390 nM). It is very likely that the ligase A as isolated was partially adenylated, and no further consumption of NAD^+ under these conditions is needed. Mass spectroscopy analysis of purified T7 DNA ligase revealed that 30% of it was adenylated (Doherty *et al.* 1996). A previous experiment showed 110 nM ligase A was able to ligate 1 nM of the same nicked plasmids in the absence of NAD^+ (not shown). Thus, further experiments in the presence of NAD^+ are needed to examine the effect of ligase A at lower concentration.

These data also resemble the outcomes of a DNA replication assay with the Pol III system with the singly-nicked plasmid instead of the primed M13 template conducted by Dr. Slobodan Jergić. The result showed that the ε subunit associated with the Pol III α subunit was needed to digest a few nucleotides from the 3'-end of the nicked site to

allow 5'–3' DNA replication (SD synthesis) by the α subunit to occur (data not shown). All in all, the assay demonstrated Pol I is able to initiate SD even at a nick, and this probably requires its 3'–5' exonuclease activity (**Figure 4.19**). Ligase A seems to compete with the SD activity of Pol I, presumably by recognition and adenylation of the nicked site, leading to ligation (lanes 1–3 in **Figure 4.19**). This leaves no substrate for Pol I, thus no SD was observed even with the presence of *Ec*-SSB (lane 1). This highlights the events in the last steps of Okazaki fragment synthesis: as soon as Pol I finishes nick translation, the nicked site is immediately occupied through tight interaction of ligase A for ligation. This avoids the risk of the nicked site being processed by other enzymes. This is also reflected in the large DNA binding sites (for protection of the nick) on *E. coli* ligase A in the ligase A:nicked DNA co-crystal structure (Nandakumar *et al.,* 2007). The composition of the heavy band resulting from the reaction with F-SSB (lane 5) is not clear; however, we know F-SSB can bind dsDNA.

Enzymatic activity of RNase HI and RNase HII were tested in a Pol III HE DNA replication assay (**Figure 4.20**). Studies showed that *E. coli* RNase HI digests RNA primers discontinuously in the 3'–5' direction (Hogrefe *et al.,* 1990; Crooke *et al.,* 1995), and cannot digest an RNA hybridized to a DNA strand to produce a DNA nick site as can Pol I (**Section 4.1.2**). Here, RNA-primed M13 was preincubated with RNase HI and/or HII to analyze their activities in a preliminary way. However, in the experiments that follow, RNase Hs will be added with Pol III to investigate their functions in concurrent DNA replication. The first result (**Figure 4.20**) shows that RNase HI and a combination of RNase HI and HII are able to digest RNA primers from RNA-primed M13, resulting in total abolition of primer extension (lanes 1 and 3). However, pretreatment of RNA-primed M13 with RNase HII alone did not result in prevention of DNA replication. A fully replicated M13 was observed in this condition (lane 2). This indicates that RNase HI is probably the enzyme digesting the full RNA primer. RNAse HII seems to have no nuclease activity.

The reactions with RNase HI and RNase HII treated flap-primed M13 and 5'-phosphorylated DNA-primed M13 give rise to SD synthesis, without showing unconsumed M13 templates (lanes 4–9). This indicates that neither RNase HI nor RNase HII digest partially or fully complementary DNA primers. The Pol III SD with

different primers is further studied and discussed in the following experiment.

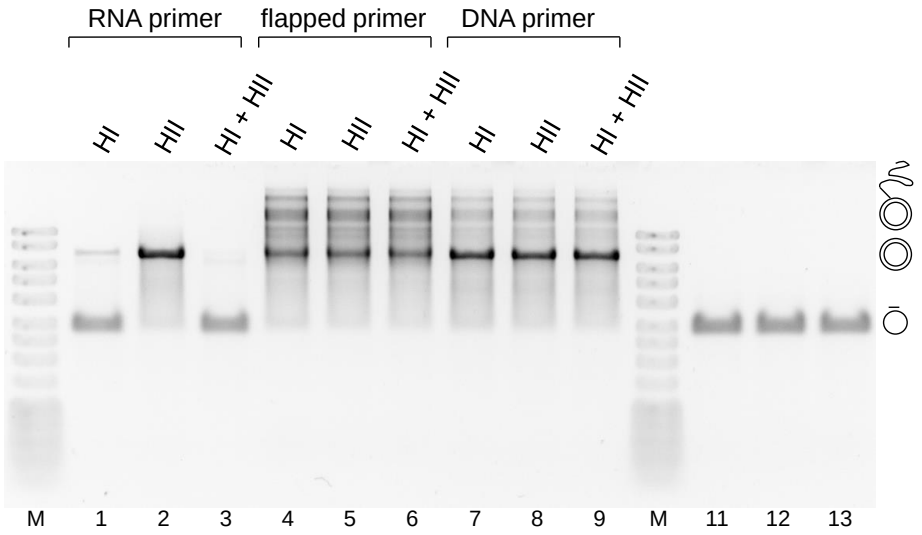

Figure 4.20 RNase HI and RNase HII tested in the Pol III HE DNA replication assay for their enzymatic activity. Individual RNase HI (lanes 1, 4 and 7), RNase HII (lanes 2, 5 and 8) or a combination of both (lanes 3, 6 and 9) were preincubated with RNA-primed M13 (lanes 1–3), flap-primed M13 (lanes 4–6) or 5'-phosphorylated DNA-primed M13 (with fully complementary DNA primer, **Section 4.2.7.1**; lanes 7–9). To the reaction mixtures were then added $\tau_3\delta\delta'\psi\chi$, $\alpha\varepsilon\theta$, β_2 and *Ec*-SSB to initiate DNA replication. Specifically, 6 nM of RNA-primed M13, flap-primed M13 and 5'-phosphorylated DNA-primed M13 were mixed with 210 nM of RNase HI, 210 nM of RNase HII or both RNase HI and RNase HII (210 nM of each) in reaction buffer A containing 20 mM Tris-HCl, pH 7.6, 10 mM $MgCl_2$, 120 mM NaCl, 1 mM ATP, 328 µM of each dNTP, 6.7 mM DTT and 23.5 µM NAD^+, and incubated at 30˚C for 10 min to digest the primer. Then the reaction mixtures were added to buffer B containing $\tau_3\delta\delta'\psi\chi$, $\alpha\varepsilon\theta$, β_2, *Ec*-SSB in buffer A to obtain a final reaction buffer containing 20 mM Tris-HCl, pH 7.6, 10 mM $MgCl_2$, 120 mM NaCl, 1 mM ATP, 328 µM of each dNTP, 6.7 mM DTT, 23.5 µM NAD^+, 30 nM $\tau_3\delta\delta'\psi\chi$, 60 nM $\alpha\varepsilon\theta$, 200 nM β_2 and 533 nM *Ec*-SSB, and 3 nM variously primed M13 templates, 105 nM RNase HI (lanes 1, 4 and 7), 105 nM RNase HII (lanes 2, 5 and 8) or combination of the two RNase Hs with 105 nM of each (lanes 3, 6 and 9). The reaction mixtures were incubated at 30˚C for 20 min. The reactions were analyzed by 0.7% agarose gel electrophoresis without EtBr. The M13 with digested primers do not provide a Pol III HE binding site, therefore result into no DNA replication (lanes 1 and 3). Full primer extension (lane 2) and SD (lanes 4–9) were observed, indicating no primer digestion by RNase H. The lanes 11, 12 and 13 were loaded with the RNA-primed M13, flap-primed M13 and 5'-hosphorylated DNA-primed M13, respectively.

Nevertheless, neither RNase HI nor RNase HII can properly process the RNA primer, to allow ligase A to ligate the nick to give a continuous DNA double strand. Here, in a similar ligation assay in the presence of Pol I as described earlier (**Figures 4.17** and **4.18**), RNase HI and RNase HII were added (**Figure 4.21A**). Additionally, two of the dNTPs (dATP and dCTP) were added with Pol III HE to allow it to assemble on the primed site, and then the other two were added to initiate replication with the addition of Pol I, RNase HI or RNase HII. This assay allows us to compare the canonical pathway of Okazaki fragment maturation involving Pol I and the proposed alternative pathway

(involving RNase HI and/or RNase HII). The nick translated plasmid with an intact nick will be ligated in the presence of ligase A, and migrate faster in the gel than the unligated plasmid in the presence of EtBr.

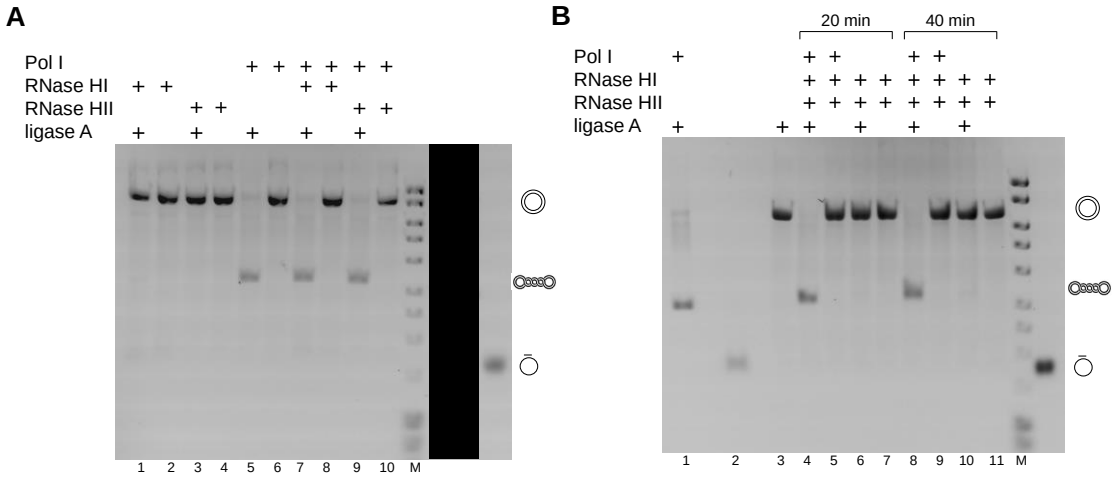

Figure 4.21 Ligation assays show the inability of RNase HI and RNase HII to properly process an RNA primer on the lagging strand. Various combinations (labelled above the gel) of Pol I, RNase HI, RNase HII and ligase A were added into the reaction mixture containing preassembled $\tau_3\delta\delta'\psi\chi$, $\alpha\varepsilon\theta$, β_2 and *Ec*-SSB (by adding dATP and dCTP instead of all four dNTPs). The reactions were initiated by adding dTTP and dGTP. **A.** Pol III HE (27 nM $\tau_3\delta\delta'\psi\chi$, 75 nM $\alpha\varepsilon\theta$ and 285 nM β_2) were first mixed with a buffer containing 20 mM Tris-HCl, pH 7.6, 10 mM $MgCl_2$, 120 mM NaCl, 1 mM ATP, 8 mM DTT, 0.3 mM dATP, 0.3 mM dCTP, 28.9 μM NAD^+, 526 nM *Ec*-SSB and 3 nM RNA primed M13 template to allow proteins to assemble on the primed site. Then were added individually or in combinations 112 nM Pol I, 24 nM ligase A, 160 nM RNase HI or 160 nM RNase HII (as indicated above), followed by 0.3 mM dTTP and dGTP The reaction mixture was incubated at 30˚C for 20 min. **B.** In another assay, Pol III HE (27 nM $\tau_3\delta\delta'\psi\chi$, 75 nM $\alpha\varepsilon\theta$ and 285 nM β_2) were first mixed with a buffer containing 20 mM Tris-HCl, pH 7.6, 10 mM $MgCl_2$, 120 mM NaCl, 1 mM ATP, 8 mM DTT, 0.3 mM dATP, 0.3 mM dCTP, 28.9 μM NAD^+, 526 nM *Ec*-SSB and 3 nM RNA primed M13 template, and incubated at 30˚C for 2 min to allow their assembly on the primed site. Then, individually or in combination were added (as indicated above): 112 nM Pol I, 24 nM ligase A, 160 nM RNase HI or 160 nM RNase HII (or the same volume of buffer containing 20 mM Tris-HCl, pH 7.6, 120 mM NaCl and 10 mM $MgCl_2$ in lane 2), followed by 0.3 mM dTTP and dGTP in all the reactions except the one in lane 2. The reaction mixtures were incubated at 30˚C for 20 min (lanes 1–7) or 40 min (lanes 8–11). The products were analyzed by 0.7% agarose gel electrophoresis in the presence of EtBr. Neither individual proteins (**A**) nor a combination (**B**) of RNase HI and RNase HII gave rise to ligated M13 dsDNA in the presence of ligase A in 20 min (**A** and **B**) or 40 min (**B**). However all mixtures containing Pol I gave rise to ligated products, indicating a properly processed RNA primer resulted from Pol I nick translation. Unmarked lanes in **A** and **B** are naked RNA-primed M13.

The M13 ssDNA was replicated to the double-stranded form in the presence of various combinations of Pol I, ligase A, RNase HI or RNase HII, but were only successfully ligated when both Pol I and ligase A were present (lanes 5, 7 and 9). None of the combinations of Pol I, ligase A, RNase HI and RNase HII hindered strand extension from the RNA primer by Pol III. Importantly, RNase HI or RNase HII could not properly process the RNA primer as does Pol I. The mechanism was further investigated

in another assay with both RNase HI and RNase HII present in the same reaction and with a longer reaction time (**Figure 4.21B**). This would show if a cooperative function of RNase HI and RNase HII exist for RNA primer processing. The DNA product from the reaction in lane 2 migrated almost at the same position as the primed M13 template (the unmarked lane) in the gel, indicating that omission of two of the four dNTPs in the reaction stalled the Pol III HE. On the other hand, the reactions with all four dNTPs present all gave rise to fully replicated M13. It is noteworthy that the fully replicated dsDNA cannot be ligated with ligase A alone (lane 3). The result functionally demonstrates the significance of Pol I in Okazaki fragment maturation, leading to a continuous strand being obtained in the presence of ligase A (lane 1 with addition of both Pol I and ligase A). More importantly, the reactions with both RNase HI and RNase HII in the presence of ligase A (lanes 6 and 10) did not lead to any ligated DNA in 20 or even 40 min, confirming the lack of RNA primer processing activity of the enzymes. Neither RNase HI nor RNase HII seems to interfere with the Pol I activity (lanes 4 and lane 8). The results demonstrate the unlikelihood of the existence in *E.* coli at least, of the alternative Okazaki fragment maturation mechanism involving RNase Hs. This is consistent with the biochemistry studies, that showed the inability of RNase H to digest the junction of the RNA primer and DNA, resulting in at least one RNA nucleotide being always left behind (Hogrefe *et al.,* 1990; Crooke *et al.,* 1995). It is also worth noticing that both of RNase HI and RNse HII seem not to hinder the activity of Pol I in the process of nick translation. However since RNase H has affinity towards RNA primers (Hogrefe *et al.,* 1990; Crooke *et al.,* 1995), it is interesting to find out whether it competes with Pol I upon binding to the primed site. A RNase HI titration assay similar to the one shown in **Figure 4.21** will shed some light on this question. Alternatively, a competition assay with RNAse H and Pol I on an immobilized primed DNA using SPR may give direct evidence for this issue.

The story about the alternative pathway for Okazaki fragment maturation is settled for now, but other interesting features observed in the ligation assay (**Figure 4.21)** can still not be explained. For example, Pol I has been demonstrated in the DNA replication assay with DNA primed M13 (**Figure 4.8**) or nicked plasmid (**Figure 4.19**) to have SD activity stimulated by *Ec*-SSB. It is known Pol I possesses 5'–3' endonuclease activity and 3'–5' exonuclease activity. With the nicked plasmid, Pol I can probably digest a few nucleotides at the 3'-end, and transition into SD synthesis. A similar activity has

been shown by Dr. Slobodan Jergić for Pol III SD stimulated by the ε proofreading subunit in assays with the singly-nicked plasmid template (data not shown). In my ligation assay, both Pol I and ε were present. However, no SD was observed in any of the present assays containing Pol III HE, *Ec*-SSB and Pol I (regardless of the presence of ligase A). What mechanism prevents SD synthesis, which would otherwise hinder Okazaki fragment maturation? Previously, Dr. Jergić observed that SD did not occur with RNA-primed M13 templates, and in some preliminary assays, I observed SD in the ligation assay with flap-primed or DNA-primed M13 in the presence of both Pol I and ligase A. Since the product of nick translation by Pol I should in theory be a suitable template for Pol III SD synthesis, our results suggest tight coupling between Pol I and ligase. Since they are both believed to interact with the β_2 sliding clamp (López de Saro and O'Donnell, 2001), it may be that this coupling is mediated *via* the clamp.

To examine the role of the RNA primer in Okazaki fragment maturation, an assay with M13 templates primed with mixed oligoribo/deoxyribonucleotides was used (**Figure 4.22**). These primers had *n* ribonucleotides (rNMPs) at the 5' end (*n* = 0, 1, 5, 10, 15, or 33) followed by (33–*n*) dNMPs, As the number of 5'-rNMPs increased, the extent of Pol III SD synthesis decreased (lanes 2, 5, 8, 11, 14 and 17).

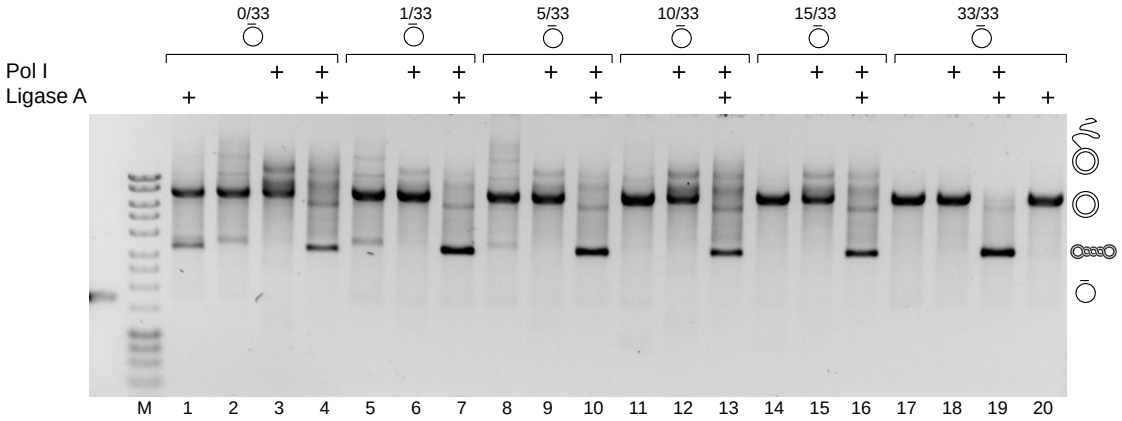

Figure 4.22 Ligation assay with Pol III HE conducted using mixed oligoribo/deoxyribonucleotide primed M13 templates. Reactions were conducted with $\tau_3\delta\delta'\psi\chi$, $\alpha\varepsilon\theta$, β_2, *Ec*-SSB, variously primed M13s and combinations of Pol I and ligase A. Specifically, 500 nM Pol I and 375 nM ligase A (as indicated above) were added into the reaction buffer containing 20 mM Tris-HCl, pH 7.6, 110 mM NaCl, 1.14 mM ATP, 475 μM of each dNTP, 28 μM NAD^+, 7.6 mM DTT, 34 nM $\tau_3\delta\delta'\psi\chi$, 75 nM $\alpha\varepsilon\theta$, 476 nM β_2 and 760 nM *Ec*-SSB with 3 nM M13 primed by full DNA (33 dNMPs, lanes 1–4), 1 rNMP + 32 dNMPs (lanes 5–7), 5 rNMPs + 28 dNMPs (lanes 8–10), 10 rNMPs + 23 dNMPs (lanes 11–13), 15 rNMPss + 18 dNMPs (lanes 14–16) ot the full RNA primer (33 rNMPs, lanes 17–20). The templates were kind gifts of Dr. Slobodan Jergić. The reaction mixtures were then incubated in 30˚C for 40 min. The results were analyzed by 0.7% agarose gel electrophoresis in the presence of EtBr. The unmarked lane at the left contained the naked full RNA primed M13.

This is consistent with previous experiments conducted by Dr. Jergić (data not shown). However, interestingly, the addition of Pol I to the reactions seemed to give rise to the same extent of SD products with variously primed templates (lanes 3, 6, 9, 12 and 15), except that with the full RNA primer (33 rNMPs, lane 18). The SD synthesis on the shorter RNA-primed species was not reduced when ligase A was also present (lanes 4, 7, 10, 13, 16 and 19). The reason for this is not clear. It may indicate a certain number of rNMPs (between 15 and 33) in the primer are needed for a successful chain of events that lead to Okazaki fragment maturation. Some other interesting features were also observed. For example, the reaction with the fully DNA primed template has resulted in a slightly reduced efficiency of SD in the presence of ligase A (compare lane 1 with ligase and lane 2 without it), and some ligated species were also observed (lane 1). The primers used did not contain a 5'-phosphate group, as required for ligation, so it is not clear what caused the Pol I-independent ligation. The reduction in SD synthesis observed in lane 1 may be caused by ligase competing with Pol III for binding at a nick site generated by Pol III.

Template slippage happens during DNA replication, which can cause severe damage to DNA such as deletion mutation. It has been shown that replication slippage happens during DNA replication by enzymes including *E. coli* Pol III HE, DNA polymerase I (Pol I) and DNA polymerase II, as well as phage T4 and T7 DNA polymerases (Canceill *et al.,* 1999). *E. coli* SSB was shown to stimulate SD for Pol I and T7 polymerase, at the same time inhibiting the occurrence of template slippage. Interestingly, slippage during replication by Pol III is in fact stimulated by SSB, especially in higher salt conditions (Canceill and Ehrlich, 1996). We may raise the question of which protein is actually preventing this devastating slippage from happening during Pol III DNA replication. I speculate that for the leading strand polymerase, this is done by the DnaB helicase. However, on the lagging strand, it is probably done by RNA primers. This explains why it is necessary to have a certain number of rNMPs in the primer to suppress slippage or SD by Pol III and Pol I. Template slippage or SD synthesis will not give rise to species that are able to be ligated, explaining the reduced yield of ligated products seen in lanes 4, 7, 10, 13 and 16 *cf*. lane 19 in **Figure 4.22**).

Pol III SD synthesis requires SSB, which is believed to bind to the displaced strand. SSB does not bind strongly to RNA, so its access to DNA on the displaced strand

depends on how far ahead of the polymerase active site strand separation by the holoenzyme complex occurs. These experiments suggest this distance is at least 15 nucleotides, which is surprisingly far. It is also clear that lagging strand primers being made of RNA cannot be the sole factor that prevents Pol III SD synthesis from occurring *in vivo* when the replisome approaches the 5'-end of a preceding Okazaki fragment. While the DnaG primase alone is able to synthesize RNA primers ≥12 Nt long, work in the Kornberg group in the 1970s suggested that Pol III takes over primers from DnaG when they are just a few nucleotides long (Rowen and Kornberg, 1978; Bouché *et al*., 1978).

4.3.9 Single-molecule DNA replication assays suggest that *Ec*-SSB is probably recycled on the ssDNA at the replication fork

Single-molecule experiments have gained increasing popularity in recent years due to their ability to reveal information on individual molecules, whereas traditional bulk phase experiments can only show ensemble information about the whole system. Single molecule experiments are particularly useful for studying very dynamic systems such as DNA replication.

An *in vivo* single molecule experiment showed fluorescently-labelled *Ec*-SSB localized to the same position as Pol III HE (Reyes-Lamothe *et al.,* 2010). There would on average be around eight *Ec*-SSB tetramers on the lagging strand at each DNA replication fork assuming it adopts the $(SSB)_{65}$ binding mode. The observed number of *Ec*-SSB tetramers actually varied from 5 to 11, presumably resulting from the balance between the unwinding of dsDNA by DnaB helicase (generating ssDNA) and DNA synthesis by Pol III (consuming it) on the lagging strand. The temporal variation of bound *Ec*-SSB at the replication fork may indicate the actions of DnaB and Pol III on the lagging strand are not tightly coupled to progress at the same instantaneous speed. This was also apparently shown in another *in vivo* single molecule experiment where bursts instead of a constant number of fluorescent *Ec*-SSB tetramers were observed (Lia *et al.,* 2012, since retracted). One problem with the *in vivo* experiments to date was that the strains used contained both wild type and C-terminally tagged *Ec*-SSB (note that C-terminal tagging of *Ec*-SSB with a fluorescent protein does not produce active protein because the C-terminus is required for protein–protein interactions). It is assumed the

two forms exist in these cells as mixed tetramers that are fully functional, but this has not been demonstrated.

Previously, a monomeric fluorescent protein mKikGR (modified from a homotetramer of wild type KikGR protein) whose fluorescence can be switched on and off was developed (Habuchi *et al.*, 2008). The KikGR used throughout the thesis is actually the mKikGR. Its use expands the tool kit of the fluorescent proteins, and empowers the single molecule experiments. An *in vitro* single molecule experiment involving a KikGR labelled *Ec*-SSB was hatched previously. The experiment would reveal how *Ec*-SSB dissociates and associates to and from the ssDNA at the replication fork during coupled leading- and lagging-strand replication, and also enable easy quantification and localization of ssDNA in uncoupled replication and helicase assays of various types. Unfortunately, an N-terminally KikGR-tagged *Ec*-SSB tetramer purified by Dr. Claire Mason failed to stimulate Pol III DNA replication *in vitro*. This was not surprising because even an N-terminal His_6 tag had been shown previously in our laboratory to affect the properties of *Ec*-SSB (unpublished data).

Therefore, I proceeded to construct another labelled *Ec*-SSB (*Ec*-SSB~KikGR) by genetically splicing the KikGR to the C-terminus of *Ec*-SSB, mindful that the KikGR protein will block the interactions between proteins (e.g., the χ subunit) and the C-terminus of *Ec*-SSB. We solved this problem by expressing and purifying a C-terminally His_6-tagged tetrameric protein: *Ec*-SSB~KikGR-His_6, and exchanging its subunits with the wild type *Ec*-SSB tetramer to obtain the **[***Ec*-SSB$]_{2.6}$[*Ec*-SSB~KikGR-$His_6]_{1.4}$ (see the following). Addition of this protein to a bulk phase DNA replication assay did not inhibit primer extension or SD synthesis by Pol III HE (shown below). It was then used in an *in vitro* single-molecule assay.

A mixed [*Ec*-SSB$]_{(4-n)}$[*Ec*-SSB~KikGR-$His_6]_n$ tetrameric protein (ideally with n ~1) was needed for the fluorescence based single-molecule assays. This protein ideally contains three wild-type SSB monomers and one SSB fused to the KikGR-His_6 protein. The protein actually purified was a mixture of tetramers with n = 1 and 2 in an ~65:35 ratio, so it is denoted as [*Ec*-SSB$]_{2.6}$[*Ec*-SSB~KikGR-$His_6]_{1.4}$. Procedures for its generation by subunit exchange and its isolation are described in **Section 4.2.2.3**, while its characterization is described below.

A ratio of 3:1 (*Ec*-SSB:*Ec*-SSB~KikGR-His_6) was initially targetted for the mixed SSB tetramer. However, the intensity of bands of *Ec*-SSB and *Ec*-SSB~KikGR-His_6 in the SDS-PAGE suggest a ~2.6:1.4 ratio based on their intensities (**Figure 4.23**). The estimated mol. wt. and extinction coefficient (ε_{280}) for the tetramer were 113.5 kDa and 157,438 $M^{-1}cm^{-1}$ based on this estimation.

The estimated parameters were further validated by SDS-PAGE of a KikGR~*Ec*-SSB protein (with known concentration, previously purified by Dr. Claire Mason) in parallel with the purified mixed tetramer (**Figure 4.23**). A sample comprising 4 μg of KikGR~*Ec*-SSB (lane 1) was analysed alongside amounts of the mixed tetramer predicted to contain 4 μg of *Ec*-SSB~KikGR-His_6 based on the assumption that the *Ec*-SSB:*Ec*-SSB~KikGR-His_6 ratio is 2:2 (lane 2), 3:1 (lane 3) or 2.6:1.4 (lane 4). The intensity of the KikGR~*Ec*-SSB band in lane 1 is apparently weaker than the band in lane 3 but stronger than the band in lane 2. So the ratio of *Ec*-SSB:*Ec*-SSB~KikGR-His_6 must be between 2:2 and 3:1. This is in accordance with the fact that the band in lane 1 has very similar intensity to the band in lane 4 (assumed *Ec*-SSB:*Ec*-SSB~KikGR-His_6 ratio of 2.6:1.4). Therefore the estimated mol. wt. and value of ε_{280} based on this ratio are close to the real situation. So it is assumed that about 65% of tetramers have one *Ec*-SSB~KikGR-His_6 monomer, while about 35% have two.

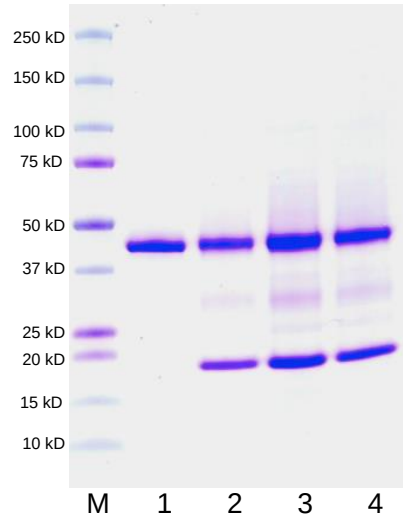

Figure 4.23 Validation of the stoichiometry of [*Ec*-SSB]$_{2.6}$[*Ec*-SSB~KikGR-His_6]$_{1.4}$ by SDS-PAGE. Four μg of KikGR~*Ec*-SSB (lane 1) were loaded in parallel with 4 μg of *Ec*-SSB~KikGR-His_6 in the mixed tetramer by assuming the *Ec*-SSB:*Ec*-SSB~KikGR-His_6 ratio is 2:2 (lane 2), 3:1 (lane 3) or 2.6:1.4 (lane 4). The intensity of KikGR~*Ec*-SSB (lane 1) is similar to *Ec*-SSB~KikGR-His_6 (lane 4), however not to that in lane 2 or 3, demonstrating the estimated ratio of 2.6:1.4 is close to the real ratio.

However, native ESI mass spectroscopy showed only the normal SSB tetramer, with smaller apparent amounts of the tetramer with two *Ec*-SSB and two *Ec*-SSB~KikGR-His_6 monomers. The subunit exchanged *Ec*-SSB and *Ec*-SSB~KikGR-His_6 protein was dialyzed in 3 changes of 300 mL of 1 M NH_4OAc (pH 8.3) at 4˚C. The sample showed a heavy precipitate, which was removed by centrifugation. The supernatant, containing ~2 μM of protein, was subject to nanoESI-MS (**Figure 4.24**). In the spectrum, both tetrameric *Ec*-SSB and [*Ec*-$SSB]_2$[*Ec*-SSB~KikGR-$His_6]_2$ were observed, although *Ec*-SSB tetramers gave more prominent peaks. The expected peaks of [*Ec*-$SSB]_3$[*Ec*-SSB~KikGR-$His_6]_1$ (or any other tetrameric species) were not observed. This could be due to additional subunit exchange during the dialysis, which results in the precipitation of the other species. It was tried to directly dilute the sample into 1 M NH_4OAc (pH 8.3) just before mass spectroscopy to avoid the unwanted subunit exchange. However no spectrum was obtained. Another possibility is that [*Ec*-$SSB]_3$[*Ec*-SSB~KikGR-$His_6]_1$ does not ionize as well as [*Ec*-$SSB]_2$[*Ec*-SSB~KikGR-$His_6]_2$ in the mass spectrometer, so we cannot observe it in the spectrum. Although the mass spectroscopy shows only partial agreement with the prediction based on the SDS-PAGE, the result shows direct evidence of the existence of hybrid tetramers.

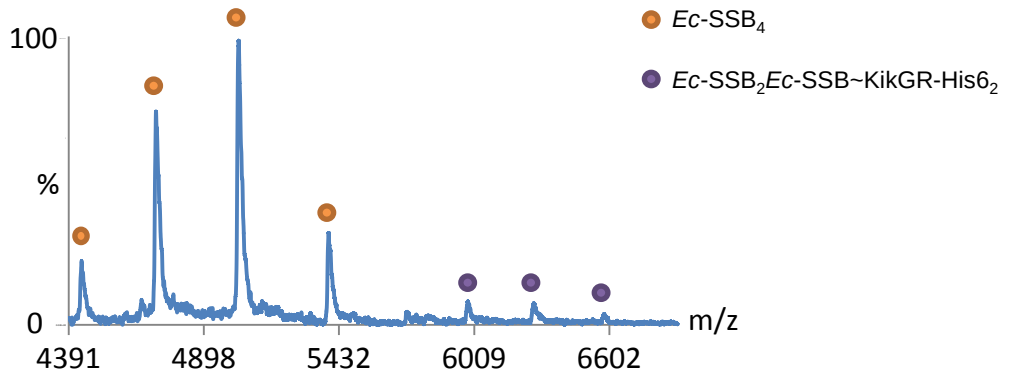

Mass (Da)	*Ec*-SSB_4	*Ec*-SSB_2*Ec*-SSB~KikGR-$His6_2$
Theoretical	75375.2	131375.9
In ESI-MS	75449 ± 7	131503 ±16

Figure 4.24 Native ESI-MS shows *Ec*-SSB_4 and [*Ec*-$SSB]_2$[*Ec*-SSB~KikGR-$His_6]_2$ species. Subunit exchanged protein was dialyzed in 1 M NH_4OAc (pH 8.3), and subjected to nanoESI-MS. The protein species and the charge state of each species are labelled on the spectrum. The theoretical and the derived masses for each species are listed in the table below.

The activity of [*Ec*-$SSB]_{2.6}$[*Ec*-SSB~KikGR-$His_6]_{1.4}$ was analyzed by bulk phase SD

assay (**Figure 4.25**) in which it stimulated SD synthesis optimally at 800 nM concentration (calculated based on the 2.6:1.4 ratio of *Ec*-SSB and *Ec*-SSB~KikGR-His_6). The wild type *Ec*-SSB also gave maximum stimulation of SD at 800 nM (lanes 4 and 9 in **Figure 4.25**), a concentration at which *Ec*-SSB (in the 35 binding mode) theoretically saturated the 4 nM M13 template in the reaction mixture.

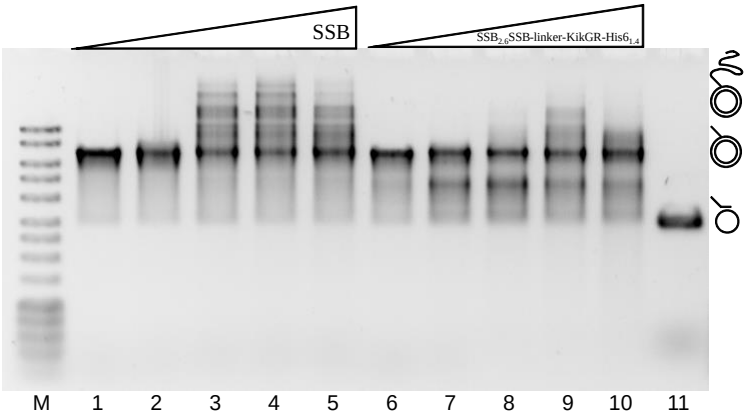

Figure 4.25 [*Ec*-SSB]$_{2.6}$[*Ec*-SSB~KikGR-His_6]$_{1.4}$ stimulates Pol III HE SD synthesis. *Ec*-SSB and **[***Ec*-SSB]$_{2.6}$[*Ec*-SSB~KikGR-His_6]$_{1.4}$ were titrated (0, 200, 400, 800 and 1600 nM) in the reaction buffer containing Pol III HE in the presence of 110 mM NaCl. Specifically, 0 (lanes 1 and 6), 200 (lanes 2 and 7), 400 (lanes 3 and 8), 800 (lanes 4 and 9) and 1600 nM (lanes 5 and 10) of *Ec*-SSB (lanes 1–5) or **[***Ec*-SSB]$_{2.6}$[*Ec*-SSB~KikGR-His_6]$_{1.4}$ (lanes 6–10) were titrated into the reaction buffer containing 20 mM Tris-HCl, pH 7.6, 10 mM $MgCl_2$, 1 mM ATP, 6.8 mM DTT, 0.42 mM of each dNTP, 68 nM αεθ, 32 nM $\tau_3\delta\delta'\chi\psi$, 400 nM β_2, 4 nM flap-primed M13 DNA template and 110 mM NaCl. Reaction mixtures were incubated at 30˚C for 20 min, and then analyzed by 0.7% agarose gel electrophoresis without EtBr. Both proteins stimulate SD to the highest extent at 800 nM (lanes 4 and 9), although the **[***Ec*-SSB]$_{2.6}$[*Ec*-SSB~KikGR-His_6]$_{1.4}$ renders less stimulation in the whole concentration range compared with its counterpart (wild type *Ec*-SSB). Lane 11 shows the DNA template used in the assay.

Both *Ec*-SSB and [*Ec*-SSB]$_{2.6}$[*Ec*-SSB~KikGR-His_6]$_{1.4}$ inhibited the SD to a certain extent at 1600 nM (lanes 5 and 10 in **Figure 4.25**). The result also proved the estimated protein concentration as well as the value of ε_{280} were at least approximately right. The impaired stimulatory role of [*Ec*-SSB]$_{2.6}$[*Ec*-SSB~KikGR-His_6]$_{1.4}$ in Pol III SD synthesis compared with wild type *Ec*-SSB is likely due to the reduced availability of the *Ec*-SSB C-termini for interaction with the χ subunit at the replication fork. More assays would be needed to demonstrate the validity of this theory.

A single-molecule rolling-circle DNA replication assay (conducted by Miss Lisanne Spenkelink in the University of Groningen, the Netherlands) was used to study the dynamics of *Ec*-SSB at the replication fork. The set-up of the experiment is based on that reported by Tanner *et al.* (2008), and is described in **Figure 4.26**.

To test the switching characteristics of the KikGR labelled *Ec*-SSB, 4 pM M13 ssDNA and 15 nM SYTOX Orange was injected in to the flow cell chamber at a flow rate of 5 μL/min. the SYTOX orange was then washed out. The $[Ec\text{-SSB}]_{2.6}[Ec\text{-SSB}\sim\text{KikGR-His}_6]_{1.4}$ (250 nM) was then injected into the chamber at a flow rate of 10 μL/min. A 405 nm light pulse was used to switch on the KikGR fluorophore which was visualized with another higher wavelength light pulse (532 nm) by its red fluorescence (**Figure 4.27**). The result showed the KikGR on the *Ec*-SSB was switched on (**Figure 4.28**) and localized on M13 ssDNA.

Figure 4.26 Schematic illustration the set-up of the single-molecule M13 rolling-circle assay. To construct the DNA template, circular M13 ssDNA was annealed to a primer with the 5'-biotin tagged end and filled in by T7 DNA polymerase before attachment to a streptavidin (SA)-coated surface. A constant flow of buffer over the surface was used to stretch the DNA, and a constant temperature of 37˚C was applied to the chamber. The DNA replication assay was carried out by flowing reaction mixture containing 30 nM DnaBC complex (as hexamer), 30 nM αεθ, 30 nM β_2, 15 nM $\tau_3\delta\delta'\psi\chi$, 300 nM DnaG, 250 nM *Ec*-SSB tetramer, 20 nM PriA, 40 nM PriB, 320 nM PriC, 480 nM DnaT, 1 mM ATP, 250 μM each of CTP, GTP, and UTP, 50 μM of each dNTP, 5 mM DTT and 15 nM SYTOX Orange. DNA replisome components (Pol III HE) of *E. coli* will bind to the 3' end of the primer and carry out leading-strand DNA replication. The tail will grow in the flowing buffer due to DNA unwinding by DnaB helicase and DNA synthesis by Pol III HE. In the meantime, the replaced ssDNA will be converted to dsDNA in the presence of DnaG primase by discontinuous lagging strand DNA synthesis. The replicated DNA was visualized by adding an intercalating dye, SYTOX Orange. The black circle is M13 dsDNA template, annealed to the biotin labelled primer (black). The green thread represents the newly synthesised leading strand DNA with an arrow indicates the direction of the DNA synthesis. The newly synthesised lagging strand DNA is represented by discontinuous threads in purple. The flow of buffer is from the left to the right.

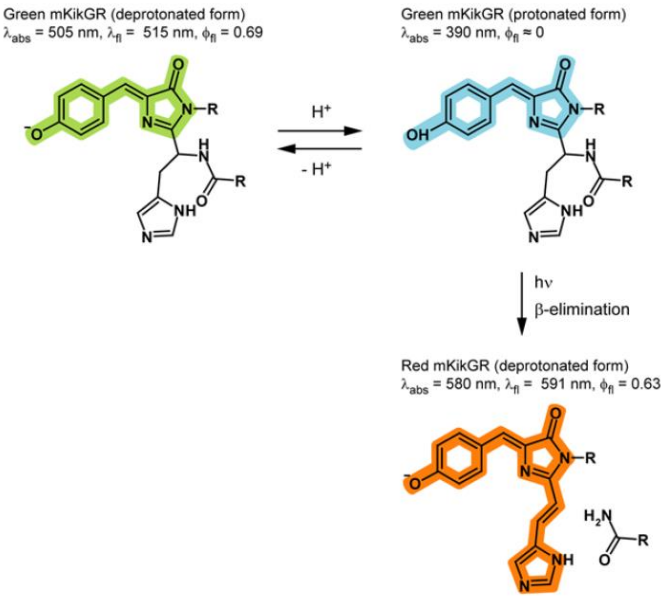

Figure 4.27 Schematic of the reaction of the photoswitching from green to red KikGR.

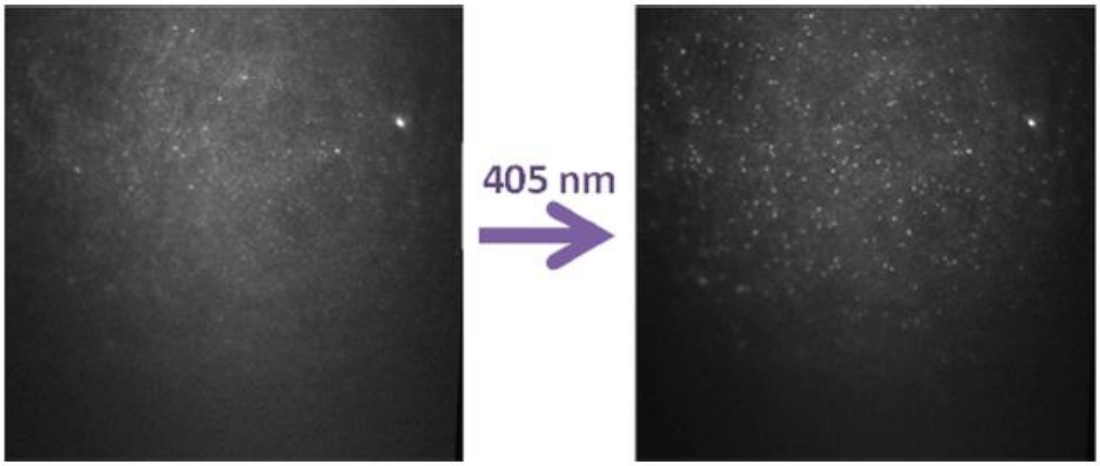

Figure 4.28 Photoswitching [*Ec*-SSB]$_{2.6}$[*Ec*-SSB~KikGR-His$_6$]$_{1.4}$ proteins on M13 ssDNA. The left picture shows a sum of three frames before imposing 405 nm activation pulses. The picture on the right shows a sum of three frames after the activation.

The replication assay was carried out by flowing the single-molecule reaction mixture (**Figure 4.26**) with 250 nM [*Ec*-SSB]$_{2.6}$[*Ec*-SSB~KikGR-His$_6$]$_{1.4}$ in place of *Ec*-SSB tetramer. A 404 nm activation pulse was applied to the surface every 10 s, while a 532 nm imaging light was constantly on to visualize the fluorescent *Ec*-SSB at the replication fork (**Figure 4.29**). By using a total internal reflection fluorescence (TIRF) microscope, the activation pulses were introduced just to the surface where DNA and proteins were bound.

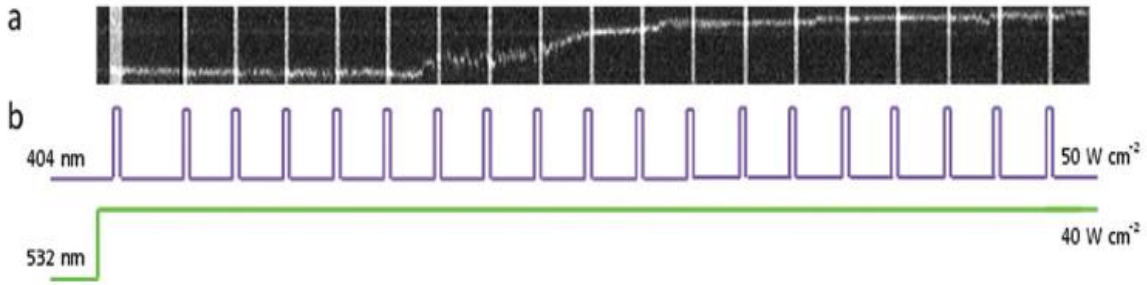

Figure 4.29 A sample kymograph of the movement of **[***Ec*-SSB]$_{2.6}$[*Ec*-SSB~KikGR-His$_6$]$_{1.4}$ at the replication fork. The kymograph is shown in **a**, and the timing of the 404-nm activation pulse (every 10 s with an intensity of 50 W/cm^2) and the 532-nm imaging light (applied constantly with an intensity of 40 W/c^{-2}) shown in **b**.

Thus, in a flow of buffer, only the bound fluorescent proteins are visualized. The unbound "dark" fluorescent proteins in the buffer are not seen. In the kymograph (**Figure 4.29a**), the direction of flow is from the bottom to the top, with time on the *x*-axis and distance (in base pairs replicated) on the *y*-axis. The bright dots are the [*Ec*-SSB]$_{2.6}$[*Ec*-SSB~KikGR-His$_6$]$_{1.4}$ at the replication fork. A preliminary measurement of the speed of fluorescence movement is 550 ± 47 bp/s, which is typical of rates determined in such assays with unmodified proteins (Tanner *et al*., 2009). This again demonstrates the normal replication activity of the labelled mixed *Ec*-SSB tetramers (**Section 4.3.9.2**).

Interestingly, **Figure 4.29a** shows the fluorescence after being switched on by each activation pulse remains at the replication fork at least until the next pulse (more than 10 s), and does not localize to any significant extent on the replicated DNA (which must therefore predominantly be double-stranded). If new "dark" *Ec*-SSBs from the buffer were to bind to the fork, the fluorescence would dim during the 10 s periods between pulses (a new Okazaki fragment should be made on the lagging strand every 2–4 s under these condition. On the other hand, if new "dark" *Ec*-SSBs were to bind to the fork and were then switched on, the fluorescence should increase due to the activation pulse applied every 10 s. Neither of these events was observed. This suggests that the *Ec*-SSBs at the replication fork being displaced by the Pol III on the lagging strand are recycled directly to the nascent ssDNA generated by the DnaB helicase. Thus the population of the *Ec*-SSBs at the replication fork is relatively constant.

This theory was tested by another experiment (data not shown**)** where the [*Ec*-

SSB]$_{2.6}$[*Ec*-SSB~KikGR-His$_6$]$_{1.4}$ was switched on and then bleached using high power 532 nm light (an intensity of 410 W/cm^2). Interestingly, after the *Ec*-SSBs at the fork had been bleached, no new *Ec*-SSBs were switched on for about 20 s. This suggests that during that time, no (or few) new *Ec*-SSBs from the buffer bound to the fork. Only after about 20 s, some new *Ec*-SSBs could be switched on at the fork. This again supports the proposition that *Ec*-SSB is recycled directly at the replication fork. However, after bleaching the movement of the fork became hard to track. More work is required to further substantiate these preliminary experiments.

The potential recycling of *Ec*-SSB at the replication fork may shed light on our understanding of Pol III SD synthesis and Okazaki fragment maturation. It only takes about 10–20 s for Pol III HE to fill the ssDNA gap on M13 (~6400 nucleotides long) in the presence of *Ec*-SSB (**Figure 4.12**), and it is well established to do this processively, without dissociation. The subsequent SD synthesis is much slower, and has more limited processivity (Yuan and McHenry, 2009). It may be that the conformation of Pol III HE (with *Ec*-SSB) needs to adjust during the transition from primer extension mode to SD mode. Furthermore, it seems that the RNA primer plays similar role in disrupting SD, and stimulating Okazaki fragment maturation (**Figure 4.22**). It suggests an RNA primer somehow signals the Pol III to release from the replication fork, possibly during the conformational transittion. *Ec*-SSB has much lower affinity for ssRNA than ssDNA, which probably supports the signalling process. However, when a DNA primer (especially a flapped primer) is used, *Ec*-SSB can immediately associate with the replaced ssDNA. Recycling of *Ec*-SSB at the fork would compete with this process because in a coupled reaction at a true replication fork, all of the SSB would have been transferred to new ssDNA generated by DnaB, and would not be available for SD synthesis.

This Chapter described stimulatory roles of SSB, the $\gamma_3\delta\delta$' clamp loader, and the Pol III χ subunit in DNA replication and SD synthesis in bulk phase assays, under conditions that have not been described before. Single-molecule assays suggested that SSB is recycled at the replication fork. Furthermore, the significant role of Pol I in Okazaki fragment maturation was further consolidated, while a proposed pathway involving RNase HI and HII was denied. Although many results described here are preliminary, they clearly suggest that DNA replication involves many weak protein–protein and

protein–nucleic acid interactions that are yet to be discovered. To elucidate the mechanisms behind all the results, new techniques are probably needed in the future.

CHAPTER 5

INTRAMOLECULAR DNA WRAPPING MODE OF F-PLASMID DERIVED SSB

5.1 Introduction

The sequence of the *ssf* gene that codes for the *E. coli* F sex factor-derived SSB (F-SSB), determined 30 years ago (Chase *et al.,* 1983) shows that F-SSB has extensive sequence similarity to the chromosomally-encoded SSB (*Ec*-SSB) in their N-terminal OB-domains (**Figure 3.3**). The *ssf* gene product of 178 amino acids has a calculated mol. wt. of 19505 (excluding the processed N-terminal methionine). Despite its early discovery, no information in terms of the structure and clear function of F-SSB has been reported (Kolodkin *et al.,* 1983; Howland *et al.,* 1989; Rees and Wilkins, 1990; Porter *et al.,* 1991). Some early data showed that F-SSB is not carried with the ssDNA to the recipient bacterium during F-mediated conjugation (Rees and Wilkins, 1990). It was speculated that F-SSB is expressed in the host cell after conjugation. However, its activity in the recipient cell is still unknown. On the other hand, SSB in *Agrobacterium tumefaciens* was shown to participate in the inter-kingdom transfer of T-DNA (Zhou and Christie, 1999). Although F-SSB protein is not carried to the recipient cell during the conjugation process, the presence of the F plasmid can partially complement the temperature-sensitive *ssb-1* mutation in *E. coli*, in which F-SSB is responsible for this rescuing process (Kolodkin *et al.,* 1983). But no report thus far showed the existence of F-SSB in cells containing F plasmid. It was later reported that the *ssf* gene can also complement a total deletion of the native *ssb* from the *E. coli* chromosome, but the *ssf* dependent bacteria showed signs of difficulty in DNA replication (Porter *et al.,* 1991). Considerable progress has been made in understanding the process of bacterial conjugation since its discovery almost 70 years ago (Lederberg and Tatum, 1946). However, conjugation has not been reconciled with other vital processes in bacteria, such as DNA replication and cell division (reviewed by de la Cruz *et al.,* 2010).

The native *Ec*-SSB has been found to be not only a “guardian” for protection of ssDNA from nuclease attack but also a protein binding "hub" that interacts with more than a dozen different proteins (**Section 3.1.1**). It adopts a cooperative ssDNA binding mode, called the $(SSB)_{35}$ mode, at low ionic strength and at a high ratio of SSB to ssDNA. On the other hand, a less cooperative ssDNA binding mode, called the $(SSB)_{65}$ mode, is adopted at high ionic strength and when SSB is limiting (**Section 3.1.1**). Many of the *Ec*-SSB residues that have been identified as being involved in ssDNA binding,

including Trp-40, Trp-54, Trp-88, His-55, Phe-60 and Tyr-70, are well conserved in F-SSB (**Figure 3.3**). It is also relevant to note that that *Ec*-SSB slides, rather than rolls, on ssDNA even when its C-terminal flexible tail is occupied by a binding partner such as RecO (**Section 3.1.1**).

By comparing the structures of ssDNA complexes of OB domains from various proteins, a "standard polarity" for ssDNA binding to the OB fold was proposed: ssDNA runs 5' to 3' from strands 4 and 5 to strand 2 of the fold (Theobald *et al.,* 2003; **Figure 5.1B** and **D**). However the polarity of ssDNA binding on the *E. coli* SSB tetramer revealed by the structure of the complex with two molecules of $(dC)_{35}$ in the $(SSB)_{65}$ mode is opposite to this typical polarity (Raghunathan *et al.,* 2000; discussed in Antony *et al.,* 2012). Interestingly, the other reported structures of ssDNA:SSB complexes reported thus far [*Mycobacterium smegmatis* SSB, Protein Data Bank (PDB) code: 3A5U; *Helicobacter pylori* SSB (Chan *et al.,* 2009); *Bacillus subtilis* SSB (Yadav *et al.,* 2012), *Plasmodium falciparum* SSB (Antony *et al.,* 2012) and *Sulfolobus solfataricus* SSB (Gamsjaeger *et al.,* 2015)] show the same "standard polarity" of ssDNA, making *Ec*-SSB the only exception to the rule. It should be noted that the *Ec*-SSB:ssDNA structure (Raghunathan *et al.,* 2000) was the first OB domain–ssDNA complex to be structurally characterized crystallographically, at moderate resolution (2.8 Å). It is unclear if data at this resolution could actually define the ssDNA binding polarity confidently; structure factors were not deposited with the PDB file, and the raw data are no longer available to allow this to be reassessed (personal communication from Prof. Gabriel Waksman to Prof. Nick Dixon, 2014).

In this Chapter, a structure of the OB-domain of the F-SSB protein in complex with ssDNA is described. It is the first structure of F-SSB solved since its discovery 30 years ago (Chase *et al.,* 1983), and is the first plasmid-derived SSB structure solved so far, either from horizontal bacterial conjugation or inter-kingdom gene transfer systems. It shows a very similar tetrameric structure and the "baseball seam" type of ssDNA wrapping as seen with the native *Ec*-SSB. However unlike the *Ec*-SSB structure (Raghunathan *et al.,* 2000), the bound ssDNA on the F-SSB is strikingly symmetric and adopts the opposite ("standard") polarity. Further studies showed that F-SSB and *Ec*-SSB can form hybrid tetramers with any combination of their monomers (**Section 4.3.2**). DNA replication assays (with the *E. coli* Pol III holoenzyme or a downsized SSB-dependent system, as described in **Chapter 4**) with the hybrid tetramer mixtures as

well as homogenous tetramers composed of elaborately made tagged monomers, all show primer extension, as the vital process for cell replication, can proceed on ssDNA bound to both *Ec*-SSB, F-SSB, and the mixed tetramers (**Section 5.3.4**). However, strand displacement (SD) DNA synthesis is not stimulated by F-SSB (**Section 5.3.4**). Since the polarity of ssDNA wrapping on *Ec*-SSB is yet to be properly defined, and the direction of ssDNA on the published *Ec*-SSB:$(dC)_{35x2}$ crystal structure (Raghunathan *et al.,* 2000) runs opposite to that in the new F-SSB:$(dT)_{63}$ structure, it is still an open question as to whether *Ec*-SSB might be able to bind ssDNA in *both* polarities. Based on the F-SSB:$(dT)_{63}$ structure and the published *Ec*-SSB:$(dC)_{35x2}$ structure, a new ssDNA binding path on SSB is proposed. Additionally, the DNA replication assays also unveiled a new feature of the unconserved C-terminal flexible regions of SSB. Given extensive sequence similarities between F-SSB and *Ec*-SSB, the structure also carries valuable information about SSB–DNA and SSB–protein interactions. Indeed it may shed light on the long standing question of whether the OB folds are derived from a common ancestral origin (Murzin, 1993, 1998; Suck, 1997).

5.2 Materials and methods

5.2.1 Expression and purification of proteins

Proteins (including clamp loaders of compositions $\gamma_3\delta\delta'$ and $\tau_3\delta\delta'\chi\psi$, Pol III $\alpha\varepsilon\theta$ core, the α subunit, and the β_2 clamp) required for the Pol III HE DNA replication assays were prepared as described in **Section 4.2.5**. *Ec*-SSB and *Ec*-SSBT* were prepared as described in **Section 3.2.1**. The preparations of F-SSB, F-SSBT*, *Ec*-SSB–F-SSBc, F-SSB–*Ec*-SSBc, *Ec*-SSB–F-SSB and F-SSB–*Ec*-SSB were described in **Chapter 4**.

5.2.2 Crystallization and structure determination

To obtain F-SSBT*:$(dT)_{63}$ crystals, F-SSBT* (100 μM, as tetramers, in 50 mM Tris-HCl, pH 7.6, 1 mM DTT, 1 mM EDTA, 500 mM NaCl and 30% glycerol) was mixed with equimolar $(dT)_{63}$ (100 μM, in TE buffer, see **Section 2.3.3**; synthesized and HPLC purified by Geneworks, Adelaide, Australia), and dialyzed at 4˚C in buffer containing

10 mM Tris-HCl, pH 7.6 and 1 mM DTT. Because of the high concentration of NaCl and glycerol in the F-SSBT* sample, the volume of the mixture increased. The volume was reduced to the same as before dialysis by ultrafiltration using Amicon centrifugal filter devices (3 kDa MWCO; Millipore). It should be noted that F-SSBT* (and also *Ec*-SSBT*) is nearly completely insoluble in these buffer conditions in the absence of ssDNA.

In attempts to obtain F-SSBT*:$(dC)_{63}$ and *Ec*-SSBT*:$(dC)_{63}$ crystals, the same procedures were followed, except $(dC)_{63}$ (also synthesized and HPLC purified by Geneworks) was used. However, no ssDNA was observed in either crystal structure, but the crystals yielded high-resolution structures of *apo*-F-SSBT* and *apo*-*Ec*-SSBT* (**Section 5.3.1**). It was subsequently shown that the $(dC)_{63}$ sample used was probably considerably shorter than anticipated due to the difficulty of chemical synthesis of long $(dC)_n$ homopolymers (data not shown); nevertheless, the ssDNA was capable of maintaining the two different SSB-T*s in solution at low ionic strength. It may also be that the $(dC)_n$ ssDNA was degraded by trace nuclease contamination during crystallization over several weeks at 18˚C.

Crystals were grown by vapour diffusion using sitting-drop methods in conditions from the Nucleix Suite kit (QIAGEN), by mixing 1 µL of protein:DNA solution with 1 µL of precipitant, and equilibrating against 60 µL of precipitant at 18˚C. Nucleix conditions 13 (50 mM sodium cacodylate, pH 6.0, 15 mM magnesium acetate and 1.7 M ammonium sulphate), 3 (50 mM MES, pH 5.6, 0.1 M magnesium acetate, and 20% MPD) and 16 (50 mM sodium cacodylate, pH 6.0, 40 mM magnesium acetate, and 30% MPD) were used for crystallization of F-SSBT*:$(dT)_{63}$, F-SSBT*:$(dC)_{63}$ and *Ec*-SSBT*:$(dC)_{63}$, respectively. Crystals of F-SSBT*:$(dT)_{63}$, F-SSBT* and *Ec*-SSBT* appeared after 3, 4 and 7 weeks, respectively. F-SSBT*:$(dT)_{63}$ crystals were stored in a cryo-protectant of 50 mM sodium cacodylate, pH 6.0, 15 mM magnesium acetate and 1.7 M lithium sulphate. F-SSBT* and *Ec*-SSBT* crystals were stored directly in their crystallization buffers. All crystals were frozen in liquid nitrogen.

Diffraction data for F-SSBT*:$(dT)_{63}$ were collected at the Australian Synchrotron, beamline MX-2. Diffraction data were processed with MOSFLM (Leslie and Powell, 2007) and SCALA (Evans, 2005) programs from the CCP4 suite**.** Diffraction data for F-SSBT* were collected in-house on a Mar345dtb detector using Cu-Kα X-rays produced

by a Rigaku 007HF X-ray generator. These diffraction data were processed using the HKL2000 package (Otwinowski and Minor, 1997). All data were collected at 100 K. Data collection and structure refinement for F-SSBT*:$(dT)_{63}$ (data collected on Australian Synchrotron; **Table 5.1**) and F-SSBT* (data collected on in-house; **Table 5.2**) crystals were conducted by Assoc. Prof. Aaron Oakley. Data collection and structure refinement for the *Ec*-SSBT* (data collected on in-house; **Table 5.3**) crystal were conducted by Dr. Nan Li.

5.2.3 Subunit exchanged *Ec*-SSB and F-SSB for DNA replication assay

Subunit exchange between *Ec*-SSB and F-SSB was carried out similarly to that described in **Section 4.3.2**. Briefly, *Ec*-SSB and F-SSB were dialyzed individually into 10 mM NH_4OAc (pH 7.2) and 1 M NH_4OAc (pH 7.2) with 1 mM DTT, respectively. Then 10 μL of 40 μM *Ec*-SSB and F-SSB were mixed and incubated at 55°C for 2 h to obtain the hybrid tetramer species. The samples, treated as a total concentration of 40 μM hybdid tetramers, were then added in the DNA replication assays (as described below and in Figure legends). The subunit exchanged species were confirmed in ESI-MS (**Figure 4.6)**. For the control experiment, homogenous tetramers of *Ec*-SSB (40 μM) and F-SSB (40 μM) were dialyzed individually in the same NH_4OAc buffers, and underwent the same incubation procedures. The whole procedures for the subunit exchange were repeated in storage buffer (50 mM Tris-HCl, pH 7.6, 1 mM DTT, 1 mM EDTA, 500 mM NaCl and 30 % glycerol), and the resulting protein samples were added in the same DNA replication assay in order to eliminate the possible influence of the buffers.

5.2.4 *In vitro* ssDNA-binding assay

Agarose (0.7%) gel electrophoresis in 2×TAE buffer (**Section 2.3.5**) under native conditions was used to examine the ssDNA binding ability of F-SSB. In the experiment, 4 nM of M13 ssDNA template (6408 Nt) was mixed with 0.18–1.8 μM of *Ec*-SSB, F-SSB and F-SSBT*, respectively, in 10 mM Tris-HCl, pH 7.6, 10 mM $MgCl_2$, 8 mM DTT and 40 mM NaCl, then loaded into wells of the gel, which was electrophoresed for

3 h at 30 V at room temperature. The DNA was visualized following staining with SYBR gold nucleic acid stain.

Table 5.1 Data collection and refinement statistics for F-SSBT*:(dT)$_{63}$

X-ray data	
Space group	I_{432}
Unit cell parameters	$a = b = c$ = 156.4 Å; α = β = γ = 90°
Resolution range (Å)	64−2.70 (2.85−2.70)[†]
Total No. of observations	379855 (56135)
No. of unique reflections	9297 (1323)
$\langle I/\sigma_I \rangle$[‡]	22.6 (3.5)
R_{merge} (%)[§]	14.1 (150)
Completeness (%)	100.0 (100.0)
Multiplicity	40.9 (42.4)
$\langle B \rangle$ from Wilson plot (Å^2)	63.3
Refinement statistics	
Resolution range (Å)	64–2.70 (2.77−2.70)
No. of reflections used in refinement	8853
No. of reflections (R_{free} set)	444
R_{work} (%)[¶]	22.4 (31.4)
R_{free} (%)[¶]	26.4 (36.5)
No. of atoms	1198
$\langle B \rangle$ of structure (Å^2)	37.2
r.m.s.d. from ideal geometry	
Bond lengths (Å)	0.015
Bond angles (°)	1.94
Chiral centres (Å^3)	0.115
General planes (Å)	0.008

[†]Numbers in parentheses pertain to the highest resolution bin.
[‡]Angle brackets refer to mean values.
[§]$R_{merge} = \Sigma_h \Sigma_i \left| I_{hi} - \langle I_h \rangle \right| / \Sigma_h \Sigma_i I_h$.
[¶]$R = \Sigma_h \left| \left| F_o \right| - \left| F_c \right| \right| / \Sigma_h \left| F_o \right|$, where F_o and F_c are the observed and calculated structure factors, respectively. R_{free} was calculated from 5% of the diffraction data not used in refinement.

Table 5.2 Data collection and refinement statistics for F-SSBT*

X-ray data	
Space group	$P4_12_12$
Unit cell parameters	$a = b = 54.0$, $c = 208.6$; $\alpha = \beta = \gamma = 90°$
Resolution range (Å)	52−2.60 (2.64−2.60)[†]
Total No. of observations	72074
No. of unique reflections	9425 (229)
$\langle I \rangle / \langle \sigma_I \rangle$[‡]	38.2 (2.83)
R_{merge} (%)[§]	6.2 (34.7)
Completeness (%)	91.0 (46.0)
Multiplicity	7.6 (4.0)
$\langle B \rangle$ from Wilson plot (Å^2)	68.8
Refinement statistics	
Resolution range (Å)	52–2.60 (2.67−2.60)
No. of reflections used in refinement	8929
No. of reflections (R_{free} set)	445
R_{work} (%)[¶]	23.7 (37.8)
R_{free} (%)[¶]	30.7 (34.4)
No. of atoms	1743
$\langle B \rangle$ of structure (Å^2)	44.9
r.m.s.d. from ideal geometry	
Bond lengths (Å)	0.012
Bond angles (°)	1.71
Chiral centers (Å^3)	0.096
General planes (Å)	0.005

[†]Numbers in parentheses pertain to the highest resolution bin.
[‡]Angle brackets refer to mean values.
[§]$R_{merge} = \Sigma_h \Sigma_i \left| I_{hi} - \langle I_h \rangle \right| / \Sigma_h \Sigma_i I_h$.
[¶]$R = \Sigma_h \left| \left| F_o \right| - \left| F_c \right| \right| / \Sigma_h \left| F_o \right|$, where F_o and F_c are the observed and calculated structure factors, respectively. R_{free} was calculated from 5% of the diffraction data not used in refinement.

Table 5.3 Data collection and refinement statistics for *Ec*-SSBT*

X-ray data	
Space group	$P2_12_12$
Unit cell parameters	a = 46.0, b = 65.1, c = 81.6; α = β = γ = 90°
Resolution range (Å)	30−2.22 (2.3−2.22)[†]
Total No. of observations	85672
No. of unique reflections	11846
$\langle I \rangle / \langle \sigma_I \rangle$[‡]	30.13 (5.80)
R_{merge} (%)[§]	4.5 (38.3)
Completeness	93.48 (62.50)
Multiplicity	6.8 (5.8)
$\langle B \rangle$ from Wilson plot (Å^2)	26.9
Refinement statistics	
Resolution range (Å)	27.66−2.22 (2.3−2.22)
No. of reflections used in refinement	11239
No. of reflections (R_{free} set)	564
R_{work} (%)[¶]	21.6 (27.5)
R_{free} (%)[¶]	25.8 (35.5)
No. of atoms	1859
protein	1781
water	78
$\langle B \rangle$ of structure (Å^2)	39.0
r.m.s.d. from ideal geometry	
Bond lengths (Å)	0.013
Bond angles (°)	1.79
Ramachandran favoured (%)	99
Ramachandran outliers (%)	0
Clashscore	10.35

[†]Numbers in parentheses pertain to the highest resolution bin.

[‡]Angle brackets refer to mean values.

[§]$R_{merge} = \Sigma_h \Sigma_i \left| I_{hi} - \langle I_h \rangle \right| / \Sigma_h \Sigma_i I_h$

[¶]$R = \Sigma_h \left| \left| F_o \right| - \left| F_c \right| \right| / \Sigma_h \left| F_o \right|$, where F_o and F_c are the observed and calculated structure factors, respectively. R_{free} was calculated from 5% of the diffraction data not used in refinement

5.2.5 *In vitro* DNA replication assay

The reaction procedures for the coupled strand extension and strand displacement DNA replication assays by Pol III HE were the same as those described in **Section 4.3.3**. Specific procedures for the assays are described in **Figures 5.7** and **5.8**. The products were analysed by 0.7% agarose gel electrophoresis (**Section 2.3.5**).

5.3 Results and discussion

5.3.1 The crystal structure of F-SSBT*:$(dT)_{63}$

The electron density maps of both protein and DNA in the F-SSBT*:$(dT)_{63}$ structure were of very good quality despite that the resolution was just 2.7 Å; this is partially due to the rare high symmetry of the crystal lattice (I_{432}) yielding a single subunit in the asymmetric unit, coupled with the high redundancy of the data (**Table 5.1**). This allowed us to visualize continuous electron density of the ssDNA on the protein surface for all but a short gap corresponding to one nucleotide per monomeric unit. In spite of this, 16 nucleotides associated with each subunit (64 per tetramer) could be built into electron density; the occupancy of all 63 Nt of the $(dT)_{63}$ chain is presumably averaged across the structure (**Figure 5.1C**).

F-SSBT* (**Figure 5.1**) adopts a very similar OB-fold layout to that of *Ec*-SSBC* (Raghunathan *et al.,* 2000). The structure consists of five β-strands and one α-helix connected by the loops between them (**Figure 5.1B**). Several interesting loops, including L1"–2, L4'–5 and L2–3, are denoted as L12, L45 and L23, respectively in the following part of the Thesis. Compared to that of *Ec*-SSB, the OB-fold of F-SSB contains a small additional structured region at the very N-terminus and slightly longer β2 and β3 strands (**Figure 5.1A** and **D**). Structural alignments (conducted in PyMOL) of these two monomers and tetramers yielded Cα RMSDs of 0.75 Å and 1.22 Å, respectively.

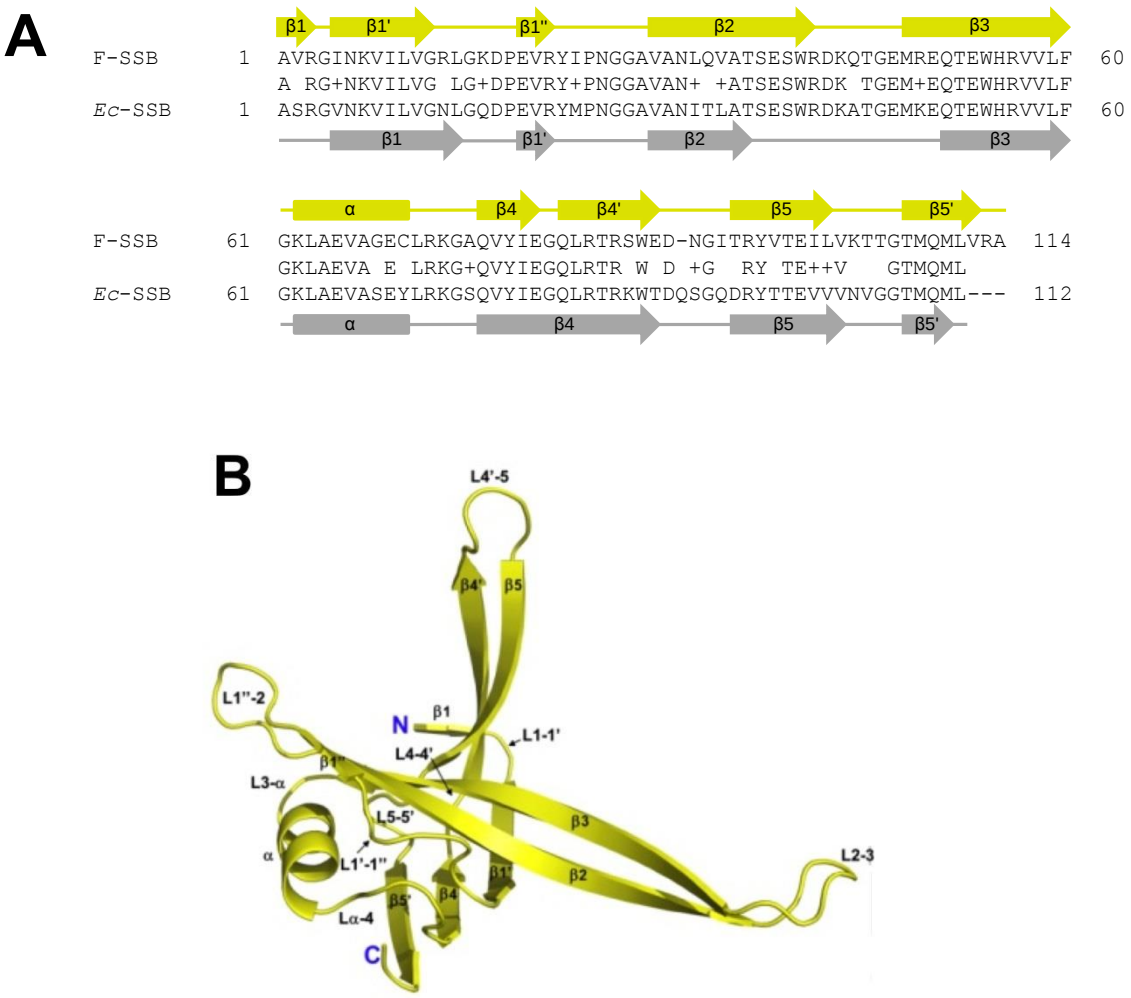

Figure 5.1 Crystal structure of F-SSBT*:$(dT)_{63}$ complex, *apo* F-SSBT* and *apo Ec*-SSBT*. (**A**) Sequence alignment of F-SSBT* and *Ec*-SSB in the structure solved by Raghunathan *et al.* (2000) shows extensive sequence similarity (87% conserved residues). Secondary structures for each protein are also shown. (**B**) Structure of the F-SSBT* monomer in the asymmetric unit of the F-SSBT*:$(dT)_{63}$ structure with labels on the secondary structural elements (continued on next page).

Surprisingly, the polarity of ssDNA wrapping on the F-SSB's OB-fold appears to be opposite to that on its counterpart of *Ec*-SSB (**Figure 5.1D**), despite that there are only 13% different residues between these two protein fragments (**Figure 5.1A** and **C**). The ssDNA wraps the F-SSB OB-domain monomer in the canonical fashion (Douglas *et al.,* 2003) with the ssDNA running in the 5'–3' direction from strands β4 and β5 to strand β2. The ssDNA on the *Ec*-SSB OB-fold seems to follow a similar binding route, but its polarity is completely opposite to that on F-SSB (**Figures 5.1D** and **5.2**).

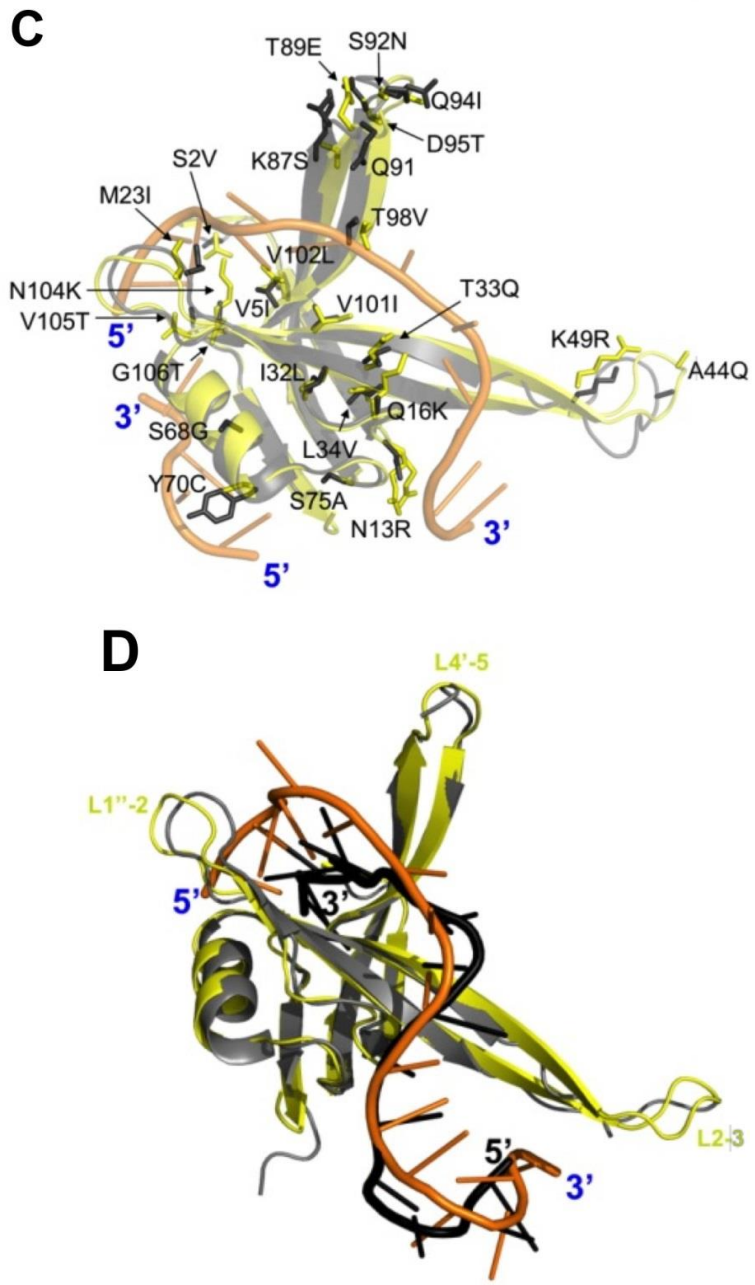

Figure 5.1 (continued from previous page). Crystal structure of F-SSBT*:$(dT)_{63}$ complex, *apo* F-SSBT* and *apo* *Ec*-SSBT*. (**C**) Overlay of the F-SSBT*:$(dT)_{63}$ monomer structure (transparent yellow) on a monomer from the *Ec*-SSB:$(dC)_{35x2}$ structure (transparent black; omitting the ssDNA; Raghunathan *et al.,* 2000) with the side chains of the non-conserved amino acids shown as solid sticks and labelled according to their sequence (*e.g.*, S2V indicates the second residue serine in *Ec*-SSB is replaced by a valine in F-SSB). All ssDNA bases interacting with each F-SSBT* monomer are shown. Shown is a ssDNA strand (dT1–dT12) on the F-SSB monomer structure and another ssDNA strand (dT13–dT16) interacting with its α helix. (**D**) Overlay of the F-SSBT*:$(dT)_{63}$ monomer structure (solid yellow; with dT1–dT16 in orange) and the *Ec*-SSB:$(dC)_{35}$ monomer structure (solid grey; with dC13–dC28 of the 28-nucleotide strand in black; Raghunathan *et al.,* 2000) with their ssDNA chains binding in opposite directions. The 5' and 3' ends of each ssDNA strand are shown (continued on next page).

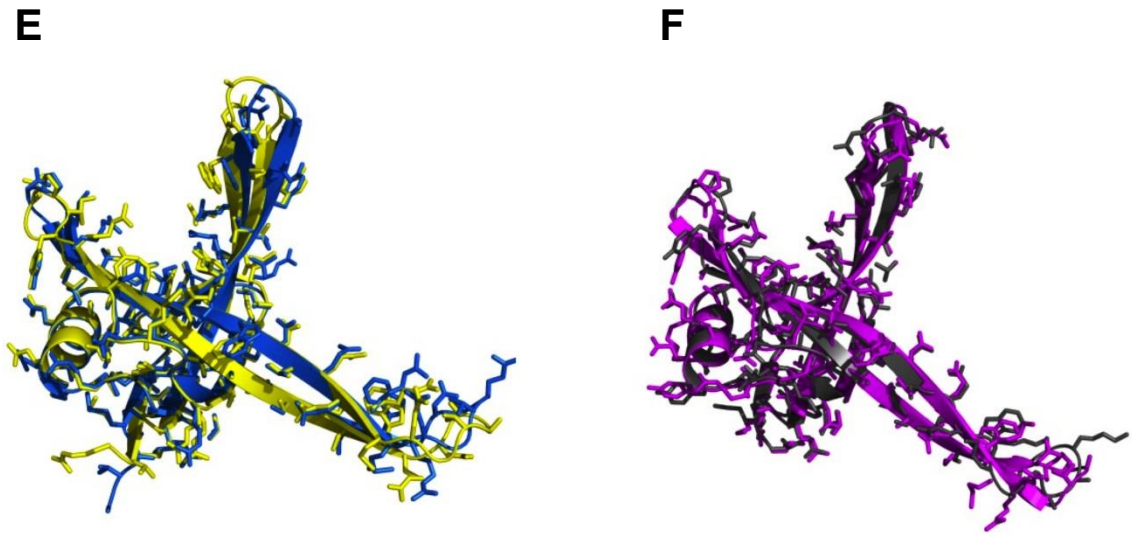

Figure 5.1 (continued from previous page). Crystal structure of F-SSBT*:$(dT)_{63}$ complex, *apo* F-SSBT* and *apo Ec*-SSBT*. (**E**) Overlay of the *apo*-F-SSBT* monomer structure (blue) and the F-SSBT*:$(dT)_{63}$ monomer structure (yellow; omitting the ssDNA) with their side chains shown as sticks. (**F**) Overlay of the *apo*-*Ec*-SSBT* monomer structure (magenta) and the *Ec*-SSB:$(dC)_{35x2}$ structure (black; omitting the ssDNA; Raghunathan *et al.,* 2000) with their side chains shown as sticks.

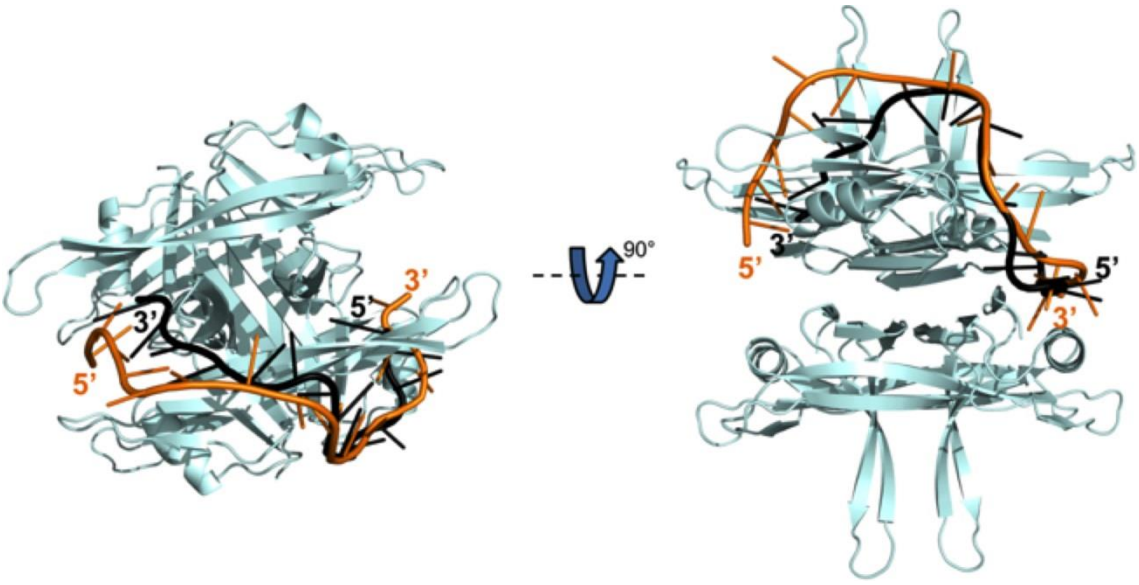

Figure 5.2 F-SSBT* tetramer (pale cyan) in complex with a $(dT)_{16}$ strand (orange) overlaid with a $(dC)_{16}$ strand of the *Ec*-SSB:DNA structure (black, dC13–dC28 of the 28-nucleotide strand, Raghunathan *et al.,* 2000) at the same region on *Ec*-SSB (not shown). The 5' and 3' ends of each strand are shown.

This raises the question: Assuming the the *Ec*-SSB:DNA structure is correct, what determines the difference in DNA binding polarity? As might be expected, all the non-conserved residues between the two SSBs are located on the protein surface (**Figure**

5.1C). A native nanoESI-MS experiment with a mixture of the two proteins proved that the *Ec*-SSB and F-SSB tetramers can exchange their subunits, and form new tetramers with any combinations of subunits from both proteins: $[Ec\text{-SSB}]_1[\text{F-SSB}]_3$, $[Ec\text{-SSB}]_2[\text{F-SSB}]_2$ and $[Ec\text{-SSB}]_3[\text{F-SSB}]_1$; indicating the monomer and dimer interfaces must predominantly be conserved in F-SSB (**Section 4.3.2**). A close look at the non-conserved residues reveals they are located either on the ssDNA binding route or on the L45 and L23 loops, which are distant from the DNA binding path (**Figure 5.1C**). It is later shown in this Chapter that the non-conserved residues in L45 and L23 abolish the typical SSB crystal packing mediated through the L45 loop, and establish a new contact at L23. Therefore, the handful of differing residues on the ssDNA binding route may be the key for determining the ssDNA binding polarity as well as some of the distinct biochemical properties of F-SSB relative to *Ec*-SSB (Ruvolo *et al.,* 1991).

Another possible reason for the two different polarities is the difference in ssDNA used, a dT homopolymer for the F-SSB structure and a dC homopolymer for the *Ec*-SSB structure. Attempting to obtain *Ec*-SSB:$(dC)_{63}$ and F-SSB:$(dC)_{63}$ crystals has surprisingly resulted in relatively high resolution *apo* structures of *Ec*-SSB (2.2 Å) and F-SSB (2.6 Å; **Section 5.2.2**). The reason for not observing ssDNA in these structures is not clear, but it is possibly due to the poor quality of the $(dC)_{63}$, its degradation or the low affinity between oligo-dC and both SSBs. Examination of the crystal packing in both cases shows insufficient room to accommodate $(dC)_{63}$ in the crystal lattices, so it is not simply that the DNA is present but disordered in the crystals.

It is noteworthy that the binding of ssDNA does not change the overall conformation of the OB-fold of *Ec*-SSB or F-SSB, except for some side chains and loop regions. Superposition of the F-SSB:$(dT)_{63}$ and the *apo*-F-SSB structures (**Figure 5.1E**) as well as *Ec*-SSB:$(dC)_{35x2}$ (Raghunathan *et al.,* 2000) and the *apo*-*Ec*-SSB structures (**Figure 5.1F**) yields the same low Cα RMSD values (0.4 Å), showing ssDNA binding has little effect on the conformation of either OB domain. It was shown that the binding of ssDNA pulls the L45 loop towards the ssDNA through the stacking interaction between Trp-88 and the base of the arbitrarily-numbered dC25 residue (Raghunathan *et al.,* 2000). A similar effect is also observed in the present *Ec*-SSB and F-SSB structures (**Figure 5.1E** and **F**).

5.3.2 Protein-DNA contacts in the crystal structure

In the F-SSBT*:$(dT)_{63}$ structure, each monomer of the protein associates with 16 nucleotides. As demanded by the high symmetry, the electron density for each $(dT)_{16}$ unit was lost at the same region at the bases of the L12 loops and L23 loops (**Figures 5.3** and **5.4**). Thus there are totally 64 nucleotides discernible bound to the F-SSB tetramer. However, $(dT)_{63}$ was used for the co-crystallization with F-SSBT*. The additional nucleotide observed in the crystal structure is likely due to the random shift of DNA on the surface of protein, and the gap between the $(dT)_{16}$ units is likely due to the flexibility of ssDNA which loses constraint from DNA–protein contacts; otherwise $(dT)_{63}$ would definitely cover at least three gaps. Therefore, the end of each observed ssDNA unit is unlikely to be the actual end of $(dT)_{63}$.

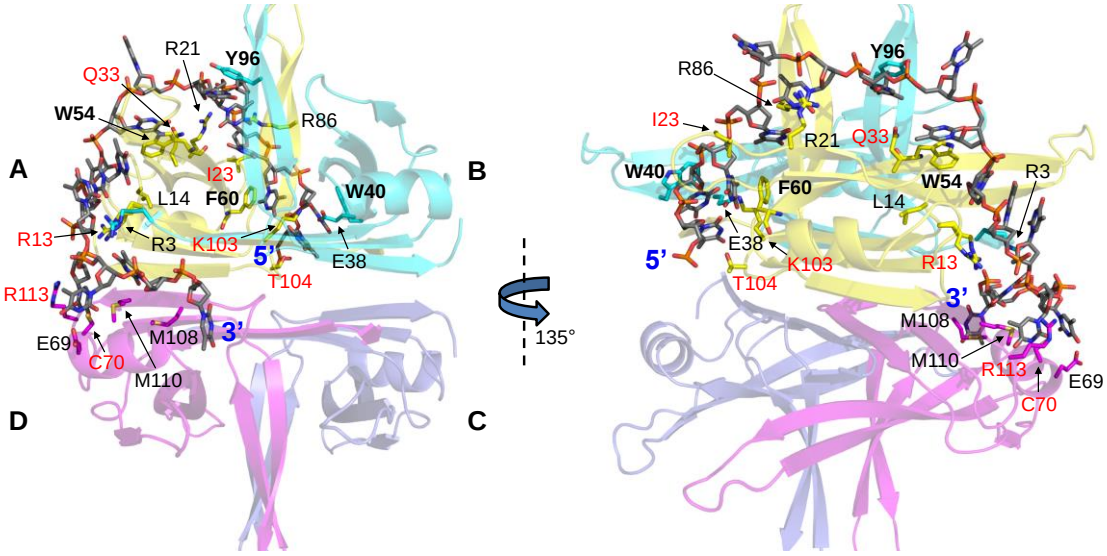

Figure 5.3 Details of F-SSBT* tetramer bound with one $(dT)_{16}$ strand. Four subunits of F-SSB are coloured yellow (subunit A), cyan (subunit B), pale blue (subunit C) and magenta (subunit D). One $(dT)_{16}$ strand runs from subunits B and A to D in the 5'–3' direction as shown as sticks. The side chains of labelled residues that interact with the ssDNA are also shown as sticks. The four aromatic residues involved in stacking interactions to bases of the ssDNA are labelled in bold. Residues that are not conserved in *Ec*-SSB are shown in red.

In the F-SSBT*:$(dT)_{63}$ structure, each $(dT)_{16}$ unit and its contacting residues on the monomer are necessarily identical to the others, which is different from the asymmetric structure of the *Ec*-SSB:$(dC)_{35x2}$ complex. In **Figure 5.3,** a $(dT)_{16}$ contacting three monomers of the tetramer runs from subunit B and A to C (**Figure 5.4**) in the 5'–3' direction.

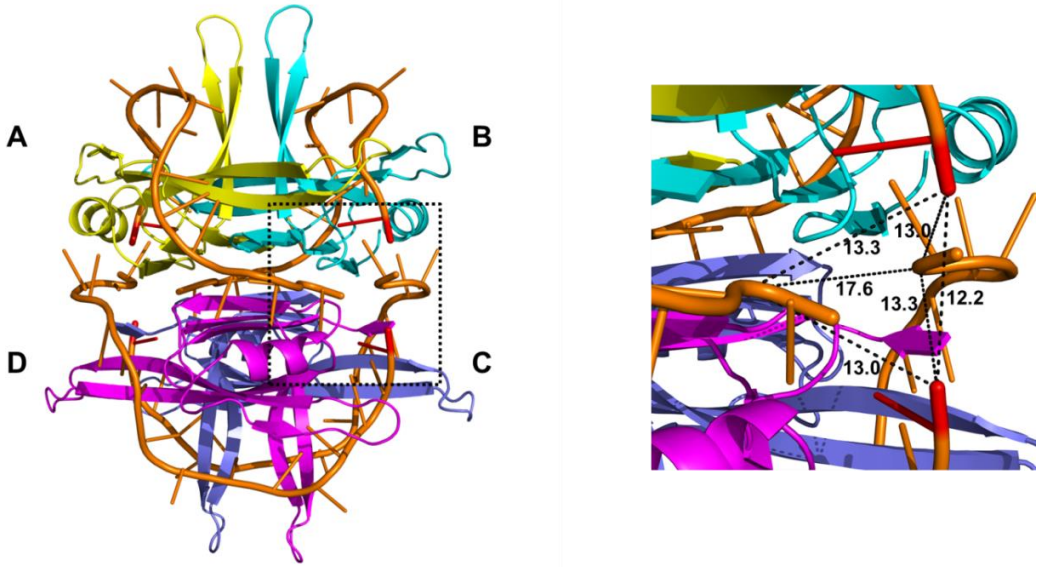

Figure 5.4 F-SSBT*:$(dT)_{63}$ tetramer structure and the distances between the ends of the $(dT)_{16}$ units. F-SSBT* structure in complex with four $(dT)_{16}$ strands (orange) is shown as cartoon (left picture). Each subunit of F-SSBT* is labelled as A (yellow), B (cyan), C (pale blue) and D (purple). ssDNA is coloured red at the 5' end. The boxed area is enlarged on the right. The distances (in Å) are measured between two termini of any $(dT)_{16}$ units (dashed lines). The distances between any two 5' and 3' ends are about 13 Å, which can accommodate one nucleotide. The distance between two 5' ends is about 12 Å. However the distance between two 3' ends is 17.6 Å, which would accommodate two nucleotides.

Nucleotide T1 binds to Thr-104 and inserts its base into a hydrophobic pocket created by Thr-104 and Lys-103. They force the 5'-end of the ssDNA to bend toward a large positively charged region where four $(dT)_{16}$ units meet. T2 interacts with Lys-103 as well as Trp-40 (π-stacking) and Glu-38 on subunit B. The side chain of T3 contacts Phe-60 through a π-stacking interaction. Trp-40 and Phe-60 in *Ec*-SSB also stack to a ssDNA base. However the bases are facing outward from the protein (**Figure 5.2**). T4 inserts its base into a hydrophobic pocket composed of Val-57, Val-58, Leu-59 and Phe-60, and its phosphate group interacts with Ile-23. These interactions bend the base of T4 toward the protein. T6 binds to Arg-86, and both phosphate groups of T5 and T6 interact with Arg-21. The hydrophobic interaction of the T4 base with the protein and its close proximity to the T6 base flips the base of T5 outward from the protein. T7 stacks with Tyr-96 on subunit B. T9 interacts with Gln-33 and Trp-54 (stacking interaction). The two-base stacking fixes the angle of the ssDNA backbone, and flips the base of T8 into space. The interactions also force a bend of ssDNA toward the protein. T10 binds to Arg-13 and Leu-14. T11 also binds to Arg-13, which also interacts with the phosphate group of T12. T12 also binds to Arg-3 on subunit B. Due to a highly positively charged

surface region, T10, T11 and T12 form extensive backbone interactions with the protein. This is similar to the *Ec*-SSB complex in the same region (**Figure 5.2**). T13 binds to Arg-113 and Cys-70 in subunit D, inserting its base into a hydrophobic pocket created by these two residues and Met-110. The hydrophobic interaction fixes the ssDNA, and allows it to bend towards the α helix of subunit D. T14 binds to Glu-69 and Met-110 of subunit D through its base. T15 binds to Arg-3 in subunit B, as well as Met-108 and Met-110 of subunit D. T16 inserts its base into a hydrophobic pocket created by Phe-60, Gly-61, Lys-62, Leu-63, Val-102, Thr-104 and Gly-106 of subunit D.

Compared to the *Ec*-SSB:$(dC)_{35}$ structure, the stacking of a nucleotide base to each of Trp-40, Trp-54 and Phe-60 is conserved. However, the stacking arrangement to Trp-88 of *Ec*-SSB is not observed in F-SSB. Instead, a stacking interaction to Tyr-96 of monomer B of F-SSB is observed. This makes the total number of observed stacking interactions between ssDNA and *Ec*-SSB or F-SSB equal. Although Trp-88 in F-SSB does not show direct stacking interaction with a DNA base, its side-chain protrudes out as does that of Tyr-96. Their aromatic rings all face towards the DNA binding cleft created by β2, β3 and the base of L45. The Trp-88 in *Ec*-SSB was proposed to play a role in promoting the $(SSB)_{35}$ binding mode to redirect the DNA into the next SSB tetramer, mediated by the L45 crystal contact (Raghunathan *et al.,* 2000). Given that the crystal contact observed for F-SSB is different (mediated by L23) from *Ec*-SSB, and the highly acidic L45 region clearly creates an obstacle for protein interaction as well as DNA interaction (**Figure 5.5**), it is unlikely that F-SSB can adopt the same cooperative binding mode.

5.3.3 F-SSB binds to ssDNA and forms a large protein–DNA complex

Agarose gel electrophoresis was used to demonstrate the ssDNA binding of F-SSB (**Figure 5.6**). Assuming all the SSB species adopt the $(SSB)_{35}$ binding mode, the M13 ssDNA should be saturated with about 720 nM protein. Indeed, no apparent shift of M13 was observed by raising the concentration of *Ec*-SSB from 720 nM (lane 4) to 1.8 μM (lane 5). The same concentrations of F-SSB (lanes 6–8) shifted the M13 to about the same position in the gel as *Ec*-SSB (lanes 2–4), which hints that F-SSB may adopt a similar ssDNA binding mode. Surprisingly, mixing 1.8 μM F-SSB or F-SSBT* with

M13 gave rise to a DNA species much larger than individual M13 circles saturated with *Ec*-SSB (lanes 9 and 13). The products are so large that they do not even enter the gel. This observation suggests additional contacts between the molecules are responsible for the oligomerization.

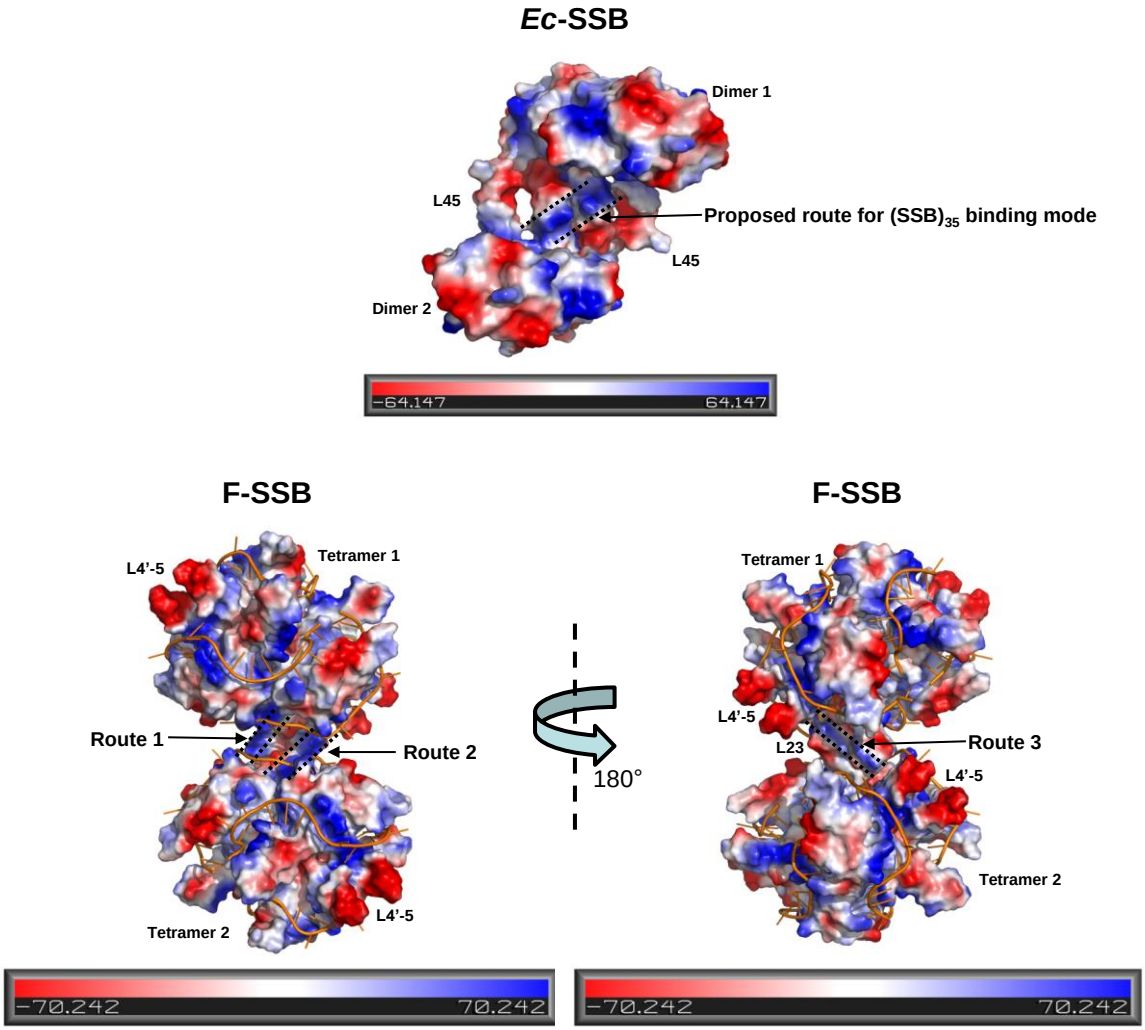

Figure 5.5 Surface electrostatic potential of the OB domains of *Ec*-SSB (Raghunathan *et al.,* 2000) and F-SSBT*. Two *Ec*-SSB OB-domain dimers associated through the crystal contact at L45 are shown above. Two F-SSBT* tetramers associated through the crystal contact at L23 are shown at the bottom. The proposed route (Raghunathan *et al.,* 2000) for ssDNA passing from one tetramer to another in the $(SSB)_{35}$ binding mode is shown. Three proposed routes for ssDNA passing from one tetramer to another on F-SSB, mediated by the L23 crystal contact, are proposed. The ssDNA segments on F-SSB are shown in orange.

In the F-SSBT*:$(dT)_{63}$ structure, only one crystal contact was observed, which is mediated through L23. The contact through L45 in the *Ec*-SSB:$(dC)_{35}$ complex is absent from the F-SSBT*:$(dT)_{63}$ structure probably due to the high negative charge on the L45 loop (**Figure 5.5**). Unlike in the *Ec*-SSB:$(dC)_{35x2}$ structure, two L45 loops on the F-SSB dimer repel each other to achieve a wide open form. As demanded by the symmetry, one

F-SSBT* tetramer contact four other F-SSBT* tetramers through its four L23 loops. Moreover, all the ends of $(dT)_{16}$ segments meet at a common area located at the base of two L12 and two L23 loops. Therefore the ssDNA is speculated to run from one tetramer to another through the L23 connection. Three potential routes are highlighted in **Figure 5.5**, which all involve positively charged areas flanked by negatively charged ones. Further studies using longer ssDNA are needed to confirm the speculation.

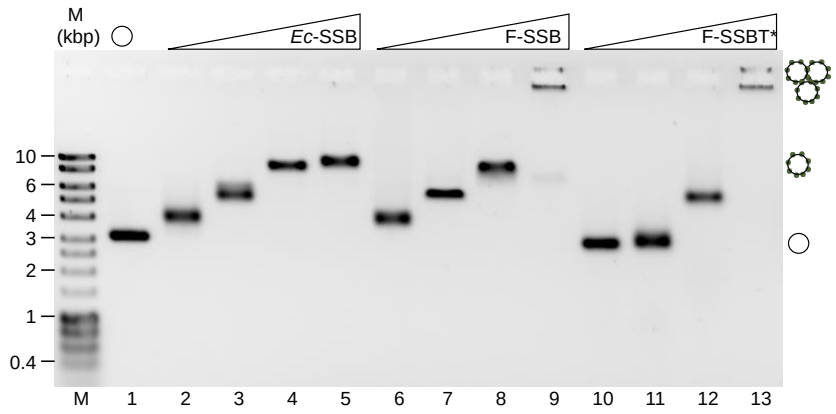

Figure 5.6 ssDNA binding assay for *Ec*-SSB, F-SSB and F-SSBT*. In the experiment, 4 nM of M13 ssDNA template (6407 nucleotides; lane 1) was mixed with 180 nM (lanes 2, 6 and 10), 360 nM (lanes 3, 7 and 11), 720 nM (lanes 4, 8 and 12) and 1.8 μM (lanes 5, 9 and 13) of *Ec*-SSB, F-SSB and F-SSBT*, respectively, in 10 mM Tris-HCl, pH 7.6, 10 mM $MgCl_2$, 8 mM DTT and 40 mM NaCl. The mixtures were analysed by 0.7% agarose gel electrophoresis. DNA was visualized by being stained with SYBR gold nucleic acid stain. The marker (M) and the schematics are shown at the left and right of the picture, respectively. Circles represent M13ssDNA. Small beads represent various SSB species.

5.3.4 *E. coli* can carry out DNA replication on parental ssDNA associated with F-SSB.

Studies showed F-SSB is probably expressed in the recipient cells after bacterial conjugation since the protein is not involved in the conjugation process itself (Rees and Wilkins, 1990). Furthermore, the *ssf* gene can complement a conditional *ssb* mutation (Kolodkin *et al.,* 1983) or *ssb* gene deletion in *E. coli* (Porter *et al.,* 1991). Here we have shown a crystal structure of an F-SSB:ssDNA complex with similar ssDNA binding fashion as that of the *Ec*-SSB:ssDNA complex. For bacteria to survive, the chromosome has to be replicated and distributed into its daughter cells. But the mechanism by which the replisome removes the SSB tightly bound to the ssDNA is not entirely clear. On the other hand, *in vitro* DNA replication assays have shown *Ec*-SSB can stimulate Pol III-

mediated DNA replication (**Chapter 4**). Our new F-SSBT*:$(dT)_{63}$ structure is very similar to that of *Ec*-SSB:$(dC)_{35x2}$, except that it shows opposite ssDNA binding polarity. Our finding raises two questions: (i) Does F-SSB stimulate *E. coli* DNA replication? (ii) Does the DNA binding polarity on SSB affect replication of the DNA.

A good way to answer these questions is to use homogenous tetramers of *Ec*- and F-SSB and compare them with hybrid tetramers of the two proteins (since hybrid tetramers can potentially exist in the cell; **Section 4.3.2**) in a DNA replication system. An *in vitro* DNA replication assay with *E. coli* Pol III HE (including the Pol III core, αεθ; the clamp loader, $\tau_3\delta\delta'\chi\psi$; and the clamp, β_2) supplemented with various SSB species (including the hybrid tetramers) was carried out (**Section 5.2**). To eliminate the influence of buffer, samples of subunit exchanged *Ec*-SSB and F-SSB used in the assay were obtained in both NH_4OAc buffer and Tris-HCl storage buffer (**Section 5.2**). The result shows reactions with all three SSB species give rise to TFII (fully double-strand circular product), indicating the *E. coli* Pol III HE can utilize F-SSB as an alternative of the native *Ec*-SSB to carry out primer extension (**Figure 5.7B**). However, the replication with F-SSB seems to be slower than that with the *Ec*-SSB, and F-SSB does not stimulate strand-displacement (SD) synthesis. This is probably not due to a stronger binding affinity of F-SSB to ssDNA, but rather to some unknown function of the unconserved part of the C-terminal region (residues between 113 and 170). This is reflected in the reactions using various homogenous tetramers of chimeric *Ec*/F-SSB species (**Figure 5.7C**). The reaction with F-SSB–*Ec*-SSB (**Section 4.2.1**) renders the same rate of DNA replication as that with *Ec*-SSB–F-SSBc (**Section 4.2.1**) and wild type *Ec*-SSB, indicating the DNA replication is not determined by the binding affinity of the OB-domains of these SSBs. Moreover, these data unambiguously show that SSB with ssDNA wrapped in either polarity does not have any influence on DNA replication (if ssDNA truly binds the two proteins with different polarities).

Additionally, all reactions with proteins containing the C-terminal domain residues 113 to 170 of F-SSB (F-SSB, *Ec*-SSB–F-SSB and F-SSB–*Ec*-SSBc; **Section 4.2.1**) did not give rise to SD synthesis, which establishes that SD is determined (at least partially) by the corresponding unconserved region in the SSB C-terminal domain (**Section 4.3**). Therefore, the assay may also shed light on the mechanism of SD synthesis.

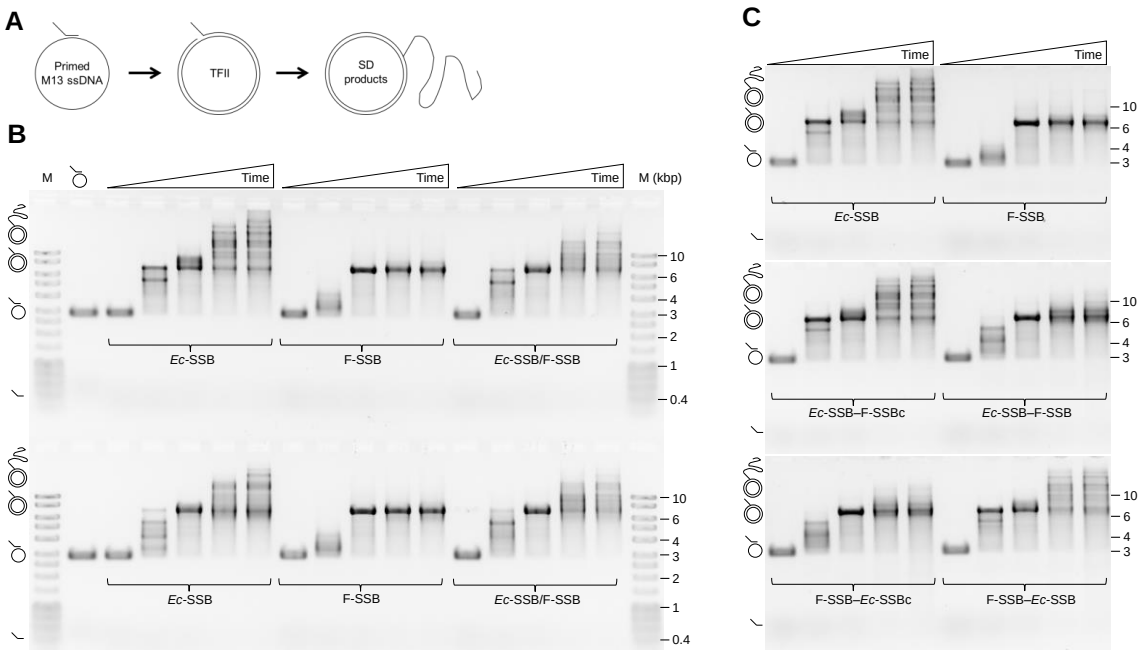

Figure 5.7 *In vitro* DNA replication assays with various F-SSB and *Ec*-SSB species. (**A**) Schematics of *in vitro* DNA replication and the products TFII and SD. (**B**) Time-course DNA replication assay with *E. coli* Pol III HE and various SSB species (*Ec*-SSB, F-SSB and hybrid tetramers composed from both proteins: *Ec*-SSB/F-SSB). The hybrid tetramers were obtained by treatment at 55°C for 2 h (**Section 5.2.4**). The homogenous tetramers of *Ec*-SSB and F-SSB were also treated separately in the same way. In the assay, 720 nM *Ec*-SSB, F-SSB or *Ec*-SSB/F-SSB subunit-exchanged proteins (SSBs used in upper and lower panel were treated with subunit-exchange procedures in Tris-HCl buffer and NH_4OAc buffer, respectively; **Section 5.2.3**) were mixed with reaction buffer containing 20 mM Tris-HCl, pH 7.6, 10 mM $MgCl_2$, 110 mM NaCl, 1 mM ATP, 8 mM DTT, 425 μM of each dNTP, 68 nM αεθ, 42 nM $\tau_3\delta\delta'\chi\psi$, 430 nM β_2 and 4 nM flap-primed M13 ssDNA, and incubated at 30°C. Aliquots (10 μL) were taken out at 0, 0.5, 1.5, 10 and 25 min, and quenched by addition of EDTA to 150 mM and SDS to 1%, and analysed by 0.7% agarose gel electrophoresis. DNA in each assay was visualized by being stained with SYBR gold nucleic acid stain (Invitrogen). (**C**) Time-course DNA replication assays with *E. coli* Pol III HE and various homogenous SSB tetramers composed of chimeric monomers (**Section 5.2.1**). The reactions were conducted in the same fashion as in (**B**), except various chimeric *Ec*/F-SSBs were used.

It was believed that *Ec*-SSB stimulates SD solely by interacting with the χ subunit of the clamp loader through the highly conserved C-terminal eight residues: DFDDDIPF (Yuan & McHenry, 2009; Jergic *et al.,* 2013). SPR measurements confirmed that the χ subunit interacts with F-SSB–*Ec*-SSB, *Ec*-SSB–F-SSBc, *Ec*-SSB–F-SSB and F-SSB–*Ec*-SSBc with very similar affinity (**Figure 4.14** and **Table 4.1**) through their C-termini (**Figure 3.6** and **Table 3.2**). Combined with the preliminary results discussed previously (**Figure 4.15**), this assay shows, for the first time, a clear dependence of SD synthesis on the unconserved region of *Ec*-SSB. On the other hand, the reactions with the hybrid SSB tetramers result in SD (**Figure 5.7B**), indicating the Pol III HE probably does not need all four intact C-terminal regions to carry out SD. A recent study shows *E. coli* can

survive with only two of the four intact *Ec*-SSB C-termini (Antony *et al.,* 2013), which is in accordance with our results.

F-SSB can also partially replace *Ec*-SSB in a second SSB-dependent DNA replication system. This downsized Pol III system involves only the α polymerase subunit, the $\gamma_3\delta\delta$' clamp loader, β_2, and *Ec*-SSB. The DNA replication assay shows absolute dependence on the β_2 clamp and *Ec*-SSB (**Figure 5.8**) in physiological salt conditions (Yin *et al.,* 2014), indicating a stimulatory role of *Ec*-SSB on DNA polymerase (α subunit).

Similar to Pol III HE-dependent DNA replication (**Figure 5.7**), only the reactions with *Ec*-SSB–F-SSBc and F-SSB–*Ec*-SSB rendered similar activity to wild type *Ec*-SSB, although the reactions with F-SSB–*Ec*-SSB was slower. Neither the other fusion proteins nor F-SSB was able to fully stimulate the reaction to TFII. The difference is clearly caused by the unconserved region of SSB (as discussed for **Figure 5.7C**). However, the facts that all SSB species stimulate Pol III primer extension and switching the OB domain of *Ec*-SSB to F-SSB does not affect its stimulatory role also suggest that the ssDNA binding polarity on SSB does not pose an obstacle for DNA replication. Efforts have been taken to solve *Ec*-SSBT*:$(dC)_{30}$ and *Ec*-SSBT*$(dT)_{62}$ crystal structures, but so far only *apo* protein structures or complex structures with poor electron density for ssDNA have been obtained (data not shown). Assigning ssDNA in both directions in these structures has resulted in similar *R* factors. Therefore there is still a lack of direct evidence for the unusual ssDNA binding polarity on *Ec*-SSB. It is likely that the ssDNA in the *Ec*-SSB:$(dC)_{35}$ structure solved by Raghunathan *et al.* (2000) was built into a poor electron density map, and the direction of ssDNA could not be unambiguously assigned. Further studies are needed.

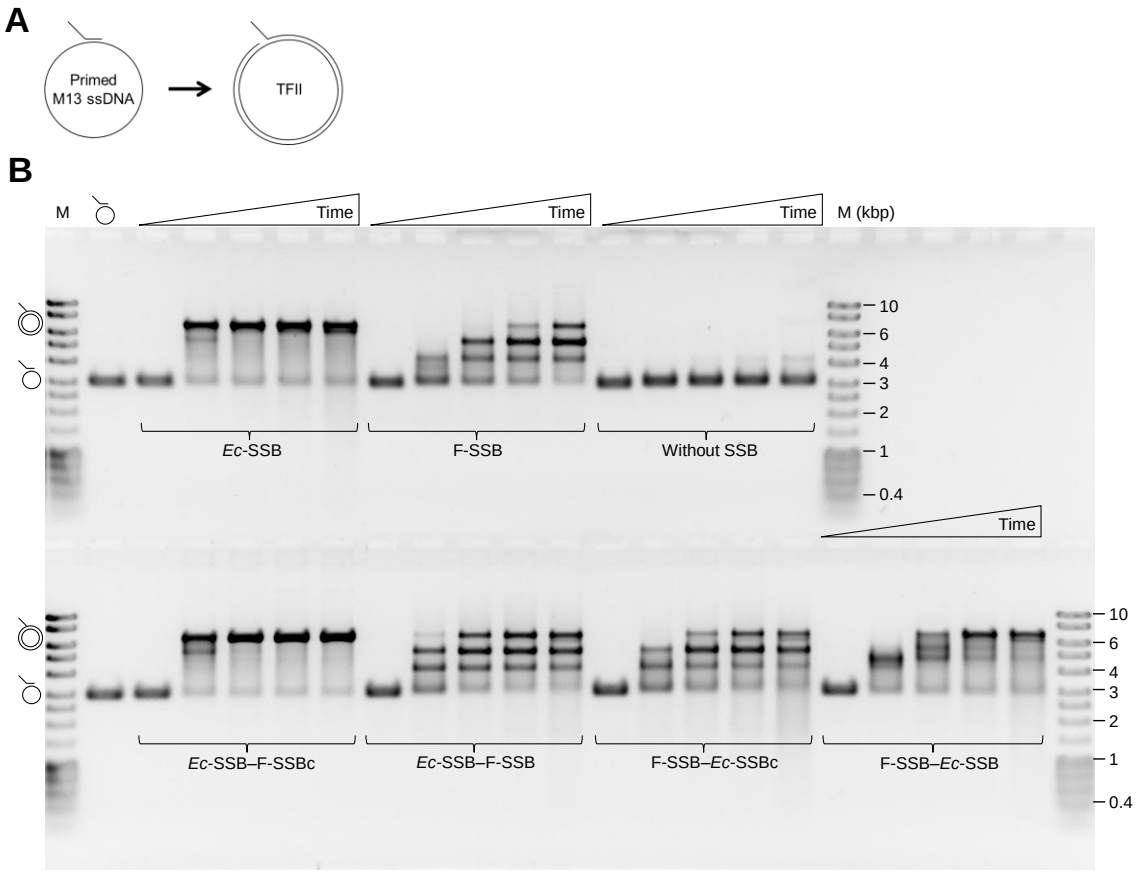

Figure 5.8 A SSB-dependent *E. coli* Pol III DNA replication assay with F-SSB, *Ec*-SSB and their fusion proteins. (**A**) Schematics of this *in vitro* DNA replication assay and the TFII products. (**B**) Time-course DNA replication assay with a minimized *E. coli* Pol III system (involving only α, $\gamma_3\delta\delta$' and β_2 subunits) and various SSB species (*Ec*-SSB, F-SSB and homogenous SSB tetramers composed of fusion monomers). In the reaction, 730 nM *Ec*-SSB, F-SSB, or their chimeric versions were mixed with reaction buffer containing 20 mM Tris-HCl, pH 7.6, 10 mM $MgCl_2$, 120 mM NaCl, 1 mM ATP, 9 mM DTT, 540 μM of each dNTP, 188 nM α, 37 nM $\gamma_3\delta\delta$', 216 nM β_2 and 3 nM flap-primed M13 ssDNA. The reactions were conducted at 30˚C. Aliquots (10 μL) of samples were taken out at 0, 10, 20, 30 and 60 min, and quenched by addition of EDTA to 150 mM and SDS to 1%, and analysed by 0.7% agarose gel electrophoresis. DNA was visualized by being stained with SYBR gold nucleic acid stain (Invitrogen).

5.3.5 A new proposed path of ssDNA on *Ec*-SSB and F-SSB hybrid tetramer species

Assuming the F-SSB and *Ec*-SSB actually do have opposite ssDNA binding polarity, the hybrid tetramers used in the DNA replication assay (**Figure 5.7B**) must have the ssDNA wrapped in a way distinct from both homogenous tetramers. It is difficult to discuss the ssDNA binding on all the hybrid tetramers. Therefore, I take the abundant species of *Ec*-SSB_2F-SSB_2 as a representative to propose a new ssDNA binding path (**Figure 5.9**). In the DNA replication assay, 110 mM NaCl and 10 mM $MgCl_2$ were

present in the reaction buffer, in which a mixture of $(SSB)_{35–65}$ binding modes should exist (Lohman and Overman, 1985; Bujalowski *et al.,* 1988).

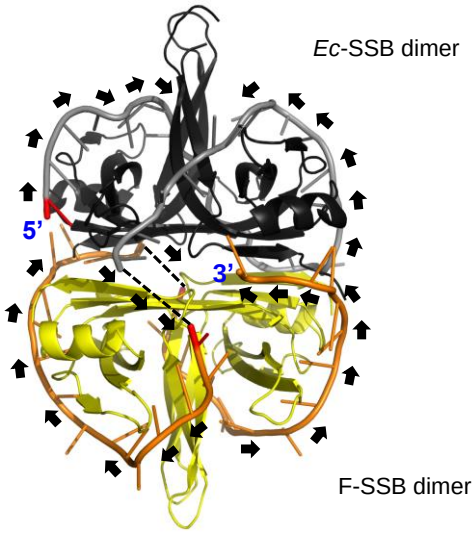

Figure 5.9 A new ssDNA binding path is proposed on a hybrid tetramer model of *Ec*-SSB_2F-SSB_2. The ssDNA running (black arrows) from 5' (red) to 3' end is connected by dashed lines. The newly proposed path (the dashed line connecting the 3'-end of the ssDNA on an *Ec*-SSB dimer and the 5'-end of the ssDNA on an F-SSB dimer) lies between the 5' (blue letter) and 3' (blue letter) ends of a continuous strand in the $(SSB)_{65}$ mode.

Here I propose a new model based on the $(SSB)_{65}$ binding mode where all four subunits engage in ssDNA binding. A hybrid *Ec*-SSB_2F-SSB_2 tetrameric structure was built by superimposing the *Ec*-SSB:$(dC)_{35}$ structure (PDB code: 1EYG) and our F-SSB:$(dT)_{63}$ structure in Pymol, and deleting a dimer (and associated ssDNA) from each structure. The resulting protein:ssDNA complex (**Figure 5.9**) contains a *Ec*-SSB dimer (black) wrapped by the $(dC)_{28}$ strand (grey) and a F-SSB dimer (yellow) wrapped by two $(dT)_{16}$ strands (orange). Based on the ssDNA binding in the crystal structures, the only possible path at the gaps is proposed (the dashed line between the 3'-end of the ssDNA on the *Ec*-SSB dimer and the 5'-end of the ssDNA on the F-SSB dimer, and the dashed line between the two ssDNA segments on the F-SSB dimer; **Figure 5.9**). This new path connecting the two dimers connects the 3' and 5' termini of a continuous ssDNA, which was not proposed in any other model. When the F-SSB is expressed in wild-type *E. coli*, this binding path could be employed by the hybrid tetramers formed between F-SSB and *Ec*-SSB. The abundance of hybrid tetramers in an F^+ cell needs to be investigated in future experiments in order to show how biologically relevant this model is. This new model as well as the DNA replication assays shows a very flexible feature of SSB OB-

fold domains and distinct features of the full-length proteins. It shows the diverse functions of different SSBs in the largely unconserved C-terminal regions.

This Chapter described a crystal structure of the F-SSB OB-domain tetramer in complex with a $(dT)_{63}$ ssDNA. Compared with *apo* structures of F-SSB and *Ec*-SSB, the overall structure of the F-SSB OB-domain is well conserved except for small distortions of the L45 loop towards the ssDNA binding site. However the binding polarity of ssDNA is strikingly opposite to that in the *Ec*-SSB:$(dC)_{35x2}$ structure (Raghunathan *et al.,* 2000). The validity of ssDNA binding polarities on both proteins have not yet been further addressed using other techniques, although efforts to reproduce the *Ec*-SSB:$(dC)_{35}$ structure have led to a electron density map with poor definition of the ssDNA that can fit ssDNA in either direction. DNA replication assays showed F-SSB can partially stimulate primer extension, but not strand displacement synthesis. Using hybrid and chimeric tetramers of F-SSB and *Ec*-SSB in the same assays revealed that the stimulatory role in primer extension is played by the well conserved OB- and Ct-domains of both proteins, but the inhibitory role in SD is related to the unconserved C-terminal regions between these two domains. Based on the subunit exchange property (**Section 4.3.2**) and opposite ssDNA binding polarities of *Ec*-SSB and F-SSB, a new ssDNA binding route was proposed. However it remains to be further established by experimental measurements.

CHAPTER 6

CONCLUDING SUMMARY

This Thesis contributes to the understanding of the role of *Ec*-SSB, as well as weak interactions among macromolecules that participate in lagging-strand DNA synthesis by the *E. coli* replisome. The transient interactions between the highly conserved *Ec*-SSB-Ct and its N-terminal OB-domain, DnaGC, χ and RNase HI were characterized either biochemically or structurally. The biological relevance of some of these interactions was explored using *in vitro* DNA replication assays. The results showed that *Ec*-SSB-Ct and the unconserved C-terminal linker domain play significant roles in primer extension and strand displacement (SD) DNA synthesis at physiological salt concentrations. The assays also showed that the *Ec*-SSB N-terminal domain alone is able to stimulate both Pol I and Pol III SD at low salt concentrations, which supports the notion that the strong interaction between this domain and ssDNA prevents DNA replication fork regression and thus facilitates SD (Manosas *et al.,* 2012). The devastating SD as Pol III approaches the previous lagging strand primer is prevented by longer RNA primers and Pol I nick translation activity, which results in a nick that is then efficiently ligated by ligase A (Kornberg and Baker, 1991). Neither RNase HI or RNase HII, nor both in combination, is able to process the RNA primer as does Pol I. An *Ec*-SSB analogue, F-SSB, encoded on the F plasmid, has a very similar amino acid sequence in the N-terminal OB-domain, but distinctive amino acid composition in the C-terminal region. An F-SSB:$(dT)_{63}$ crystal structure showed a very similar OB-domain arrangement but opposite ssDNA binding polarity to an *Ec*-SSB:$(dC)_{35x2}$ crystal structure (Raghunathan *et al.,* 2000). The function of F-SSB in DNA replication was explored, and the functions relating to the ssDNA binding polarities and the distinctive C-terminal domain were discussed.

Ec-SSB protects ssDNA from nucleolytic attack through high affinity interaction between its OB-domain and ssDNA. More and more studies also show *Ec*-SSB is able to recruit an array of different proteins to ssDNA through its highly conserved Ct-domain. There is evidence showing *Ec*-SSB regulates these interactions, including those to both ssDNA and proteins, through its Ct-domain (reviewed by Shereda *et al.,* 2008). As many of these interactions significantly influence DNA synthesis by Pol III (Yuzhakov *et al.*, 1999; Yuan & McHenry, 2009), understanding the multiple roles of *Ec*-SSB is of crucial importance to understanding of *E. coli* DNA replication. In **Chapter 3**, weak interactions between *Ec*-SSB or F-SSB and several DNA and RNA metabolic enzymes, as well as the Ct-domain of *Ec*-SSB and its OB-domain, were explored. The SPR results showed that an *Ec*-SSB tetramer immobilized through

binding to an oligodeoxynucleotide can interact with multiple molecules of the same protein (The C-terminal domain of DnaG primase, *i.e.,* DnaGC, RNase HI and the χ subunit of Pol III) simultaneously with K_D in the low μM range. Sequence alignment of *Ec*-SSB and its analogue F-SSB showed extensive sequence similarity in the N-terminal OB-domain and the very C-terminal 8 residues. Repeating the same SPR experiment with F-SSB yielded similar values of K_D and stoichiometries, which strengthens the notion that *Ec*-SSB interacts with almost all its binding partners through the Ct-domain. Additionally, this work provided the first evidence of the interactions between F-SSB and DnaG, RNase HI and χ. This Chapter also revealed the structural basis of the interaction between the *Ec*-SSB-Ct (Asp-174 and Phe-172) and the ssDNA-binding site in its OB-domain (Val-30 and Val-59) through NMR studies at pH 3.4 where *Ec*-SSB is a monomer. However, this interaction is surprisingly weak (K_D is in the mM range) at neutral pH even in the absence of ssDNA, suggesting *Ec*-SSB can readily interact with its binding partners through its Ct-domain without pre-associating with ssDNA. This seems to contradict results from previous studies (summarized in **Sections 3.1.1** and **4.1.1**), which showed signs that the C-terminus of *Ec*-SSB regulates itself on binding to ssDNA. This regulatory role of the Ct-domain was reflected in the following Chapters where primer extension assays by Pol III were clearly stimulated by the C-termini of *Ec*-SSB. More studies are needed in the future to understand the regulatory role of *Ec*-SSB.

Ec-SSB plays an important role in lagging strand DNA synthesis as it coordinates the actions of DnaG primase and the χ subunit on the clamp loader through weak interactions (Yuzhakov *et al.*, 1999; Yuan & McHenry, 2009). Its new role in stimulating Pol III SD was revealed more recently (Yuan & McHenry, 2009). It was found this process is mediated through weak interaction between the SSB-Ct and the χ subunit in physiological conditions. The Pol III proofreading ε subunit is also required in the process (Jergic *et al.*, 2013). However, larger, more complete replication systems were often used in previous studies, which because of their complexity often cannot reveal direct interaction between two particular proteins. In **Chapter 4**, several downsized replication systems were developed to probe new interactions among components (especially the *Ec*-SSB) of the *E. coli* replication machinery during lagging-strand synthesis. A well-established rolling circle system with a primed phage M13 ssDNA circle was used. The Pol III SD was re-examined in the rolling circle

reaction in the presence of Pol III HE and *Ec*-SSB, which revealed additional stimulatory roles of the OB-domain and non-conserved C-terminal domain in SD beside the stimulatory role of *Ec*-SSB-Ct mediated by interaction with χ. Specifically, *Ec*-SSB without its Ct-domain or the entire C-terminal region could support Pol III SD in lower salt conditions, which indicates that the high affinity between the OB-domain and ssDNA may be enough to facilitate the opening of the replication fork. This is reflected in Pol I SD as well, where just the OB-domain of *Ec*-SSB is capable of stimulating SD to the same extent as does the wild type *Ec*-SSB in low salt. Moreover, the stimulatory role of the non-conserved *Ec*-SSB C-terminal region was revealed by use of *Ec*-SSB and F-SSB chimeric fusion proteins in the Pol III SD reactions (in physiological salt conditions). Only the chimeric SSB species that contained the *Ec*-SSB C-terminal non-conserved region stimulated Pol III SD, although a ssDNA binding assay and SPR measurements showed F-SSB binds to ssDNA and the χ subunit in similar fashion as does *Ec*-SSB.

However, F-SSB showed dsDNA binding capacity in another assay, and this may contribute to its inhibitory role in Pol III SD. The dsDNA binding region of F-SSB is likely to be near the C-terminus. Fusion proteins with other SSB species should be used in future experiments for elucidating the role of the non-conserved SSB C-terminal domain in DNA replication. The biological significance of SD is still under debate, but it is clearly devastating to Okazaki fragment maturation. Assays showed both Pol I and a long RNA primer are required for stopping SD and supporting Okazaki fragment maturation, while RNase HI and RNase HII cannot replace Pol I's role. The latter results were in agreement with previous findings.

However, to fully understand the complex machinery of Pol III HE, using the downsized Pol III systems could give us the advantage of investigating interactions in a system with a smaller numbers of proteins. An SSB-dependent β_2-dependent Pol III α subunit primer extension assay showed both the *Ec*-SSB-Ct and the C-terminal non-conserved region contribute to DNA synthesis. F-SSB could not stimulate the reaction to the same extent. This may be due to the regulatory role of the *Ec*-SSB-Ct on ssDNA binding, or additional interaction between the *Ec*-SSB C-terminal domain and other components. To rule out the influence of the clamp loader in the reaction, a further downsized system was used. Surprisingly, the result showed that in lower salt the clamp

loader ($\gamma_3\delta\delta'$) together with *Ec*-SSB stimulates Pol III α subunit primer extension in the absence of the β_2 clamp. A similar effect was observed in Pol I primer extension as well, but *Ec*-SSB was not required. The result showed uncharacterized interactions between the clamp loader and the polymerases may exist. Surprisingly, adding *Ec*-SSB into a Pol I primer extension assay in physiological salt conditions inhibited the reaction, which contrasts with the SSB-dependent β_2-dependent Pol III α subunit primer extension assay. DNA polymerase needs to remove SSB that is tightly associated with ssDNA ahead of it for DNA synthesis to proceed. These results indicate that certain DNA polymerases (*e.g.*, the Pol III α subunit) can achieve this more efficiently than others (*e.g.*, Pol I), and interaction between the polymerases and SSB should be examined more closely. In the last part of **Chapter 4**, a hybrid *Ec*-SSB tetramer with a covalently linked mKikGR fluorescent protein was used in a single molecule assay to help visualize the movement of the replication fork. Preliminary results indicated that *Ec*-SSB is likely to be recycled at the replication fork, presumably from a position ahead of the polymerase to one behind the helicase. However, more experiments are required to elucidate this mechanism.

Despite its similarity to *Ec*-SSB in terms of amino acid sequence and biochemical properties, the function of F-SSB remains unknown. In **Chapter 4**, many new features of F-SSB were revealed, including its inhibitory role in Pol III DNA synthesis and its interaction with dsDNA. Results indicated the non-conserved C-terminus of F-SSB may be responsible for these features. But is this true? In **Chapter 5**, a F-SSB:$(dT)_{63}$ crystal structure was described. Interestingly, despite adopting a similar ssDNA binding route to *Ec*-SSB, F-SSB has its bound ssDNA running in the opposite direction to the dC oligonucleotide on the *Ec*-SSB (Raghunathan *et al.,* 2000). Sequence alignment showed these two proteins are very well conserved in the N-terminal OB-domain, and a structural alignment showed only six non-conserved residues on the ssDNA binding route. Therefore these six residues may contribute to the distinct ssDNA binding polarities on these two proteins. Since the *Ec*-SSB:$(dC)_{35x2}$ complex was the first SSB:ssDNA cocrystal structure to be solved, and is the only SSB with ssDNA running opposite to that on all other SSBs, reproduction of the crystal structure was necessary. However, efforts to reproduce the *Ec*-SSB:$(dC)_{35x2}$ crystal yielded structures with poor electron density maps of DNA that were not sufficient to distinguish its polarity. It is unclear if the published *Ec*-SSB:$(dC)_{35x2}$ crystal structure with relatively low resolution

(2.8 Å) could actually define the ssDNA binding polarity confidently; structure factors and amplitudes were not deposited with the PDB file and the raw data are no longer available to allow this to be reassessed. Assuming the *Ec*-SSB:$(dC)_{35x2}$ crystal structure is correct, Pol III SD and *Ec*-SSB-dependent β_2-dependent Pol III α subunit primer extension assays with hybrid tetramers and fusion proteins of *Ec*-SSB and F-SSB were carried out to determine if the ssDNA binding polarities on SSB influence Pol III DNA replication. The results showed F-SSB has the ability to partially support Pol III DNA primer extension and SD, but replacing F-SSB's C-terminal domain with that of *Ec*-SSB increased this ability to an extent that was almost equivalent to *Ec*-SSB. This result would seem to indicate that SSB bound with either ssDNA polarity can support Pol III DNA synthesis. Furthermore, it is likely F-SSB coexists with *Ec*-SSB in F^+ *E. coli* strains and forms hybrid tetramers. Such hybrid tetramers with a continuous ssDNA strand running in opposite directions may exist as well. Based on the *Ec*-SSB:$(dC)_{35x2}$ and F-SSB:$(dT)_{63}$ structures, a SSB tetramer model with two *Ec*-SSB monomers and two F-SSB monomers was built with their own ssDNA. A new ssDNA binding route was proposed for the $(SSB)_{65}$ binding mode in this situation. However, more experiments are needed to validate this presumption.

This Thesis contains many preliminary results. Follow-up studies are currently being conducted for some experiments described in it. For example, NMR, MS and SPR are currently being used to study the ssDNA binding polarity on *Ec*-SSB and the dsDNA binding property of F-SSB.

REFERENCES

Antony, E., Weiland, E.A., Korolev, S., and Lohman, T.M. (2012). *Plasmodium falciparum* SSB tetramer wraps single-stranded DNA with similar topology but opposite polarity to *E. coli* SSB. *J. Mol. Biol., 420*, 269–283.

Antony, E., Weiland, E.A., Yuan, Q., Manhart, C.M., Nguyen, B., Kozlov, A.G., McHenry, C.S., and Lohman, T.M. (2013). Multiple C-terminal tails within a single *E. coli* SSB homotetramer coordinate DNA replication and repair. *J. Mol. Biol., 425*, 4802–4819.

Ariyoshi, M., Vassylyev, D.G., Iwasaki, H., Nakamura, H., Shinagawa, H., and Morikawa, K. (1994). Atomic structure of the RuvC resolvase: a Holliday junction-specific endonuclease from *E. coli*. *Cell, 78*, 1063–1072.

Argiriadi, M.A., Goedken, E.R., Bruck, I., O'Donnell, M., and Kuriyan, J. (2006). Crystal structure of a DNA polymerase sliding clamp from a Gram-positive bacterium. *BMC Struct. Biol*., *6*, 2.

Ason, B., Handayani, R., Williams, C.R., Bertram, J.G., Hingorani, M.M., O'Donnell, M., Goodman, M.F., and Bloom, L.B. (2003). Mechanism of loading the *Escherichia coli* DNA polymerase III β sliding clamp on DNA. Bona fide primer/templates preferentially trigger the γ complex to hydrolyze ATP and load the clamp. *J. Biol. Chem*., *278*, 10033–10040.

Babu, C.S., Dudev, T., Casareno, R., Cowan, J.A., and Lim, C. (2003). A combined experimental and theoretical study of divalent metal ion selectivity and function in proteins: Application to *E. coli* ribonuclease H1. *J. Am. Chem. Soc*., *125*, 9318–9328.

Ban, C., Junop, M., and Yang, W. (1999). Transformation of MutL by ATP binding and hydrolysis: a switch in DNA mismatch repair. *Cell, 97*, 85–97.

Ban, C., and Yang, W. (1998). Crystal structure and ATPase activity of MutL: implications for DNA repair and mutagenesis. *Cell, 95*, 541–552.

Barsky, D., Laurence, T.A., and Venclovas, C. (2011). How proteins slide on DNA. Biophysics of DNA-Protein Interactions: From Single Molecules to Biological Systems, New York: Springer , 39-68.

Becker, A., Lyn, G., Gefter, M., and Hurwitz, J. (1967). The enzymatic repair of DNA, II: Characterization of phage-induced sealase. *Proc. Natl. Acad. Sci. U.S.A*., *58*, 1996–2003.

Beese, L.S., and Steitz, T.A., (1991). Structural basis for the 3'–5' exonuclease activity of *Escherichia coli* DNA polymerase I: a two metal ion mechanism. *EMBO J., 10*, 25–33.

Blackburn, G.M., and Gait, M.J. (1996). *Nucleic Acids in Chemistry and Biology*, Oxford University Press, New York.

Blaszczyk, J., Tropea, J.E., Bubunenko, M., Routzahn, K.M., Waugh, D.S., Court, D.L., and Ji, X. (2001). Crystallographic and modeling studies of RNase III suggest a mechanism for double-stranded RNA cleavage. *Structure, 9*, 1225–1236.

Bonner, G., Patra, D., Lafer, E.M., and Sousa, R. (1992). Mutations in T7 RNA polymerase that support the proposal for a common polymerase active site structure. *EMBO J.*, *11*, 3767–3775.

Bouché, J.P., Rowen, L., and Kornberg, A. (1978). The RNA primer synthesized by primase to initiate phage G4 DNA replication. *J Biol Chem., 253*, 765–769.

Bowman, G.D., O'Donnell, M., and Kuriyan, J. (2004). Structural analysis of a eukaryotic sliding DNA clamp–clamp loader complex. *Nature, 429*, 724–730.

Brutlag, D., Atkinson, M.R., Setlow, P., and Kornberg, A. (1969). An active fragment of DNA polymerase produced by proteolytic cleavage. *Biochem. Biophys. Res. Commun., 37*, 982–989.

Buiacz, G., Jaskolski, M., Alexandratos, J., Wlodawer, A., Merkel, G., Katz, R.A., and Skalka, A.M. (1996). The catalytic domain of avian sarcoma virus integrase: conformation of the active-site residues in the presence of divalent cations. *Structure, 4*, 89–96.

Bujalowski, W., Overman, L.B., and Lohman, T.M. (1988). Binding mode transitions of *Escherichia coli* single strand binding protein–single-stranded DNA complexes. Cation, anion, pH, and binding density effects. *J. Biol. Chem.*, *263*, 4629–4640.

Broccoli, S., Rallu F., Sanscartier, P., Cerritelli, S.M., Crouch R.J., and Drolet, M. (2004). Effects of RNA polymerase modifications on transcription-induced negative supercoiling and associated R-loop formation. *Mol. Microbiol., 52*, 1769–1779.

Brody, R.S., and Frey, P.A., (1981). Unambiguous determination of the stereochemistry of nucleotidyl transfer catalyzed by DNA polymerase I from *Escherichia coli*. *Biochemistry*, *20***,** 1245–1252.

Bujalowski, W., and Lohman, T.M. (1986). *Escherichia coli* single-strand binding protein forms multiple, distinct complexes with single stranded DNA. *Biochemistry, 25*, 7799–7802.

Bunting, K.A., Roe, S.M., and Pearl, L.H. (2003). Structural basis for recruitment of translesion DNA polymerase Pol IV/DinB to the β-clamp. *EMBO J., 22*, 5883–5892.

Burnouf, D.Y., Oliéric, V., Wagner, J., Fujii, S., Reinbolt, J., Fuchs, R.P.P., and Dumas, P. (2004). Structural and biochemical analysis of sliding clamp/ligand interactions suggest a competition between replicative and translesion DNA polymerases. *J. Mol. Biol., 335*, 1187–1197.

Butland, G., Peregrin-Alvarez, J.M., Li, J., Yang, W., Yang, X., Canadien, V., Starostine, A., Richards, D., Beattie, B., Krogan, N., Davey, M., Parkinson, J., Greenblatt, J., and Emili, A. (2005). Interaction network containing conserved and essential protein complexes in *Escherichia coli*. *Nature, 433*, 531–537.

Canceill, D., and Ehrlich, S.D. (1996). Copy-choice recombination mediated by DNA polymerase III holoenzyme from *Escherichia coli. Proc. Natl. Acad. Sci. U.S.A.*, *93*,

6647–6652.

Canceill, D., Viguera, E., and Ehrlich, S.D. (1999). Replication slippage of different DNA polymerases is inversely related to their strand displacement efficiency. *J. Biol. Chem.*, *274*, 27481–27490.

Carter, J.R., Franden, M.A., Lippincott, J.A., and McHenry, C.S. (1993a). Identification, molecular cloning and characterization of the gene encoding the χ subunit of DNA polymerase III holoenzyme of *Escherichia coli*. *Mol. Gen. Genet.*, *241*, 399–408.

Carter, J.R., Franden, M.A., Aebersold, R., and McHenry, C.S. (1993b). Identification, isolation, and overexpression of the gene encoding the ψ subunit of DNA polymerase III holoenzyme. *J. Bacteriol.*, *175*, 5604–5610.

Chan, K.W., Lee, Y.J., Wang, C.H., Huang, H., and Sun, Y.J. (2009). Single-stranded DNA-binding protein complex from *Helicobacter pylori* suggests an ssDNA binding surface. *J. Mol. Biol.*, *388*, 508–519.

Chapados, B.R., Hosfield, D.J., Han, S., Qiu, J., Yelent, B., Shen, B., and Tainer, J.A. (2004). Structural basis for FEN-1 substrate specificity and PCNA-mediated activation in DNA replication and repair. *Cell*, *116*, 39–50.

Chase, J.W., L'Italien, J.J., Murphy, J.B., Spicer, E.K., and Williams, K.R. (1984). Characterization of the *Escherichia coli* SSB-113 mutant single-stranded DNA-binding protein. Cloning of the gene, DNA and protein sequence analysis, high pressure liquid chromatography peptide mapping, and DNA-binding studies. *J. Biol. Chem.*, *259*, 805–814.

Chase, J.W., Merrill, B.M., and Williams, K.R. (1983). F sex factor encodes a single-stranded DNA binding protein (SSB) with extensive sequence homology to *Escherichia coli* SSB. *Proc. Natl. Acad. Sci. U.S.A.*, *80*, 5480–5484.

Clark, A.B., Valle, F., Drotschmann, K., Gary, R.K., and Kunkel, T.A. (2000). Functional interaction of proliferating cell nuclear antigen with MSH2–MSH6 and MSH2–MSH3 complexes. *J. Biol. Chem.*, *275*, 36498–36501.

Chrysogelos, S., and Griffith, J. (1982). *Escherichia coli* single-strand binding protein organizes single-stranded DNA in nucleosome-like units. *Proc. Natl. Acad. Sci. U.S.A.*, *79*, 5803–5807.

Crooke, S. T., Lemonidis, K.M., Neilson, L., Griffey, R., Lesnik, E.A., and Monia, B.P. (1995). Kinetic characteristics of *Escherichia coli* RNase HI: cleavage of various antisense oligonucleotide RNA duplexes. *Biochem. J.*, *312*, 599–608.

Crooks, G.E., Hon, G., Chandonia, J.M., and Brenner, S.E. (2004). WebLogo: a sequence logo generator. *Genome Res.*, *14*, 1188–1190.

Crouch, R.J., and Dirksen, M.L. (1982). In *Nucleases*, Linn, S., and Roberts, R. (eds.), Cold Spring Harbor Laboratory Press, NY.

Curth, U., Genschel, J., Urbanke, C., and Greipel, J. (1996). *In vitro* and *in vivo* function of the C-terminus of *Escherichia coli* single-stranded DNA binding protein, *Nucleic Acids Res., 24*, 2706–2711.

Dalrymple, B.P., Kongsuwan, K., Wijffels, G., Dixon, N.E., and Jennings, P. (2001). A universal protein–protein interaction motif in the eubacterial DNA replication and repair systems. *Proc. Natl. Acad. Sci. U.S.A., 98*, 11627–11632.

Davey, M.J., Fang, L., McInerney, P., Georgescu, R.E., and O'Donnell, M. (2002a). The DnaC helicase loader is a dual ATP/ADP switch protein. *EMBO J., 21*, 3148–3159.

Davey, M.J., Jeruzalmi, D., Kuriyan, J., and O'Donnell, M. (2002b). Motors and switches: AAA+ machines within the replisome. *Nat. Rev. Mol. Cell. Biol., 3*, 826–835.

de la Cruz, F., Frost L.S., Meyer, R.J. and Zechner, E.L. (2010). Conjugative DNA metabolism in Gram-negative bacteria. *FEMS Microbiol. Rev., 34*, 8–40.

Doherty, A.J., Ashford, S.R., Subramanya, H.S., and Wigley, D.B. (1996). Bacteriophage T7 DNA ligase. Overexpression, purification, crystallization, and characterization. *J. Biol. Chem., 271*, 11083–11089.

Dohrmann, P.R., and McHenry, C.S. (2005). A bipartite polymerase–processivity factor interaction: Only the internal β binding site of the α subunit is required for processive replication by the DNA polymerase III holoenzyme. *J. Mol. Biol., 350*, 228–239.

Dougherty, G. (1983). The unwinding of circular DNA by intercalating agents as determined by gel electrophoresis. *Biosci. Rep., 3*, 453–460.

Drolet, M. (2006). Growth inhibition mediated by excess negative supercoiling: the interplay between transcription elongation, R-loop formation and DNA topology. *Mol. Microbiol., 59*, 723–730.

Dyda, F., Hickman, A.B., Jenkins, T.M., Engelman, A., Craigie, R., and Davies, D.R. (1994). Crystal structure of the catalytic domain of HIV-1 integrase: similarity to other polynucleotidyl transferases. *Science, 266*, 1981–1986.

Echols, H., and Goodman, M.F. (1991). Fidelity mechanisms in DNA replication. *Annu. Rev. Biochem., 60*, 477–511.

Elvin, C.M., Thompson, P.R., Argall, M.E., Hendry, P., Stamford, N.P.J., Lilley, P.E., and Dixon, N.E. (1990). Modified bacteriophage λ promoter vectors for overproduction of proteins in *Escherichia coli*. *Gene, 87*, 123–126.

Evans, P.R. (2005). Scaling and assessment of data quality. *Acta Crystallogr. D*, *62*, 72–82.

Fay, P.J., Johanson, K.O., McHenry, C.S., and Bambara, R.A., (1981). Size classes of products synthesized processively by DNA polymerase III and DNA polymerase III holoenzyme of *Escherichia coli., J. Biol. Chem.*, 256, 976–83.Flower, A.M., and McHenry, C.S. (1990). The γ subunit of DNA polymerase III holoenzyme of

Escherichia coli is produced by ribosomal frameshifting. *Proc. Natl. Acad. Sci. U.S.A.*, 87, 3713–3717.

Frank-Kamenetskii, M.D. (1987). How the double helix breathes. *Nature, 328*, 17–18.

Fukushima, S., Itaya, M., Kato, H., Ogasawara, N., and Yoshikawa, H. (2007). Reassessment of the *in vivo* functions of DNA polymerase I and RNase H in bacterial cell growth. *J. Bacteriol., 189*, 8575–8583.

Gajiwala, K.S., and Pinko, C. (2004). Structural rearrangement accompanying NAD^+ synthesis within a bacterial DNA ligase crystal. *Structure, 12*, 1449–1459.

Gamsjaeger. R., Kariawasam. R., Gimenez. A.X., Touma. C., McIlwain. E., Bernardo R.E., Shepherd. N.E., Ataide. S.F., Dong. Q., Richard. D.J., White. M.F., and Cubeddu. L. (2015). The structural basis of DNA binding by the single-stranded DNA-binding protein from *Sulfolobus solfataricus*. *Biochem. J., 465*, 337–346.Gao, D., and McHenry, C.S. (2001a). τ binds and organizes *Escherichia coli* replication through distinct domains. Partial proteolysis of terminally tagged τ to determine candidate domains and to assign Domain V as the α binding domain. *J. Biol. Chem., 276*, 4433–4440.

Gao, D., and McHenry, C.S. (2001b). τ binds and organizes *Escherichia coli* replication proteins through distinct domains. Domain III, shared by γ and τ, binds δ, δ' and χψ. *J. Biol. Chem., 276*, 4447–4453.

Gajjar, L., Dubey, R.S., and Srivastava, R.C. (1994). Activation and stabilization of enzymes entrapped into reversed micelles. Studies on hydrolyzing enzymes – protease and α-amylase. *Appl. Biochem. Biotechnol., 49*, 101–112.

Gefter, M.L., Becker, A., and Hurwitz, J. (1967). The enzymatic repair of DNA, I: Fformation of circular DNA. *Proc. Natl. Acad. Sci. U.S.A., 58*, 240–247.

Gellert, M. (1967). Formation of covalent circles of λ DNA by *E. coli* extracts. *Proc. Natl. Acad. Sci. U.S.A., 57*, 148–155.

Georgescu, R.E., Kim, S.S., Yurieva, O., Kuriyan, J., Kong, X.-P., and O'Donnell, M. (2007). Structure of a sliding clamp on DNA. *Cell, 132*, 43–54.

Glover, B.P., and McHenry, C.S. (1998). The χψ subunits of DNA polymerase III holoenzyme bind to single-stranded DNA-binding protein (SSB) and facilitate replication of an SSB-coated template. *J. Biol. Chem., 273*, 23476–23484.

Glover, B.P., and McHenry, C.S. (2000). The DnaX-binding subunits δ' and ψ are bound to γ and not τ in the DNA polymerase III holoenzyme. *J. Biol. Chem., 275*, 3017–3020.

Goedken, E.R., Kazmirski, S.L., Bowman, G.D., O'Donnell, M., and Kuriyan, J. (2005). Mapping the interaction of DNA with the *Escherichia coli* DNA polymerase clamp loader complex. *Nat. Struct. Mol. Biol., 12*, 183–190.

Goedken, E.R., and Marqusee, S. (2001). Co-crystal of *Escherichia coli* RNAse HI with Mn^{2+} ions reveals two divalent metals bound in the active site. *J. Biol. Chem., 276*,

7266–7271.

Goldgur, Y., Dyda, F., Hickman, A.B., Jenkins, T.M., Craigie, R., and Davies, D.R. (1998). Three new structures of the core domain of HIV-1 integrase: an active site that binds magnesium. *Proc. Natl. Acad. Sci. U.S.A., 95*, 9150–9154.

Greve, J., Maestre, M., Moise, H., and Hosoda, J. (1978). Circular dichroism studies of the interaction of a limited hydrolysate of T4 gene 32 protein with T4 DNA and poly[d(A-T)].poly[d(A-T)]. *Biochemistry, 17*, 893–898.

Griffith, J.D., Harris, L.D., and Register, J. (1984). Visualization of SSB–ssDNA complexes active in the assembly of stable RecA–DNA filaments. *Cold Spring Harb. Symp. Quant. Biol*., *49*, 553–559.

Gueron, M., Kochoyan, M., and Leroy, J.L. (1987). A single mode of DNA base-pair opening drives imino proton exchange. *Nature, 328*, 89–92.

Gueron, M., and Leroy, J.L. (1995). Studies of base pair kinetics by NMR measurement of proton exchange. *Methods Enzymol., 261*, 383–413.

Gulbis, J.M., Kazmirski, S.L., Finkelstein, J., Kelman, Z., O'Donnell, M., and Kuriyan, J. (2004). Crystal structure of the χ:ψ sub-assembly of the *Escherichia coli* DNA polymerase clamp-loader complex. *Eur. J. Biochem., 271*, 439–449.

Gulbis, J.M., Kelman, Z., Hurwitz, J., O'Donnell, M., and Kuriyan, J. (1996). Structure of the C-terminal region of p21 (WAF1/CIP1) complexed with human PCNA. *Cell, 87*, 297–306.

Gumport, R.I., and Lehman, I.R. (1971). Structure of the DNA ligase adenylate intermediate: lysine (3-amino)-linked adenosine monophosphoramidate. *Proc. Natl. Acad. Sci. U.S.A., 68*, 2559–2563.

Habuchi, S., Tsutsui, H., Kochaniak, A.B., Miyawaki, A., and van Oijen, A.M. (2008). mKikGR, a monomeric photoswitchable fluorescent protein. *PLoS ONE*, *3*, e3944-1–e3944-9.

Hogrefe, H.H., Hogrefe, R.I., Walder, R.Y., and Walder, J.A. (1990). Kinetic analysis of *Escherichia coli* RNase H using DNA-RNA-DNA/DNA substrates. *J. Biol. Chem*., *265*, 5561–5566.

Hosoda, J., and Moise, H. (1978). Purification and physicochemical properties of limited proteolysis products of T4 helix destabilizing protein (gene 32 protein). *J. Biol. Chem., 253*, 7547–7555.

Howland, C.J., Rees, C.E., Barth, P.T., and Wilkins, B.M. (1989). The *ssb* gene of plasmid colIb-P9. *J. Bacteriol*., *171*, 2466–2473.

Hsieh, T. S., and Capp, C. (2005). Nucleotide- and stoichiometry-dependent DNA supercoiling by reverse gyrase. *J. Biol. Chem., 280*, 20467–20475.

Hughes, A.J., Bryan, S.K., Chen, H., Moses, R.E., and McHenry, C.S. (1991).

Escherichia coli DNA polymerase II is stimulated by DNA polymerase III holoenzyme auxiliary subunits. *J. Biol. Chem.*, *266*, 4568–4573.

Indiani, C., McInerney, P., Georgescu, R.E., Goodman, M.F., and O'Donnell, M. (2005). A sliding-clamp toolbelt binds high and low fidelity DNA polymerases simultaneously. *Mol. Cell.*, *19*, 805–815.

Indiani, C., and O'Donnell, M. (2003). Mechanism of the δ wrench in opening the β sliding clamp. *J. Biol. Chem.*, *278*, 40272–40281.

Jergić, S., Horan, N.P., Elshenawy, M.M., Mason, C.M., Urathamakul, T., Ozawa, K., Robinson, A., Goudsmits, J.M.H., Wang, Y., Pan, X., Beck, J.L., van Oijen, A.M., Huber, T., Hamdan, S.M., and Dixon, N.E. (2013). A direct proofreader–clamp interaction stabilizes the Pol III replicase in the polymerization mode. *EMBO J.*, *32*, 1322–1333.

Jergić, S., Ozawa, K., Williams, N.K., Su, X.-C., Scott, D.D., Hamdan, S.M., Crowther, J.A., Otting, G., and Dixon, N.E. (2007). The unstructured C-terminus of the τ subunit of *Escherichia coli* DNA polymerase III holoenzyme is the site of interaction with the α subunit. *Nucleic Acids Res.*, *35*, 2813–2824.

Jeruzalmi, D., Yurieva, O., Zhao, Y., Young, M., Stewart, J., Hingorani, M., O'Donnell, M., and Kuriyan, J. (2001a). Mechanism of processivity clamp opening by the δ subunit wrench of the clamp loader complex of *E. coli* DNA polymerase III. *Cell*, *106*, 417–428.

Jeruzalmi, D., O'Donnell, M., and Kuriyan, J. (2001b). Crystal structure of the processivity clamp loader γ complex of *E. coli* DNA polymerase III. *Cell*, *106*, 429–441.

Jo, K., and Topal, M.D. (1998). Step-wise DNA relaxation and decatenation by *NaeI-43K*. *Nucleic Acids Res.*, *26*, 2380–2384.

Johnson, A., and O'Donnell, M. (2005). Cellular DNA replicases: Components and dynamics at the replication fork. *Annu. Rev. Biochem.*, *74*, 283–315.

Joyce, C. M., and Grindley, N.D. (1984). Method for determining whether a gene of *Escherichia coli* is essential: application to the *polA* gene. *J. Bacteriol.*, *158*, 636–643.

Kanaya, S. (1998). Enzymatic activity and protein stability of *E. coli* ribonuclease HI. In *Ribonucleases H* (Crouch, R. J. and Toulme, J. J., eds), INSERM, Paris.

Kanaya, S., and Ikehara, M. (1995). Functions and structures of ribonuclease H enzymes. In *Subcellular Biochemistry* (Biswas, B. B. and Roy, S., eds), Plenum Press, New York.

Katayanagi, K., Okumura, M., and Morikawa, K. (1993). Crystal structure of *Escherichia coli* RNAse HI in complex with Mg^{2+} at 2.8 Å resolution: proof for a single Mg^{2+}-binding site. *Proteins*, *17*, 337–346.

Katayanagi, K., Miyagawa, M., Matsushima, M., Ishikawa, M., Kanaya, S., Ikehara, M., Matsuzaki, T., Raghunathan, S., Kozlov, A.G., Lohman, T.M., and Waksman, G. (2000). Structure of the DNA binding domain of *E. coli* SSB bound to ssDNA. *Nat. Struct. Biol.*, *7*, 648–652.

Kath, J.E., Jergic, S., Heltzel, J.M.H., Jacob, D., Dixon, N.E., Sutton, M.D., Walker, G.C., and Loparo, J.J. (2014) Polymerase exchange on single DNA molecules reveals processivity clamp control of translesion synthesis. *Proc. Natl. Acad. Sci. U.S.A.*, *111*, 7647–7652.

Kazmirski, S.L., Podobnik, M., Weitze, T.F., O'Donnell, M., and Kuriyan, J. (2004). Structural analysis of the inactive state of the *Escherichia coli* DNA polymerase clamp-loader complex. *Proc. Natl. Acad. Sci. U.S.A.*, *101*, 16750–16755.

Keck, J.L., Goedken, E.R., and Marqusee, S. (1998). Activation/attenuation model for RNase H. A one-metal mechanism with second-metal inhibition. *J. Biol. Chem*., *273*, 34128–34133.

Kelman, Z., Yuzhakov, A., Andjelkovic, J., and O'Donnell, M. (1998). Devoted to the lagging strand—the χ subunit of DNA polymerase III holoenzyme contacts SSB to promote processive elongation and sliding clamp assembly. *EMBO J*., *17*, 2436–2449.

Kim, Y., Grable, J.C., Love, R., Greene, P.J., and Rosenberg, J.M. (1990). Refinement of *Eco*RI endonuclease crystal structure: a revised protein chain tracing. *Science, 249*, 1307–1309.

Kobayashi, M., Itoh, K., Suzuki, T., Osanai, H., Nishikawa, K., Katoh, Y., Takagi, Y., and Yamamoto, M. (2002). Identification of the interactive interface and phylogenic conservation of the Nrf2-Keap1 system, *Genes Cells.*, *7*, 807–820.

Kogoma, T., and Foster, P.L. (1998). Physiological functions of *E. coli* RNase HI. In *Ribonucleases H* (Crouch RJ and Toulme JJ, eds), INSERM, Paris.

Kolodkin, A.L., Capage, M.A., Golub, E.I., and Low, K.B. (1983). F sex factor of *Escherichia coli* K-12 codes for a single-stranded DNA binding protein. *Proc. Natl. Acad. Sci. U.S.A.*, *80*, 4422–4426.

Kong, X.-P., Onrust, R., O'Donnell, M.E., and Kuriyan, J. (1992). Three-dimensional structure of the β subunit of *E. coli* DNA polymerase III holoenzyme: a sliding DNA clamp. *Cell*, *69*, 425–437.

Kornberg, A., and Baker, T.A. (1992). *DNA Replication.* W. H. Freeman and Company, New York, NY.

Kornberg, A., Lehman, I.R., Bessman, M.J., and Simms, E.S. (1956). Enzymic synthesis of deoxyribonucleic acid. *Biochim. Biophys. Acta*., *21*, 197–198.

Kostrewa, D., and Winkler, F.K. (1995). Mg^{2+} binding to the active site of *Eco*RV endonuclease: a crystallographic study of complexes with substrate and product DNA at 2 Å resolution. *Biochemisty*, *34*, 683–696.

Kozlov, A.G., and Lohman, T.M. (2002). Kinetic mechanism of direct transfer of *Escherichia coli* SSB tetramers between single-stranded DNA molecules. *Biochemistry*, *41*, 11611–11627.

Kozlov, A.G., Jezewska, M.J., Bujalowski, W., and Lohman, T.M. (2010). Binding

specificity of *E. coli* SSB protein for the χ subunit of DNA pol III holoenzyme and PriA helicase. *Biochemistry, 49*, 3555–3566.

Kozlov, A.G., Cox, M.M., and Lohman, T.M. (2010). Regulation of single-stranded DNA binding by the C-termini of *Escherichia coli* single-stranded DNA-binding (SSB) protein. *J. Biol. Chem.*, *285*, 17246–17252.

Krauss, G., Sindermann, H., Schomburg, U., and Maass, G. (1981). *Escherichia coli* single-strand deoxyribonucleic acid binding protein: Stability, specificity, and kinetics of complexes with oligonucleotides and deoxyribonucleic Acid. *Biochemistry, 20*, 5346–5352.

Krishna, T.S., Kong, X.-P., Gary, S., Burgers, P.M.J., and Kuriyan, J. (1994). Crystal structure of the eukaryotic DNA polymerase processivity factor PCNA. *Cell, 79*, 1233–1243.

Kunst, F., Ogasawara, N., Moszer, I., Albertini, A.M., Alloni, G., Azevedo, V., Bertero, M.G., Bessières, P., Bolotin, A., Borchert, S., Borriss, R., Boursier, L., Brans, A., Braun, M., Brignell, S.C., Bron, S., Brouillet, S., Bruschi, C.V., Caldwell, B., Capuano, V., Carter, N.M., Choi, S.K., Codani, J.J., Connerton, I.F., Danchin, A., *et al.* (1997). The complete genome sequence of the Gram positive bacterium *Bacillus subtilis*. *Nature, 390*, 249–256.

Kurz, M., Dalrymple, B., Wijffels, G., and Kongsuwan, K. (2004). Interaction of the sliding clamp β-subunit and Hda, a DnaA-related protein. *J. Bacteriol., 186*, 3508–3515.

LaDuca, R.J., Fay, P.J., Chuang, C., McHenry, C.S., and Bambara, R.A. (1983). Site-specific pausing of deoxyribonucleic acid synthesis catalyzed by four forms of *Escherichia coli* DNA polymerase III. *Biochemistry, 22*, 5177–5188.

Lederberg, J., and Tatum, E.L. (1946). Gene recombination in *Escherichia coli*. *Nature*, 158–558.

Lee, J.Y., Chang, C., Song, H.K., Moon, J., Yang, J., Kim, H.K., Kwon, S.T., and Suh, S.W. (2000). Crystal structure of NAD^+-dependent DNA ligase: modular architecture and functional implications. *EMBO J., 19*, 1119–1129.

Lehman, I.R., and Richardson, C.C. (1964). The deoxyribonucleases of *Escherichia coli* IV. An exonuclease activity present in purified preparations of deoxyribonucleic acid polymerase. *J. Biol. Chem., 239*, 233–241.

Leslie, A.G.W., and Powell, H.R. (2007). *Evolving Methods for Macromolecular Crystallography*, Springer Netherlands.

Leu, F.P., and O'Donnell, M. (2001). Interplay of clamp loader subunits in opening the β sliding clamp of *Escherichia coli* DNA polymerase III holoenzyme. *J. Biol. Chem., 276*, 47185–47194.

Li, X., and Marians, K.J. (2000). Two distinct triggers for cycling of the lagging strand

polymerase at the replication fork. *J. Biol. Chem*., *275*, 34757–34765.

Lia, G., Michel, B., and Allemand, J.F. (2012). Polymerase exchange during Okazaki fragment synthesis observed in living cells. *Science*, *335*, 328–331 (retracted 2014).

Little, J.W., Zimmerman, S.B., Oshinsky, C.K., and Gellert, M. (1967). Enzymatic joining of DNA strands, II: an enzyme-adenylate intermediate in the DPN-dependent DNA ligase reaction. *Proc. Natl. Acad. Sci. U.S.A.*, *58*, 2004–2011.

Lo, A.T. (2012). *Protein Dynamics on the Lagging Strand during DNA Synthesis*. Ph.D. Thesis, University of Wollongong.

Lohman, T.M., and Overman, L.B. (1985). Two binding modes in *Escherichia coli* single strand binding protein–single stranded DNA complexes. Modulation by NaCl concentration. *J. Biol. Chem., 260*, 3951–3954.

Lohman, T.M., Overman, L.B., and Datta, S. (1986). Salt-dependent changes in the DNA binding co-operativity of *Escherichia coli* single strand binding protein. *J. Mol. Biol., 187*, 603–615.

Lohman, T.M., and Mascotti, D.P. (1992). Thermodynamics of ligand–nucleic acid interactions. *Methods Enzymol., 212*, 400–424.

Lonberg, N., Kowalczykowski, S.C., Paul, L.S., and von Hippel, P.H. (1981). interactions of bacteriophage T4-coded gene 32 protein with nucleic acids. III. Binding properties of two specific proteolytic digestion products of the protein (G32P*I and G32P*III). *J. Mol. Biol., 145*, 123–138.

López de Saro, F.J., Georgescu, R.E., Goodman, M.F., and O'Donnell, M. (2003a). Competitive processivity-clamp usage by DNA polymerases during DNA replication and repair. *EMBO J., 22*, 6408–6418.

López de Saro, F.J., Georgescu, R.E., and O'Donnell, M. (2003b). A peptide switch regulates DNA polymerase processivity. *Proc. Natl. Acad. Sci. U.S.A., 100*, 14689–14694.

López de Saro, F.J., Marinus, M.G., Modrich, P., and O'Donnell, M. (2006). The β sliding clamp binds to multiple sites within MutL and MutS. *J. Biol. Chem., 281*, 14340–14349.

López de Saro, F.J., and O'Donnell, M. (2001). Interaction of the β sliding clamp with MutS, ligase and DNA polymerase I. *Proc. Natl. Acad. Sci. U.S.A., 98*, 8376–8380.

Love, C.A., Lilley, P.E., and Dixon, N.E. (1996). Stable high-copy-number bacteriophage λ promoter vectors for overproduction of proteins in *Escherichia coli*. *Gene*, *176*, 49–53.

Ludwig, C. 1856. *Sitzungsber. Akad. Wiss. Wien: Math.-Naturwiss.*

Lundquist, R.C., and Olivera, B.M. (1982). Transient generation of displaced single-stranded DNA during nick translation. *Cell, 31*, 53–60.

Luria, S.E., and Burrous, J.W. (1957). Hybridization between *Escherichia coli* and Shigella. *J. Bacteriol*., *74*, 461–476.

Maignan, S., Guilloteau, J.P., Zhou-Liu, Q., Clement-Mella, C., and Mikol, V. (1998). Crystal structures of the catalytic domain of HIV-1 integrase free and complexed with its metal cofactor: high level of similarity of the active site with other viral integrases. *J. Mol. Biol*., *282*, 359–368.

Maki, H. and Kornberg, A. (1987). Proofreading by DNA polymerase III of *Escherichia coli* depends on cooperative interaction of the polymerase and exonuclease subunits. *Proc. Natl. Acad. Sci. U. S. A. 84*, 4389–4392.

Manosas, M., Spiering, M.M., Ding, F., Bensimon, D., Allemand, J.F., Benkovic, S.J., and Croquette, V. (2012). Mechanism of strand displacement synthesis by DNA replicative polymerases. *Nucleic Acids Res.*, *40*, 6174–6186.

Marceau, A.H., Bahng, S., Massoni, S.C., George, N.P., Sandler, S.J., Marians, K.J. and Keck, J.L. (2011). Structure of the SSB–DNA polymerase III interface and its role in DNA replication. *EMBO J.*, *30*, 4236–4247.

Marchetti, A., Jehle, S., Felletti, M., Knight, M.J., Wang, Y., Xu, Z.-Q., Park, A.Y., Otting, G., Lesage, A., Emsley, L., Dixon, N.E., and Pintacuda, G. (2012). Backbone assignment of fully protonated solid proteins by ^{1}H detection and ultrafast magic-angle-spinning NMR spectroscopy. *Angew. Chem. Int. Ed.*, *51*, 10756–10759.

Marintcheva, B., Hamdan, S.M., Lee, S.J., and Richardson, C.C. (2006). Essential residues in the C-terminus of the bacteriophage T7 gene 2.5 single-stranded DNA-binding protein. *J. Biol. Chem.*, *281*, 25831–25840.

Marintcheva, B., Marintchev, A., Wagner, G., and Richardson, C.C. (2008). Acidic C-terminal tail of the ssDNA-binding protein of bacteriophage T7 and ssDNA compete for the same binding surface. *Proc. Natl. Acad. Sci. U.S.A.*, *105*, 1855–1860.

Mason, C.E., Jergić, S., Lo, A.T., Wang, Y., Dixon, N.E., and Beck, J.L. (2013). *Escherichia coli* single-stranded DNA-binding protein: nanoESI-MS studies of salt-modulated subunit exchange and DNA binding transactions. *J. Am. Soc. Mass Spectrom.*, *24*, 274–285.

Matsumiya, S., Ishino, Y., and Morikawa, K. (2001). Crystal structure of an archaeal DNA sliding clamp: Proliferating cell nuclear antigen from *Pyrococcus furiosus*. *Protein. Sci.*, *10*, 17–23.

Matsumoto, T., Morimoto, Y., Shibata, N., Kinebuchi, T., Shimamoto, N., Tsukihara, T., and Yasuoka, N. (2000). Roles of functional loops and the C-terminal segment of a single-stranded DNA binding protein elucidated by X-ray structure analysis. *J. Biochem.*, *127*, 329–335.

Maul, R.W., Sanders, L.H., Lim, J.B., Benitez, R. and Sutton, M.D. (2007). Role of *Escherichia coli* DNA polymerase I in conferring viability upon the *dnaN159* mutant strain. *J. Bacteriol.*, *189*, 4688–4695.

McHenry, C.S. (2000). The DnaX-binding subunits δ′ and ψ are bound to γ and not τ in the DNA polymerase III holoenzyme. *J. Biol. Chem*., *275*, 3017–3020.

McHenry, C.S. (2003). Chromosomal replicases as asymmetric dimers: studies of subunit arrangement and functional consequences. *Mol. Microbiol*., *49*, 1157–1165.

Meselson, M., and Stahl, F.W. (1958). The replication of DNA in *Escherichia coli*. *Proc. Natl. Acad. Sci. U.S.A*., *44*, 671–682.

Miller, E.M., and Nickoloff, J.A. (1995). *Escherichia coli* electrotransformation. In *Electroporation Protocols for Microorganisms*, Nickoloff, J.A., Ed.. Humana Press, Totowa, New Jersey, 105–114.

Mitra, S. and Kornberg, A. (1966). Enzymatic mechanisms of DNA replication. *J. Gen. Physiol.* 49, 59–79.

Moise, H., and Hosoda, J. (1976). T4 gene 32 protein model for control of activity at replication fork. *Nature*, *259*, 455–458.

Mol, C.D., Kuo, C.F., Thayer, M.M., Cunningham, R.P., and Tainer, J.A. (1995). Structure and function of the multifunctional DNA-repair enzyme exonuclease III. *Nature*, *374*, 381–386.

Molineux, I.J., Pauli, A., and Gefter, M.L. (1975). Physical studies of the interaction between the *Escherichia coli* DNA binding protein and nucleic acids. *Nucleic Acids Res*., *2*, 1821–1837.

Morikawa, K. (1990). Three-dimensional structure of ribonuclease H from *E. coli*. *Nature*, *347*, 306–309.

Morrison, D.A. (1979). Transformation and preservation of competent bacterial cells by freezing. *Methods Enzymol. 68*, 326–331.

Mulcair, M.D., Schaeffer, P.M., Oakley, A.J., Cross, H.F., Neylon, C., Hill, T.M. and Dixon, N.E. (2006). A molecular mousetrap determines polarity of termination of DNA replication in *E. coli*. *Cell, 125*, 1309–1319.

Murzin, A.G. (1993). OB (oligonucleotide/oligosaccharide binding)-fold: common structural and functional solution for nonhomologous sequences. *EMBO J.*, *12*, 861–867.

Murzin, A.G. (1998). How far divergent evolution goes in proteins. *Curr. Opin. Struct. Biol.*, *8*, 380–387.

Nagata, Y., Mashimo, K., Kawata, M., and Yamamoto, K. (2002). The roles of Klenow processing and flap processing activities of DNA polymerase I in chromosome instability in *Escherichia coli* K12 strains. *Genetics*, *160*, 13–23.

Nakamura, T., Zhao, Y., Yamagata, Y., Hua, Y., and Yang, W. (2012). Watching DNA polymerase η make a phosphodiester bond. *Nature, 487*, 196–201.

Naktinis, V., Onrust, R., Fang, L., and O'Donnell, M. (1995). Assembly of a chromosomal replication machine: two DNA polymerases, a clamp loader, and sliding clamps in one holoenzyme particle. II. Intermediate complex between the clamp loader and its clamp. *J. Biol. Chem.*, *270*, 13358–13365.

Naktinis, V., Turner, J., and O'Donnell, M. (1996). A molecular switch in a replication machine defined by an internal competition for protein rings. *Cell*, *84*, 137–145.

Nandakumar, J., Nair, P.A., and Shuman, S. (2007). Last stop on the road to repair: structure of *E. coli* DNA ligase bound to nicked DNA–adenylate. *Mol. Cell*, *26*, 257–271.

Neylon, C., Brown, S.E., Kralicek, A.V., Miles, C.S., Love, C.A., and Dixon, N.E. (2000). Interaction of the *Escherichia coli* replication terminator protein (Tus) with DNA: a model derived from DNA binding studies of mutant proteins by surface plasmon resonance. *Biochemistry*, *39*, 11989–11999.

Neuwald, A.F., Aravind, L., Spouge, J.L., and Koonin, E.V. (1999). AAA+: A class of chaperone-like ATPases associated with the assembly, operation, and disassembly of protein complexes. *Genome Res.*, *9*, 27–43.

Nishino, T., Komori, K., Ishino, Y., and Morikawa, K. (2003). X-ray and biochemical anatomy of an archaeal XPF/Rad1/Mus81 family nuclease: similarity between its endonuclease domain and restriction enzymes. *Structure*, *11*, 445–457.

Nowotny, M., Gaidamakov, S.A., Crouch, R.J., and Yang, W. (2005). Crystal structures of RNase H bound to an RNA/DNA hybrid: substrate specificity and metal dependent catalysis. *Cell*, *121*, 1005–1016.

Nowotny, M., and Yang, W. (2006). Stepwise analyses of metal ions in RNase H catalysis from substrate destabilization to product release. *EMBO J.*, *25*, 1924–1933.

Oakley, A.J., Heinrich, T., Thompson, C.A., and Wilce, M.C.J. (2003). Characterisation of a family 11 xylanase from *Bacillus subtilis* B230 used for paper bleaching. *Acta Crystallogr. D*, *59*, 627–636.

Oakley, A.J., Prosselkov, P., Wijffels, G., Beck, J.L., Wilce, M.C.J., and Dixon, N.E. (2003). Flexibility revealed by the 1.85 Å crystal structure of the β sliding-clamp subunit of *Escherichia coli* DNA polymerase III. *Acta Crystallogr. D*, *59*, 1192–1199.

Oakley, G.G., Patrick, S.M., Dixon, K., and Turchi, J.J. (2005). DNA damage induced hyper-phosphorylation of replication protein A. 2. Characterization of DNA binding activity, protein interactions, and activity in DNA replication and repair. *Biochemistry*, *44*, 8438–8448.

Oda, Y., Yoshida, M., and Kanaya, S. (1993). Role of histidine 124 in the catalytic function of ribonuclease HI from *Escherichia coli*. *J. Biol. Chem.*, *268*, 88–92.

O'Donnell, M., and Studwell, P.S. (1990). Total reconstitution of DNA polymerase III holoenzyme reveals dual accessory protein clamps. *J. Biol. Chem*., *265*, 1179–1187.

Ohtani, N., Haruki, M., Morikawa, M., Crouch, R.J., Itaya, M., and Kanaya, S. (1999). Identification of the genes encoding Mn^{2+}-dependent RNase HII and Mg^{2+}-dependent RNase HIII from *Bacillus subtilis*: classification of RNases H into three families. *Biochemistry*, *38*, 605–618.

Ohtani, N., Haruki, M., Morikawa, M., and Kanaya, S. (1999). Molecular diversities of RNase H. *J. Biosci. Bioeng*., *88*, 12–19.

Okazaki, T., and Okazaki, R. (1969). Mechanism of DNA chain growth. IV. Direction of synthesis of T4 short DNA chains as revealed by exonucleolytic degradation. *Proc. Natl. Acad. Sci. U.S.A.*, *64*, 1242.

Olivera, B.M., and Lehman, I.R. (1967a). Linkage of polynucleotides through phosphodiester bonds by an enzyme from *Escherichia coli. Proc. Natl. Acad. Sci. U.S.A.*, *57*, 1426–1433.

Olivera, B.M., and Lehman, I.R. (1967b). Diphosphopyridine nucleotide: a cofactor for the polynucleotide-joining enzyme from *Escherichia coli. Proc. Natl. Acad. Sci. U.S.A.*, *57*, 1700–1704.

Olivera, B.M., Hall, Z.W., and Lehman, I.R. (1968). Enzymatic joining of polynucleotides, V: a DNA-adenylate intermediate in the polynucleotide-joining reaction. *Proc. Natl. Acad. Sci. U.S.A.*, *61*, 237–244.

Ollis, D.L., Brick, P., Hamlin, R., Xuong, N.G., and Steitz, T.A. (1985). Structure of large fragment of *Escherichia coli* DNA polymerase I complexed with dTMP. *Nature*, *313*, 762–766.

Olson, M.W., Dallmann, H.G., and McHenry, C.S. (1995). DnaX complex of *Escherichia coli* DNA polymerase III holoenzyme. The χψ complex functions by increasing the affinity of τ and γ for δδ' to a physiologically relevant range. *J. Biol. Chem.*, *270*, 29570–29577.

Onrust, R., Finkelstein, J., Turner, J., Naktinis, V., and O'Donnell, M. (1995). Assembly of a chromosomal replication machine: two DNA polymerases, a clamp loader, and sliding clamps in one holoenzyme particle. I. Organization of the clamp loader. *J. Biol. Chem.*, *270*, 13348–13357.

Otwinowski, Z., and Minor, W. (1997). Processing of X-ray diffraction data collected in oscillation mode, *Methods Enzymol.*, *276*, 307–326.

Overman, L.B., Bujalowski, W., and Lohman, T.M. (1988). Equilibrium binding of *E. coli* single strand binding protein to single stranded nucleic acids in the $(SSB)_{65}$ binding mode. Cation and anion effects and polynucleotide specifecity. *Biochemistry*, *27*, 456–471.

Overman, L.B., and Lohman, T.M. (1994). Linkage of pH, anion and cation effects in protein–nucleic acid equilibria. *E. coli* SSB protein–single stranded nucleic acid equilibria. *J. Mol. Biol*., *236*, 165–178.

Ozawa, K., Jergić, S., Crowther, J.A., Thompson, P.R., Wijffels, G., Otting, G., and

Dixon, N.E. (2005). Cell-free *in vitro* protein synthesis in an autoinduction system for NMR studies of protein–protein interactions. *J. Biomol. NMR., 32*, 235–241.

Pant, K., Nimitpattana, S., Silva, M.C., Sefcikova, J., Beuning, P.J., and Williams, M.C. (2013). Simultaneous interaction of *E. coli* single stranded DNA binding protein and replicative DNA polymerase III alpha subunit with single-stranded DNA molecules. *Biophysical Journal, 104*, p74a. (meeting abstract)

Pascal, J.M., O'Brien, P.J., Tomkinson, A.E., and Ellenberger, T. (2004). Human DNA ligase I completely encircles and partially unwinds nicked DNA. *Nature, 432*, 473–478.

Petzold, C., Marceau, A.H., Miller, K.H., Marqusee, S., and Keck, J.L. (2012). Structural basis for the interaction between *E. coli* RNase HI and SSB. *FASEB J., 26* (meeting abstract)

Pomerantz, R.T., and O'Donnell, M. (2007). Replisome mechanics: insights into a twin DNA polymerase machine. *Trends Microbiol., 15*, 156–164.

Prescott, D.M., and Kuempel, P.L. (1972). Bidirectional replication of the chromosome in *Escherichia coli*. *Proc. Natl. Acad. Sci. U.S.A., 69*, 2842–2845.

Porter, R.D., and Black, S. (1991). The single-stranded-DNA-binding protein encoded by the *Escherichia coli* F factor can complement a deletion of the chromosomal *ssb* gene. *J. Bacteriol., 173*, 2720–2723.

Pritchard, A.E., Dallmann, H.G., Glover, B.P., and McHenry, C.S. (2000). A novel assembly mechanism for the DNA polymerase III holoenzyme DnaX complex: association of δδ' with $DnaX_4$ forms $DnaX_3$δδ'. *EMBO J., 19*, 6536–6545.

Pritchard, J.K., Stephens, M., and Donelly, P. (2000). Inference of population structure using multilocus genotype data. *Genetics, 155*, 945–959.

Raghunathan, S., Kozlov, A.G., Lohman, T.M., and Waksman, G. (2000). Structure of the DNA binding domain of *E. coli* SSB bound to ssDNA. *Nat. Struct. Biol., 7*, 648–652.

Record, M.T., Jr, Lohman, T.M., and De Haseth, P.L. (1976). Ion effects on ligand–nucleic acid interactions. *J. Mol. Biol., 107*, 145–158.

Record, M.T., Jr, Anderson, C.F., and Lohman, T.M. (1978). Thermodynamic analysis of ion effects on the binding and conformational equilibria of proteins and nucleic acids: the roles of ion association or release, screening, and ion effects on water activity. *Quart. Rev. Biophys., 11*, 103–178.

Rees, C.E.D., and Wilkins, B.M. (1990). Protein transfer into the recipient cell during bacterial conjugation: studies with F and RP4. *Mol. Microbiol., 4*, 1199–1205.

Reyes-Lamothe, R., Sherratt, D.J., and Leake, M.C. (2010). Stoichiometry and architecture of active DNA replication machinery in *Escherichia coli*. *Science, 328*, 498–501.

Rice, P., and Mizuuchi, K. (1995). Structure of the bacteriophage Mu transposase core:

a common structural motif for DNA transposition and retroviral integration. *Cell, 82*, 209–220.

Ricchetti, M., and Buc, H. (1993). *E. coli* DNA polymerase I as a reverse transcriptase. *EMBO J., 12*, 387–396.

Robins, P., Pappin, D.J., Wood, R.D., and Lindahl, T. (1994). Structural and functional homology between mammalian DNase IV and the 5'-nuclease domain of *Escherichia coli* DNA polymerase I. *J. Biol. Chem., 269*, 28535–28538.

Robinson, A., and van Oijen, A.M. (2013). Bacterial replication, transcription and translation: mechanistic insights from single-molecule biochemicals studies. *Nature Reviews Microbiology*, *11*, 303–315.

Rothwell, P.J., and Waksman, G. (2005). Structure and mechanism of DNA polymerases. *Adv. Protein Chem.*, *71***,** 401–440.

Rowen, L., and Kornberg, A. (1978). A ribo-deoxyribonucleotide primer synthesized by primase. *J. Biol. Chem*., *253*, 770–774.

Roy, R., Kozlov, A.G., Lohman, T.M., and Ha, T. (2009). SSB protein diffusion on single-stranded DNA stimulates RecA filament formation. *Nature, 461*, 1092–1097.

Russu, I.M. (2004). Probing site-specific energetics in proteins and nucleic acids by hydrogen exchange and nuclear magnetic resonance spectroscopy. *Methods Enzymol., 379*, 152–175.

Ruvolo, P.P., Keating, K.M., Williams, K.R., and Chase, J.W. (1991). Single-stranded DNA binding proteins (SSBs) from prokaryotic transmissible plasmids. *Proteins, 9*, 120–134.

Ruyechan, W.T., and Wetmur, J.G. (1975). Studies on the cooperative binding of the *Escherichia coli* DNA unwinding protein to single-stranded DNA. *Biochemistry, 14*, 5529–5534.

Sambrook, J., Fritsch, E.F., and Maniatis, T. (1989). *Molecular Cloning: A Laboratory Manual, 2nd ed.*, Cold Spring Harbor Laboratory Press, Cold Spring Harbor, New York.

Schmitz, C., Vernon, R., Otting, G., Baker, D., and Huber, T. (2012). Protein structure determination from pseudocontact shifts using ROSETTA. *J. Mol. Biol*., *416*, 668–677.

Scott, J.F., Eisenberg, S., Bertsch, L.L., and Kornberg, A. (1977). A mechanism of duplex DNA replication revealed by enzymatic studies of phage ϕX174: catalytic strand separation in advance of replication. *Proc. Natl. Acad. Sci. U.S.A., 74*, 193–197.

Setlow, P., Brutlag, D., and Kornberg, A. (1972). DNA polymerase: Two distinct enzymes in one polypeptide. I. A proteolytic fragment containing the polymerase and 3'→5' exonuclease functions. *J. Biol. Chem., 247*, 224–231.

Shamoo, Y., and Steitz, T.A. (1999). Building a replisome from interacting pieces:

sliding clamp complexed to a peptide from DNA polymerase and a polymerase editing complex. *Cell, 99*, 155–166.

Shereda, R.D., Kozlov, A.G., Lohman, T.M., Cox, M.M., and Keck, J.L. (2008). SSB as an organizer/mobilizer of genome maintenance complexes. *Crit. Rev. Biochem. Mol. Biol., 43*, 289–318.

Shishmarev, D., Wang, Y., Mason, C.E., Su, X.-C., Yagi, H., Oakley, A.J., Graham, B., Huber, T., Dixon, N.E. and Otting, G. (2014). Intramolecular binding mode of the C-terminus of *E. coli* single-stranded DNA binding protein (SSB) determined by nuclear magnetic resonance spectroscopy. *Nucleic Acids Res.*, *42*, 2750–2757.

Shlyakhtenko, L.S., Lushnikov, A.Y., Miyagi, A., and Lyubchenko, Y.L. (2012). Specificity of binding of single-stranded DNA-binding protein to its target. *Biochemistry, 51***,** 1500–1509.

Shuman, S. (2009). DNA ligases: Progress and prospects. *J. Biol. Chem.*, *284*, 17365–17369.

Simmons, L.A., Davies, B.W., Grossman, A.D., and Walker, G.C. (2008). β clamp directs localization of mismatch repair in *Bacillus subtilis*. *Mol. Cell*., *29*, 291–301.

Simonetta, K.R., Kazmirski, S.L., Goedken, E.R., Cantor, A.J., Kelch, B.A., McNally, R., Seyedin, S.N., Makino, D.L., O'Donnell, M., and Kuriyan, J. (2009). The mechanism of ATP-dependent primer–template recognition by a clamp loader complex. *Cell, 137*, 659–671.

Singleton, M.R., Håkansson, K., Timson, D.J., and Wigley, D.B. (1999). Structure of the adenylation domain of an NAD^+-dependent DNA ligase. *Structure*, *7*, 35–42.

Sinha, N.K., Morris, C.F., and Alberts, B.M. (1980). Efficient *in vitro* replication of double-stranded DNA templates by a purified T4 bacteriophage replication system. *J. Biol. Chem., 255*, 4290–4293.

Snyder, A.K., Williams, C.R., Johnson, A., O'Donnell, M., and Bloom, L.B. (2004). Mechanism of loading the *Escherichia coli* DNA polymerase II sliding clamp. II. Uncoupling the β and DNA binding activities of the γ complex. *J. Biol. Chem., 279*, 4386–4393.

Srivastava, S.K., Tripathi, R.T., and Ramachandran, R. (2005). NAD^+-dependent DNA ligase (Rv0314c) from *Mycobacterium tuberculosis*: Crystal structure of the adenylylation domain and identification of novel inhibitors. *J. Biol. Chem.*, *280*, 30273–30281.

Studier, F.W., Rosenberg, A.H., Dunn, J.J., and Dubendorff, J.W. (1990). Use of T7 RNA polymerase to direct expression of cloned genes. *Methods Enzymol*., *185*, 60–89.

Studwell-Vaughan, P.S. and O'Donnell, M. (1993) DNA polymerase III accessory proteins. V. θ encoded by *holE*. *J. Biol. Chem. 268*, 11785–11791.

Stukenberg, P.T., Studwell-Vaughan P.S., O'Donnell, M. (1991). Mechanism of the sliding β-clamp of DNA polymerase III holoenzyme. *J. Biol. Chem., 266*, 11328–11334.

Stukenberg, P.T., Turner, J., and O'Donnell, M. (1994). An explanation for lagging strand replication: polymerase hopping among DNA sliding clamps. *Cell, 78*, 877–887.

Su, X.-C., Wang, Y., Yagi, H., Shishmarev, D., Mason, C.E., Smith, P.J., Vandevenne, M., Dixon, N.E. and Otting, G. (2014). Bound or free: interaction of the C-terminal domain of *Escherichia coli* single-stranded DNA-binding protein (SSB) with the tetrameric core of SSB. *Biochemistry*, *53*, 1925–1934.

Suck, D. (1997). Common fold, common function, common origin? *Nat. Struct. Biol.*, *4*, 161–165.

Sutton, M.D., and Duzen, J.M. (2006). Specific amino acid residues in the β sliding clamp establish a DNA polymerase usage hierarchy in *Escherichia coli. DNA Repair, 408*, 318–340.

Sutton, M.D., and Walker, G.C. (2001). Managing DNA polymerases: Coordinating DNA replication, DNA repair, and DNA recombination. *Proc. Natl. Acad. Sci. U.S.A., 98*, 8342–8349.

Sutton, M.D. (2004). The *Escherichia coli dnaN159* mutant displays altered DNA polymerase usage and chronic SOS induction. *J. Bacteriol., 186*, 6738– 6748

Tadokoro, T., and Kanaya, S. (2009). Ribonuclease H: Molecular diversities, substrate binding domains, and catalytic mechanism of the prokaryotic enzymes. *FEBS J., 276*, 1482–1493.

Taft-Benz, S.A. and Schaaper, R.M. (2004). The θ subunit of *Escherichia coli* DNA polymerase III: A role in stabilizing the ε proofreading subunit. *J. Bacteriol. 186*, 2774–2780.

Tang, X.F., Ezaki, S., Atomi, H., and Imanaka, T. (2000). Biochemical analysis of a thermostable tryptophan synthase from a hyperthermophilic archaeon. *Eur. J. Biochem., 267*, 6369–6377.

Tanner, N.A., Hamdan, S.M., Jergić, S., Loscha, K.V., Schaeffer, P.M., Dixon, N.E., and van Oijen A.M. (2008). Single-molecule studies of fork dynamics in *Escherichia coli* DNA replication. *Nat. Struct. Mol. Biol., 15*, 170–176.

Tanner, N.A., Loparo, J.J., Hamdan, S.M., Jergic, S., Dixon, N.E., and van Oijen A.M., (2009). Real-time single-molecule observation of rolling-circle DNA replication. *Nucleic Acids Res.*, 37, e27.

Tatum, E.L., and Lederberg, J. (1947). Gene recombination in the bacterium *E. coli*. *J Bacteriol.*, *53*, 673–684.

Theobald, D.L., Mitton-Fry, R.M., and Wuttke, D.S. (2003). Nucleic acid recognition by OB-fold proteins. *Annu. Rev. Biophys. Biomol. Struct., 32*, 115–133.

Tougu, K., and Marians, K.J. (1996a). The interaction between helicase and primase sets the replications fork clock. *J. Biol. Chem., 271,* 21398–21405.

Tougu, K., and Marians, K.J. (1996b). The extreme C terminus of primase is required for interaction with DnaB at the replication fork. *J. Biol. Chem., 271,* 21391–21397.

Tsunaka, Y., Haruki, M., Morikawa, M., Oobatake, M., and Kanaya, S. (2003). Dispensability of glutamic acid 48 and aspartic acid 134 for Mn^{2+}-dependent activity of *Escherichia coli* ribonuclease HI. *Biochemistry, 42,* 3366–3374.

Tsuchihashi, Z., and Kornberg, A. (1990). Translational frameshifting generates the γ subunit of DNA polymerase III holoenzyme. *Proc. Natl. Acad. Sci. U.S.A., 87,* 2516–2520.

Tsutakawa, S.E., Jingami, H., and Morikawa, K. (1999). Recognition of a TG mismatch: the crystal structure of very short patch repair endonuclease in complex with a DNA duplex. *Cell, 99,* 615–623.

Tsutakawa, S.E., Muto, T., Kawate, T., Jingami, H., Kunishima, N., Ariyoshi, M. (1999). Crystallographic and functional studies of very short patch repair endonuclease. *Mol. Cell, 3,* 621–628.

Vasudevan, S.G., Armarego, W.L.F., Shaw, D.C., Lilley, P.E., Dixon, N.E. and Poole, R.K. (1991). Isolation and nucleotide sequence of the *hmp* gene that encodes a haemoglobin-like protein in *Escherichia coli* K-12. *Mol. Gen. Genet.*, *226*, 49–58.

Wagner, J., and Nohmi, T. (2000). *Escherichia coli* DNA polymerase IV mutator activity: genetic requirements and mutational specificity. *J. Bacteriol., 182,* 4587–4595.

Walker, G.T., Fraiser, M.S., Schram, J.L., Little, M.C., Nadeau, J.G., and Malinowski, D.P. (1992). Strand displacement amplification — an isothermal, *in vitro* DNA amplification technique. *Nucleic Acids Res., 20,* 1691–1696.

Warbrick, E. (2000). The puzzle of PCNA's many partners. *BioEssays, 22,* 997–1006.

Watson, J.D., and Crick, F.H.C. (1953a). The structure of DNA. *Nature, 171,* 123–131.

Watson, J.D., and Crick, F.H.C. (1953b). Genetical implications of the structure of deoxyribonucleic acid. *Nature, 171,* 964–966.

Wei, T.F., Bujalowski, W., and Lohman, T.M. (1992). Cooperative binding of polyamines induces the *Escherichia coli* single-strand binding protein–DNA binding mode transitions. *Biochemistry, 31,* 6166–6174.

Weiner, J.H., Bertsch, L.L., and Kornberg, A. (1975). The deoxyribonucleic acid unwinding protein of *Escherichia coli. J. Biol. Chem., 250,* 1972–1980.

Weiss, B., and Richardson, C.C. (1967a). Enzymatic breakage and joining of deoxyribonucleic acid, I: repair of single-strand breaks in DNA by and enzyme system from *Escherichia coli* infected with T4 bacteriophage. *Proc. Natl. Acad. Sci. U.S.A., 57,* 1021–1028.

Weiss, B., and Richardson, C.C. (1967b). Enzymatic breakage and joining of deoxyribonucleic acid, III: an enzyme-adenylate intermediate in the polynucleotide ligase reaction. *J. Biol. Chem*., *242*, 4270–4278.

William, T.R., and James, G.W. (1975). Studies on the cooperative binding of the *Escherichia coli* DNA unwinding protein to single-stranded DNA. *Biochemistry, 14*, 5529–5534.

Williams, K.R., and Konigsberg, W. (1978). Structural changes in the T4 gene 32 protein induced by DNA polynucleotides. *J. Biol. Chem*., *253*, 2463–2470.

Williams, K.R., Spicer, E.K., Lopresti, M.B., Guggenheimer, R.A., and Chase, J.W. (1983). Limited proteolysis studies on the *Escherichia coli* single-stranded DNA binding protein. Evidence for a functionally homologous domain in both the *Escherichia coli* and T4 DNA binding proteins. *J. Biol. Chem.*, *10*, 3346–3355.

Williams, L.E., and Gregory, A. (2004). Changes in the expression pattern of the plasma membrane H^+-ATPase in developing *Ricinus communis* cotyledons undergoing the sink/source transition. *Planta*, *218*, 562–568.

Williams, N.K., Prosselkov, P., Liepinsh, E., Line, I., Sharipo, A., Littler, D.R., Curmi, P.M.G., Otting, G., and Dixon, N.E. (2002). *In vivo* protein cyclization promoted by a circularly-permuted *Synechocystis* sp. PCC6803 DnaB mini-intein. *J. Biol. Chem.*, *277***,** 7790–7798.

Winkler, F.K., Banner, D.W., Oefner, C., Tsernoglou, D., Brown, R.S., and Heathman, S.P. (1993). The crystal structure of *Eco*RV endonuclease and of its complexes with cognate and non-cognate DNA fragments. *EMBO J.*, *12*, 1781–1795.

Witte, G., Urbanke, C., and Curth, U. (2003). DNA polymerase III χ subunit ties single-stranded DNA binding protein to the bacterial replication machinery. *Nucleic Acids Res*., *31*, 4434–4440.

Wu, C.A., Zechner, E.L., Hughes, A.J., Jr., Franden, M.A., McHenry, C.S., and Marians, K.J. (1992). Coordinated leading- and lagging-strand synthesis at the *Escherichia coli* DNA replication fork. IV. Reconstitution of an asymmetric, dimeric DNA polymerase III holoenzyme. *J. Biol. Chem.*, *267*, 4064–4073.

Xiao, H., Crombie, R., Dong, Z., Onrust, R., and O'Donnell, M. (1993a). DNA polymerase III accessory proteins. III. *holC* and *holD* encoding χ and ψ. *J. Biol. Chem*., *268*, 11773–11778.

Xiao, H., Dong, Z., and O'Donnell, M. (1993b). DNA polymerase III accessory proteins. IV. Characterization of χ and ψ. *J. Biol. Chem*., *268*, 11779–11784.

Yadav, T., Carrasco, B., Myers, A.R., George, N.P., Keck, J.L., and Alonso, J.C. (2012). Genetic recombination in *Bacillus subtilis*: a division of labor between two single-strand DNA-binding proteins. *Nucleic Acids Res.*, *40*, 5546–5559.

Yang, W., Hendrickson, W.A., Crouch, R.J., and Satow, Y. (1990). Structure of ribonuclease H phased at 2 Å resolution by MAD analysis of the selenomethionyl

protein. *Science*, *249*, 1398–1405.

Yang, W., Lee, J.Y., and Nowotny, M. (2006). Making and breaking nucleic acids: two-Mg^{2+} -ion catalysis and substrate specificity. *Mol. Cell*, *22*, 5–13.

Yang, W., and Steitz, T. (1995). Recombining the structures of HIV integrase, RuvC and RNase H. *Structure, 3*, 131–134.

Yin, Z., Wang, Y., Whittell, L.R., Jergic, S., Liu, M., Harry, E., Dixon, N.E., Kelso, M.J., Beck, J.L. and Oakley, A.J. (2014). DNA replication is the target for the antibacterial effects ofnon-steroidal anti-inflammatory drugs. *Chem. Biol.*, 21, 481–487.

Yuan, Q., and McHenry, C.S. (2009). Strand displacement by DNA polymerase III occurs through a τ–ψ–χ link to single-stranded DNA-binding protein coating the lagging strand template. *J. Biol. Chem.*, *284*, 31672–31679.

Yuzhakov, A., Kelman, Z., and O'Donnell, M. (1999). Trading places on DNA – a three-point switch underlies primer handoff from primase to the replicative DNA polymerase. *Cell*, *96*, 153–163.

Zechner, E.L., Wu, C.A., and Marians, K.J. (1992). Coordinated leading- and lagging-strand synthesis at the *Escherichia coli* DNA replication fork. II. Frequency of primer synthesis and efficiency of primer utilization control Okazaki fragment size. *J. Biol. Chem.*, *267*, 4045–4053.

Zimmerman, S.B., Little, J.W., Oshinsky, C.K., and Gellert, M. (1967). Enzymatic joining of DNA strands: a novel reaction of diphosphopyridine nucleotide. *Proc. Natl. Acad. Sci. U.S.A.*, *57*, 1841–1848.

Zhang, D.Y., and Seelig, G. (2011). Dynamic DNA nanotechnology using strand-displacement reactions. *Nat. Chem.*, *3*, 103–113.

Zhou, R., Kozlov, A.G., Roy, R., Zhang, J., Korolev, S., Lohman, T.M., and Ha, T., (2011). SSB functions as a sliding platform that migrates on DNA *via* reptation. *Cell*, *146*, 222–232.

Zhou, X.R., and Christie, R.J. (1999). Mutagenesis of the *Agrobacterium* VirE2 single-stranded DNA-binding protein identifies regions required for self-association and interaction with VirE1 and a permissive site for hybrid protein construction. *J. Bacteriol.*, *181*, 4342–4352.